SEISMIC WAVE MODELLING USING THE BOUNDARY ELEMENT METHOD

MURAT SARI B.Sc.

A submission presented in partial fulfilment of the
requirements of the University of Glamorgan / Prifysgol Morgannwg
for the degree of Doctor of Philosophy.

School of Technology
Division of Mathematics and Statistics

August 2000

CERTIFICATE OF RESEARCH

This is to certify that, except where specific reference is made, the work presented within this thesis is the result of the investigation undertaken by the candidate.

Candidate: .....

Director of Studies: .....

Date: 14/2/00 .....

DECLARATION

This is to certify that neither this thesis or any part of it has been presented or is currently being submitted in candidature for any other degree other than the degree of Doctor Philosophy of the University of Glamorgan / Prifysgol Morgannwg.

Candidate: 

I would like to give my deepest thanks and sincere gratitude to my director of studies, Prof. R J Wiltshire, and to my former director of studies Dr R W Williams for their help, encouragement, guidance and constructive criticism provided during this research project.

I am grateful to the Pamukkale University for their financial support during my research period.

I would like to express my deepest gratitude to my wife Fatma, my mother, brothers and sisters for their support and constant encouragement during the period of accomplishing this thesis.

Also, I would like to thank my friends Dr H Ulucan, Mr I B Soysal and Mr M Demirci for always being supportive.

Finally, my thanks go to all my colleagues, the secretaries, computer technicians and the Head of School, Prof. A. Ryley.

Thank you all.

The main objective of this thesis is to use the boundary element method as an efficient and advantageous numerical approach to model the seismic signals received at selected receiver points due to a source located within a geophysical structure. These signals may travel through different geophysical structures. This work determines whether rock interfaces can be identified from the signals received at selected points. The method proves to be most satisfactory and more easily applicable for unbounded media than for bounded media.

Each layer in the media of interest is assumed to be linearly elastic, homogeneous and isotropic. This assumption is used for both two- and three-dimensional geometries. Throughout this research linear and constant time approximations are used to represent the displacements and tractions, respectively. With the use of these temporal variations all time integrations are evaluated analytically. The two-dimensional boundary kernels and internal flux kernels have been derived. New kernels for boundary and internal points have also been obtained for three-dimensional scalar waves. In addition, the three-dimensional elastodynamic boundary kernels have been evolved.

Constant elements are normally employed to discretize the boundary. To determine the dynamical response constant elements are seen to be well suited for the geometries used here. The improper integrals are evaluated analytically in two dimensions. In three dimensions two different techniques are used to cope with the singularities.

Some available computer codes for the boundary nodes are extended to determine material behaviour at internal points. For three-dimensional cases some programs are developed with the help of the two-dimensional programs. For layered materials these codes are expanded for each layer as subprogram.

In spite of the fact that the existence of the interfaces makes the solution of the problem tend to instability, this analysis shows that the BEM is capable of treating layered media problems. In general, the examples presented show that the time domain direct BEM is stable for practical applications. Some supplemental layered media results are also presented to show the usefulness and range of the method in real applications. These results also demonstrate the validity of the extended and developed programs in this thesis. Where possible the current work is compared with that of others.

Strong interface and other reflections are visible in all seismograms though somewhat weaker in the case of three dimensions.

The potential and flux changes across a plane body have been examined in two and three dimensions.

$\boldsymbol{a}$	Acceleration
θ, θ_i, γ	Angles
$\varnothing$	Empty set
x_1, x_2, x_3	Cartesian co-ordinates
ζ	One-dimensional homogeneous co-ordinate
ζ_k	Two-dimensional homogeneous co-ordinates
μ^m, η^m	Time interpolation functions
φ_k, ψ_k	Space interpolation functions
∇^2	Laplacian
J	Jacobian
$\mathbf{y}^i$	Load point
b_k	Body force components
f	Body source
K	Bulk modulus
c	Speed of wave propagation
c_1	Compresional wave velocity
c_2	Shear wave velocity
ρ	Density
∂	Differential operator
u	Displacement vector for the actual state
$\mathbf{u}^s$	Displacement vector for the for the solution state
r, R	Distance between the load and field points
Ω	Domain of the body
B	Boundary of the body
BEM	Boundary Element Method
FDM	Finite Difference Method
FEM	Finite Element Method
Δx	Element size
n	Unit outward vector normal to the boundary
H(t)	Heaviside function

$\delta(t)$	Dirac delta function
u_i	Displacement components
p_i	Traction components
σ_{km}	Stress components
u_{lk}^s	Fundamental displacement components
p_{lk}^s	Fundamental traction components
σ_{lkm}^s	Fundamental stress components
δ_{ij}	Kronecker delta
λ	Lame elastic constant
υ	Poisson's ratio
μ	Shear modulus
ε_{ij}	Strain components
e_{ijk}	Permutation symbol
t	Time
τ	Time in which an impulse is applied
Δt	Time increment
$\mathbf{e}$	Unit vector
ϕ	Scalar potential for the actual state
q	Derivative of ϕ with respect to normal
ϕ^s	Scalar potential for the solution state
q^s	Derivative of ϕ^s with respect to normal
E	Young modulus

CHAPTER 1

INTRODUCTION

1.1 Wave Propagation

In almost all physical sciences, the study of wave motion plays a very important role. The effect of a sharply applied disturbance in a medium transmits to other parts of the medium. This simple fact forms a basis of the study of *wave propagation*. An elastic wave is a motion in a medium in which, when particles are displaced, a force proportional to the displacement acts on the particles to restore them to their initial position. There are two basic types of elastic waves:

i. Body waves, which propagate within a body of a rock.

ii. Surface waves, whose motion is restricted to near the surface.

Surface waves are beyond the scope of this study.

Two main types of body waves propagate through the geophysical structures:

i. P-waves, also called primary or longitudinal, or compressional waves.

ii. S-waves, also called secondary or transverse, or shear waves.

Thus, like acoustic waves, the P-waves can travel through both solid and liquid material, unlike the S-waves, which can only travel through solids. The P-waves are characterized by particle motion back and forth along the direction of propagation, whereas the S-waves are characterized by particle motion at right angles to the direction of propagation as can be clearly seen in Figure (1.1). The two waves are elastic waves in a homogeneous and isotropic medium, each one with a fixed velocity. This velocity is called material velocity or wave velocity. The material and particle velocities should not be mixed up. So the P-

waves shake the ground in the direction they are propagating while the S-waves shake perpendicularly or transverse to the direction of propagation. That is why P-waves travel faster than the S-waves.

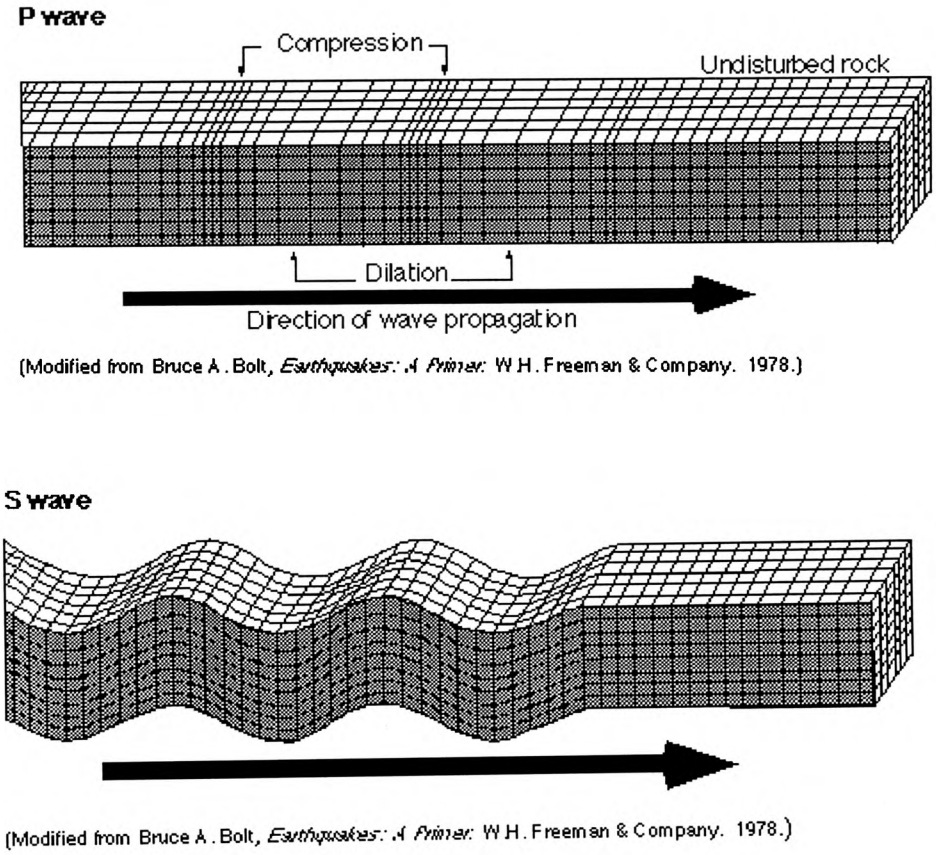

Figure 1.1 Motion during passage of a wave: P- and S-waves

Seismic waves are elastic waves which mean that they deform the media that they travel through but the medium returns to its original form after the passage of the wave. They are generated by disturbances of the ground such as earthquakes, blasts, atomic bombs, landslides, meteor impacts, magma movements etc. However, for seismic waves to be detectable, the source must be energetic. More details can be found in, for example, Bullen (1976) and Hudson (1980).

1.2 Seismology

Seismology is the study of seismic waves and it is an important branch of Earth science and geophysics, providing most of our knowledge of the structure of the Earth. Seismic waves are waves of energy caused by, for example, an explosion. This work concerns the method of explosion seismology in relation to crustal structure. The method brings a degree of control to seismological analyses, since origin times and locations of explosions are known, unlike natural earthquakes. Explosion experiments can be planned in advance, so that seismograms with much finer detail can be obtained. More details can be found in, for example, Bullen (1976) and White et al. (1987).

1.2.1 Seismographs

Seismic waves are detected and recorded by an instrument called a *seismograph*. The seismograph is obtained from data, which are records of mechanical vibrations of the Earth and is as important to seismology as is the telescope to astronomy. The aim of a seismograph is to record as much information as possible concerning the nature of the earth's movement, which is recorded in the vicinity of a particular point of the earth surface. More details can be found in, for example, Bullen (1976) and White et al. (1987).

1.2.2 Earthquakes

Astronomy existed long before the telescope, likewise seismology is older than the seismograph; but our information about early earthquakes is mainly provided by unscientific sources. Ancient accounts of earthquakes do not give much information; they are incomplete, and accuracy is usually sacrified to make the most of a good story. Useful and helpful reports begin in the eighteenth century (Doyle, 1995).

Vibrations in the Earth's crust are caused by earthquakes when rocks in which elastic strain has been increasing suddenly rupture, and then rebound. More details can be found in, for example, Bullen (1976) and Doyle (1995).

1.2.3 Developments in Seismology

In the last few decades, seismology has made tremendous progress mainly because of the advent of computers, and improvements in data acquisition systems. These developments have enabled seismologists to make measurements with greater sophistication and precision than was previously possible. Advanced computational analyses have been applied to high-quality data, and elaborate theoretical models have been devised to interpret them.

Seismology began with the study of earthquakes. Later transmission of elastic waves was used, by researchers such as Hooke in the study of earthquakes. Navier derived the differential equations of the theory of elasticity in 1821, and after that Somiglina produced formal solutions to Navier equations for a wide class of sources and boundary conditions (Graff, 1975). Cauchy developed the pure theory of elasticity, including the dynamical equations of motion in an elastic solid in 1822, and Poisson investigated the theory of seismic waves through an elastic solid body and showed the existence of two body waves in 1828 (Ben-Menahem et al., 1981). Stokes (1849) first investigated elastic wave motion due to body forces. In 1887, Lord Rayleigh predicted elastic surface waves on an elastic medium (Graff, 1975). In 1911, Love developed the fundamental theory of point sources in an infinite elastic space, and also Lamb laid the theoretical foundation for propagation of seismic waves in layered media in 1904 (Graff, 1975). A complete historical

development of early investigations carried out by Poisson, Cauchy, Green, Lame, Stokes etc. can be found in the books by Love (1944), Graff (1975), Hudson (1980) and Ben-Menahem et al. (1981).

Modern approaches to the investigation of wave propagation can be found in, for example, Morse and Feshbach (1953), Eringen and Suhubi (1975) and Achenbach (1975). Various numerical methods have been used to deal with the wave propagation problems, such as Boundary Element Methods (BEM), Finite Difference Method (FDM), Finite Element Method (FEM), experimental methods etc. These numerical methods are briefly and comparatively considered in the following section.

1.3 Numerical Methods in Dynamics

The most widely used and well known numerical methods are the FEM, the FDM and the BEM which emerged during the last three decades as a powerful computational tool. The FEM and FDM are based on the differential of the governing equation, whilst the BEM is based on an integral formulation of the partial differential equation to be solved.

Since it is sometimes difficult to obtain an analytical solution to a dynamic problem, and since the advent of computers in technology, popularity of the numerical methods has increased much especially in the last couple of decades. Among the numerical techniques, probably the most popular and well-established one is the FEM which can deal with intricate geometries, inhomogeneous media and non-linearities (Zienkiewicz, 1977). However, the FEM as well as the FDM requires to discretize the full domain under consideration. In these domain techniques, an entire discretization is also not feasible for the case of semi-infinite or infinite domain. Artificial boundaries are created at the ends of the mesh in which the discretization ends. In the BEM, as a result of the advantage of the

infinity cases, the regularity and radiation conditions (no reflected waves come from the infinity) are satisfied.

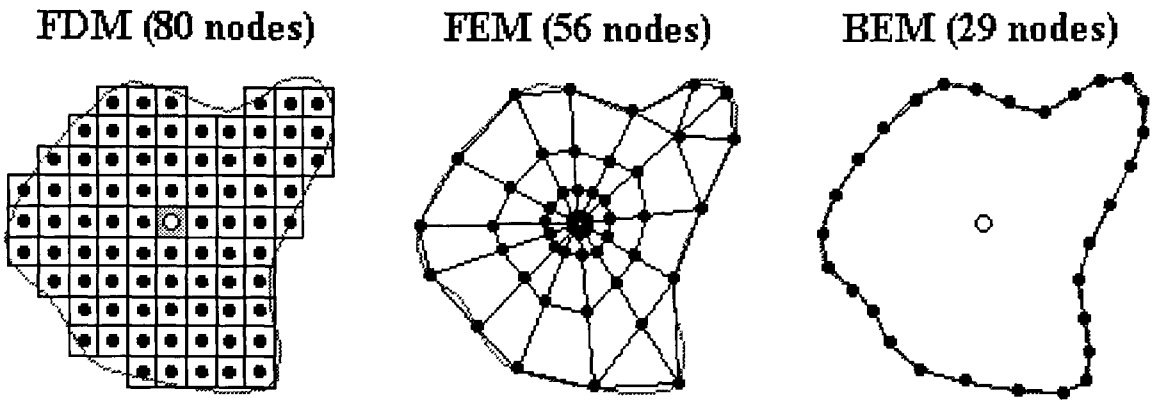

Figure 1.2 Comparison of different discretization schemes

There are some features of the BEM that give clear advantages for the analysis of continuum mechanic problems. For instance, the problem is formulated only on the boundary as shown in Figure (1.2). Therefore, the resulting system of equations is one dimension smaller in the BEM. This reduction of the problem's dimension is a great advantage of the BEM for dynamic problems, since a large amount of computer memory is needed to record a long history for a transient dynamic problem.

On the other hand, the BEM has not been used before to solve very large problems and is very new in comparison with the rival domain methods. The mathematics used in the BEM formulations is very intricate. However, many FEM numerical procedures are directly applicable to boundary element solutions (Dominguez, 1993). In the BEM, since each element is affected by all other elements, the system matrix is fully populated for a

homogeneous region and the matrix is block banded when more than one region is involved.

The BEM is now a well-established numerical technique, which provides an efficient alternative to the FDM and FEM for the solution of a wide range of engineering and applied science problems. Because of the above advantages, the BEM is used in the present study for different geometries and with time variation to solve our seismic problems.

1.3.1 The BEM Types

There are two types of integral equation formulations. One contains unknowns with a clear physical meaning. In these terms, the known boundary conditions are given and this class is called the direct BEM formulation. Different procedures have been adopted to derive the direct BEM formulation. To obtain an integral equation relating the internal and boundary field variables, in elastostatics, Betti's reciprocal theorem and Kelvin's solution was used by Rizzo (1967). To derive the same integral equation the weighted residuals method was used by Brebbia (1978).

The second type of formulation is known as indirect BEM formulation, in which the basic unknown quantities have no physical interpretation. As the indirect BEM is no longer widely used, the direct BEM is used throughout this thesis. For the scalar wave and elastodynamic problems, the direct BEM formulation in terms of dynamical reciprocity theorem and the corresponding fundamental solutions will be considered in the following chapter.

1.3.2 The BEM in Dynamics

Dynamic problems exist in many different engineering disciplines and applied sciences such as mechanical engineering, civil engineering, seismology etc. Wave propagation is a branch of dynamics. Two types of dynamic problems, steady state and transient, take place.

In recent years, the literature available tells us that two approaches have been considered to design elasticity and potential problems in terms of the BEMs. One of them is the transform domain approach, whilst the second is a time domain approach. In the first approach, the problem under consideration is expressed concisely and solved using Laplace or Fourier integral transforms. As the solution is obtained in the transform domain, it is transformed back into the time domain. On the other hand, in the time domain approach, the problem is solved directly using a time-stepping technique.

Both approaches have advantages and disadvantages. The principal advantage of the transform domain methods is that the problem is easy to formulate in that domain. On the other hand, the main advantage of the time domain over the transform domain is that it is more suitable for the extension to nonlinear material behavior (e.g. Manolis, 1983, Dominguez, 1993). The time domain technique is well suited for linear and nonlinear problems with sharply changing time histories of short duration, whereas the transform domain approaches are well suited for linear problems with long and slowly varying time histories (e.g. Birgisson, 1996). Therefore, nonlinear elastodynamic problems need to be solved using the time domain approach.

The time-domain approach is based on the dynamical reciprocity theorem and the fundamental solution (or so-called generalized Green's function) for a concentrated point

load in an infinite medium. Although the studies on the time domain formulation and implementation of the BEM have, especially over the last two decades, increased, this increase is rather small. Some reasons can be found why there are less time domain studies than transform domain implementations. Firstly, it can be seen that the time domain formulation is considerably more complex as a structure than the transform domain one. Another reason is that the time domain formulation can be obtained considering the transform domain. As the time history becomes longer, the time domain technique tends to be inefficient, because the solution obtained for the current time step is formulated using all the previous time steps. Manolis (1983) and Spyrakos and Antes (1986) gave some comparative studies to these approaches. In the present work, the solutions are obtained with the use of the time domain approach, since this technique is very well suited for linear problems with rapidly changing time histories (Birgisson, 1996).

1.3.3 Main Steps in the BEM

In the following chapters, the major steps of the method will be considered in detail. Here for the sake of completeness, the main steps generally used will be summarized with the help of Figure (1.3).

Firstly, the boundary problem to be solved is transformed into an integral equation with the use of the dynamical reciprocity theorem. Then the boundary integral equation is discretized temporally and spatially. This boundary element equation is converted to a set of algebraic equations after the specification of the boundary conditions. Solutions to the linear equation system are obtained for unspecified boundary variables for each time step.

Finally, internal field variables for the points chosen are calculated in terms of these boundary values for the related time step.

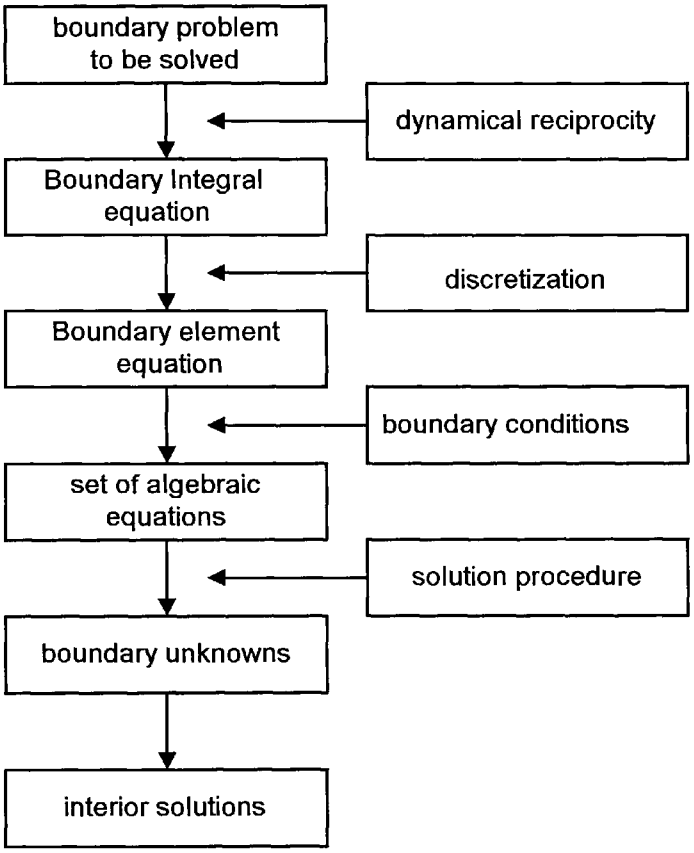

Figure 1.3 Main steps of the BEM solution of a boundary value problem (from Nowak et al., 1994)

1.4 Historical Development of the BEMs

Some textbooks describe the theoretical background of the linear elastodynamics using integral methods, for example, Wheeler and Sternberg (1968), Achenbach (1975), Graff (1975), Eringen and Suhubi (1975), Aki and Richards (1980), Hudson (1980) and Ben-Menahem et al. (1981). General books describing elasticity and potential problems using

the BEM are Banerjee and Butterfield (1981), Brebbia (1978), Brebbia et al. (1984), Beskos (1987a), Manolis and Beskos (1988), Brebbia et al. (1992), Partridge et al. (1992), Dominguez (1993), Nowak et al. (1994), Banerjee (1994), Hall (1994) and Bonnet (1998).

The BEM is based on the integral formulations of potential and elasticity problems. In 1889, Somiglina was the first person to establish an integral equation involving potential problems, and in 1905, Fredholm used Somiglina's identity to prove the existence and uniqueness of the potential fundamental solutions to Laplace equation (Ben-Menahem et al., 1981).

Muskhelishivili (1963) formulated the two-dimensional elastostatic problems. The direct BEM formulation was implemented by Symm (1963) and Jaswon (1963) with some papers for static potential problems and later with a paper by Rizzo (1967) for elastostatic problems. In those works, the numerical solution of the integral equation and segmentation of the boundary were studied. Cruse (1969,1974) studied the boundary element solution of elastostatic problems in three dimensions. Lachat (1975), Lachat and Watson (1976) studied the three-dimensional elastostatic problems using the BEM. A great contribution to the integral formulations with discontinuity and singularity was made by Mikhlin (1957).

The first developments of the BEM for dynamical problems were independent of the aforementioned works on the direct formulation of the method. The first dynamical works on the numerical solution of elasticity problems using the boundary integral formulation were obtained by Banaugh and Goldsmith (1963). Cruse and Rizzo (1968) and Cruse (1968) deduced the direct elastodynamic BEM taking into consideration the Laplace

transform domain to solve a wave propagation problem in a half-plane. In their scheme first the boundary integral equation is formulated and then solved through discretization in the Laplace domain. Manolis and Beskos (1981) developed the approach of Cruse and Rizzo to obtain transient solutions of elastodynamic problems, in terms of the Laplace transform approach. As mentioned above, both Manolis (1983) and Spyrakos and Antes (1986) gave comparative studies in terms of the time domain and transform domain approaches in the BEM for two-dimensional elastodynamic problems. Although Das and Aki (1977) studied two-dimensional problems in an infinite homogeneous elastic medium, this formulation was not a general one.

The first time-domain BEM produced for acoustics was that of Friedman and Shaw (1962). Cole et al. (1978) presented a time-domain BEM formulation for two-dimensional anti-plane elastodynamic problems. Although there are some restrictions in their approach, they gave the first contribution close to a general two-dimensional boundary element formulation in the time domain. The general time-domain formulation was studied by Mansur (1983) and Mansur and Brebbia (1982, 1985) for the scalar and elastic wave propagation problems in detail. Antes (1985) extended Mansur's study to include non-zero initial conditions. Spyrakos and Antes (1986) employed an alternative formulation for the time domain problems. Nardini and Brebbia (1983, 1985) brought out a BEM scheme so-called Dual Reciprocity approach to solve dynamic problems with non-zero body forces. When the body forces are not zero, the Multiple Reciprocity BEM of Nowak et al. (1994) can also be used as an alternative to the Dual Reciprocity BEM. A comparison of the two reciprocity methods was given by Brebbia (1991). Karabalis and Beskos (1984,1986) for the first time analyzed the time-domain formulation, and its

implementation for three-dimensional elastodynamic problems with a constant spatial and temporal discretization of the field variables. Banerjee and his co-workers (1986-1988) used this approach as well and extended it by considering a linear temporal variation of the field variables (Ahmad and Banerjee, 1988).

In recent years, the number of researchers who have been using the BEM has increased very rapidly. The transient wave propagation problems with initial conditions in isotropic elastic media were studied by Antes (1985). Banerjee and his co-workers, see for example Israil and Banerjee (1990a, 1990b), used a BEM, which requires bounded domains. Wang and Takemiya (1992) presented a two-dimensional scalar BEM under the condition of straight-line elements to evaluate the integrals analytically in both space and time.

During the derivation of the kernels in the scalar wave and elastodynamic problems, Israil and Banerjee (1990a, 1990b) used an explicit derivation, whilst Mansur (1983), Antes (1985) and Dominguez (1993) accepted an implicit approach in two dimensions. Adopting the same approach, Israil and Banerjee (1991a, 1991b) derived interior flux and stress kernels using, the linear temporal variation for both field variables. In their work, during the derivation of internal flux kernels, attention was drawn to some difficulties of Mansur's approach. Considering the two-dimensional scalar waves, Mansur and Carrer (1993) and Carrer and Mansur (1994) discussed time and spatial integration of the kernels. Carrer and Mansur (1996) worked on the two-dimensional scalar wave problems without neglecting initial conditions. In 1998 Mansur et al. considered a different time approximation from the commonly used one for the boundary tractions. To solve two-dimensional elastodynamic transient problems, Wang et al. (1997) took part in the discussion of temporal and space variation of the field variables. While the debate was

carrying on by means of different points of the method, Birgisson and Crouch (1998) presented a paper that considered the two-dimensional elastodynamic problems. In their work all integrals were evaluated analytically, to increase the accuracy and stability of the solution, using straight-line elements. They gave a very good comparative summary of the achievements of earlier works. Birgisson (1996) also studied piecewise homogeneous media using two-dimensional direct BEM. Time domain two-dimensional direct and indirect BEMs were used by Tian (1990), and a comparison was made between the two methods. In that work it was emphasized that the direct approach gave better results than the indirect one. Also an indirect time domain BEM was used by Antes et al. (1991) to analyze stress distribution. Gallego and Dominguez (1996) studied the obtaining of hypersingular integrals in transient elastodynamic problems. Carrer and Mansur (1999) studied internal stress and velocity components in two-dimensional elastodynamics. In their work all of the expressions required were presented *explicitly*.

There is less literature for three dimensions than for two. The first works on the time domain three-dimensional problems were mentioned previously. Both Mack (1991) and Loken (1992) studied indirect time-domain BEM to solve their problems by considering the 'fictitious stress' (Crouch and Starfield, 1983) and 'displacement discontinuity', which is a special case of the direct BEM (Mack, 1991) methods, respectively. Both Mack and Loken used linear-in-time and constant-in-space functional variations on flat rectangular elements. To obtain a new general time domain BEM, Rizos and Karabalis (1994) proposed to use the so-called 'B-spline fundamental solutions' to eliminate the restriction on temporal variation order of the field variables, without invalidating results. Coda and Venturini (1995, 1996) presented a different fundamental solution, which was obtained

considering a different body force from the common one in their formulation. Recently Wen et al. (1999), to solve their problems in a time domain BEM, developed a method by assuming temporal variation to be one-time-step piecewise continuity. For that temporal variation, the kernels were presented.

The BEM has proven to be an accurate numerical method (Beskos, 1987a, Dominguez, 1993, Trevelyan, 1994). Growing evidence of numerical instabilities in the BEMs led some researchers to work on this problem. Siebrits and Peirce (1995) and Siebrits et al. (1997) studied the stability properties of the direct and indirect time domain elastodynamic BEM and drew attention to evidence of instabilities. Peirce and Siebrits (1996) used model problems to investigate the stability properties in the method. Peirce and Siebrits (1997) again and Birgisson et al. (1999) focused on the problem and suggested some methods to improve the numerical stability of the method. Arai et al. (1999) also joined the discussion with a paper using the Laplace transformation for two-dimensional elastodynamic problems. Yu et al. (1999) suggested using the linear temporal variation for traction as well, in terms of the so-called linear θ method, without any mathematical proof. Yu et al. (2000) used Galerkin type formulations to improve stability in the BEM scalar wave propagation analysis, without giving any mathematical proof, in an example. It is important to realize that the method is at best conditionally stable.

BEM researchers often find Mackerle et al. (1988) to be a valuable source of reference. In this reference book the BEM textbooks, proceedings, publications and different BEM software available until 1987 were reviewed. Also, rigorous reviews of the BEMs were made by Beskos (1987b, 1997).

It can then be said that the method is now widespread and with increasing interest, even though it is very new in comparison to the rival methods.

Recent BEM research has been devoted to many points at issue. For example:

i. Evaluation of singular integrals,

ii. Temporal and spatial variation of the field variables,

iii. Use of the time or transform domain approaches,

iv. The BEM Types (direct or indirect, mostly the direct),

v. And lately, the stability of the methods.

The following sections are devoted to give the main aims, computer codes and an outline of the present work.

1.5 Objectives of This Research

The main objectives of this research are to produce satisfactory numerical models for the propagation of seismic waves in two- and three-dimensional physical homogeneous and inhomogeneous environments.

The 2D and 3D numerical models are based on the direct BEM in which the field variables are expressed in terms of each other by means of an algebraic equation system.

To develop a numerical model based on the BEM, the known displacements and tractions need to be integrated in space and time, and the integrated terms in time are called kernels. Therefore, derivation of the boundary and internal kernels are essential components of the present work. Since evaluation of the singular integrals is vital for the stability of the solution, careful treatment of the singular integrals is also of fundamental importance.

An additional goal is to determine potential and flux distributions through a two- and three-dimensional geophysical geometry.

To accomplish the stated aims, this research incorporates the following assumptions:

i. Small displacement theory,

ii. Each layer in media is taken to be homogeneous, isotropic and linearly elastic,

iii. Body forces and initial conditions are assumed to be zero,

iv. Equilibrium of tractions and continuity of displacements are assumed across the interfaces between different media,

v. The boundary under consideration is approximated by a set of straight-line (flat rectangular) elements in two (three) dimensions,

vi. Displacements and tractions are usually assumed to be constant over each element in space,

vii. Displacements and tractions are approximated by linear-in-time and constant-in-time interpolation functions, respectively,

viii. Homogeneous (Dirichlet or Neumann) and inhomogeneous Dirichlet boundary conditions are specified for external and internal boundaries, respectively (inhomogeneous boundary conditions are prescribed for an external boundary in two and three-dimensional distributions).

1.6 Development of the Programs

The theory of the wave equation is employed to produce computer code written in FORTRAN 77 to solve wave problems in time domain.

The computer code written solves the two-dimensional scalar wave equation at internal and boundary points of a domain. The code is valid for homogeneous isotropic elastic materials. To extend the validity of the programs for complex heterogeneous media, additional programs are produced for each layer. During the programming, special

attention is paid to irregular interfaces between different media. In addition, the programs calculate the internal flux distributions.

In addition, programs are encoded to solve two-dimensional elastic wave problems for a single layer. These programs compute the internal displacements as well as the boundary variables. Using additional code, the above programs are validated for piecewise homogeneous media.

To solve the scalar wave equation for three-dimensional geometries, further computer code is created. The potential and flux variables are computed on the boundary surface and inside the domain of interest. In addition, the programs are extended to heterogeneous media.

New code is also developed for the three-dimensional elastic wave formulations. Elastic responses of a three-dimensional geophysical structure are computed. The field variables are calculated both on the surface and inside the region under consideration.

It is important to notice that, the programs are not only valid for bounded domains but also for unbounded domains. The code for the two-dimensional problems is based on the simple media programs of Dominguez (1993).

1.7 Outline of Thesis

In Chapter 2, wave motion in elastic materials is examined, and the governing equations of transient wave propagation problems in the cases of scalar and elastodynamics are studied in general. Analysis of stresses and strains on a linearly elastic body, together with convenient differential equations, initial and boundary conditions are also discussed. Only the essential equations, the ideas needed to obtain the boundary element solution of

transient elastic and scalar wave propagation problems are investigated. A short analysis of the behaviour of wave motion in layered media is also given.

Chapter 3 contains the BEM solutions to the two-dimensional scalar waves, which are easier than fully developed elastic waves, in homogeneous and piecewise homogeneous media. The time-domain direct BEM formulation for the scalar waves in two dimensions is given by means of the solution and actual states. Derivation of the fundamental solution is also considered. In this chapter, establishment of the method is described in detail to provide a good base for the following chapters. New solutions are presented for layered media as well as the internal distributions. To show the validity of the method, different types of layered media results are presented. New internal flux kernels are derived and, relevant results produced are compared with the obtained FDM results. A discussion on the numerical stability of the method is given in this chapter. This discussion can also be generalized for results contained in later.

Chapter 4 is devoted to a description of the two-dimensional elastic wave problem in the same fashion as Chapter 3. The time domain direct boundary element formulation for the elastic waves in two dimensions is developed in terms of the dynamical reciprocity applied to the fundamental solution and actual states. The BEM solutions of the Cauchy-Navier equations are also shown for isotropic elastic homogeneous media as well as piecewise homogeneous media. This chapter demonstrates stability of the results, and the versatility of the method. These elastic results for different materials are presented, although there are no results for layered media with which to compare them.

Chapter 5 contains results for three-dimensional scalar waves for which the principles are easier to illustrate than for three-dimensional elastic waves. The three-dimensional direct

BEM formulation for the scalar waves is established in a similar fashion of the two-dimensional case, and analytical integration of the kernels are given in time. In the case of a singularity, spatial integrals are carried out using two different methods, and according to the two approaches the results obtained are compared in homogeneous, and piecewise homogeneous media. Also in this chapter, flux kernels for the interior points are derived and related results are presented. It is believed that the results produced and kernels obtained in the current chapter are new. The approaches of the evaluation of improper integrals are also a novelty for dynamic problems.

Chapter 6 concentrates on three-dimensional elastic waves. The relevant direct BEM formulation is developed, and the time integration of the kernels is evaluated analytically. The improper integrals are treated in two different approaches, which are the subtriangle and analytical methods. The new BEM solutions are presented for the two cases of media of interest. The kernels derived and related results are also believed to be novel. Increasing complexity of the mathematics used in this case, increases the importance of the work carried out here.

Finally, Chapter 7 presents main conclusions from the present work. Also this chapter includes recommendations for further work based on that carried out here.

CHAPTER 2

BASIC EQUATIONS AND PROPERTIES OF WAVE PROPAGATION

2.1 Introduction

In this chapter, wave motion in elastic materials is analysed and the governing equations of transient elastodynamics and transient scalar wave propagation are studied. Analysis of stresses and strains on a body together with relevant differential equations, initial and boundary conditions, are also considered. Only the essential equations and ideas needed to obtain the boundary element solution of transient elastic and scalar wave propagation problems are studied.

2.2 Mathematical Preliminaries

Lightface letters will be used to denote scalar quantities, whilst vectors or second order tensors will be written in boldface. Here for example $\mathbf{u}(\mathbf{x},t)$, $\mathbf{u}\in\mathbb{R}^3$, denotes a displacement vector at time t as a function of the position vector $\mathbf{x}\in\mathbb{R}^3$ expressed in Cartesian co-ordinates. The Einstein summation convention will be used to express summations so that as usual,

$$\sigma_{ij}n_j \equiv \sum_{j=1}^{3}\sigma_{ij}n_j \tag{2.1}$$

In addition frequent use will be made of the Kronecker delta,

$$\delta_{ij} = \begin{cases} 1 & \text{if } i=j \\ 0 & \text{otherwise} \end{cases} \tag{2.2}$$

and the permutation symbol

$$e_{ijk} = \begin{cases} 0 & \text{if any two suffixes are equal} \\ -1 & \text{for anticyclic order of } i,j,k \\ 1 & \text{for cyclic order of } i,j,k \end{cases} \tag{2.3}$$

The first partial derivative of the vector component $u_i \equiv u_i(\mathbf{x},t)$ i=1,2,3 with respect to time t, in the direction x_j, j=1,2,3 is denoted respectively by

$$\dot{u}_i \equiv \frac{\partial u_i}{\partial t}, \qquad u_{i,j} \equiv \frac{\partial u_i}{\partial x_j} \tag{2.4}$$

and for second derivatives:

$$\ddot{u}_i \equiv \frac{\partial^2 u_i}{\partial t^2}, \qquad u_{i,jk} \equiv \frac{\partial^2 u_i}{\partial x_j \partial x_k} \tag{2.5}$$

The familiar notation $h * g$ will be used to denote the Reimannian convolution of two scalar continuous regular functions $h(\mathbf{x},t)$ and $g(\mathbf{x},t)$. Thus

$$h * g(\mathbf{x},t) \equiv \int_0^t h(\mathbf{x},t-\tau)g(\mathbf{x},\tau)d\tau \tag{2.6}$$

2.3 Basic Equations of Linear Elastodynamics

2.3.1 Stress

The stress tensor σ (or traction) is measured as force per unit area with dimension of the Pascal (Pa=N/m^2). The stress acting upon each of the six faces of an elementary box whose normal is parallel to the axis of the co-ordinate system is shown in Figure (2.1).

If one considers a normal to a given face of the box, then the components of the stress are reckoned positive if the force acts in directions of increasing x_i provided that the normal has the same sense as the positive direction of the axis to which the face is perpendicular. On the other hand, if the normal to a given face points in direction opposite to that of the positive axis, then the positive values of the stress components are associated with forces directed opposite to the positive directions of axes. The normal stresses are defined to be σ_{11}, σ_{22}, σ_{33} and the shear stresses are σ_{ij}, $i \neq j$; i,j=1,2,3, where the first subscript

indicates the face of the box and the second indicates stress direction. Since isotropic homogeneous materials are considered, the stress tensor is symmetrical, that is $\sigma_{ij} = \sigma_{ji}$.

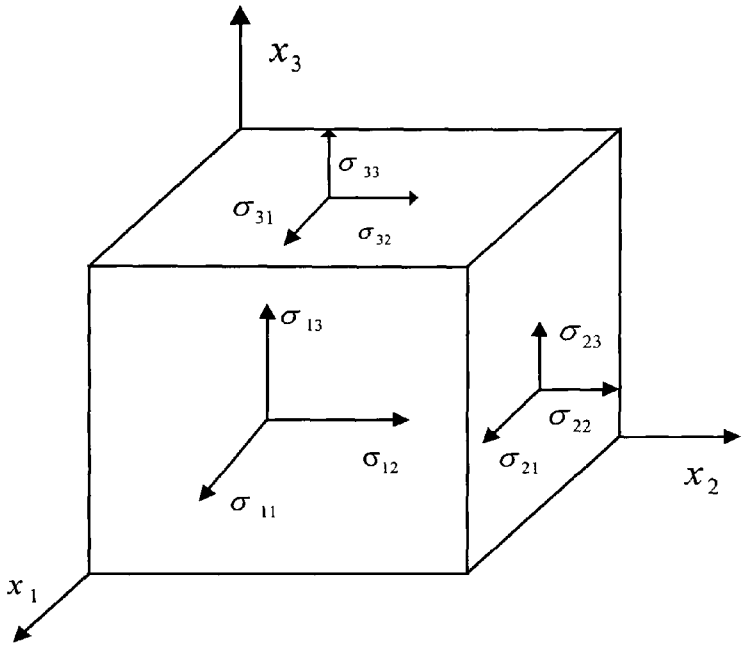

Figure 2.1 Components of the stress tensor

2.3.2 Strain

The strain components in an elastic body under the effect of forces which are distributed throughout the body varying with time and space are deformations, and can be represented by the strain tensor. The strain tensor $\varepsilon=\varepsilon(\mathbf{x},t)$ explicitly is:

$$\varepsilon = \begin{bmatrix} \varepsilon_{11} & \varepsilon_{12} & \varepsilon_{13} \\ \varepsilon_{21} & \varepsilon_{22} & \varepsilon_{23} \\ \varepsilon_{31} & \varepsilon_{32} & \varepsilon_{33} \end{bmatrix} \tag{2.7}$$

For small values of strain ε, the following kinematical relationship between strain and displacement $\mathbf{u}$ at a point $\mathbf{x}$ of a body at time t can be defined (Dominguez, 1993, Sokolnikoff, 1956) by:

$$\varepsilon_{ij} = \frac{1}{2}(u_{i,j} + u_{j,i}) \tag{2.8}$$

Thus, the diagonal and off-diagonal terms are, respectively:

$$\varepsilon_{11} = u_{1,1}, \quad \varepsilon_{22} = u_{2,2}, \quad \varepsilon_{33} = u_{3,3} \tag{2.9}$$

$$\begin{aligned} \varepsilon_{12} = \varepsilon_{21} &= \frac{1}{2}(u_{1,2} + u_{2,1}), \\ \varepsilon_{13} = \varepsilon_{31} &= \frac{1}{2}(u_{1,3} + u_{3,1}), \\ \varepsilon_{23} = \varepsilon_{32} &= \frac{1}{2}(u_{2,3} + u_{3,2}) \end{aligned} \tag{2.10}$$

The strain components can be uniquely found, when the displacement components are specified continuous functions of the co-ordinates x_i. On the other hand, when the strains ε_{ij} are specified functions of the co-ordinates, then it will not be possible to determine uniquely the displacement components. The reason is that the strain components include only pure deformation, while the displacements u_i also include rigid body displacement as well as the deformation.

2.3.3 Hooke's Law

One expression of the relationship between the stress and strain is known as Hooke's law (Sokolnikoff, 1956, Muskhelishvili, 1963, Bullen, 1976) which is valid for small strains. In this work, only isotropic and homogeneous (or piecewise homogeneous) media will be considered and so the linear relation between stresses and strains depends on just two elastic constants. Thus Hooke's law is:

$$\sigma_{ij} = \lambda\delta_{ij}\varepsilon_{kk} + 2\mu\varepsilon_{ij} \tag{2.11}$$

where λ and μ are known as the Lamé constants. These constants can be related (Brebbia et al., 1992) to more familiar elastic constants through the following relations,

$$\mu = \frac{E}{2(1+\upsilon)}, \quad \lambda = \upsilon \frac{E}{(1+\upsilon)(1-2\upsilon)}, \quad K = \lambda + \frac{2}{3}\mu \tag{2.12}$$

Here E is Young's modulus, which is the stress-strain ratio for tension or compression, and υ is Poisson's ratio which is the ratio of lateral contraction to the longitudinal extension, and K is the bulk modulus (or incompressibility) that shows the stress-strain ratio for simple hydrostatic pressure. Each of these elastic constants may be expressed as a function of two of the remaining constants. Thus, any two of the constants can be used to define the elastic properties of a homogeneous isotropic material.

2.3.4 Scalar Wave Equation

The scalar wave equation describes the motion of an elastic body under the influence of external forces, for example, pressure for the acoustic waves. To derive the scalar wave equation, a particular case of the Navier-Cauchy equations, only longitudinal normal stresses are considered.

Now, the longitudinal normal stress and the component of the body force in the x_3 direction only, will be a function of x_3 and t only. Thus the small strain in this direction in terms of displacement is:

$$\varepsilon_{33} = u_{3,3} \tag{2.13}$$

Also, the longitudinal normal stress forces in the x_3 direction on the top and bottom faces of the elemental cube as shown in Figure (2.2) are, respectively:

$$\begin{aligned} (\sigma_{33})_1 &= \sigma_{33}(x_3 - \frac{\Delta x_3}{2}, t) \\ (\sigma_{33})_2 &= \sigma_{33}(x_3 + \frac{\Delta x_3}{2}, t) \end{aligned} \tag{2.14}$$

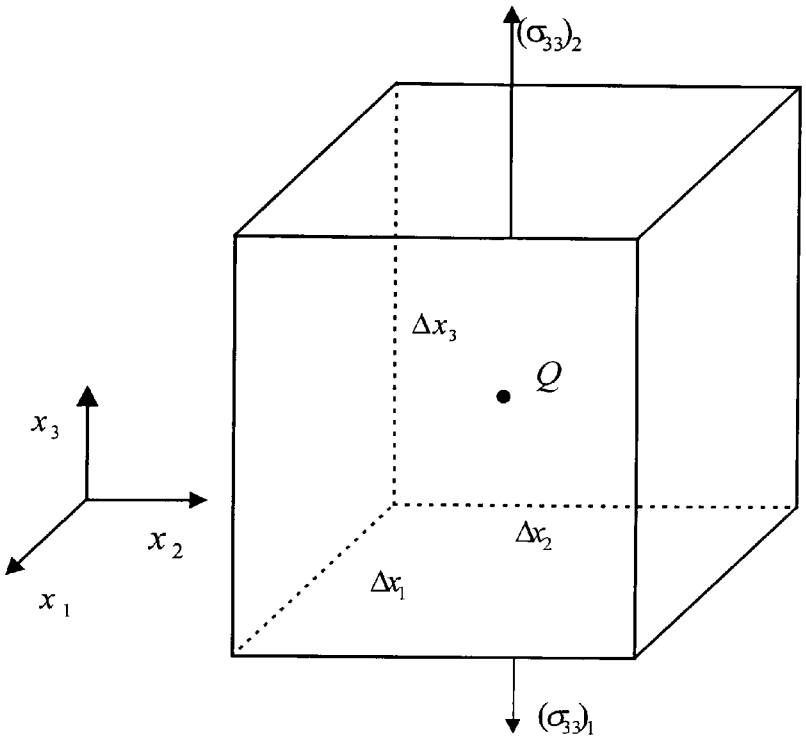

Figure 2.2 The longitudinal normal stress

Here the point Q is the box centre. Basically, this is a case of normal stress with zero shear contributions. Taking into account the above definitions and the net force in the x_3 direction, Newton's second law of motion may be expressed through

$$[(\sigma_{33})_2 - (\sigma_{33})_1]\Delta x_2 \Delta x_1 + \Delta m b_3 = \Delta m a_3 \tag{2.15}$$

where $\Delta m, b_3$ are the mass of the box, the body force (or gravitational force) in the x_3 direction respectively, and a_3 the acceleration in the x_3 direction. Dividing equation (2.15) by $\Delta x_1 \Delta x_2 \Delta x_3$ and taking the limit with $\Delta x_3 \to 0$, the stress equation of motion is formed to be:

$$\sigma_{33,3} + \rho b_3 = \rho a_3 \tag{2.16}$$

In the above, ρ is the mass density and $\Delta m = \rho \Delta x_1 \Delta x_2 \Delta x_3$. Through Hooke's law (Achenbach, 1975) for this special case, the normal components of the stress tensor are:

$$\sigma_{11} = 0 \Rightarrow \lambda(\varepsilon_{11} + \varepsilon_{22} + \varepsilon_{33}) + 2\mu\varepsilon_{11} = 0 \tag{2.17a}$$

$$\sigma_{22} = 0 \Rightarrow \lambda(\varepsilon_{11} + \varepsilon_{22} + \varepsilon_{33}) + 2\mu\varepsilon_{22} = 0 \tag{2.17b}$$

$$\sigma_{33} = (\lambda + 2\mu)\varepsilon_{33} + \lambda(\varepsilon_{11} + \varepsilon_{22}) \tag{2.17c}$$

It follows from equations (2.17a) and (2.17b) that

$$\varepsilon_{11} = \varepsilon_{22} = -\frac{\lambda}{2(\lambda + \mu)}\varepsilon_{33} \tag{2.18}$$

Employing equations (2.13), (2.17c) and (2.18) the following equation is obtained:

$$\sigma_{33} = E u_{3,3} \tag{2.19}$$

Substituting equation (2.19), into (2.16) and with small values of acceleration where $a_3 = \ddot{u}_3$, it is easy to obtain the equation,

$$c^2 u_{3,33} + b_3 = \ddot{u}_3 \tag{2.20}$$

where $c^2 = \frac{E}{\rho}$.

The same argument can be given for the x_1 and x_2 directions. Thus in the direction of x_2:

$$\sigma_{11} = 0 \Rightarrow \lambda(\varepsilon_{11} + \varepsilon_{22} + \varepsilon_{33}) + 2\mu\varepsilon_{11} = 0 \tag{2.21a}$$

$$\sigma_{22} = (\lambda + 2\mu)\varepsilon_{22} + \lambda(\varepsilon_{11} + \varepsilon_{33}) \tag{2.21b}$$

$$\sigma_{33} = 0 \Rightarrow \lambda(\varepsilon_{11} + \varepsilon_{22} + \varepsilon_{33}) + 2\mu\varepsilon_{33} = 0 \tag{2.21c}$$

For in the direction x_1:

$$\sigma_{11} = (\lambda + 2\mu)\varepsilon_{11} + \lambda(\varepsilon_{22} + \varepsilon_{33}) \tag{2.22a}$$

$$\sigma_{22} = 0 \Rightarrow \lambda(\varepsilon_{11} + \varepsilon_{22} + \varepsilon_{33}) + 2\mu\varepsilon_{22} = 0 \tag{2.22b}$$

$$\sigma_{33} = 0 \Rightarrow \lambda(\varepsilon_{11} + \varepsilon_{22} + \varepsilon_{33}) + 2\mu\varepsilon_{33} = 0 \tag{2.22c}$$

Since only normal stresses are considered, see Figure (2.2), the final equation of motion is:

$$c^2 u_{i,ii} + b_i = \ddot{u}_i \tag{2.23}$$

where c is the speed of the wave propagation with units of m/s.

This equation may be expressed in an alternative more compact form using Helmholtz decomposition (Eringen et al., 1975, Bedford et. al., 1994, Banerjee, 1994), in which the displacement **u** of a medium may be presented as the sum of gradient of a scalar potential $\phi(\mathbf{x},t)$ and the curl of a vector potential $\mathbf{\Psi}(\mathbf{x}, t)$, which are known (Eringen et al., 1975, Achenbach, 1975) as Lamé potentials,

$$u_i = \phi_{,i} + e_{ijk}\Psi_{\mathrm{k,j}} \tag{2.24}$$

Following the same line of thought, the body force vector **b** may be written (Eringen et al., 1975), for a scalar- and a vector-valued functions f and **F** in the similar way as:

$$b_i = f_{,i} + e_{ijk}F_{\mathrm{k,j}} \tag{2.25}$$

The divergence of equations (2.24) and (2.25) results in

$$\nabla.\mathbf{u} = u_{i,i} = \phi_{,ii}, \qquad \nabla.\mathbf{b} = b_{i,i} = f_{,ii} \tag{2.26}$$

It may be seen that in the second parts of the equations (2.24) and (2.25) are divergence free.

Thus, using the divergence of equation (2.23), it can be shown that

$$c^2\phi_{,ii} + f = \ddot{\phi} + g \tag{2.27}$$

where g is a harmonic function and is usual to take $g = 0$. Here ϕ, $\mathbf{x}$, t and f are the potential, position vector, time and body source, respectively. The normal derivative of the potential is given by:

$$q(\mathbf{x},t) = \frac{\partial \phi(\mathbf{x},t)}{\partial n} \tag{2.28}$$

2.3.4.1 Boundary and Initial Conditions

For a well-posed boundary problem, it is necessary to specify the initial and boundary conditions. In such a problem, there will be some points on the boundary B of the body Ω where the potential ϕ is prescribed and others where the normal derivative of the potential q is prescribed.

For all points $\mathbf{x}$ of the boundary B with time $t \in \mathbb{R}$, the boundary conditions may be specified conveniently using the two known functions $\bar{\phi}(\mathbf{x},t)$, $\bar{q}(\mathbf{x},t)$ defined by:

$$\phi(\mathbf{x},t) = \begin{cases} \bar{\phi}(\mathbf{x},t) & \text{if } t > 0 \\ 0 & \text{if } t < 0 \end{cases} \tag{2.29}$$

where $\mathbf{x} \in B_2 \subseteq B$, and:

$$q(\mathbf{x},t) = \frac{\partial \phi(\mathbf{x},t)}{\partial n} = \begin{cases} \bar{q}(\mathbf{x},t) & \text{if } t > 0 \\ 0 & \text{if } t < 0 \end{cases} \tag{2.30}$$

with $\mathbf{x} \in B_1 \subseteq B$. Here, $\mathbf{n}$ is the outward unit normal vector at the position vector $\mathbf{x}$, B_1 and B_2 are parts of boundary $B = B_1 + B_2$ and where $B_1 \cap B_2 = \varnothing$. For a boundary value problem q is unknown on B_2 and ϕ is unknown on B_1 as displayed for a two-dimensional case in Figure (2.3).

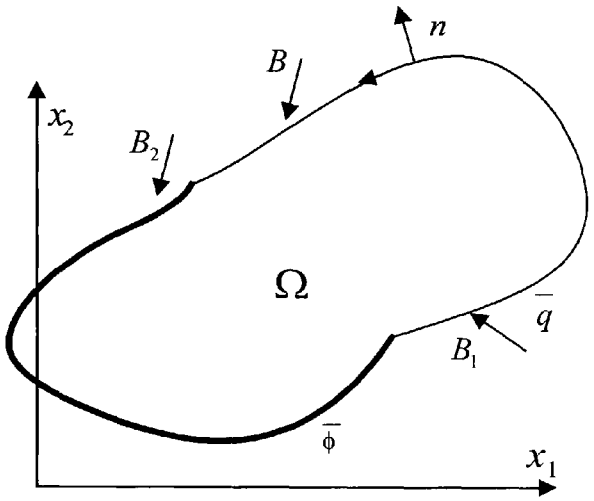

Figure 2.3 Geometric definition of the boundary conditions

The equations (2.29) and (2.30) are known respectively as essential (or Dirichlet) and natural (or Neumann) boundary conditions. If the prescribed value is a relationship between the potential and flux, then the boundary condition is known as a mixed boundary condition.

Finally the initial conditions in the body Ω at time t=0 are:

$$\phi(\mathbf{x},0) = \phi_0(\mathbf{x})$$

$$\dot{\phi}(\mathbf{x},0) = v_0(\mathbf{x}). \tag{2.31}$$

It should be noted that the conditions given for two-dimensional geometries can also be generalised to three-dimensions.

2.3.4.2 Reciprocal Relation for the Scalar Case

The dynamic reciprocal relation is needed for the scalar BEM formulation in Chapters 3 and 5. Therefore, in this section, the dynamic reciprocal theorem (Eringen et al., 1975,

Dominguez, 1993, Achenbach, 1975) will be discussed. It is an extension of Betti's classical reciprocal theorem (Eringen et al., 1975) in elastostatics, and was for the first time stated by Graffi in 1946 (Achenbach, 1975). Later, it was generalised to include unbounded regions by Wheeler et al. (1968). The divergence theorem is used to derive this theorem (Sokolnikoff, 1956).

Let (f^s, q^s, ϕ^s) be another state for the scalar wave equation on the same domain Ω with the boundary B. Then from equation (2.27)

$$c^2 \phi^s_{,ii} + f^s = \ddot{\phi}^s \tag{2.32}$$

Taking the second scalar field ϕ^s, for the domain Ω, the following weighted residual may be written (Dominguez, 1993, Eringen et al., 1975)

$$\int_\Omega c^2 (\phi_{,ii} * \phi^s)(\mathbf{x},t) d\Omega + \int_\Omega (f * \phi^s)(\mathbf{x},t) d\Omega = \int_\Omega (\ddot{\phi} * \phi^s)(\mathbf{x},t) d\Omega \tag{2.33}$$

Integrating by parts gives rise to:

$$\begin{aligned} \int_\Omega c^2 (\phi_{,ii} * \phi^s)(\mathbf{x},t) d\Omega = \int_\Omega c^2 (\phi * \phi^s_{,ii})(\mathbf{x},t) d\Omega + \int_B c^2 (q * \phi^s)(\mathbf{x},t) dB \\ - \int_B c^2 (\phi * q^s)(\mathbf{x},t) dB \end{aligned} \tag{2.34}$$

In equation (2.33), the right-hand side may also be written (Eringen et al., 1975) as:

$$\begin{aligned} \int_\Omega (\ddot{\phi} * \phi^s)(\mathbf{x},t) d\Omega = \int_\Omega (\phi * \ddot{\phi}^s)(\mathbf{x},t) d\Omega + \int_\Omega [v_0^s(\mathbf{x})\phi(\mathbf{x},t) + \phi_0^s(\mathbf{x})\dot{\phi}(\mathbf{x},t)] d\Omega \\ - \int_\Omega [v_0(\mathbf{x})\phi^s(\mathbf{x},t) + \phi_0(\mathbf{x})\dot{\phi}^s(\mathbf{x},t)] d\Omega \end{aligned} \tag{2.35}$$

Arranging equations (2.32), (2.33), (2.34) and (2.35), for two distinct states (Wheeler et al., 1968, Eringen et al., 1975) of body sources, fluxes, potentials (f, q, ϕ) and

(f^s, q^s, ϕ^s) defined on the same domain Ω bounded by a boundary B with initial conditions, while $t \geq 0$, the dynamic reciprocal relation may be expressed through

$$\int_B c^2 (q * \phi^s)(\mathbf{x},t)dB - \int_B c^2 (q^s * \phi)(\mathbf{x},t)dB = \int_\Omega [(f^s * \phi)(\mathbf{x},t) + \phi_0^s(\mathbf{x})\dot{\phi}(\mathbf{x},t) + v_0^s(\mathbf{x})\phi(\mathbf{x},t)]d\Omega$$

$$- \int_\Omega [(f * \phi^s)(\mathbf{x},t) + \phi_0(\mathbf{x})\dot{\phi}^s(\mathbf{x},t) + v_0(\mathbf{x})\phi^s(\mathbf{x},t)]d\Omega \tag{2.36}$$

where

$$q^s = \frac{\partial \phi^s}{\partial n}. \tag{2.37}$$

As a result of this theorem, it may be concluded that in a well-posed boundary problem the unknown boundary potentials and fluxes can be computed from the specified potentials and fluxes on the boundary. This will be used to establish the BEM for the scalar wave equations. More details on the reciprocal relation of two states can be found for instance in references (Dominguez, 1993, Eringen et al., 1975, Achenbach, 1975, Sokolnikoff, 1956, Becker, 1992).

2.3.5 Cauchy Equations

Cauchy's equation describes the motion of an elastic body under stress. To derive the Cauchy's equations of motion for any continuum, consider an elementary box of elastic material under stress at time t and determine how the stresses vary from one point to another within the material. For the points of the box, Cauchy's equations of motion can be derived from the application of Newton's second law of motion.

Consider an elementary box of elastic material of sides $\Delta x_1, \Delta x_2, \Delta x_3$ with centre $Q(x_1, x_2, x_3)$. It may be seen that the stresses of the elastic material in the x_3 axis (see Figure 2.4) are:

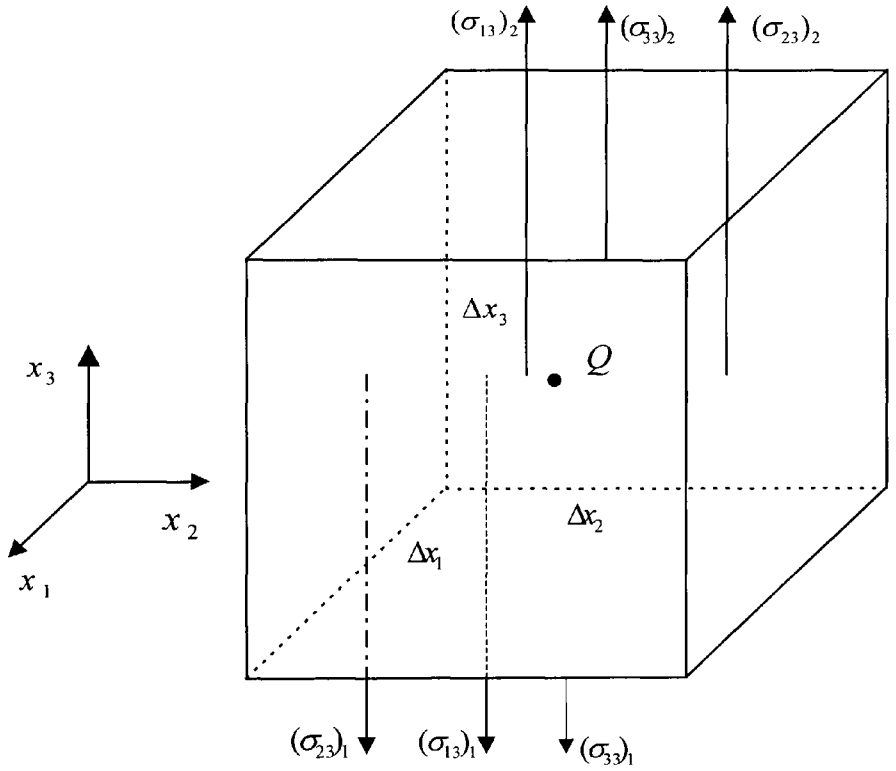

Figure 2.4 Stress components in one direction

$$(\sigma_{13})_1 = \sigma_{13}(x_1 - \frac{\Delta x_1}{2}, x_2, x_3, t)$$

$$(\sigma_{13})_2 = \sigma_{13}(x_1 + \frac{\Delta x_1}{2}, x_2, x_3, t)$$

$$(\sigma_{23})_1 = \sigma_{23}(x_1, x_2 - \frac{\Delta x_2}{2}, x_3, t)$$

$$(\sigma_{23})_2 = \sigma_{23}(x_1, x_2 + \frac{\Delta x_2}{2}, x_3, t)$$

$$(\sigma_{33})_1 = \sigma_{33}(x_1, x_2, x_3 - \frac{\Delta x_3}{2}, t) \tag{2.38}$$

$$(\sigma_{33})_2 = \sigma_{33}(x_1, x_2, x_3 + \frac{\Delta x_3}{2}, t)$$

Using these definitions and by considering the net force in the x_3 direction Newton's second law of motion takes the form

$$[(\sigma_{33})_2 - (\sigma_{33})_1]\Delta x_2 \Delta x_1 + [(\sigma_{23})_2 - (\sigma_{23})_1]\Delta x_1 \Delta x_3 + [(\sigma_{13})_2 - (\sigma_{13})_1]\Delta x_2 \Delta x_3 + \Delta m b_3 = \Delta m a_3 \tag{2.39}$$

where Δm, b_3, a_3 are the mass of the box, the third component of the body force (or gravitational force) vector **b**, and the third component of the acceleration vector **a** respectively. Dividing equation (2.39) by $\Delta x_1 \Delta x_2 \Delta x_3$ and with $\Delta x_i \to 0$, it may be seen that

$$\sigma_{33,3} + \sigma_{23,2} + \sigma_{13,1} + \rho b_3 = \rho a_3 \equiv \sigma_{i3,i} + \rho b_3 \tag{2.40}$$

In the above, ρ is the mass density and $\Delta m = \rho \Delta x_1 \Delta x_2 \Delta x_3$. The above argument may be repeated for directions x_1 and x_2 so that the Cauchy's equations of motion can be written as:

$$\sigma_{ij,j} + \rho b_i = \rho \ddot{u}_i, \quad i,j=1,2,3 \tag{2.41}$$

with small values of acceleration $a_i = \ddot{u}_i$, where σ is the stress tensor, **b** is the body force per unit mass.

2.3.5.1 Navier-Cauchy Equations

By eliminating σ_{ij}, ε_{ij} using the equations (2.8), (2.11) and (2.41), one can obtain the displacement equations of motion,

$$\mu u_{i,jj} + (\lambda + \mu) u_{j,ji} + \rho b_i = \rho \ddot{u}_i \tag{2.42}$$

They are known as the Navier-Cauchy equations. In terms of P-wave (compressional wave) and S-wave (shear wave) velocities, c_1 and c_2 respectively, the above equation can be rewritten as follows (Dominguez, 1993, Banerjee, 1994),

$$c_2^{\,2} u_{i,jj} + (c_1^{\,2} - c_2^{\,2}) u_{j,ji} + b_i = \ddot{u}_i \tag{2.43}$$

where $c_1 = \left(\dfrac{\lambda + 2\mu}{\rho} \right)^{\frac{1}{2}}$ and $c_2 = \left(\dfrac{\mu}{\rho} \right)^{\frac{1}{2}}$. The two values, c_1 and c_2, have the dimensions of velocity (m / s).

The dynamic equilibrium equations, Hooke's law and the equations of motion are to be satisfied at every internal point of the medium of interest.

2.3.5.2 Boundary and Initial Conditions

These are defined in a similar way to that already presented in section (2.3.4.1). For all the points **x** on the boundary B for the body Ω with time $t \in \mathbb{R}$, the boundary conditions may be specified conveniently using the two known functions $\overline{p}_i(\mathbf{x},t)$, $\overline{u}_i(\mathbf{x},t)$ defined by:

$$p_i(\mathbf{x},t) = \sigma_{ij} n_j = \begin{cases} \overline{p}_i(\mathbf{x},t) & \text{if } t > 0 \\ 0 & \text{if } t < 0 \end{cases} \tag{2.44}$$

where $\mathbf{x} \in B_1 \subseteq B$ and

$$u_i(\mathbf{x},t) = \begin{cases} \bar{u}_i(\mathbf{x},t) & \text{if } t > 0 \\ 0 & \text{if } t < 0 \end{cases} \tag{2.45}$$

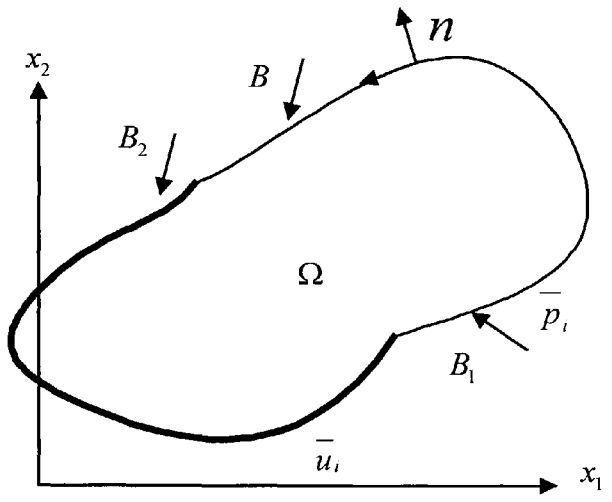

Figure 2.5 Geometric definition of the boundary conditions

where $\mathbf{x} \in B_2 \subseteq B$. Here $\mathbf{n}$ is the outward unit normal vector of the boundary B. The functions p_i and u_i show the traction and displacement in the i-direction on the boundary B. As can be seen from Figure (2.5), B_1 and B_2 are the parts of boundary $B = B_1 + B_2$ and where $B_1 \cap B_2 = \varnothing$. Either of B_1 or B_2 may be taken to represent the whole of boundary B. For a boundary value problem, p_i is unknown on B_2 and u_i is unknown on B_1. It can be seen that p_i is acting on the boundary in positive $\mathbf{n}$ direction (away from the boundary). The equations (2.44) and (2.45) are known respectively, as natural (or Neuman) and essential (or Dirichlet) boundary conditions (see Figure 2.5). If the prescribed value is a combination of the traction and the displacement, then the boundary condition is known as a mixed boundary condition.

To complete the specification of the problem, the initial conditions in the body Ω, at time t=0, are prescribed by:

$$u_i(\mathbf{x},0) = u_{0i}(\mathbf{x})$$
$$\dot{u}_i(\mathbf{x},0) = v_{0i}(\mathbf{x}) \tag{2.46}$$

It should be noted that the conditions given for two-dimensional geometries can be generalised to three-dimensions.

2.3.5.3 Reciprocal Relation in Elastodynamics

The elastodynamic reciprocal relation is needed for the elastodynamic BEM formulation in Chapters 4 and 6. The proof of the theorem can be found for this case in Eringen et al. (1975) and Dominguez (1993).

When there exist two distinct elastodynamic states (Wheeler et al., 1968) of body forces, tractions, displacements such as (b_k, p_k, u_k) and (b_k^s, p_k^s, u_k^s) defined over the same domain Ω under equilibrium with its boundary B by taking the initial conditions, then, for $t \geq 0$,

$$\int_B (p_k * u_k^s)(\mathbf{x},t)dB - \int_B (p_k^s * u_k)(\mathbf{x},t)dB =$$
$$\int_\Omega \rho[(b_k^s * u_k)(\mathbf{x},t) + u_{0k}^s(\mathbf{x})\dot{u}_k(\mathbf{x},t) + v_{0k}^s(\mathbf{x})u_k(\mathbf{x},t)]d\Omega - \tag{2.47}$$
$$\int_\Omega \rho[(b_k * u_k^s)(\mathbf{x},t) + u_{0k}(\mathbf{x})\dot{u}_k^s(\mathbf{x},t) + v_{0k}(\mathbf{x})u_k^s(\mathbf{x},t)]d\Omega$$

This theorem now specifies a relationship between two distinct states of body forces, tractions, displacements where they satisfy the Cauchy's equations (2.42) on the domain under consideration. This relation states essentially that the work done by the stress

forces of the first state on the displacements of the second state is equal to the work done by the stress forces of the second state on the displacements of the first state. In other words, the displacement wave travelled of the second state (u_k^s) because of the first state tractions (p_k) is equal to the displacement wave travelled of the first state (u_k) because of the second state tractions (p_k^s). Here (b_k, p_k, u_k) is the first state in which the boundary displacements and tractions are unknown whilst (b_k^s, p_k^s, u_k^s) is the second state in which the boundary displacements and tractions are specified. This will be used to design a linear algebraic BEM equation system for obtaining a unique (Achenbach, 1975, Eringen et al., 1975) solution.

Similar to the scalar case, it may be said that in a well-posed boundary problem the unknown boundary displacements and tractions can be computed from the specified displacements and tractions on the boundary.

2.4 Reflection and Refraction

As has already been mentioned there are two types of body waves in seismology, firstly longitudinal, push, or compressional, or the primary, P, waves and secondly, transverse, shake, or shear, or the secondary, S, waves. Both types of waves can travel through a solid, isotropic, homogeneous medium of infinite extent. A wave with infinite energy will be required to reach infinity. P-waves propagate through the medium when the particle velocity is parallel to the propagation direction, whilst S-waves travel through the medium when the particle velocity is perpendicular to the propagation direction as shown in Figure (2.6). In general, waves which encounter the interface between two media, may be reflected or refracted. Those entering the discontinuity are called incident refracted waves; if the waves come back from the interface then they are called reflected waves.

Those that pass through are refracted or transmitted waves. The change in direction of the raypath when it crosses a boundary is expressed by Snell's law (see Figure 2.6) which can be stated, in terms of angles and wave velocities, as follows,

$$\frac{\sin\theta_1}{c_{11}} = \frac{\sin\theta_4}{c_{21}} = \frac{\sin\theta_2}{c_{12}} = \frac{\sin\theta_3}{c_{22}} \tag{2.48}$$

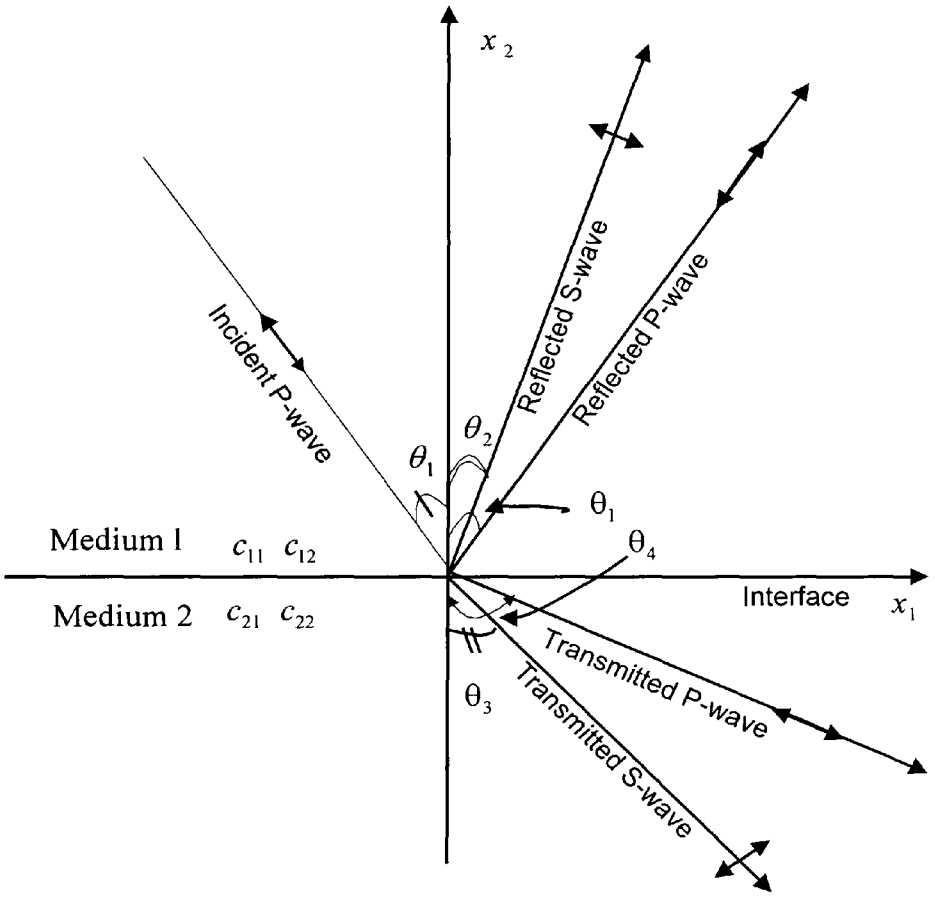

Figure 2.6 Waves generated at the interface by an incident P-wave

where $c_{11}, c_{12}; c_{21}, c_{22}$ are P-wave and S-wave velocities for the first medium and the second medium, respectively. As can be seen from Figure (2.6), the angles θ_1, θ_4 are the

angles of the reflected and transmitted P-waves, and the angles θ_2, θ_3 are the angles of reflected and transmitted S-waves, respectively.

In general, when a P-wave interacts with a boundary, it produces not only a reflected and a refracted P-wave but it can also produce a reflected and a refracted S-wave. Conversely, an S-wave that interacts with boundaries can produce reflected and refracted P-waves. These 'changes' from P to S and S to P-waves are called mode conversions. When an incident (P or S) wave is normal to interface only a single type of (P or S) wave is produced (Achenbach, 1975). Scalar waves (acoustic waves, electromagnetic waves, water waves etc.) only generate waves of their own type (Graff, 1975).

2.5 Summary

In this Chapter, the fundamentals of linear elastodynamics have been taken into consideration. To properly define the problem to be solved, appropriate initial and boundary conditions have been treated as well as the dynamic reciprocal relations which will be used in later chapters.

CHAPTER 3

TWO DIMENSIONAL TIME DOMAIN BEM FOR SCALAR WAVE PROPAGATION

3.1 Introduction

The scalar waves are considered in this chapter as they are easier than fully developed elastic waves and yet their concepts are similar. The two-dimensional time domain direct boundary element formulation for the scalar waves is established by means of the dynamic reciprocal relation applied to the fundamental solution state and the actual state. Also, the BEM solutions are obtained for homogeneous and inhomogeneous media. At the same time, the internal flux kernels are derived and comparative results related to these kernels are presented.

3.2 Integral Equation Formulation for Two Dimensional Scalar Wave

In Chapter 2, it was shown that the governing equation for the two-dimensional scalar wave equation corresponding to a homogeneous isotropic elastic body Ω enclosed by the boundary B is given by:

$$c^2\phi_{,ii} + f = \ddot{\phi} \tag{3.1}$$

In this equation ϕ, f and $\ddot{\phi}$ are functions of position and time, and represent potential, body source and acceleration respectively, whilst c is the speed of wave propagation. When the dynamic reciprocity is applied, the scalar field of the actual problem will be defined by ϕ, and the fundamental solution of the field by ϕ^s. Clearly ϕ^s satisfies equation (3.1) namely

$$c^2\phi^s_{,ii} + f^s = \ddot{\phi}^s \tag{3.2}$$

3.2.1 Fundamental Solutions

As long as a fundamental solution of the governing partial differential equation is given, then the BEM can be applied. For the corresponding domain and its boundary, the fundamental solution is a solution that satisfies the equation (3.2) for an unbounded region subject to a unit impulse body source f^s. The source selected is of the type (Eringen et al., 1975, Achenbach, 1975)

$$\frac{1}{c^2} f^s(\mathbf{x},t) = \delta(t)\delta(\mathbf{x}-\mathbf{y}^i) \tag{3.3}$$

acting at a point $\mathbf{y}^i$ for t=0 and propagating to infinity. Here $\delta(\mathbf{x})$ is the Dirac delta function. It follows that equation (3.2) becomes

$$\phi^s_{,ii} + \delta(t)\delta(\mathbf{x}-\mathbf{y}^i) = \frac{1}{c^2}\ddot{\phi}^s \tag{3.4}$$

The two-dimensional fundamental solution is obtained (Greenberg, 1971, Achenbach, 1975, Eringen et al., 1975) from its three-dimensional counterpart by integrating along the third spatial direction. As can be seen from Figure (3.1), the fundamental solution corresponds to an infinite line of sources along the x_3 direction perpendicular to the $x_1 - x_2$ plane.

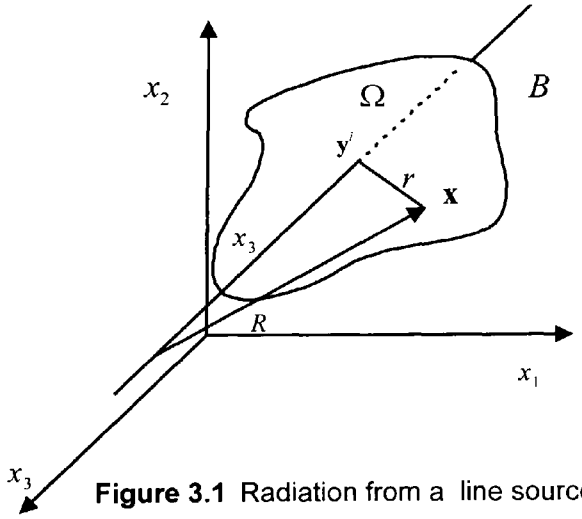

Figure 3.1 Radiation from a line source

It follows that

$$\phi^s_{2D} = \int_{-\infty}^{\infty} \phi^s_{3D} dx_3 \tag{3.5}$$

where ϕ^s_{3D} is the three-dimensional fundamental solution, which will be derived later in Chapter 5, is given (e.g. Greenberg, 1971) by:

$$\phi^s_{3D} = \frac{c}{4\pi R}\delta(ct - R) \tag{3.6}$$

where R is the distance between the field and load points in the three-dimensional fundamental solution. Using equation (3.6) and the geometric definitions from Figure (3.1), equation (3.5) can be rewritten as:

$$\phi^s_{2D} = \frac{c}{4\pi}\int_{-\infty}^{\infty} \frac{\delta[ct - (r^2 + x_3^2)^{1/2}]}{(r^2 + x_3^2)^{1/2}} dx_3 \tag{3.7}$$

where r is the distance between the field $\mathbf{x}$ and load point $\mathbf{y}^i$ in the two-dimensional fundamental solution, because the field and load points are in the $x_1 - x_2$ plane, namely $r^2 = (x_j - y^i_j)(x_j - y^i_j)$.

To simplify equation (3.7), consider the property of the delta function (Eringen and Suhubi, 1975) given by:

$$\delta[g(x)] = \sum_{k=1}^{n} \frac{\delta(x - x_k)}{|g'(x_k)|} \tag{3.8}$$

where x_k are the roots of function $g(x)$ with $g'(x_k) \neq 0$. In the case of (3.7)

$$g(x_3) = ct - (r^2 + x_3^2)^{1/2} \tag{3.9}$$

with roots

$$x_3 = \pm(c^2t^2 - r^2)^{1/2} \tag{3.10}$$

It follows that

$$|g'(x_3)| = \frac{(c^2t^2 - r^2)^{1/2}}{ct} \tag{3.11}$$

Using equation (3.9) it may be seen that

$$\delta[ct - (r^2 + x_3^2)^{1/2}] = \frac{ct}{(c^2t^2 - r^2)^{1/2}}\{\delta[x_3 - (c^2t^2 - r^2)^{1/2}] + \delta[x_3 + (c^2t^2 - r^2)^{1/2}]\} \tag{3.12}$$

From (3.12), (3.8) substituted into (3.7) and omitting the subscript "2D", it follows that (Morse et al., 1953, Eringen et al., 1975)

$$\phi^s(\mathbf{x}, t; \mathbf{y}^i) = \frac{c}{2\pi}\frac{1}{\left(c^2t^2 - r^2\right)^{1/2}}H(ct - r) \tag{3.13}$$

where r is the distance from the load point $\mathbf{y}^i$ to any point under consideration in the $x_1 - x_2$ plane. As previously stated, R shows the distance between the field and load points in three-dimensional space. Here, H is the Heaviside function, which is used because the arguments of the Dirac delta function have no zero on the x_3-axis if $ct < r$, in which case $\phi^s = 0$. For time $t = 0$, the fundamental solution is zero. It may be noted that ϕ^s represents the field at time t and position $\mathbf{x} = (x_1, x_2)$ due to a line source.

Similar derivations of the two-dimensional fundamental solution may also be found in Achenbach (1975). To evaluate the two-dimensional fundamental solution from the three-dimensional fundamental solution, the Hadamard's method of descent is used.

As can be seen from the fundamental solution (3.13), the disturbance sent initially from the load point $\mathbf{y}^i$ is received at field point $\mathbf{x}$ at time $\frac{r}{c} < t$, and decays as t increases.

When the load is applied at time τ, the variable t in the fundamental solution is replaced by $t - \tau$ during the Riemann convolution. Thus, equation (3.13) can be written as:

$$\phi^s(\mathbf{x},t;\mathbf{y}^i,\tau)=\frac{c}{2\pi}\frac{1}{[c^2(t-\tau)^2-r^2]^{1/2}}H[c(t-\tau)-r] \tag{3.14}$$

The normal derivative of the fundamental solution may be found to be:

$$\begin{aligned} q^s(\mathbf{x},t;\mathbf{y}^i,\tau)&=\frac{\partial\phi^s(\mathbf{x},t;\mathbf{y}^i,\tau)}{\partial n}=\frac{\partial r}{\partial n}\frac{\partial\phi^s}{\partial r} \\ &=\frac{c}{2\pi}\frac{\partial r}{\partial n}\{-\frac{\delta[c(t-\tau)-r]}{[c^2(t-\tau)^2-r^2]^{1/2}}+\frac{rH[c(t-\tau)-r]}{[c^2(t-\tau)^2-r^2]^{3/2}}\} \end{aligned} \tag{3.15}$$

The two-dimensional fundamental solution has the following properties (Eringen and Suhubi, 1975):

i) Causality:

$$\phi^s(\mathbf{x},t;\mathbf{y}^i,\tau)=0 \quad \text{if} \quad c(t-\tau)<r$$

which means that the field point does not experience any disturbance if the wave has not reached the field point **x**.

ii) Reciprocity:

$$\phi^s(\mathbf{x},t;\mathbf{y}^i,\tau)=\phi^s(\mathbf{x},t-\tau;\mathbf{y}^i,0)=\phi^s(\mathbf{y}^i,-\tau;\mathbf{x},-t)$$

iii) Time translation:

$$\phi^s(\mathbf{x},t+t_1;\mathbf{y}^i,\tau+t_1)=\phi^s(\mathbf{x},t;\mathbf{y}^i,\tau)$$

3.2.2 Integral Representation

The integral representation of the two-dimensional scalar wave equation was first presented by Volterra in 1894 (Mansur, 1983).

When the unit impulse body source (3.3) is applied at an interior point $\mathbf{y}^i$, with the help of the sifting property of the Dirac delta function, the scalar reciprocal equation (2.36) may be transformed into

$$\phi(\mathbf{y}^i,t) = \int_B (\phi^s * q)(\mathbf{x},t)dB - \int_B (q^s * \phi)(\mathbf{x},t)dB$$
$$+ \int_\Omega \frac{1}{c^2}[(f * \phi^s)(\mathbf{x},t) + \phi_0(\mathbf{x})\dot{\phi}^s(\mathbf{x},t) + v_0(\mathbf{x})\phi^s(\mathbf{x},t)]d\Omega \tag{3.16}$$

In the absence of the body source, and when the initial conditions of the body are zero, namely, $f \equiv 0$, $\phi_0 \equiv 0$, $v_0 \equiv 0$, equation (3.16) reduces to

$$\phi(\mathbf{y}^i,t) = \int_B (\phi^s * q)(\mathbf{x},t)dB - \int_B (q^s * \phi)(\mathbf{x},t)dB \tag{3.17}$$

3.2.3 Boundary Integral Equation

Consider equation (3.17) for the case of the body source on the smooth boundary. Here special care must be taken to remove singularities which occur when the points $\mathbf{x}$ and $\mathbf{y}^i$ coincide. The Cauchy principal method will be used to remove this singularity. Hence, assuming that the boundary is smooth at point $\mathbf{y}^i$, the domain Ω can be augmented (Mansur et al., 1985, Brebbia et al. 1992, Dominguez, 1993) by a small external semi-circle of radius ε, as shown in Figure (3.2). The point $\mathbf{y}^i$ can then be considered at the centre of the small circle of infinitesimally small radius ε, with $\varepsilon \to 0$. Hence, the point $\mathbf{y}^i$ will become a point on the boundary of the domain under study.

In equation (3.17), the integrals can be evaluated when $\mathbf{y}^i = \mathbf{x}$ by consideration of Figure (3.2). Clearly the integrals in equation (3.17) can be written as the limiting process when $\varepsilon \to 0$ for boundaries B_ε and B. Thus,

$$I_1 = \int_B (\phi^s * q)(\mathbf{x},t)dB = \lim_{\varepsilon\to 0} \int_{B-B_\varepsilon} (\phi^s * q)(\mathbf{x},t)dB + \lim_{\varepsilon\to 0} \int_{B_\varepsilon} (\phi^s * q)(\mathbf{x},t)dB \tag{3.18}$$

and similarly for the second integral

$$I_2 = \int_B (q^s * \phi)(\mathbf{x},t)dB = \lim_{\varepsilon \to 0} \int_{B-B_\varepsilon} (q^s * \phi)(\mathbf{x},t)dB + \lim_{\varepsilon \to 0} \int_{B_\varepsilon} (q^s * \phi)(\mathbf{x},t)dB \qquad (3.19)$$

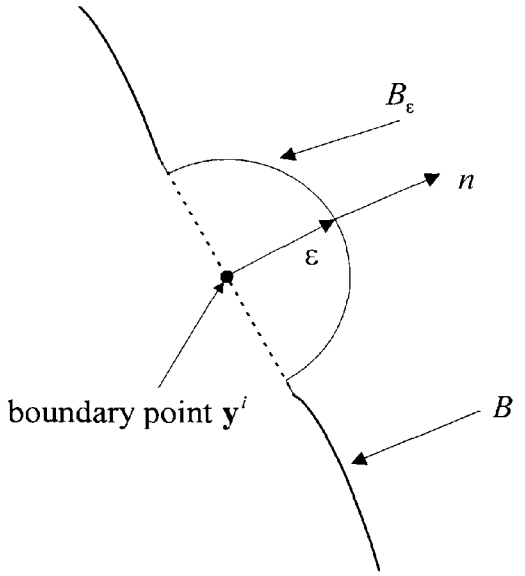

Figure 3.2 Illustration of the Cauchy principal integral

To simplify the second integral on the right hand side of equations (3.18) and (3.19), it is helpful to note the fundamental solutions of Laplace equation. The resulting solutions of Laplace equation which are given in Bonnet, (1998) and Brebbia et al. (1992) are:

$$\phi^{s1} = -\frac{1}{2\pi} \ln r, \qquad q^{s1} = -\frac{\partial r}{\partial n} \frac{1}{2\pi r} \qquad (3.20)$$

where ϕ^{s1} and q^{s1} are the potential and flux fundamental solutions, for the static case. The last integral on the right hand side of equations (3.18) and (3.19) are of the same type as in the static case, and therefore, to evaluate these integrals ϕ^s and q^s are replaced by ϕ^{s1} and q^{s1} respectively.

It is not difficult to derive solutions (3.20) and they can be found, for instance, in El-Zafrany (1993).

Thus, with the geometry of Figure (3.2), the last integrals in equations (3.18) and (3.19) are calculated for the small semi-circle when $\varepsilon \to 0$.

Thus in equations (3.18) and (3.19):

$$\lim_{\varepsilon\to 0}\int_{B_\varepsilon} q\phi^{s1}dB = \lim_{\varepsilon\to 0}[-q\frac{\pi\varepsilon}{2\pi}\ln\varepsilon] = 0 \tag{3.21}$$

$$\lim_{\varepsilon\to 0}\int_{B_\varepsilon} \phi q^{s1}dB = \lim_{\varepsilon\to 0}[-\phi\frac{\pi\varepsilon}{2\pi\varepsilon}] = -\frac{1}{2}\phi \tag{3.22}$$

where $\pi\varepsilon$ is the perimeter of the semi-circle. Note that time convolution has not been considered in equations (3.21) and (3.22) since the kernels are static. The actual states of the potential $\phi(\mathbf{x},t)$ and flux $q(\mathbf{x},t)$ are then taken as constant during the integration. Using (3.21) and (3.22), the equations (3.18) and (3.19) become:

$$I_1 = \int_B (\phi^s * q)(\mathbf{x},t)dB \tag{3.23}$$

and

$$I_2 = \int_B (q^s * \phi)(\mathbf{x},t)dB - \frac{1}{2}\phi(\mathbf{y}^i,t) \tag{3.24}$$

Employing equations (3.17), (3.23) and (3.24) the integral equation for a boundary point is:

$$\frac{1}{2}\phi(\mathbf{y}^i,t) = \int_B (\phi^s * q)(\mathbf{x},t)dB - \int_B (q^s * \phi)(\mathbf{x},t)dB \tag{3.25}$$

where the integrals have the sense of a Cauchy principal value.

It is also important to emphasise that the points $\mathbf{y}^i$ located outside $\Omega \cup B$ have zero potential. The integral equation is obtained by taking the left-hand side of equation (3.16) equal to zero, that is $\phi(\mathbf{y}^i,t) = 0$.

Thus, the integral representation for the two-dimensional scalar wave problems for any point can be summarized by:

$$\alpha^i\phi(\mathbf{y}^i,t) = \int_B (q * \phi^s)(\mathbf{x},t)dB - \int_B (\phi * q^s)(\mathbf{x},t)dB \tag{3.26}$$

where

$$\alpha^i(\mathbf{y}^i) = \begin{cases} 1. & \text{if} \quad \mathbf{y}^i \in \Omega \\ 1/2 & \text{if} \quad \mathbf{y}^i \in B \\ 0. & \text{if} \quad \mathbf{y}^i \notin (\Omega \cup B) \end{cases} \tag{3.27}$$

Similar approaches have been used for non-smooth boundaries, see for example Banerjee (1994), Dominguez (1993), Brebbia (1984), Brebbia et al. (1992), Guiggiani et al. (1990) and Paris et al. (1997).

Utilizing the convolution equation (3.26) may be written explicitly as:

$$\alpha^i\phi(\mathbf{y}^i,t) = \int_0^{t^+}\int_B \phi^s(\mathbf{x},t-\tau;\mathbf{y}^i)q(\mathbf{x},\tau)dBd\tau - \int_0^{t^+}\int_B q^s(\mathbf{x},t-\tau;\mathbf{y}^i)\phi(\mathbf{x},\tau)dBd\tau \tag{3.28}$$

where $t^+ = t+\varepsilon$. The limit $\varepsilon \to 0$ is used (Morse et al., 1953) to avoid ending the integration at the peak of the Dirac delta function.

In equation (3.28), ϕ^s and q^s are given by equations (3.14) and (3.15), respectively.

In equation (3.28) the last integral can explicitly be written as

$$I = \int_B\int_0^{t^+} q^s\phi d\tau dB = -\frac{c}{2\pi}\int_B \frac{\partial r}{\partial n}\int_0^{t^+}\phi(\mathbf{x},\tau)\frac{\delta[c(t-\tau)-r]}{[c^2(t-\tau)^2-r^2]^{1/2}}d\tau dB$$

$$+\frac{c}{2\pi}\int_B \frac{\partial r}{\partial n}\int_0^{t^+}\phi(\mathbf{x},\tau)\frac{rH[c(t-\tau)-r]}{[c^2(t-\tau)^2-r^2]^{3/2}}d\tau dB \tag{3.29}$$

The first integral in the right hand side of equation (3.29) can be reconsidered due to

presence of the Dirac delta function. Thus, the corresponding integral can be integrated by parts with respect to time τ:

$$I_1 = -\frac{1}{2\pi}\int_B \frac{\partial r}{\partial n}\int_0^{t^+} \dot{\phi}(\mathbf{x},\tau)\frac{H[c(t-\tau)-r]}{[c^2(t-\tau)^2-r^2]^{1/2}}\,d\tau dB$$

$$-\frac{1}{2\pi}\int_B \frac{\partial r}{\partial n}\int_0^{t^+} \phi(\mathbf{x},\tau)\frac{c^2(t-\tau)H[c(t-\tau)-r]}{[c^2(t-\tau)^2-r^2]^{3/2}}\,d\tau dB \tag{3.30}$$

Note that $H[c(t-t^+)-r]=0$ and $u_0(\mathbf{x})=0$ are used in the above partial integration. Substitution of equation (3.30) into equation (3.29) and re-substitution of this result in equation (3.28) gives:

$$\alpha^i\phi(\mathbf{y}^i,t) = \int_0^{t^+}\int_B \phi^s(\mathbf{x},t-\tau;\mathbf{y}^i)q(\mathbf{x},\tau)dBd\tau - \int_0^{t^+}\int_B z^s(\mathbf{x},t-\tau;\mathbf{y}^i)\phi(\mathbf{x},\tau)dBd\tau$$

$$-\int_0^{t^+}\int_B w^s(\mathbf{x},t-\tau;\mathbf{y}^i)\dot{\phi}(\mathbf{x},\tau)dBd\tau \tag{3.31}$$

where,

$$z^s(\mathbf{x},t-\tau;\mathbf{y}^i) = \frac{\partial r}{\partial n}\frac{c[r-(t-\tau)]}{2\pi[c^2(t-\tau)^2-r^2]^{1/2}}H[c(t-\tau)-r] \tag{3.32}$$

and

$$w^s(\mathbf{x},t-\tau;\mathbf{y}^i) = \frac{\partial r}{\partial n}\frac{1}{c}\phi^s(\mathbf{x},t-\tau;\mathbf{y}^i). \tag{3.33}$$

This integral representation is known as Volterra's integral representation. Mansur (1983) used this derivation of Volterra's formula. This approach has been used to remove the Dirac delta function in Volterra's integral equation (3.28).

3.3 Boundary Elements for 2D Scalar Wave Problems

So far the integral representation has been established in terms of the two dynamical states from the principle of dynamic reciprocity. Since an analytical solution of the boundary integral equation is impossible, except for particular geometries, it is necessary to employ numerical methods to gain a solution. In this work for numerical integration, the boundary is approximated by straight-line elements, which are called boundary elements as shown in Figure (3.3).

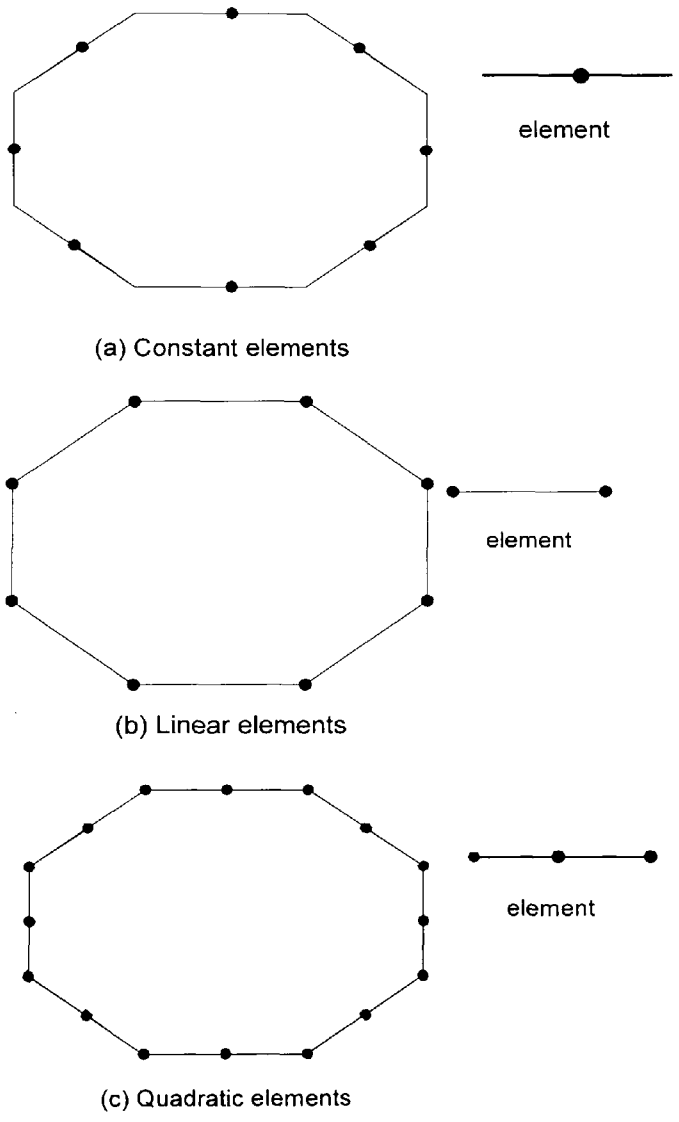

Figure 3.3 Boundary Elements

In an element, nodal points are positions where dependent variable values are to be approximately determined. If nodal points are taken to be in the middle of the element, then the boundary elements are called constant (see Figure 3.3.a), and if they are taken to be at the end points of the element, then they are called linear as shown in Figure (3.3.b). An element is called a quadratic element if the element is also required to have a node at the centre of the element (see Figure 3.3.c).

3.3.1 Time Interpolations of Boundary Variables

Temporal integration of the kernels of equation (3.31) is used to obtain a numerical solution of the partial differential equation, by applying the boundary integral equations. Temporal integration of the kernels used here for equation (3.31), can also be found in Dominguez (1993). The flux and potential are interpolated by constant and linear time variations, respectively. The use of these interpolation functions allows for discontinuity of the field variables from step to step (Gallego et al., 1996, Mansur et al., 1998). Because of that, this scheme was found to be best (Gallego et al., 1996) and the commonest in the literature, see for instance Banerjee (1994), Richter (1997). However, Mansur et al. (1998) recently suggested an alternative to be able to use linear time variation for the flux as well.

Let time be divided into n equal intervals, $t = n\Delta t$. To obtain the approximate solution of the boundary integral equation let:

$$\phi(\mathbf{x},\tau) = \sum_m \eta^m(\tau)\phi^m(\mathbf{x})$$

$$q(\mathbf{x},\tau) = \sum_m \mu^m(\tau)q^m(\mathbf{x}) \tag{3.34}$$

where $\eta^m(\tau)$ and $\mu^m(\tau)$ are temporal interpolation shape functions. In addition, ϕ^m and

q^m indicate the potential and flux respectively, at time $t_m = m\Delta t$ at point **x**. The interpolation functions can be chosen to be piecewise constant, linear, or of higher order. For the above reasons, the potentials are approximated by the linear time functions, and the fluxes are represented by the piecewise constant functions.

In principle, the time or space interpolation functions are chosen arbitrarily. However when the piecewise linear time interpolation function is used for the flux, as well as for the potential, the solution process is prone to become unstable (Cole et al., 1978).

Both for the potential and the flux, the piecewise constant time interpolation function was used for elastodynamic case by Spyrakos et al. (1986). However, Dominguez (1993) and Richter (1997) showed that in some cases, this approach gave poorer results than for the elements used in this study. Tian (1990) also used the constant time interpolation function for both field variables, and stated that this approach to be less stable than the linear time interpolation function used for both approximations.

The interpolation functions used by us, are predominantly used in the literature (Richter, 1997, Dominguez, 1993, Banerjee, 1994, Mansur et al., 1985) and are believed to define the 'best' numerical scheme for the solution of the displacement integral equation (Gallego et al., 1996). Explicitly they are (see Figures 3.4 and 3.5):

$$\eta^m(\tau) = \begin{cases} \dfrac{(\tau - \tau_{m-1})}{\Delta t} & \text{if } \tau \in [\tau_{m-1}, \tau_m] \\ \dfrac{(\tau_{m+1} - \tau)}{\Delta t} & \text{if } \tau \in [\tau_m, \tau_{m+1}] \\ 0 & \text{else} \end{cases} \tag{3.35}$$

and

$$\mu^m(\tau) = \begin{cases} 1 & \text{if } \tau \in [\tau_{m-1}, \tau_m] \\ 0 & \text{otherwise} \end{cases} \tag{3.36}$$

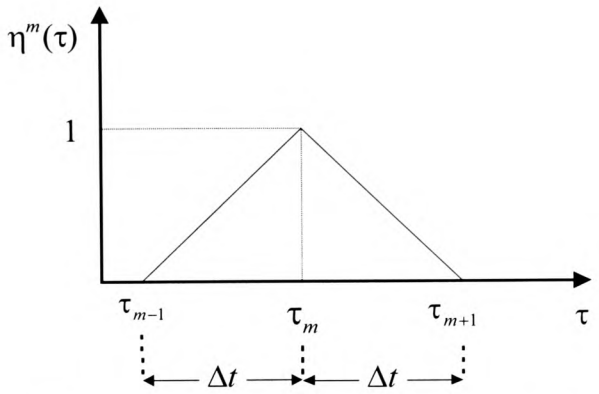

Figure 3.4 Linear time interpolation function for ϕ

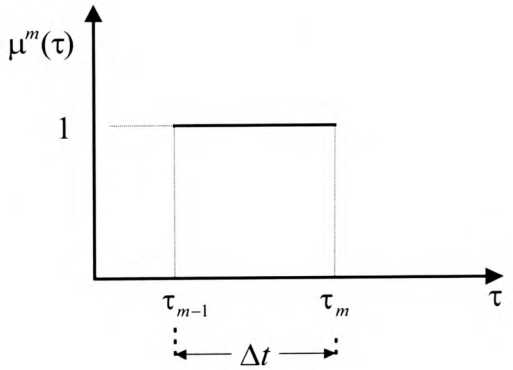

Figure 3.5 Constant time interpolation function for q

Considering the time approximations for the boundary node $\mathbf{y}^i$ at time step n equation (3.31) can be concluded as:

$$\alpha^i \phi^{ni} = \sum_{m=1}^{n} [\int_{B_j} U^{nm} q^m(\mathbf{x}) dB] - \sum_{m=1}^{n} [\int_{B_j} Q^{nm} \phi^m(\mathbf{x}) dB] \tag{3.37}$$

where

$$U^{nm} = \int_0^{t^+} \phi^s(\mathbf{x}, t-\tau; \mathbf{y}^i) \mu^m(\tau) d\tau \tag{3.38}$$

and:

$$Q^{nm} = \int_0^{t^+} [z^s(\mathbf{x}, t-\tau; \mathbf{y}^i)\eta^m(\tau) - w^s(\mathbf{x}, t-\tau; \mathbf{y}^i)\dot{\eta}^m(\tau)]d\tau \tag{3.39}$$

Here ϕ^s, z^s, w^s are given by equations (3.14), (3.32) and (3.33) respectively.

Using (3.36) and (3.38) the effect of the load at the field point $\mathbf{x}$ at time $t = t_n$ can be found (Dominguez, 1993) from equation (3.38). To obtain the time integral for the potential, three cases must be considered.

Case 1: $\tau_m < \tau^* = t_n - \dfrac{r}{c}$

Disturbances, which took place within the interval $[\tau_{m-1}, \tau_m]$, have reached the field point. In this case:

$$U^{nm} = \frac{1}{2\pi}[\cosh^{-1} a_0 - \cosh^{-1} a_1] \tag{3.40}$$

where

$$a_0 = \frac{c(t_n - \tau_{m-1})}{r} \quad \text{and} \quad a_1 = \frac{c(t_n - \tau_m)}{r}.$$

Case 2: $\tau_{m-1} < \tau^* \leq \tau_m$

The field point has received some part of the effect, but has not yet received the effect of the remaining part. Here:

$$U^{nm} = \frac{c}{2\pi} \int_{\tau_{m-1}}^{\tau^*} \frac{d\tau}{[c^2(t_n - \tau)^2 - r^2]^{1/2}} = \frac{1}{2\pi} \cosh^{-1} a_0 \tag{3.41}$$

Case 3: $\tau^* \leq \tau_{m-1}$

The field point has not yet received any effect, so that:

$$U^{nm} = 0 \tag{3.42}$$

Similarly for the time integral of the flux equation (3.39), four cases must be considered.

The interpolation time function η^m is taken to be linear. Hence, from equations (3.35) and (3.39) the time integration for the flux kernel may be found (Dominguez, 1993) as:

Case 1: $\tau_{m+1} < \tau^*$

$$Q^{nm} = -\frac{\partial r}{\partial n}\frac{1}{2\pi c\Delta t}[(a_0^2-1)^{1/2} - 2(a_1^2-1)^{1/2} + (a_2^2-1)^{1/2}] \tag{3.43}$$

where

$$a_2 = \frac{c(t_n - \tau_{m+1})}{r}.$$

Case 2: $\tau_m < \tau^* \le \tau_{m+1}$

$$Q^{nm} = -\frac{\partial r}{\partial n}\frac{1}{2\pi c\Delta t}[(a_0^2-1)^{1/2} - 2(a_1^2-1)^{1/2}] \tag{3.44}$$

Case 3: $\tau_{m-1} < \tau^* \le \tau_m$

$$Q^{nm} = -\frac{\partial r}{\partial n}\frac{1}{2\pi c\Delta t}(a_0^2-1)^{1/2} \tag{3.45}$$

Case 4: $\tau^* \le \tau_{m-1}$

$$Q^{nm} = 0 \tag{3.46}$$

It is worth noting that the flux kernel (3.43-3.46) has also been obtained by considering the fundamental solution *explicitly* with the same time function η^m. In other words, the above flux kernel can be found without using further transformations on the Dirac delta function in the fundamental solution, in equation (3.28).

On the other hand, it is important to realise that there is no singularity appearing at the wave front in the displacement and flux kernels in the above.

It is also emphasised that when time tends to infinity in equations (3.41, 3.45) the kernels tend to the static fundamental solutions.

3.3.2 Boundary Discretization

The boundary of the domain is discretized into a number of elements. Over each element, the spatial variation of the field variables (potentials and fluxes) and the geometry must be described. The variations of the field variables can be approximated using constant, linear, quadratic or higher order elements. In this study, the co-ordinates at any point over any element are expressed by means of their nodal values, using linear elements whilst the field variables are represented by constant or isoparametric quadratic elements.

The geometry of element j can be represented by the co-ordinates using linear interpolation functions,

$$\mathbf{x}(\zeta) = \varphi_k(\zeta)\mathbf{x}^k, \quad 1 \le k \le 2 \tag{3.47}$$

where

$$\varphi_1(\zeta) = \frac{1}{2}(1-\zeta), \qquad \varphi_2(\zeta) = \frac{1}{2}(1+\zeta) \tag{3.48}$$

The nodal values of the field variables on the boundary are approximated using the spatial interpolation function ψ_j for the node j to write equation (3.34),

$$\phi(\mathbf{x},\tau) = \sum_j \sum_m \eta^m(\tau)\psi_j(\mathbf{x})\phi^{mj}$$

$$q(\mathbf{x},\tau) = \sum_j \sum_m \mu^m(\tau)\psi_j(\mathbf{x})q^{mj} \tag{3.49}$$

where ϕ^{mj} and q^{mj} denote the potential and its normal derivative at node j for time $t_m = m\Delta t$ whilst the spatial interpolation function is ψ_j for the field variables (potentials and fluxes). For the points $\mathbf{x}(\zeta)$ inside an element, $\psi_j = \psi_j(\zeta)$. When the field variables are constant over the element in approximation (3.49) $\psi_j = 1$. Notice that for an isoparametric element, the interpolation functions are identical namely, $\psi_j(\zeta) = \varphi_k(\zeta)$.

The order of the spatial and time interpolation functions influences the stability of the system. The use of higher order space interpolation functions is suggested, for instance by Beer et al. (1992) and Birgisson (1996). However, when using higher order interpolation functions the integration of singular integrals poses difficulties. Since Dominguez (1989,1993) obtained similar results for space constant, and space quadratic elements which consist of linear lines, the space constant elements are usually preferred in this work. Elements are numbered successively around the boundary B. The numbering direction is anticlockwise if B is an external boundary, whilst clockwise for the internal boundary B.

Using the spatial approximations with a set of discrete elements B_j, j=1,2,...,N on the boundary B, equation (3.37) can be written as

$$\alpha^i \phi^{ni} = \sum_{m=1}^{n} \sum_{j=1}^{N} [\int_{B_j} U^{nm} \psi_j(\mathbf{x}) dB] q^{mj} - \sum_{m=1}^{n} \sum_{j=1}^{N} [\int_{B_j} Q^{nm} \psi_j(\mathbf{x}) dB] \phi^{mj} \tag{3.50}$$

In equation (3.50), N and n show the number of boundary elements and final time (i.e. $t = n\Delta t$), whilst ϕ^{ni} denotes the unknown potential at the load point $\mathbf{y}^i$ on the boundary at time step n.

3.3.2.1 Evaluation of Spatial Integrals

The basic idea here is to solve equation (3.31) numerically, by discretizing boundary values spatially as well as temporally. Once only the boundary B is discretized, as opposed to the FDM and FEM in which the domain is discretized as well, the kernel U^{nm} and its normal derivative Q^{nm} have to be integrated spatially over the all boundary elements.

If the load point $\mathbf{y}^i$ is not on the integration element, the above integrals are evaluated using a standard Gaussian quadrature of maximum fourteenth order. The order of the integration is taken quite high, because of the discontinuous variation of the fundamental solution with respect to r.

The integration to be evaluated is expressed by means of the homogeneous co-ordinate $-1 \le \zeta \le 1$ along the elements. To evaluate the integrals, the differential is expressed in the $x_1 x_2$-plane, as

$$dB = [(\frac{dx_1}{d\zeta})^2 + (\frac{dx_2}{d\zeta})^2]^{1/2} d\zeta = |J| d\zeta \tag{3.51}$$

where $|J|$ is the Jacobian of the transformation.

With the spatial discretization, equation (3.50) takes the following form for the two-dimensional scalar wave problems,

$$\alpha^i \phi^{ni} = \sum_{m=1}^{n} \sum_{j=1}^{N} [\int_{-1}^{1} U^{nm} \psi_j |J| d\zeta] q^{mj} - \sum_{m=1}^{n} \sum_{j=1}^{N} [\int_{-1}^{1} Q^{nm} \psi_j |J| d\zeta] \phi^{mj} \tag{3.52}$$

The boundary is divided into N elements and because of the constant elements considered here, the actual state values of potential ϕ and flux q are assumed to be constant over each element, and equal to the value at the mid-element node.

3.3.2.2 Evaluation of Singular Integrals

There are two types of integrals, singular and non-singular. In case of $r \neq 0$, the evaluation of the non-singular integrals has been discussed in the last section in terms of the Gaussian integration. The singular integrals appear only when the field and load points coincide at the first time step. When the field and load points are in the same element (see Figure 3.6), the integrals are performed analytically (Dominguez, 1993). In

that case, the fundamental flux solution is zero since it is an antisymmetric function. Taking equation (3.41), the integral of the potential fundamental solution is:

$$IG(s,t) = \int_0^s \cosh^{-1}(\frac{ct}{r})dr = ct[\frac{s}{ct}\cosh^{-1}(\frac{ct}{s}) + \sin^{-1}(\frac{s}{ct})] \tag{3.53}$$

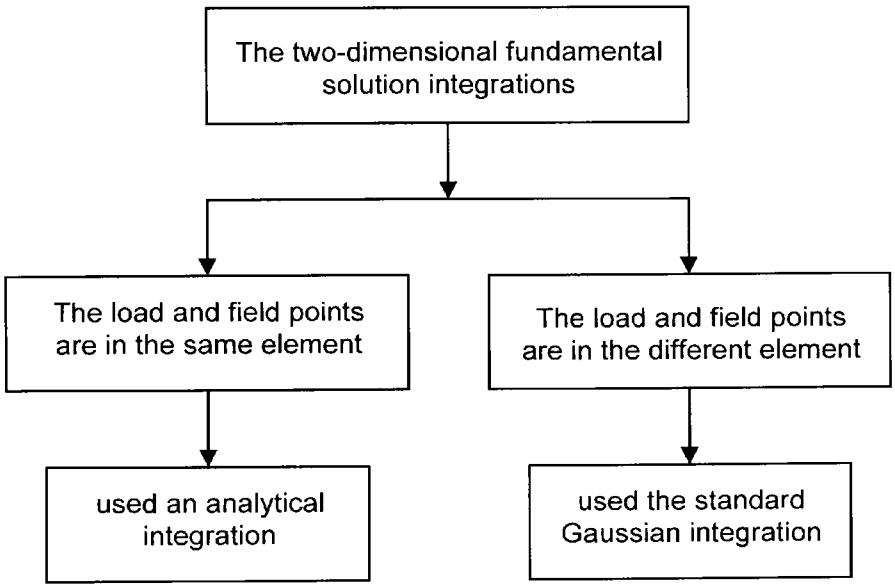

Figure 3.6 Integration scheme

The value s depends on whether or not the wave travels the whole element. So

$$G^{nmii} = \int_{B_i} U^{nm} dB_i = \frac{1}{\pi}[IG(s_0,t) - IG(s_1,t-\Delta t)] \tag{3.54}$$

where

$$s_0 = \max[1, \frac{ct}{(\Delta x/2)}], \qquad s_1 = \max[1, \frac{c(t-\Delta t)}{(\Delta x/2)}]$$

with the length of element being Δx.

3.3.3 The Boundary Element Equation

For each element one can write,

$$G^{nmij} = \int_{B_j} U^{nm}(\mathbf{x}, t-\tau; \mathbf{y}^i)\psi_j dB \tag{3.55}$$

$$\hat{H}^{nmij} = \int_{B_j} Q^{nm}(\mathbf{x}, t-\tau; \mathbf{y}^i)\psi_j dB \tag{3.56}$$

Using the jump term (α^i) in equation (3.27), equation (3.56) may be redefined by:

$$H^{nmij} = \begin{cases} \hat{H}^{nmij} + \alpha^i & \text{if} \quad i = j \quad \text{and} \quad n = m \\ \hat{H}^{nmij} & \text{if} \quad i \neq j \quad \text{or} \quad n \neq m \end{cases} \tag{3.57}$$

Here the boundary of the domain is discretized with constant elements. Now, considering the spatial integrals, equation (3.50) can be written as:

$$\sum_{m=1}^{n}\sum_{j=1}^{N} H^{nmij}\phi^{mj} - \sum_{m=1}^{n}\sum_{j=1}^{N} G^{nmij}q^{mj} = 0 \tag{3.58}$$

where N represents the total number of boundary elements. Taking into consideration all boundary elements, equation (3.58) can be rewritten in the more compact form:

$$\sum_{m=1}^{n}[\mathbf{H}^{nm}\boldsymbol{\phi}^m - \mathbf{G}^{nm}\mathbf{q}^m] = \mathbf{0} \tag{3.59}$$

where $\mathbf{G}^{nm}$ and $\mathbf{H}^{nm}$ are square matrices which are calculated by spatial integration for each element and $\boldsymbol{\phi}^m$ and $\mathbf{q}^m$ are the column vectors of boundary nodal quantities. The matrices $\mathbf{G}^{nm}$ and $\mathbf{H}^{nm}$ are also known as the influence coefficients.

3.3.4 Solution Procedure

At time t, there are as many unknowns as the number of equations in the matrix equation (3.59). If the boundary quantities $\boldsymbol{\phi}^m$ and $\mathbf{q}^m$ are known for m=1,2,...,n-1, then for each time step n, the solution can be found. Thus, taking the unknowns on the left, equation (3.59) can be rewritten as,

$$\mathbf{H}^{nn}\phi^{n} = \mathbf{G}^{nn}\mathbf{q}^{n} + \sum_{m=1}^{n-1}[\mathbf{G}^{nm}\mathbf{q}^{m} - \mathbf{H}^{nm}\phi^{m}] \tag{3.60}$$

Here, the last part of the right hand side of equation (3.60) is known. The unknowns in the above equation consist of boundary potentials or their normal derivatives. For instance, if the boundary potential quantities only are prescribed, then the fluxes are unknowns at these boundary nodes. Rearranging the columns of $\mathbf{G}^{nn}$ and $\mathbf{H}^{nn}$ according to boundary conditions, the last equation may be expressed as:

$$\mathbf{A}^{n}\mathbf{X}^{n} = \mathbf{R}^{n} \tag{3.61}$$

where the right hand side $\mathbf{R}^{n}$ is the sum of terms over the previous steps, and the known boundary conditions for time step n multiplied by their coefficient matrix. In the last equation, $\mathbf{X}^{n}$ and $\mathbf{A}^{n}$ are respectively the unknown vector and the system matrix for time step n.

For each time step, the last part of the right-hand side of equation (3.60) is reformed since the coefficient matrices $\mathbf{G}^{n1}$ and $\mathbf{H}^{n1}$ in each time step are computed, whilst the rest of them are already known. The coefficient matrices $\mathbf{G}^{nn}$, $\mathbf{H}^{nn}$ and $\mathbf{A}^{n}$ remain unchanged with time, unless the nature of the boundary conditions at each boundary node changes. So the system matrix is organised only once, thus it can be written as $\mathbf{A}^{n} \equiv \mathbf{A}$. It can also be recognised that the matrix $\mathbf{R}^{n}$ in equation (3.61) has to be computed for each time step. For the solution of equation (3.61) see the Appendix.

In addition, the field point time is n while the loading time is m with duration Δt, namely, $t_n = n\Delta t$ and $\tau_m = m\Delta t$. The coefficient matrices then depend only on the difference n-m. The procedure outlined here is that of Dominguez (1993).

3.4 Infinite Domains

For some applications, it is convenient to take the medium to be of infinite extent. For example, in the case of deep underground sources it is supposed that the rock mass extends to infinity. To explain this case, first consider a rectangle. When the right and left sides of the rectangular domain are positioned at infinity (see Figure 3.7), the behaviour of the solution is then observed. In Figure (3.7) B_2^b and B_2^t denote the external boundaries for the bottom and top edges, respectively, whilst B_1 stands for the internal boundary. The left and right boundaries are shown by B_r^l and B_r^r, respectively, when they extend to infinity. Also, $\mathbf{y}^i$ and $\mathbf{x}$ denote the load and field points, respectively. The load point belongs to the interior where the integral equation will be applied. Also note that $B = B_1 + B_2^b + B_2^t$ and $B_r = B_r^l + B_r^r$. Then, taking the external and internal boundaries, equation (3.28) can be written in the form:

$$\alpha^i \phi(\mathbf{y}^i, t) = \int_B [(\phi^s * q) - (q^s * \phi)](\mathbf{x}, t) dB + \lim_{r \to \infty} \int_{B_r} [(\phi^s * q) - (q^s * \phi)](\mathbf{x}, t) dB \qquad (3.62)$$

It can be seen that this case can be viewed as a particular situation of the general one considered in the previous sections. If all the sources causing the motion are confined to the interior of the domain Ω, then there is no wave to propagate to the interior from infinity. Therefore, the potential and its normal derivative must behave in such a way that the last integral in equation (3.62) is zero (Eringen et al., 1975). From the analytical structure of the potential and flux fundamental solutions, the field quantities satisfy:

$$\lim_{r \to \infty} r^{-1/2} \phi = 0, \qquad \lim_{r \to \infty} r^{1/2} \left(\frac{\partial \phi}{\partial r} + \frac{1}{c} \dot{\phi} \right) = 0 \qquad (3.63)$$

In equation (3.63), the first and second conditions are called the regularity and

Sommerfield radiation conditions, respectively (Eringen et al., 1975, Achenbach, 1975, Bonnet, 1998). These conditions ensure the uniqueness of the solution in an unbounded domain (Eringen et al., 1975).

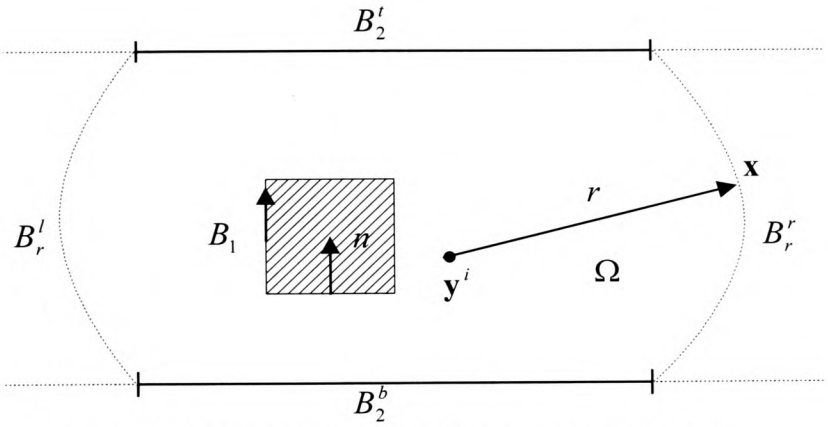

Figure 3.7 Propagation in a medium extending to infinity

Consequently, it may be seen that the boundary integral equation (3.28) is valid for domains of infinite extent as well as the confined domains. There is no need to discretize the external boundary B_r as $r \to \infty$. This is a very important advantage of the BEM over the FEM and FDM, which need a discretization that should extend to infinity (e.g. Dominguez, 1993).

3.5 Multimedia

So far the numerical implementation of the boundary integral equation has been considered for only homogeneous materials.

One of the important, yet very difficult, problems in dealing with the Earth's interior is that it is a complex heterogeneous medium in which the physical properties change continuously along boundaries. Therefore, this work will consider the problem of solving the scalar (or elastic in the following chapters) wave equation in regions containing two

or more different layers. Figure (3.8) represents this idea with a domain consisting of two subdomains which are Ω_1 and Ω_2. Applying the procedure for each subdomain separately gives, from equation (3.59),

$$\sum_{m=1}^{n}\left\{\begin{bmatrix}\mathbf{H}_{11}^{nm} & \mathbf{H}_{1I}^{nm}\end{bmatrix}\begin{bmatrix}\boldsymbol{\phi}_1^m \\ \boldsymbol{\phi}_{1I}^m\end{bmatrix}-\begin{bmatrix}\mathbf{G}_{11}^{nm} & \mathbf{G}_{1I}^{nm}\end{bmatrix}\begin{bmatrix}\mathbf{q}_1^m \\ \mathbf{q}_{1I}^m\end{bmatrix}\right\}=\mathbf{0} \tag{3.64}$$

for subdomain Ω_1.

Here, for time $t_m = m\Delta t$, $\boldsymbol{\phi}_1^m$ and $\mathbf{q}_1^m$ indicate the nodal potentials and fluxes at the boundary B_1, whilst $\boldsymbol{\phi}_{1I}^m$ and $\mathbf{q}_{1I}^m$ stand for the nodal potentials and fluxes at the interface when it belongs to B_1. It may be seen that the corresponding coefficient matrices $\mathbf{H}_{1I}^{nm}$ and $\mathbf{G}_{1I}^{nm}$ are obtained from the interface, when it belongs to boundary B_1. The matrices $\mathbf{H}_{11}^{nm}$ and $\mathbf{G}_{11}^{nm}$ are derived from the boundary B_1, excluding the interface. Similarly,

$$\sum_{m=1}^{n}\left\{\begin{bmatrix}\mathbf{H}_{22}^{nm} & \mathbf{H}_{2I}^{nm}\end{bmatrix}\begin{bmatrix}\boldsymbol{\phi}_2^m \\ \boldsymbol{\phi}_{2I}^m\end{bmatrix}-\begin{bmatrix}\mathbf{G}_{22}^{nm} & \mathbf{G}_{2I}^{nm}\end{bmatrix}\begin{bmatrix}\mathbf{q}_2^m \\ \mathbf{q}_{2I}^m\end{bmatrix}\right\}=\mathbf{0} \tag{3.65}$$

for subdomain Ω_2.

Where two subdomains have a common interface, it is necessary that the common nodal points on the boundaries B_1 and B_2 are at the same potential, and that there is dynamical equilibrium of the flux across the corresponding interface elements. These conditions can be written as:

$$\boldsymbol{\phi}_{1I}^m = \boldsymbol{\phi}_{2I}^m \tag{3.66}$$

$$\mathbf{q}_{1I}^m = -\mathbf{q}_{2I}^m \tag{3.67}$$

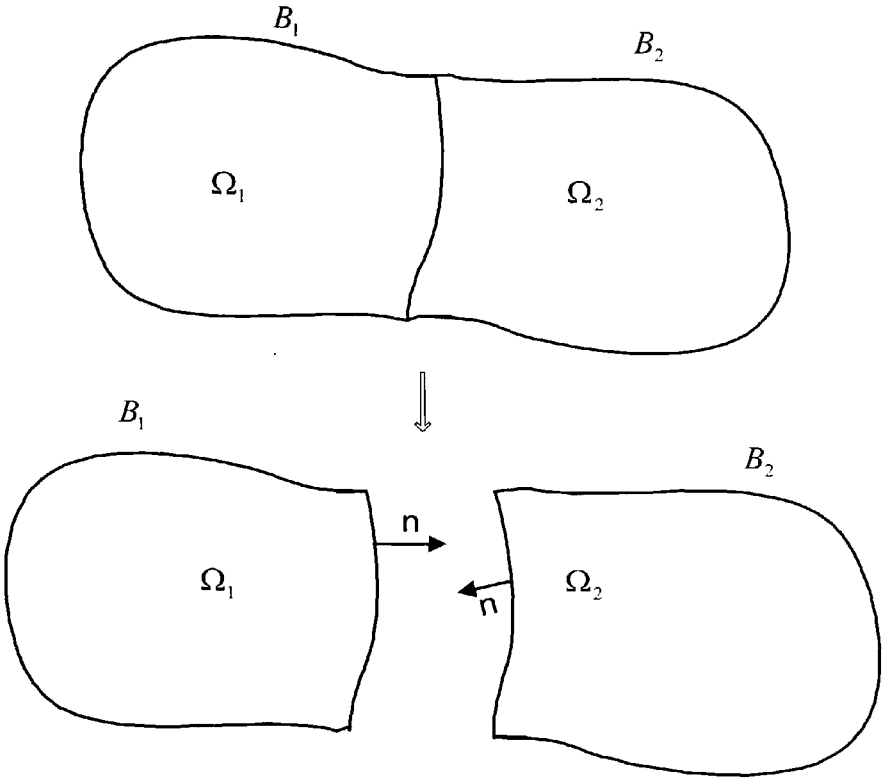

Figure 3.8 Two subdomains of the medium

Equations (3.66) and (3.67) are called (Sokolnikoff, 1956, Banerjee, 1994, Paris et al., 1997) compatibility conditions and dynamical equilibrium conditions, respectively, or, the interface conditions.

Note that for a subdomain, the integral equation is constructed in terms of the interface variables of the subdomain as well as the boundary variables (Lachat et al., 1976). At the interface, both the potential and the flux are unknown, so that the number of unknowns and knowns are not equal. However, considering equations (3.66) and (3.67) corresponding to the interface, the number of unknowns and knowns becomes equal, and the discrete equation system is constructed for the piecewise homogeneous medium, and simultaneously solved for all subdomains. It follows that the algebraic equation system by considering the interface equations can be written in a compact form as,

$$\mathbf{D}\mathbf{X}^n = \mathbf{R}^n \tag{3.68}$$

where $\mathbf{D}$ and $\mathbf{X}^n$, at time step n, are the system matrix which consists of the matrix coefficients of both subdomains and the unknown vector, which contains the interface unknowns as well. The matrix $\mathbf{D}$ can be set up in two ways:

i) Equations (3.66) and (3.67) are added directly to the system matrix obtained using the subdomains.

ii) The interface variables are eliminated.

Here, case (i) is used to consider multimedia problems. This case is more flexible than case (ii). On the one hand, in case (ii) the dimension of the system matrix is smaller than case (i).

In the coefficient matrix (3.68), interface contributions can also be scaled. The argument above can be repeated for three or more subdomains. So for each time step, the boundary and interface unknowns can be calculated from equation (3.68). Solution of equation (3.68) is stated in the Appendix.

3.6 Internal Calculations

Calculation of the internal variables and their formulations are discussed. The internal flux kernels are derived for different cases, depending on whether or not the effect of the load has been received by the field point.

3.6.1 Internal Potentials

So far, the numerical formulation stated has concentrated on solving the unspecified boundary potentials and fluxes for the domain of interest. If the boundary potentials and fluxes are known for time steps $1,2,...,n$, then it is not difficult to find the potential value at internal points selected and at time step n. From equation (3.27), it can be seen that the term α^i is unity for internal points. For the boundary node j and the internal point i,

considering the time difference *n-m*, the internal potentials can be easily calculated numerically at time step *n*. Using equations (3.52) for this case the equation is:

$$\phi^{ni} = \sum_{m=1}^{n}\sum_{j=1}^{N}(G^{nmij}q^{mj} - \hat{H}^{nmij}\phi^{mj}) \tag{3.69}$$

It is noticeable that integration of equations (3.69) is evaluated numerically, using Gaussian quadrature in a similar fashion to the boundary integrations. Note that since the point is an internal point, the kernels never become singular (the wavefronts are considered in the following).

3.6.2 Internal Fluxes

Once the boundary variables are known for time $t = \Delta t, 2\Delta t, ..., n\Delta t$, then the internal fluxes can be found using the kernels to be derived in the following. For the boundary node *j*, and the internal point *i*, considering the time difference *n-m*, the internal flux components can be easily computed numerically. By differentiating equation (3.69), the following equation can be obtained:

$$q_k^{ni} = \frac{\partial \phi^{ni}}{\partial y_k} = \sum_{m=1}^{n}\sum_{j=1}^{N}(\frac{\partial G^{nmij}}{\partial y_k}q^{mj} - \frac{\partial \hat{H}^{nmij}}{\partial y_k}\phi^{mj}) \tag{3.70}$$

Note that during the integration superfix notation '*i*' of the load point $\mathbf{y}^i$ is omitted, because of clustering notations. From the last equation,

$$\frac{\partial G^{nmij}}{\partial y_k} = \int_B \frac{\partial U^{nm}}{\partial y_k}\psi_j dB \tag{3.71}$$

where ψ_j is the same as before. Then,

$$\frac{\partial U^{nm}}{\partial y_k} = \int_{\Delta t_m} \frac{\partial}{\partial y_k}\phi^s(\mathbf{x}, t; \mathbf{y}^i)\mu^m(\tau)d\tau \tag{3.72}$$

Similar to the boundary potential kernels, three distinct cases are considered depending on whether or not the wave reached the field point:

Case 1: $\tau_m < \tau^*$

Disturbances taken place from τ_{m-1} to τ_m have reached the field point. So that:

$$\frac{\partial U^{nm}}{\partial y_k} = \frac{r_{,k}}{2\pi r}\left[\frac{a_0}{(a_0^2-1)^{1/2}} - \frac{a_1}{(a_1^2-1)^{1/2}}\right] \tag{3.73}$$

where a_0, a_1, τ^* and $\mu^m(\tau)$ are the same previously mentioned, and $r_{,k} \equiv \frac{\partial r}{\partial x_k} \equiv \frac{r_k}{r}$

with $r_k \equiv x_k - y_k$.

Case 2: $\tau_{m-1} < \tau^* \leq \tau_m$

The field point has received some part of the effect, but has not yet received the effect of the remaining part. In this case:

$$\frac{\partial U^{nm}}{\partial y_k} = \frac{r_{,k}}{2\pi r}\frac{a_0}{(a_0^2-1)^{1/2}} \tag{3.74}$$

Case 3: $\tau^* \leq \tau_{m-1}$

The field point has not received any effect yet, so that:

$$\frac{\partial U^{nm}}{\partial y_k} = 0 \tag{3.75}$$

And similarly:

$$\frac{\partial \hat{H}^{nmij}}{\partial y_k} = \int_B \frac{\partial Q^{nm}}{\partial y_k}\psi_j dB \tag{3.76}$$

where ψ_j is the same as before. Thus, considering (3.15):

$$\frac{\partial Q^{nm}}{\partial y_k} = \int_{\Delta t_m} \frac{\partial}{\partial y_k}[q^s(\mathbf{x}, t-\tau; \mathbf{y})]\eta^m(\tau)d\tau \tag{3.77}$$

Four different cases are considered as follows:

Case 1: $\tau_m < \tau^*$

$$\frac{\partial Q^{nm}}{\partial y_k} = -\frac{1}{2\pi c\Delta t}\{[\frac{r_{,k}}{r}\frac{\partial r}{\partial n}(\frac{a_0^2}{(a_0^2-1)^{1/2}} - \frac{2a_1^2}{(a_1^2-1)^{1/2}} + \frac{a_2^2}{(a_2^2-1)^{1/2}})] + [(a_0^2-1)^{1/2} - 2(a_1^2-1)^{1/2} + (a_2^2-1)^{1/2}]\frac{\partial}{\partial y_k}(\frac{\partial r}{\partial n})\} \tag{3.78}$$

where a_2 and $\eta^m(\tau)$ are the same as previously given.

In the above

$$\frac{\partial}{\partial y_k}(\frac{\partial r}{\partial n}) = \frac{1}{r}(-n_k + r_{,k}\frac{\partial r}{\partial n}) \tag{3.79}$$

Case 2: $\tau_m < \tau^* \le \tau_{m+1}$

$$\frac{\partial Q^{nm}}{\partial y_k} = -\frac{1}{2\pi c\Delta t}\{\frac{r_{,k}}{r}\frac{\partial r}{\partial n}[\frac{a_0^2}{(a_0^2-1)^{1/2}} - \frac{2a_1^2}{(a_1^2-1)^{1/2}}] + [(a_0^2-1)^{1/2} - 2(a_1^2-1)^{1/2}]\frac{\partial}{\partial y_k}(\frac{\partial r}{\partial n})\} \tag{3.80}$$

Case 3: $\tau_{m-1} < \tau^* \le \tau_m$

$$\frac{\partial Q^{nm}}{\partial y_k} = -\frac{1}{2\pi c\Delta t}[\frac{r_{,k}}{r}\frac{\partial r}{\partial n}\frac{a_0^2}{(a_0^2-1)^{1/2}} + (a_0^2-1)^{1/2}\frac{\partial}{\partial y_k}(\frac{\partial r}{\partial n})] \tag{3.81}$$

Case 4: $\tau^* \le \tau_{m-1}$

$$\frac{\partial Q^{nm}}{\partial y_k} = 0 \tag{3.82}$$

In equation (3.77), the fundamental flux solution is considered explicitly during the derivation of the internal flux kernels. In other words, here Mansur's way (1983) has not been used. This is because if this process is used to obtain the interior flux kernels, one is faced with involving an even higher order of temporal derivative of the boundary

variable, the numerical evaluation of which is very difficult. Israil et al. (1991a) also emphasised these difficulties.

During the derivation of the internal flux kernels both for (3.72) and (3.77), Israil (1990) used linear temporal variation. On the other hand, in this work, constant and linear temporal variations are considered, respectively.

It is noted that the kernels obtained do not possess a strong singularity at the wave front, and as can be seen from the kernels above, there is only a singularity of order $r^{-1/2}$. As was emphasised by Israil (1990) and Israil et al. (1991a) during the integration, this singularity does not pose any special difficulty.

The internal static flux kernels can be obtained for the case of $n = m$ and $\Delta t \to \infty$ in expressions (3.74) and (3.81), respectively, as follows:

$$\frac{\partial U^{nn}}{\partial y_k} = \frac{r_{,k}}{2\pi r} \tag{3.83}$$

$$\frac{\partial Q^{nn}}{\partial y_k} = \frac{1}{2\pi r^2}(n_k - 2r_{,k}\frac{\partial r}{\partial n}) \tag{3.84}$$

These results can also be checked using the solutions (3.20).

To calculate potential and flux values inside a subdomain, only the subdomain boundary (interface) values are used. Some subroutines have been coded to calculate the internal potential (3.69) and internal fluxes (3.70).

3.7 Numerical Aspects

In order to analyse the effects of time step size and elements size on the stability of the method, a scalar wave problem was solved at a selected internal point (25,470) using the BEM formulation due to a source located in a geophysical structure.

If a solution process is divergent or begins to oscillate, then the process is called unstable.

If a solution process requires a time step restriction from the user, then it is called conditionally stable, otherwise it is unconditionally stable. In general, a mathematical discussion on stability can be found in Gilbert et al. (1967).

The Courant-Fredericks-Lewy (CFL) condition provides an upper bound on the time step for explicit FDM and FEM methods in numerical analysis. However there are no such criteria in the BEM and the CFL condition cannot be directly applied to the BEM schemes since they are based on a different discretization and formulation of the system (Pierce et al., 1996). Since the discretized BEM equations are very complicated, researchers, for example, Pierce et al. (1996), consider model problems to determine the stability properties.

A convenient factor for measuring stability is $\beta = c\Delta t / \Delta x$, with time step size Δt, and the length of element Δx, where usually $0.5 \le \beta \le 1.5$, for example Richter (1997). In this thesis, the results obtained are usually within this interval.

The material velocity for seawater is 1500 m/s. The physical geometry of the problem is given in Figure (3.9), and boundary conditions prescribed are shown in Figure (3.10). Homogeneous and inhomogeneous boundary conditions are used for the external and internal (source) boundaries. The lengths $(\Delta x)_1$, $(\Delta x)_2$ and factors β^1, β^2 are for the external and internal boundaries, respectively. The physical system is a conservative system, so there is no energy loss.

Sensitivity of time step size and element size has been observed in the solutions in Figure (3.11). The effect of the uniformity of the elements to the solutions was also analysed considering β^1 and β^2.

In Figures (3.11a) to (3.11c), the element lengths are $(\Delta x)_1 = 5\,\mathrm{m}$, $(\Delta x)_2 = 2\,\mathrm{m}$. In these cases, the problem was solved for different β values. When the low β^1 and β^2 values have been adopted, the solution begins to oscillate (Figures 3.11a, 3.11d and 3.11h), and the resulting disturbances do not remain arbitrarily small throughout the wave path. To obtain a stable solution, following the application of arbitrary small perturbations the disturbances must remain arbitrarily small throughout the period of the investigation (Gilbert et al., 1967). When the waves reach an obstacle, they are partly reflected and partly transmitted (see Snell's law in section 2.4).

When high β^1 and β^2 values are used (see Figures3.11c, 3.11g and 3.11j), small responses in the medium can not be seen. In other words, for very large time step size small disturbances in the body are invisible.

The effect of the element size to the solution has also been observed. In Figures (3.11h), (3.11i) and (3.11j) the element length is larger those of Figures (3.11a), (3.11b) and (3.11c), while the β^1 and β^2 values are equal. Comparison of Figures (3.11b) and (3.11i) suggests the larger element size represents the wave motion less accurately. Therefore, increasing the number of elements is suggested. However, it should not be forgotten that if the element size is taken to be very small the desired stability may not be obtained. Because adoption of a small time step size means more time steps used and more accumulation of numerical errors. So this speeds up the instability of the solution.

Consideration of Figure (3.11b) tells us that even small reflections can be seen in the domain. Comparisons of Figures (3.11b-c), (3.11e-g) and (3.11i-j) lead us to see a solution with unseen reflections for the larger β^1 and β^2 values.

As can be seen from results (3.11b), (3.11f) and (3.11i), the reflections are weaker than the first wave. This is because the amplitude of the wave decreases as the radius increases since the energy in the wavefront is spread out over an ever-increasing circumference.

In results (3.11e) and (3.11f), $(\Delta x)_1 = (\Delta x)_2$ and so that $\beta = \beta^1 = \beta^2$. In the first, β is 0.6 and in the second 1.2. In the first case, the solution looks to be more sensitive to selection of time step, while the second is not as clear as in Figure (3.11b). So for uniform elements β close to 1 is recommended. In the meantime, Figure (3.11b) suggests taking β close to 1 for non-uniform elements, referring to an intermediate element. In this respect, use of uniform elements can increase the stability of the numerical solution.

A similar analysis for boundary points was carried out in a different medium by Dominguez et al. (1991a) for elastodynamic problems, and their observations agree with our observations for internal points.

The solution of the problem was analysed here for only one internal point. In the following sections, the solution of the problem for all internal points will be presented and seen to be in a good agreement with the result to be compared.

At the same time, Demir (1998) solved the same problem for a single trace using the FDM and his result also agrees with our result.

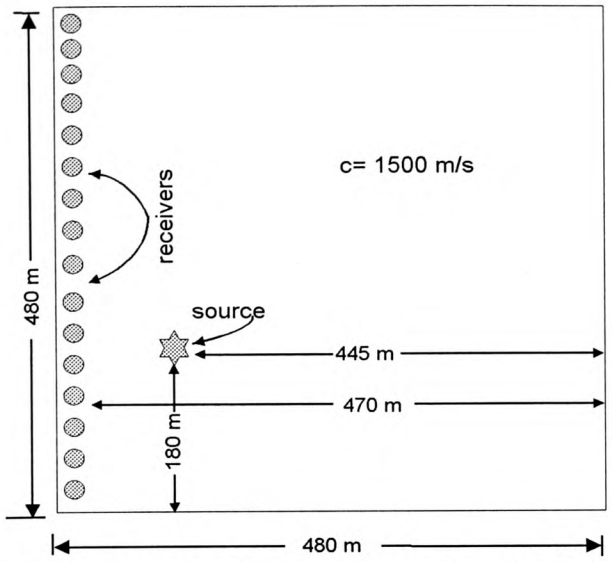

Figure 3.9 Physical the geometry of the medium used to generate seismograms in the scalar BEM Program

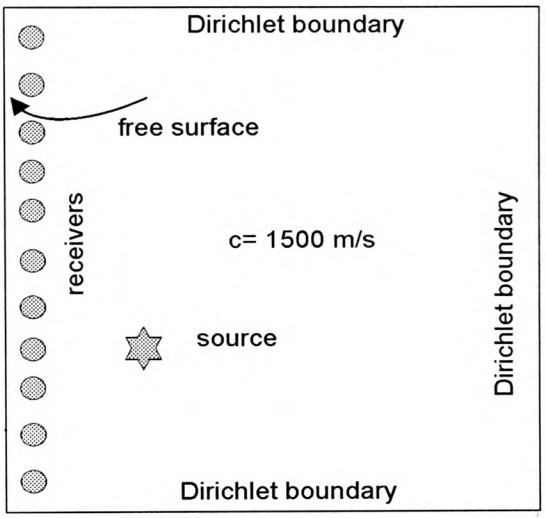

Figure 3.10 Definition of the boundary conditions of the problem.

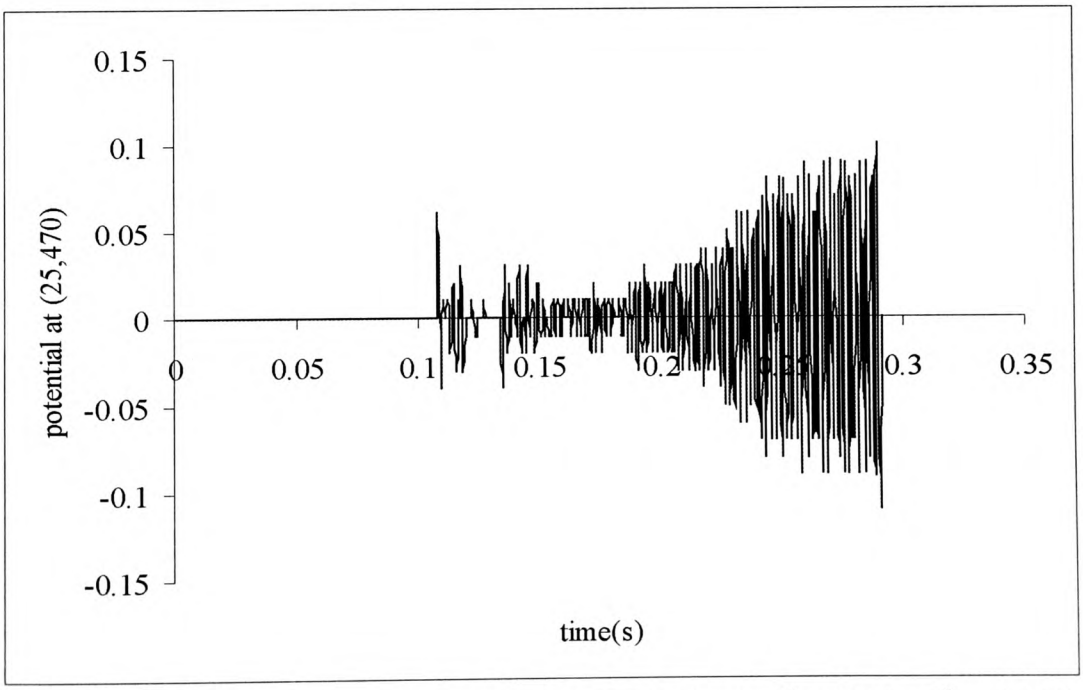

Figure 3.11a Potential ϕ versus time; for point (25,470) with $\beta^1 = 0.15$, $\beta^2 = 0.375$, $(\Delta x)_1 = 5$ m, $(\Delta x)_2 = 2$ m

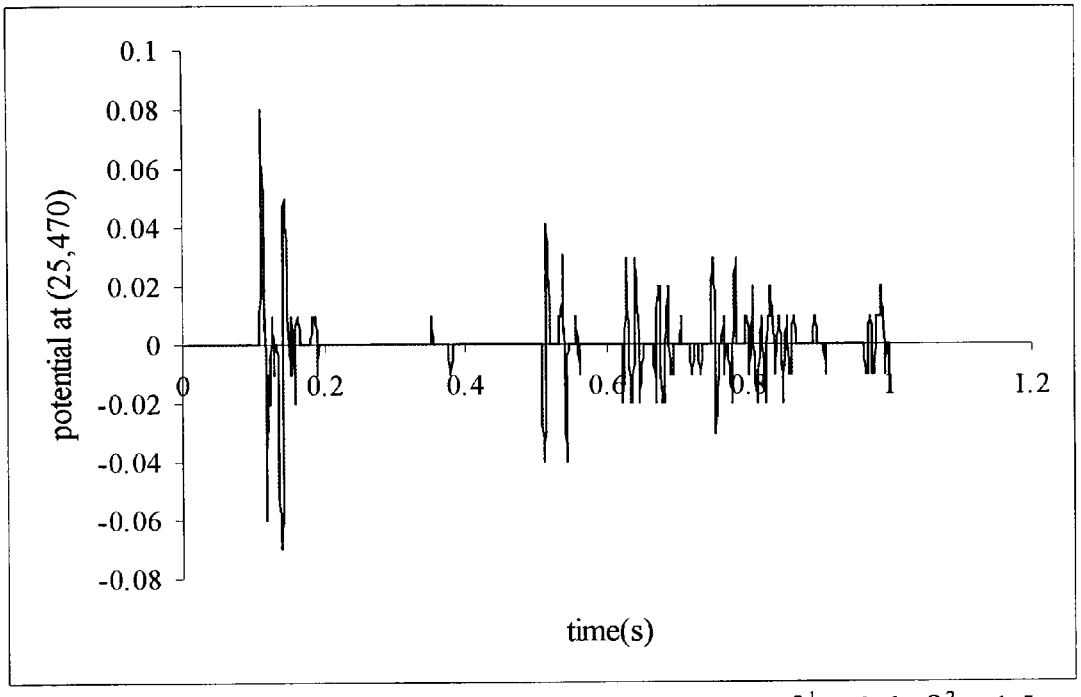

Figure 3.11b Potential ϕ versus time; for point (25,470) with $\beta^1 = 0.6$, $\beta^2 = 1.5$, $(\Delta x)_1 = 5$ m, $(\Delta x)_2 = 2$ m

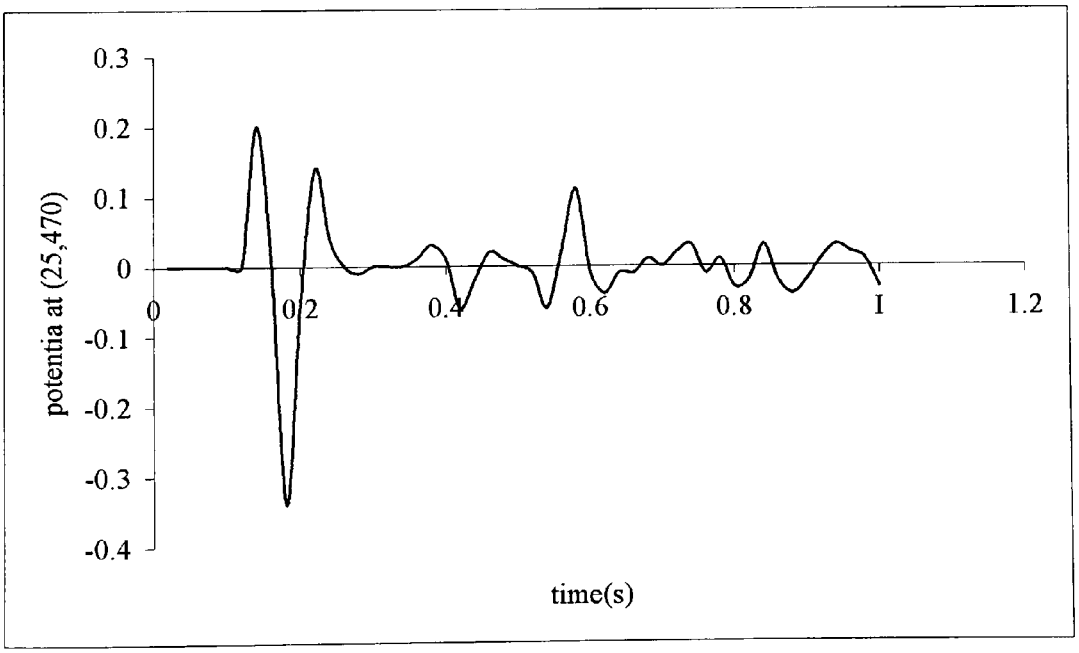

Figure 3.11c Potential ϕ versus time; for point (25,470) with $\beta^1 = 6.$, $\beta^2 = 15.$, $(\Delta x)_1 = 5$ m, $(\Delta x)_2 = 2$ m

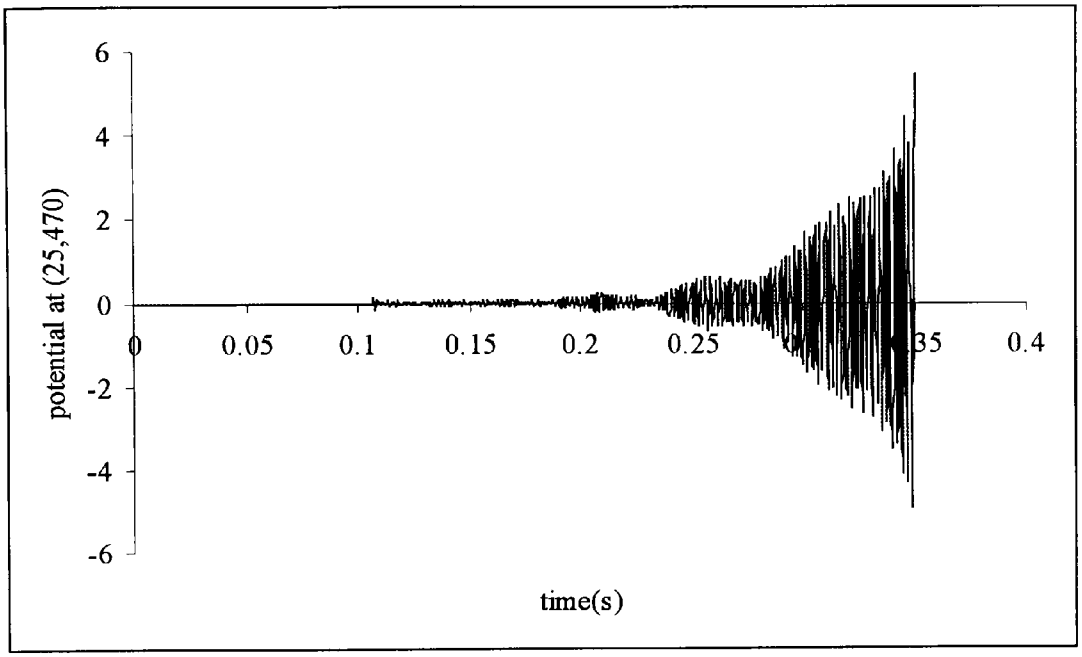

Figure 3.11d Potential ϕ versus time; for point (25,470) with $\beta^1 = \beta^2 = 0.15$, $(\Delta x)_1 = (\Delta x)_2 = 5$ m

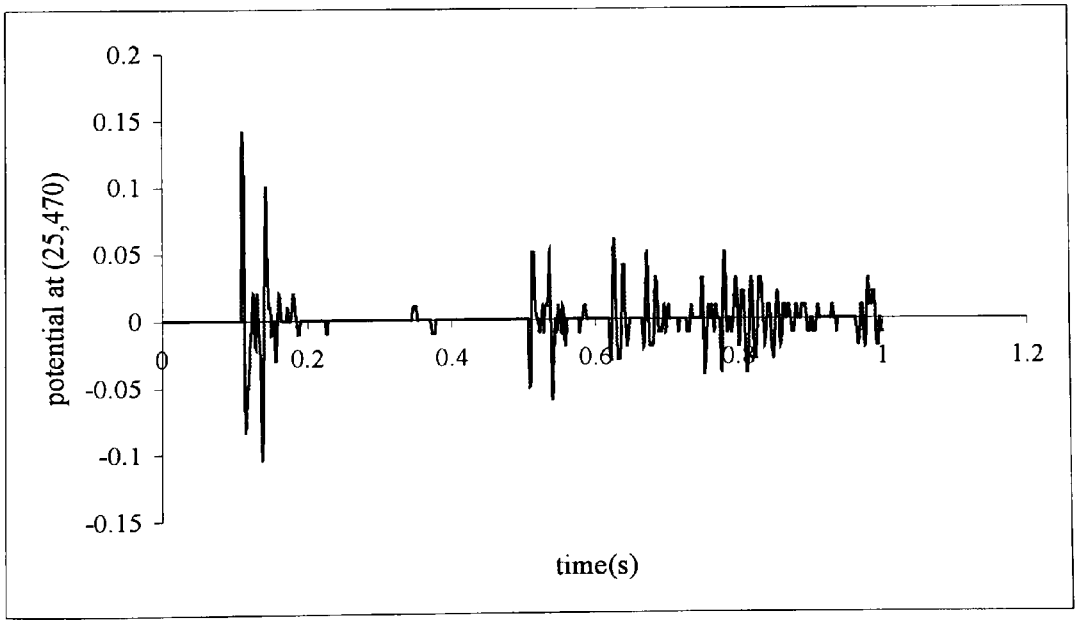

Figure 3.11e Potential ϕ versus time; for point (25,470) with $\beta^1 = \beta^2 = 0.6$, $(\Delta x)_1 = (\Delta x)_2 = 5$ m

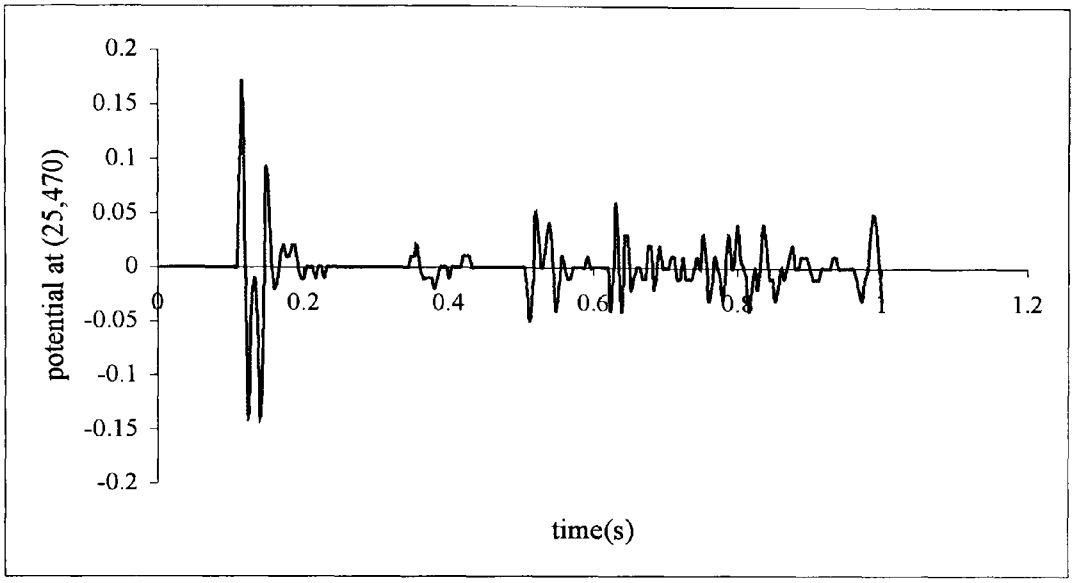

Figure 3.11f Potential ϕ versus time; for point (25,470) with $\beta^1 = \beta^2 = 1.2, (\Delta x)_1 = (\Delta x)_2 = 5$ m

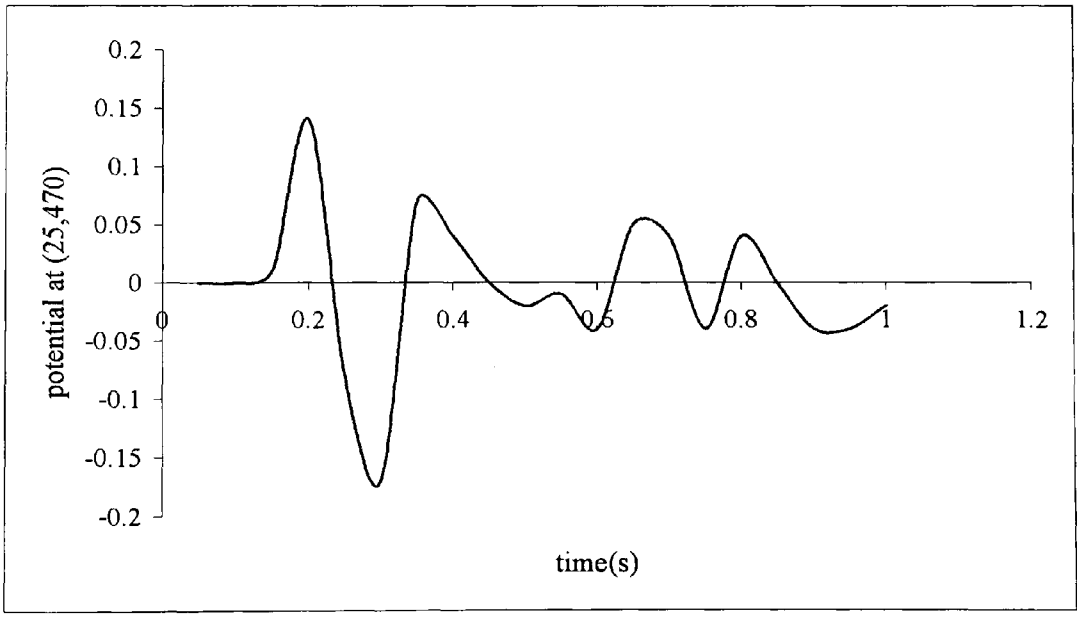

Figure 3.11g Potential ϕ versus time; for point (25,470) with $\beta^1 = \beta^2 = 15., (\Delta x)_1 = (\Delta x)_2 = 5$ m

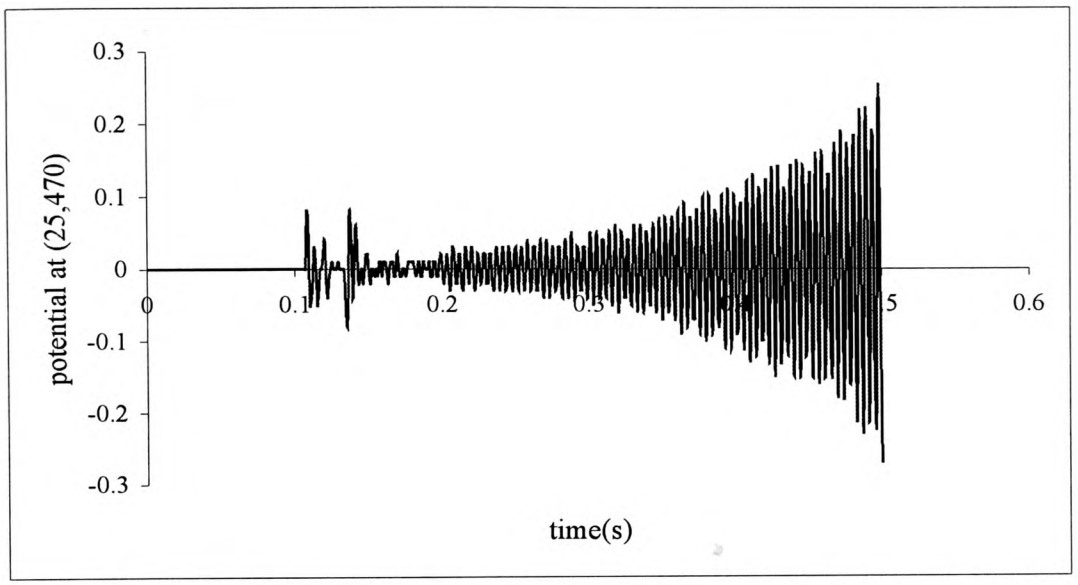

Figure 3.11h Potential ϕ versus time; for point (25,470) with $\beta^1 = 0.15$, $\beta^2 = 0.375$, $(\Delta x)_1 = 10$ m, $(\Delta x)_2 = 4$ m

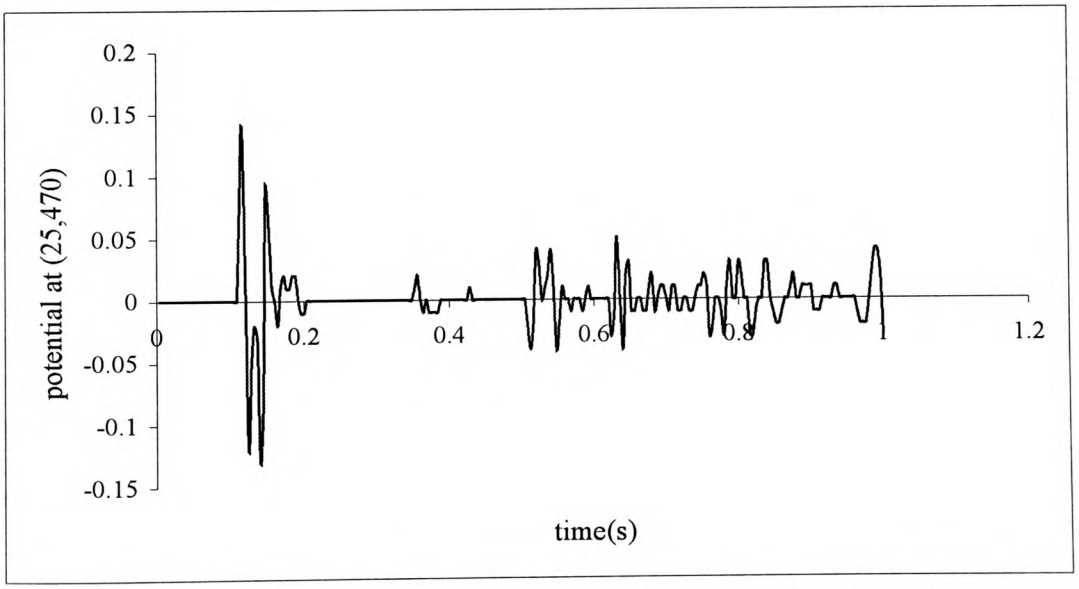

Figure 3.11i Potential ϕ versus time; for point (25,470) with $\beta^1 = 0.6$, $\beta^2 = 1.5$, $(\Delta x)_1 = 10$ m, $(\Delta x)_2 = 4$ m

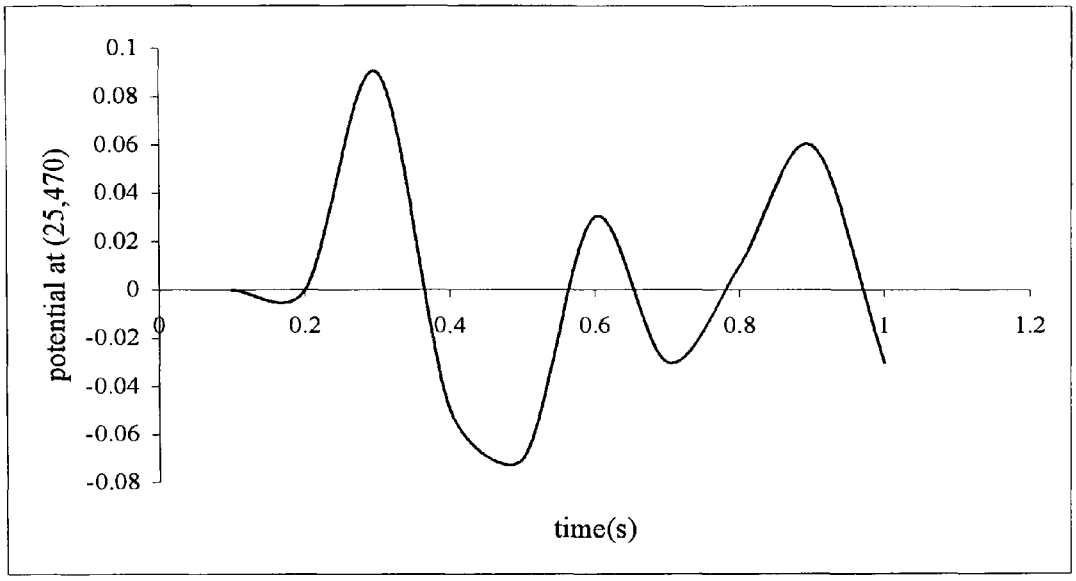

Figure 3.11j Potential ϕ versus time; for point (25,470) with $\beta^1 = 15.$, $\beta^2 = 37.5$, $(\Delta x)_1 = 10$ m, $(\Delta x)_2 = 4$ m

3.8 Interpretation of Seismograms

The traces recorded for each point are called a seismogram, and are calculated for internal points in the following sections and chapters. The seismogram can be classified, as experimental, real or synthetic depending on the data used is experimental, real field or numerical, respectively.

In considering the field data or experimental data that is collected and compared against a synthetic seismogram, there are many possible differences (White et al., 1987). The synthetic seismogram is created by controlling the reflectivity. The real field (or experimental) data is created by exploding dynamite, or by somehow exciting a point on or near the surface of the Earth, to create waves which travel into the Earth and are reflected back by the Earth's reflectivity.

Although the two dissimilar processes in the above often result in similar traces, in the literature, it is not common to compare them. Researchers often prefer two numerical (or theoretical) methods for their comparisons. This is perhaps because of the physical difficulties and the restrictions of numerical methods. Additional private communications with various researchers from other establishments were undertaken, in addition to the literature review, in order to look for additional, suitable experimental data. Their responses were similar to those observed here.

However, a real seismogram obtained by Brabham et al. (1999) will be used as a reference to show similarities between our synthetic seismograms and their real counterparts. For the sake of simplicity, only the surface of the field will be considered. Using this simplified surface, a 2D plane with only two layers, the wave equation is solved. All seismograms are produced synthetically in the following.

3.9 Results

In this section, the behaviour of the scalar wave through two-dimensional rock structures of finite and infinite extent is examined. However, the real data traces given for the field are in three dimensions. With the help of the two-dimensional main program (Dominguez, 1993), subprograms were produced to solve single medium and multimedia problems. Throughout this work for the solution of the problems, homogeneous boundary conditions are used for the external boundaries.

3.9.1 Comparison of a Real Field Result and a Numerical Result for the Simplified Surface

The seismological reaction of different rocks was investigated by Brabham et al. (1999). To achieve this, they nominated the Porth Neigwl in the Llyn Peninsula in the northwest

of Wales, UK. They also calculated the wave velocities, shown in Figure (3.12), for different types of rocks. To create the real seismograms, their geometry had a source 10-m from a 24-receiver spread (with a 2-m receiver spacing), and the signals were taken every 2-m along the boundary as the spread moved along simultaneously. With a 24-receiver system, their survey geometry allows a maximum mid point gather of some more traces which can be subsequently added to enhance weak reflection events. The real field reflections are seen in Figure (3.13). The reflections explain the heterogeneity of the field. According to the discontinuity of the material velocities, the reflections weaken gradually. More geological details can be found by referring to Brabham et al. (1999).

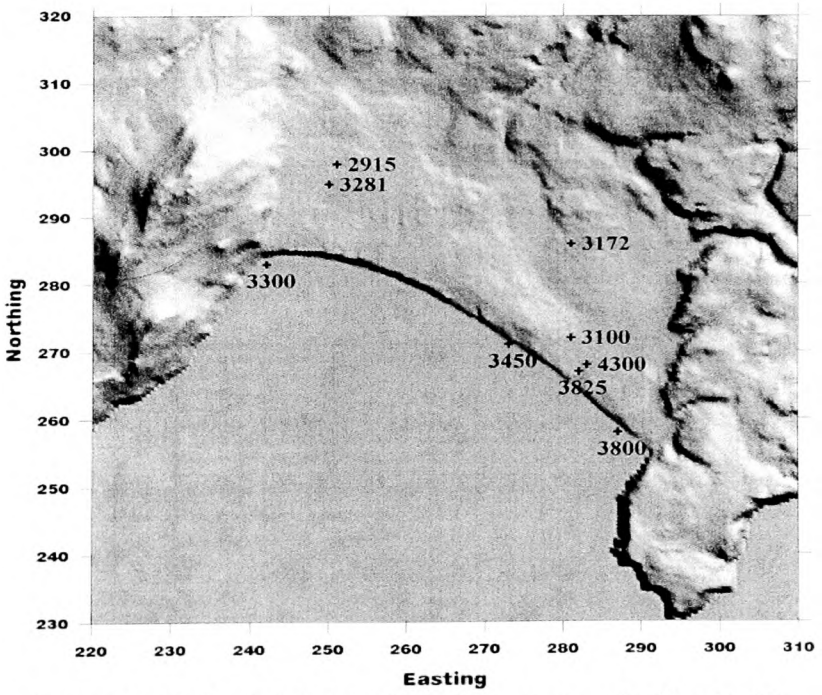

Figure 3.12 Spatial distribution of the wave velocities (m/s) given by Brabham et al. for the area in the Porth Neigwl

The work of Brabham et al. (1999) is used to produce a synthetic seismogram. This is achieved by considering only the flat surface of their region. It is noticed that the original geometry (see Figure 3.12) is heavily heterogeneous and very irregular. For simplicity, the geometry is modified so that only two homogenous layers are taken. This can be seen in Figure (3.14) where the source and receivers are positioned in a linear line 2-m below the boundary. The synthetic seismogram produced from the draft geometry is presented in Figure (3.15). Our aim in taking this draft geometry is to indicate the closeness of the synthetic and real seismograms, rather than a full comparison. This examination is similar to that for the synthetic seismograms which follow later.

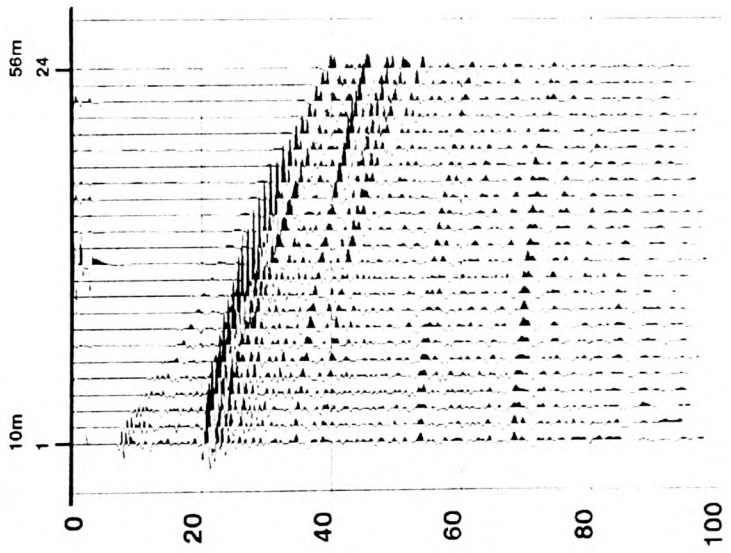

Figure 3.13 Brabham et al's seismogram illustrated as real field recording

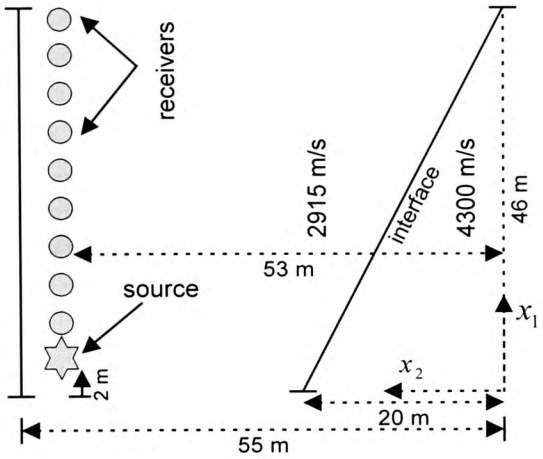

Figure 3.14 A simplified part of the field taken by Brabham et al. (1999) used to generate seismograms in the scalar BEM program

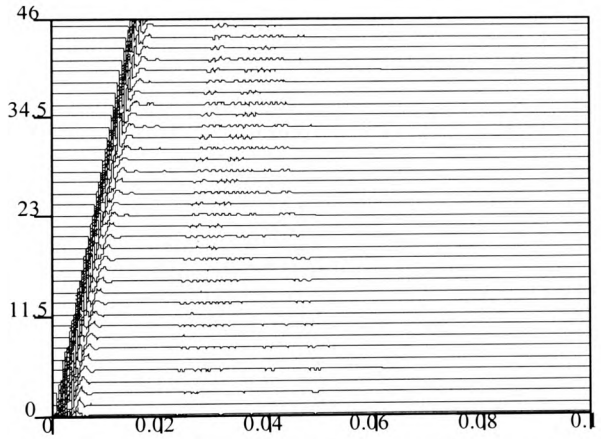

Figure 3.15 Synthetic seismogram generated from the BEM solution for the simplified field

3.9.2 Single Medium Results

Equation (3.1) is solved for a one-layered medium. The geometry of the problem was shown in Figure (3.9), and is considered for comparison with the definitive work of Reynolds (1978) who used the FDM to obtain similar results. The speed of wave propagation c is 1500 m/s for seawater. The source is located 35 m below the boundary

while the receivers are placed in a horizontal line at 10 m below the top boundary (see Figure 3.9).

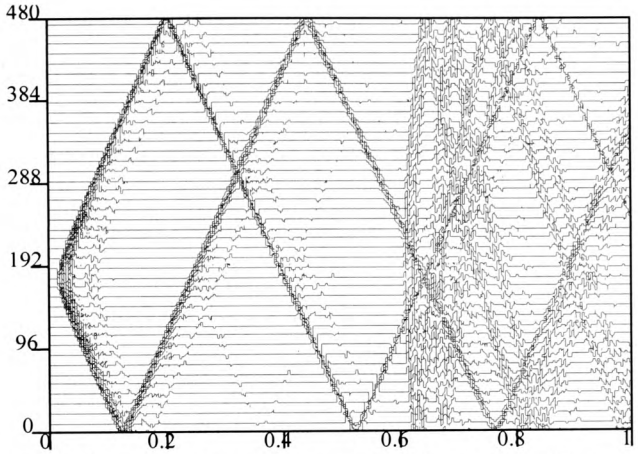

Figure 3.16 Seismogram generated from the BEM solution of the 2D scalar wave equation with the sides and the bottom Dirichlet boundary conditions and the top Neumann boundary

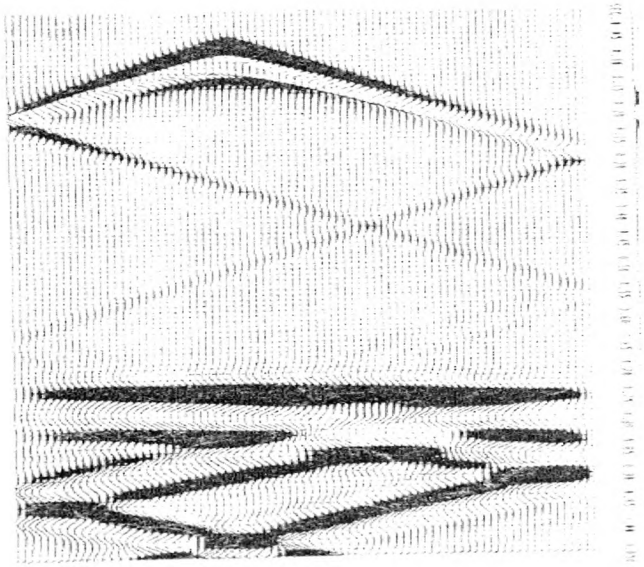

Figure 3.17 Reynolds' results with mostly Dirichlet boundary conditions

Here the topside is a free surface, $\partial\phi/\partial n = 0$, whilst the Dirichlet boundary conditions are used for the rest of the boundary as is shown in the geometrical definition (see Figure 3.10). Figure (3.16) shows the results, which contain large reflections from the side boundaries as can be seen from the criss-cross pattern. A very good qualitative agreement is obtained between Figures (3.16) and (3.17). The first wave becomes decreasingly weak as it moves further from the source. Snell's law explains why the reflections are weaker than the first wave. These observations hold for wave propagation problems in two and three dimensions.

The seismogram corresponds to the physical geometry of Figure (3.9), and has time (in seconds) on the horizontal axis and all displacement values received at the selected receiver points are on the vertical axis. The number of receivers is 95. The distance between the adjacent receiver points is equal. The vertical axis shows the length of topside of Figure (3.9) with its dimension being meters (m). To obtain this synthetic seismogram the boundary elements used are of the same size with 5 m and the total elapsed time is 1 s with 0.002 s the time increment. The source position is (180,445). In this work, the source is taken as an internal boundary, which is a small square (for three-dimensional geometries a small cube). The Dirichlet boundary condition is prescribed for the sides of the small square with length 2-m.

Reynolds' results are shown in Figure (3.17) rotated by 90 degrees. The results obtained from the BEM are in a very good qualitative agreement on comparison to those found by Reynolds (1978).

An infinity case of the physical geometry is shown by Figure (3.18) and the BEM results (Figure 3.19) obtained are compared to those found with the FDM by Reynolds (1978)

using his transparent boundary conditions to simulate a medium of infinite extent on the sides as shown in Figure (3.20) again. The BEM results give very good agreement with Reynolds' results. To display the results a MATHCAD program has been used.

In Figure (3.16), the first wave reaches the closest receiver at time 0.017 s. There is a weak wave appearing after the first wave. Another wave is detected at the receiver at about 0.3 s reflected from the source.

Registration of the waves reflected from the bottom starts at time 0.61 s and 0.7 s. The first one of these waves first travels towards the bottom and then comes back, while the latter first strikes the top side and travels in the same way as the first. In Figure (3.16) there are also some other reflected waves, arising immediately after 0.6 s. These come from the side boundaries.

In the case of the medium extending to infinity, after the first wave has arrived at the receiver after 0.017 s, the top boundary gives rise to a reflected wave which is received at 0.03 s.

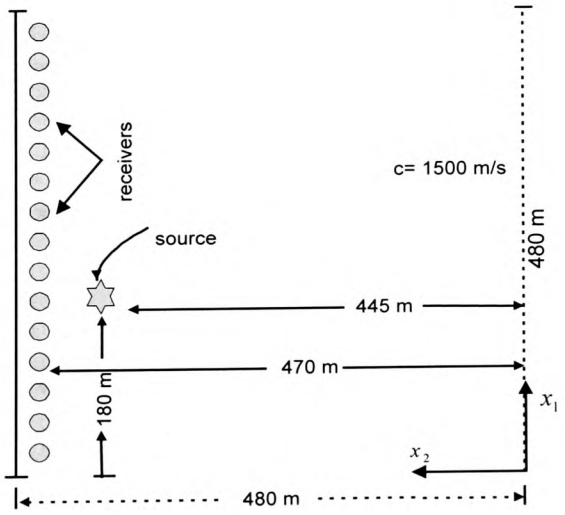

Figure 3.18 Physical model showing the medium of infinite extent used to generate seismograms in the scalar BEM program.

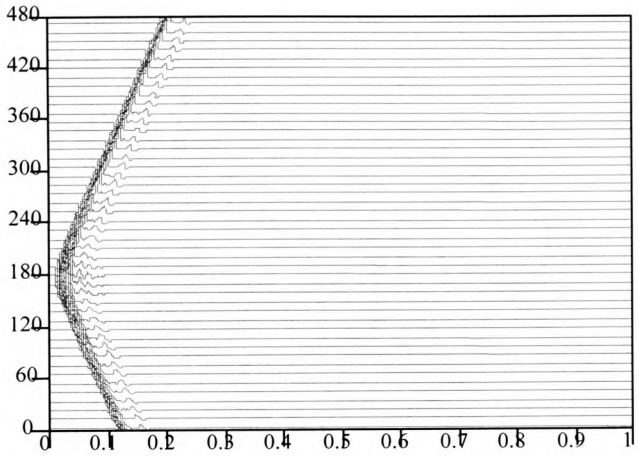

Figure 3.19 Synthetic seismogram generated from the BEM solution of the 2D scalar wave equation for the unbounded medium

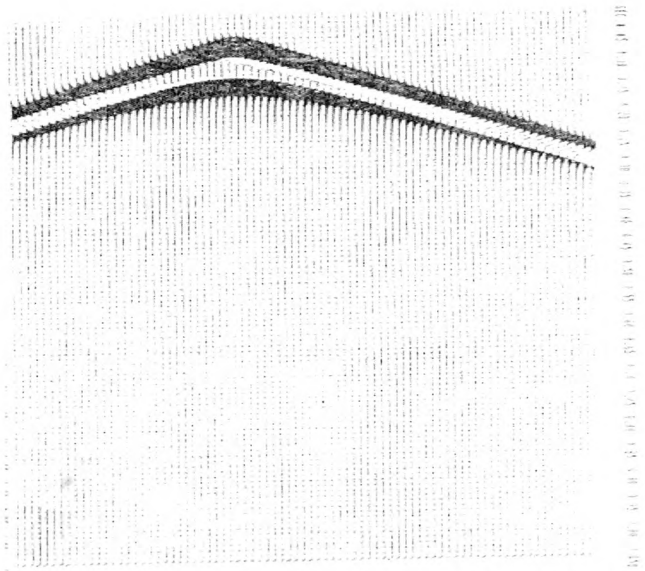

Figure 3.20 Reynolds' results with his transparent boundary conditions

3.9.3 Two Media Results

Consider now the case of two media with differing acoustic properties. With the help of the CONDPLAST (Dominguez, 1993), some programs were developed to incorporate two media for each medium as subprograms.

The material velocities as shown in Figure (3.21) are 1500 m/s for the upper seawater and 2130 m/s for the lower shale respectively, as given by Reynolds (1978). For the top boundary free surface (or Neumann) boundary conditions are used. Figure (3.22) displays the seismograms for the two media problem. The first interface wave is visible, whilst the second interface wave is not clearly visible. At the same time, the reflected waves from the sides are quite strong. Other waves appearing just after time 0.5 s and around 0.6 s reflect from the bottom boundary.

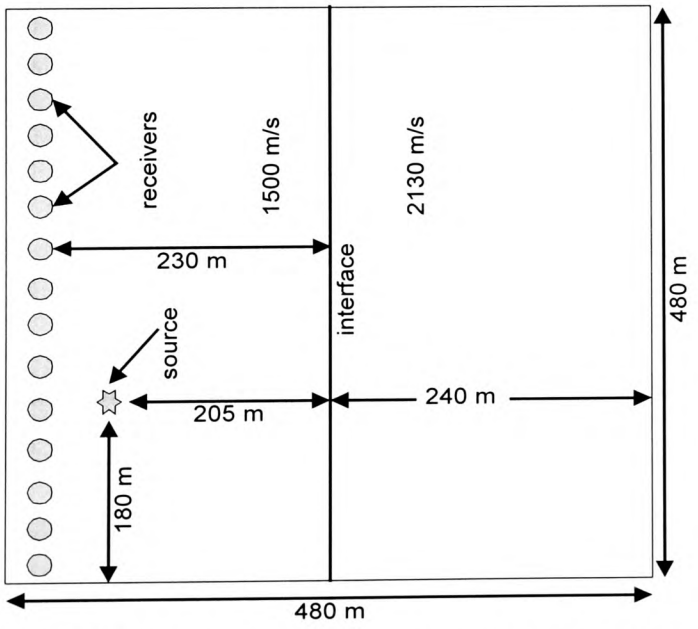

Figure 3.21 Physical model showing the geometry used to generate seismograms in the scalar BEM program for two media

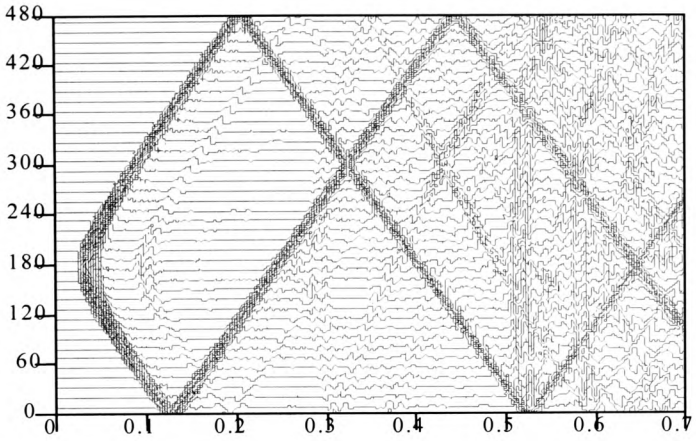

Figure 3.22 Synthetic seismogram generated from the BEM solution of the 2D scalar wave equation with the Dirichlet (for the top side- Neumann) boundary conditions for the two media

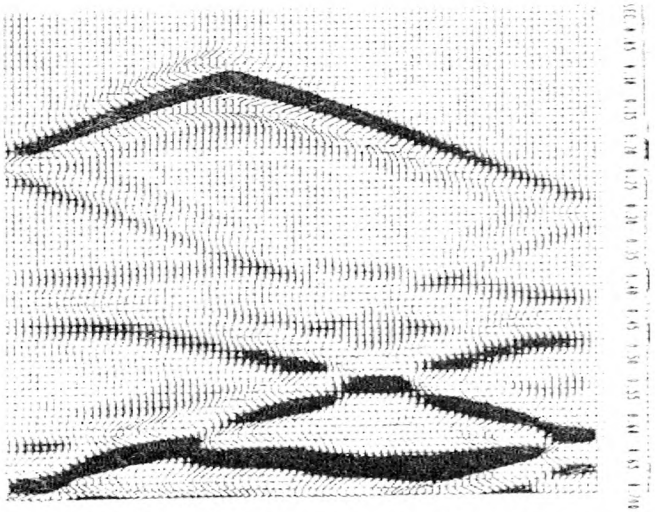

Figure 3.23 Reynolds' results with mostly Dirichlet boundary conditions

The physical medium of infinite extent is defined in Figure (3.24). For the medium of infinite extent, only the interface and top side are considered. Figures (3.22) and (3.25) are compared to the counterpart results (see Figures 3.23 and 3.26) found by Reynolds (1978).

As expected, Figure (3.25) shows no reflections from the sides and bottom, and is in very good agreement with Figure (3.26). There is a reflected wave immediately after the first

wave, coming from the source. It is also noted that the rising interface waves are visible. The first interface wave being received at 0.29 s, strikes the interface and then reflects. As for the second interface the wave appearing at time 0.336 s first hits the top side and then follows the same path as the first.

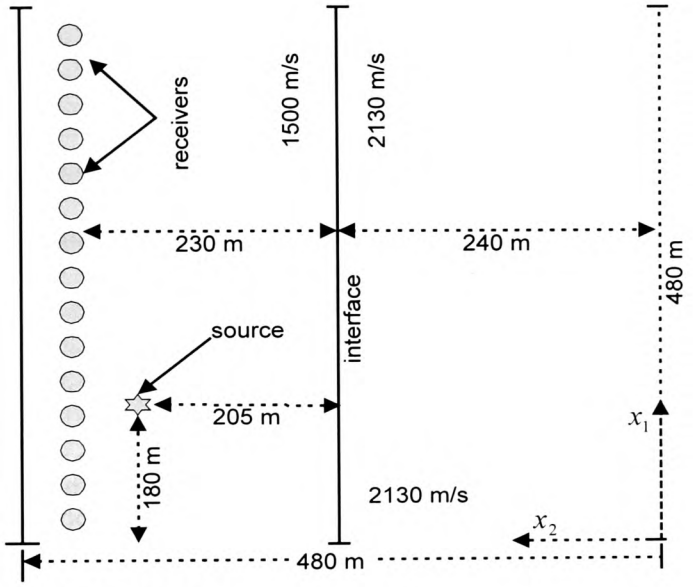

Figure 3.24 Physical model showing the geometry used to generate seismograms in the scalar BEM program a two-layered medium

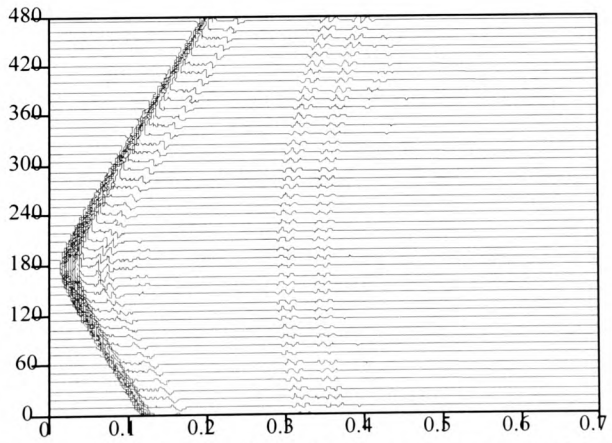

Figure 3.25 Synthetic seismogram generated from the BEM solution of the 2D scalar wave equation for the two-layered medium

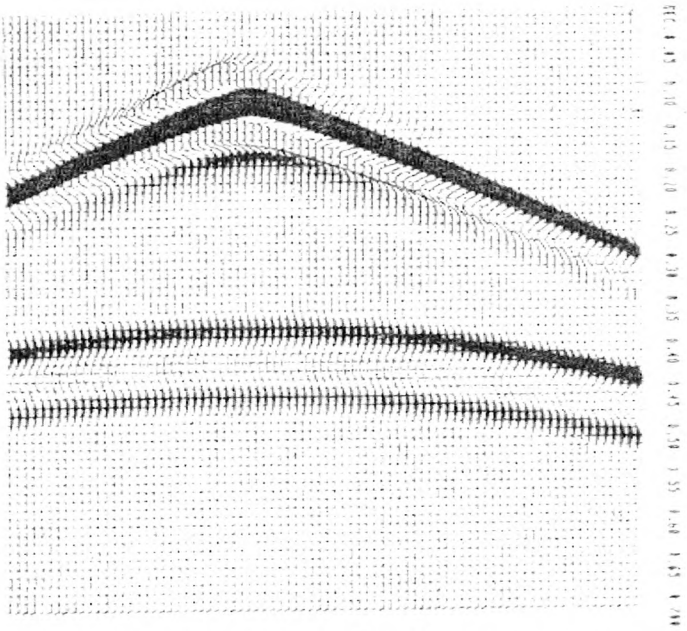

Figure 3.26 Reynolds' results with his transparent boundary conditions

3.9.4 Two Media Results (Salt Dome Model)

The salt dome geometry consists of two different media with the dome rising from the lower medium into the upper medium, as can be seen from the physical geometry (Figure 3.27). The material velocities are for the upper medium 2500 m/s, whilst for the bottom medium 4500 m/s. The source is located at (420,1790) and its size is 8 m. The element length, time increment and number of receivers used are 16 m, 0.01 s and 249 respectively. The Neumann boundary conditions are used for the top side of the salt dome geometry.

Figure (3.28) indicates the results obtained by using the BEM for the salt dome model. Figure (3.29) shows Demir's (1998) solutions obtained for the same model. The required

agreement between the results can be seen. The interface waves can be seen in Figure (3.28). The first wave reaches the closest receiver at 0.068 s, and just after the first wave there is a reflection wave, which arrives at 0.236 s, coming from the source. The first interface wave reaches the nearest receiver at 0.9 s, whilst the second interface wave arrives at 1.08 s for the flat part of the interface. Two interface waves from the dome can be seen from Figure (3.28), and the last part of the first wave arrives at 1.54 s and followed by the second wave, at time 1.67 s, reflected from the dome. This wave is slightly clearer in Demir's result. It is believed that the weakness of this wave can be redressed somewhat in the BEM, by increasing the size of the source taken.

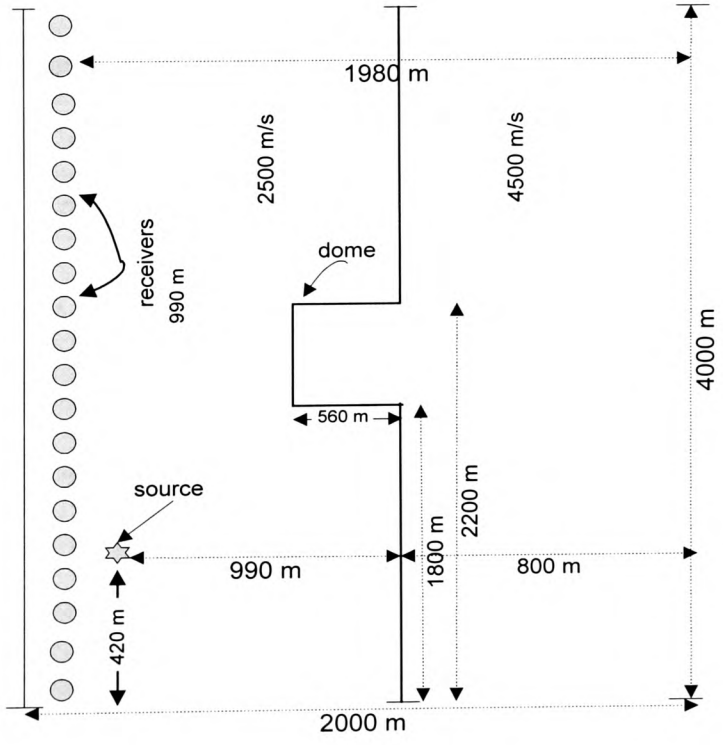

Figure 3.27 The geometry of the salt dome model used to generate seismograms in the scalar BEM program.

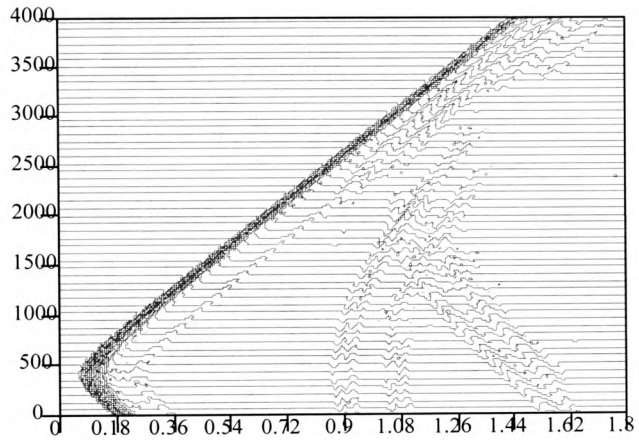

Figure 3.28 Synthetic seismogram generated from the BEM solution of the 2D scalar wave equation for the salt dome model

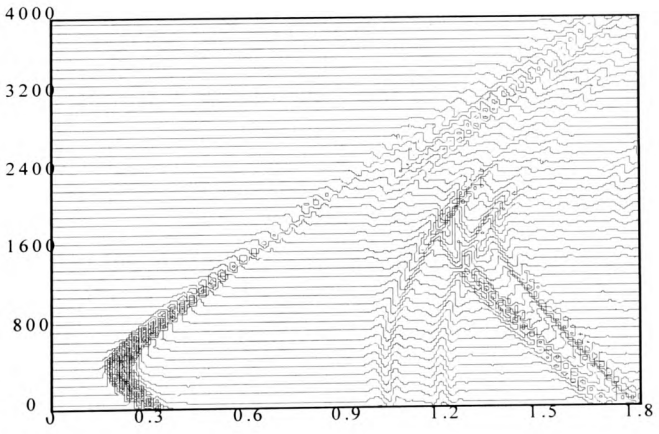

Figure 3.29 Demir's results generated from the FDM solutions of 2D scalar wave equation for the salt dome model

3.9.5 Multimedia Results

3.9.5.1 Flat-interfaced Three Media Model

In this section, multimedia problems are considered to model heterogeneous rocks. Three flat layers are used as is shown in Figure (3.30). The velocities are given from the top layer to the bottom layer respectively: 1500 m/s for sea-water, 2440 m/s for marls and 4000 m/s for granite. The multimedia geometry is shown in Figure (3.30). The co-ordinates of the source are (240,445) with size 5 m. The element size used is 5 m in this problem, and the results obtained are for the time increment 0.0025 s.

The results are depicted in a seismogram representation of the BEM solution. Figure (3.31) shows the result obtained by the BEM, incorporating the interfaces of the media. Two interface waves for each one can easily be seen from Figure (3.31). Figure (3.32) is used to show the travelling path of the wave. Looking at Figure (3.31) enables us to see a reflected wave w_2, immediately after the first wave w_1, originating from the boundary of the source.

For the first interface, the first wave w_3, which is received at 0.184 s, hits the first interface and comes back after the energy is partitioned. The second reflection wave w_4, for the first interface, hits the top edge and during the travelling strikes the interface and then reflects. This interface wave starts to reach the receivers at time 0.23 s.

For the second interface, the first wave w_6 is received at 0.32 s. This wave first hits the first interface, and then transmits into the second medium. When it encounters the second interface during the partition of energy, it then reflects and transmits back into the first interface again.

For the second interface, the second wave w_7 being received at about 0.36 s hits the top boundary, and then travels pursuing the same way as the wave w_6. It may be noticed that the last wave is very weak because the energy dissipates. The wave w_5 is a weak wave reflected from the source, and reaches the nearest receiver simultaneously with the reflected wave w_4.

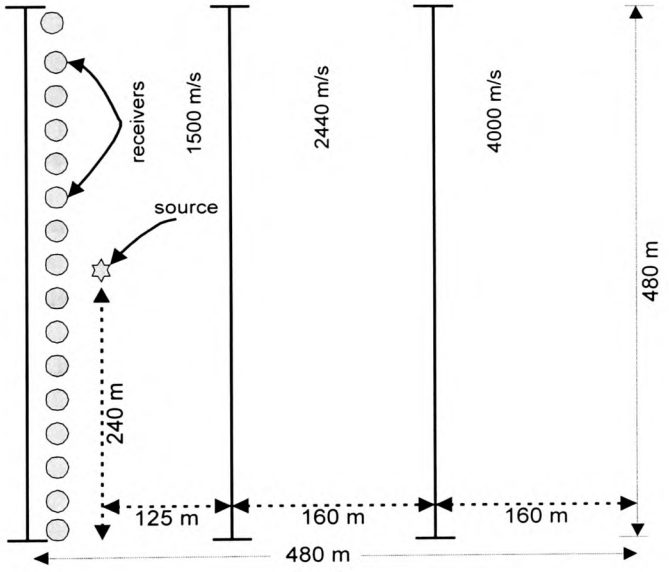

Figure 3.30 Physical model showing the geometry used to generate seismograms in the scalar BEM program for the multimedia

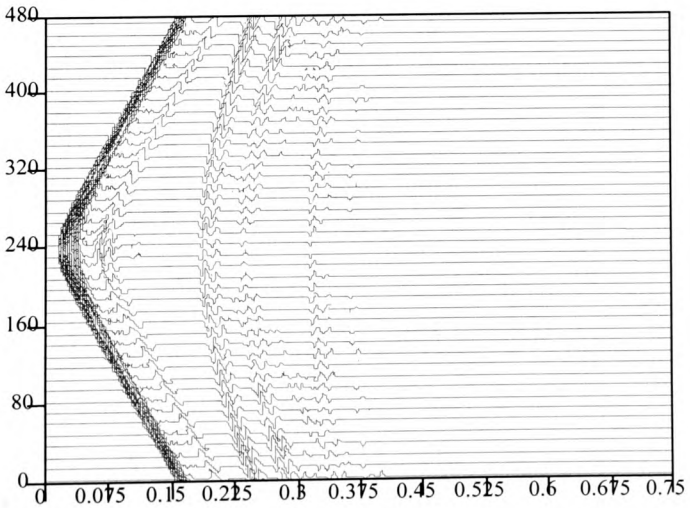

Figure 3.31 Synthetic seismogram generated from the BEM solution of the 2D scalar wave equation for the multimedia

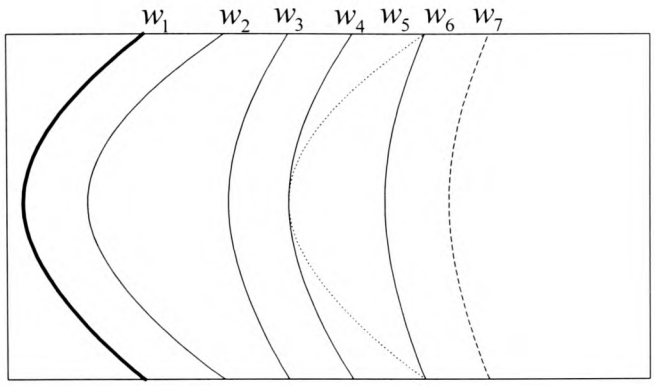

Figure 3.32 Indication of the waves in Figure 3.31

3.9.5.2 Flat and Non-flat-interfaced Model

An additional multimedia problem (see Figure 3.33) is now considered to extend the range of the method.

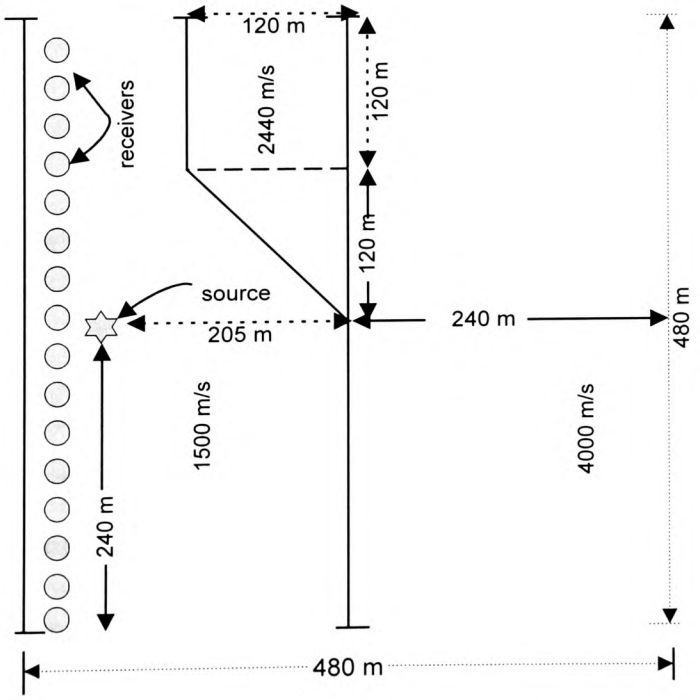

Figure 3.33 Physical model showing the geometry used to generate seismograms in the scalar BEM program for the multimedia

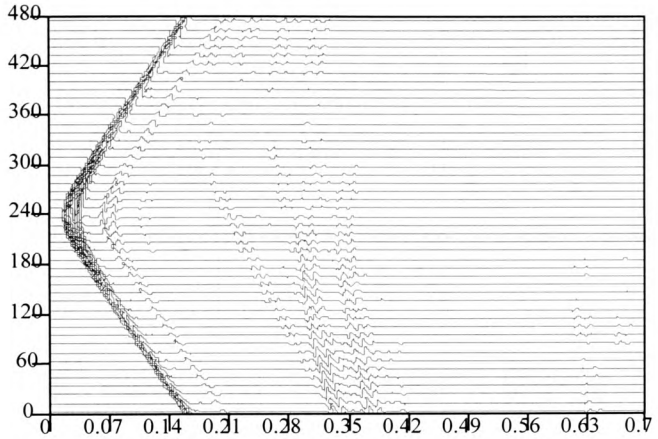

Figure 3.34 Synthetic seismogram generated from the BEM solution of the 2D scalar wave equation for the multimedia

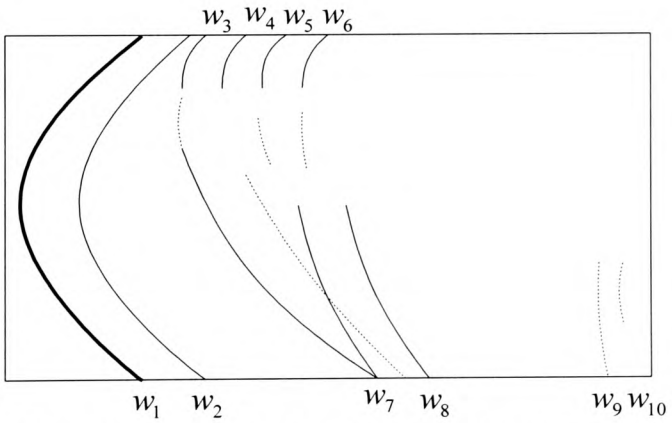

Figure 3.35 Indication of the waves in Figure 3.34

In this problem, three different media are considered with a different physical geometry, as is shown in Figure (3.33). The three media are shown in Figure (3.33) and the wave velocities are the same as in the previous three-layered problem. The source is located at (240,445) with size 4-m. The element length is 4-m (for the diagonal elements $3\sqrt{2}$ m.)

in this problem. Stable results are obtained for a time increment of 0.002 s (see Figure 3.34).

The results are shown in a seismogram representation of the BEM solution. Figure (3.34) shows the results obtained, and two interface waves for each can be seen from that figure. The first wave w_1 reaches the receivers at 0.017 s. The wave w_2, immediately after the first wave, is a reflection wave coming from the top boundary and reaches the closest receiver at 0.063 s.

The first interface wave w_3, which is received at 0.172 s, hits the first interface and then returns. The second wave w_4, impinges on the top side and during the travelling, strikes the interface and then reflects. This interface wave is registered at 0.21 s.

The first wave w_5, arrives at 0.272 s, first strikes the first interface, and then transmits into the second medium. When it arrives at the second interface during the partition of energy it then reflects and transmits back into the first interface again.

For the second interface, the second wave w_6 impinges on the top edge and then travels pursuing the same path as the wave w_5. This interface wave is received at 0.31 s.

It is noted that on the other side of the medium, the continuation of the waves w_3, w_4, w_5, w_6 can be seen even though they are very weak. On the other hand, the waves w_7 and w_8 are the first and second interface waves, respectively, while the weak waves w_9 and w_{10} are the repetition of the reflected interface waves from that interface.

3.9.5.3 Flat and Non-flat-interfaced Model

In this special case, another multimedia problem is considered. One of the interfaces is flat, whilst another is diagonal as can be seen in Figure (3.36). The velocities are given from the top layer to the bottom respectively: 1500 m/s, 2440 m/s and 4000 m/s. The co-ordinates of the source are (240,445), and its length is 4 m. The element length used is 4 m (for the diagonal elements $3\sqrt{2}$ m) in this problem. Stable results are obtained for 0.002 s as the time increment (see Figure 3.37).

The results are pictured, Figure (3.37), in a seismogram representation of the BEM solution.

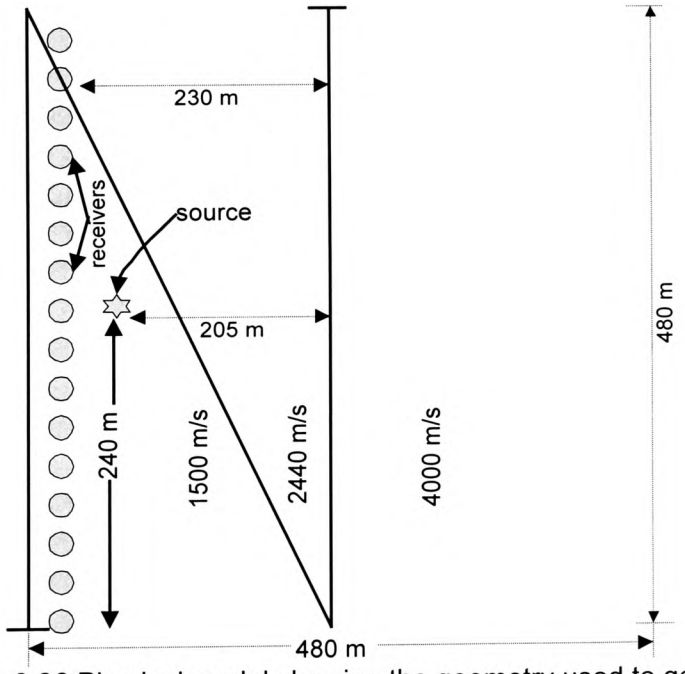

Figure 3.36 Physical model showing the geometry used to generate seismograms in the scalar BEM program for multimedia

An indication of the travel path of the wave in Figure (3.37) is given in Figure (3.38). The first wave w_1 reaches the receivers at about 0.017 s. The wave w_2, after the first wave, is a reflection wave caused by the source, and reaches the closest receiver at 0.063 s. For

the diagonal interface, the first interface wave w_3, which is received at about 0.12 s, strikes the diagonal interface and then reflects. The second interface wave w_4 to the diagonal interface, arrives at the top boundary and during the travelling strikes the diagonal interface and then reflects. The second diagonal interface wave, w_4, is received at about 0.14 s.

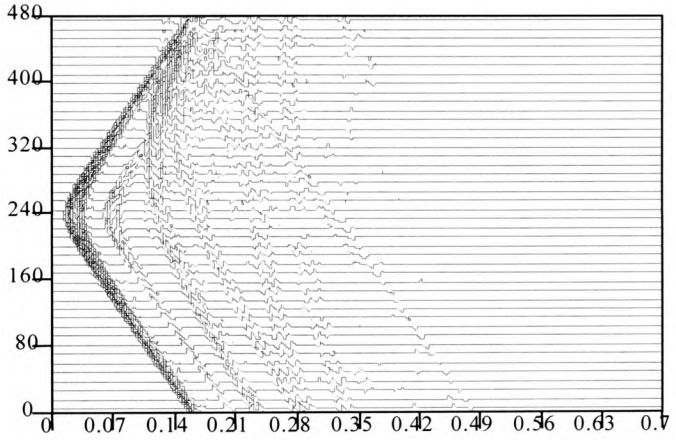

Figure 3.37 Synthetic seismogram generated from the BEM solution of the 2D scalar wave equation for the multimedia

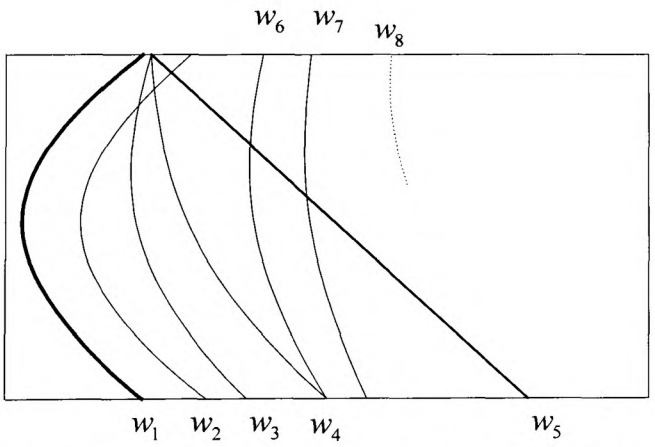

Figure 3.38 Indication of the waves in Figure 3.37

For the flat interface, the first wave w_6 is received at about 0.23 s. This wave first hits the diagonal interface and transmits into the second medium. When it encounters the flat

interface during the partition of energy, it here reflects and then transmits back into the diagonal interface again.

For the flat interface the second wave, w_7, hits the top boundary of the domain, and then travels following the same path as the wave w_6. This wave is received at about 0.28 s.

It may be seen that there is a reflection wave w_5 from the corner between the diagonal interface and top edge. At this corner, and at the other end of the diagonal, interface waves coincide (see Figures 3.37 and 3.38).

There are no results to compare with these, but the results obtained are as expected. Clearly, this indicates the versatility of the BEM.

3.10 Results of the Potential and Flux Distributions

In the previous section, the behaviour of waves through the same or different geophysical structures was observed at selected receiver points, and relevant results have been presented. In this section, potential and flux distributions through a region, in which the speed of wave propagation is taken as 1 m/s, are examined. In both methods, the distance Δx between adjacent nodes is the same and equal to 0.25 m.

Some numerical results to the domain considered have been obtained from the BEM for comparison with explicit FDM results. The relevant two-dimensional kernels obtained previously (see equations 3.73-3.75 and 3.78-3.82), are used together with prescribed boundary conditions. The geometry and boundary conditions for the following examples considered are shown in the corresponding figures, indicating the use of 16 boundary nodes and 8 quadratic elements for the isotropic homogeneous region of interest. The domains were divided into equal length element boundaries. The results obtained from

the two numerical methods are generally qualitatively and quantitatively the same. It is believed that the small differences in numbers are mainly due to differences in the numerical methods.

The unit square region has been considered to obtain the potential ϕ, boundary flux q and potential derivatives, qx_1 and qx_2, by handling the Neumann and Dirichlet boundary conditions. The graphical results obtained by these methods, using a MATHCAD program, are indicated in the following figures. The numbers on the contours show either the potential or its derivatives in the related figures. In the two time dependent applications considered; the first results are calculated by the BEM, and the second ones by the FDM.

Example 1*: Dirichlet Problem*

In the domain under consideration, the potential and potential derivatives have been calculated using both the BEM and the FDM.

The definition of the problem is given in Figure (3.39) and the results presented are for an elapsed time of 1 s. The time increment is taken as 0.333 s for the BEM (0.02 s for the FDM). The potential and its derivatives are obtained at the internal nodes and boundary nodes, where they are unknown.

Both graphs have significant similarities qualitatively and quantitatively. For instance, in both of them potential is symmetric with respect to axes of x_1 and x_2, and at the centre the potential takes a maximum value. The derivatives are zero along the lines $x_1 = 0.5$ and $x_2 = 0.5$, being skew symmetric with respect to these lines. It can also be seen that qx_1 and qx_2 have the same distribution when the qx_1 figure is rotated by 90 degrees clockwise.

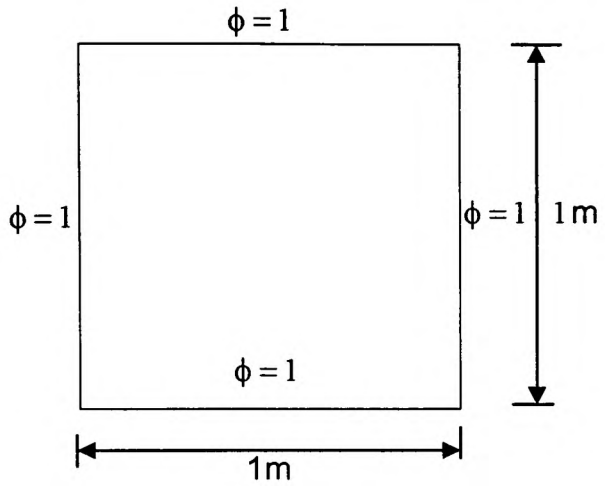

Figure 3.39 Definition of the first problem

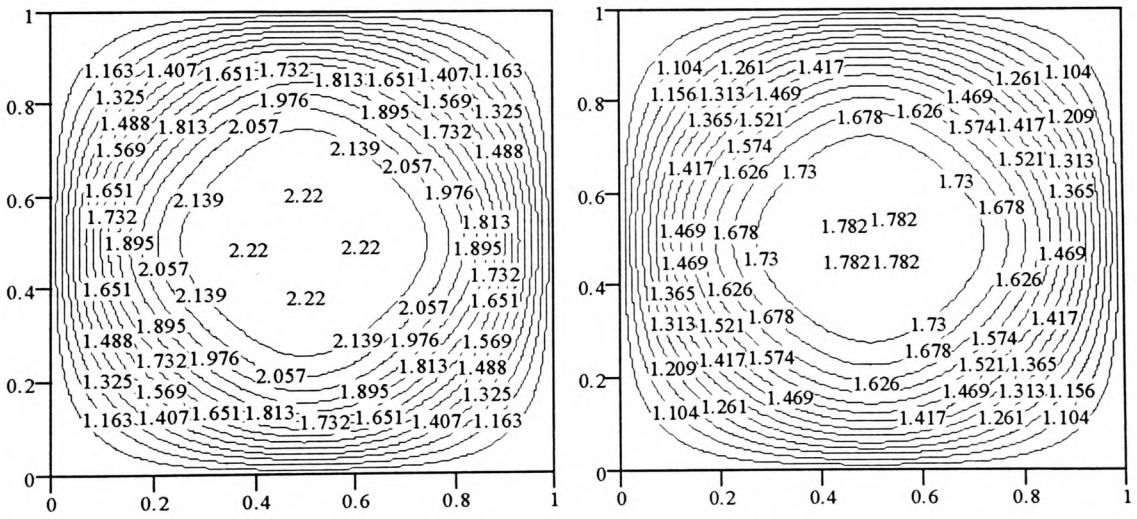

Figure 3.40a Potential distribution ϕ by the BEM and FDM, respectively

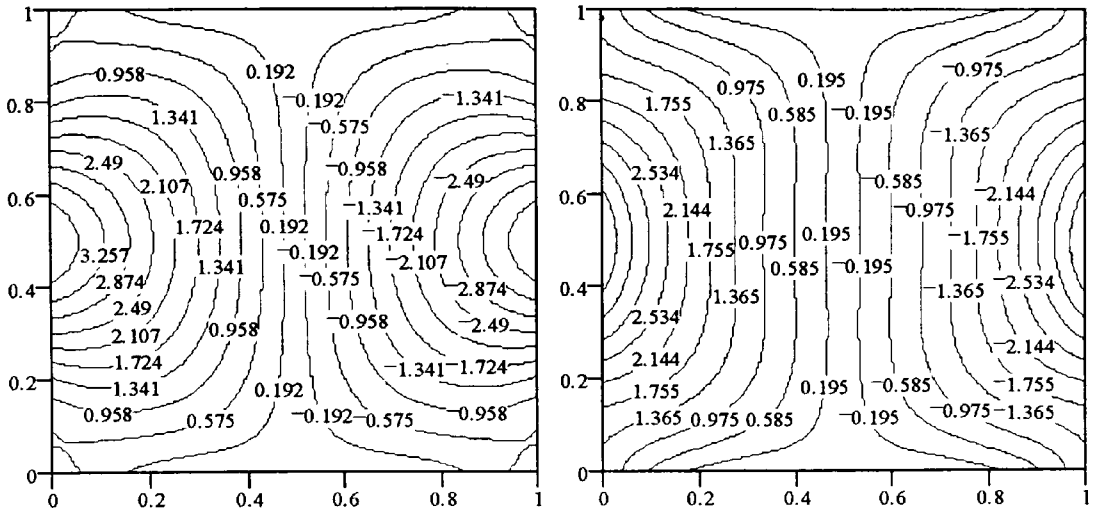

Figure 3.40b Flux distribution qx_1 by the BEM and FDM, respectively

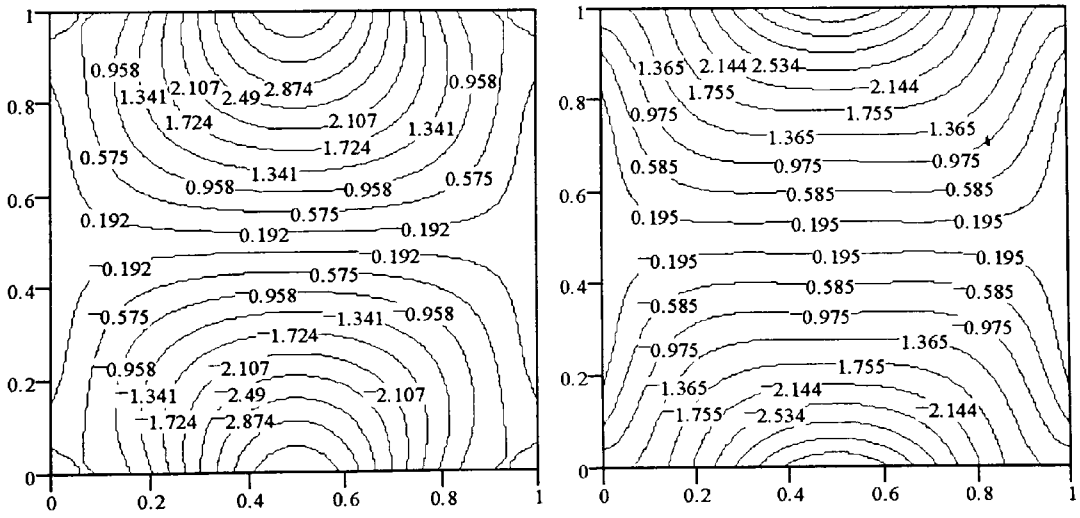

Figure 3.40c Flux distribution qx_2 by the BEM and FDM, respectively

Example 2: *Neumann Problem*

In this example, the same physical geometry is used as above with the boundary conditions being the Neumann boundary conditions defined in Figure (3.41). In this example, the time increment is taken as 0.02857 s for the BEM while 0.02 s for the FDM.

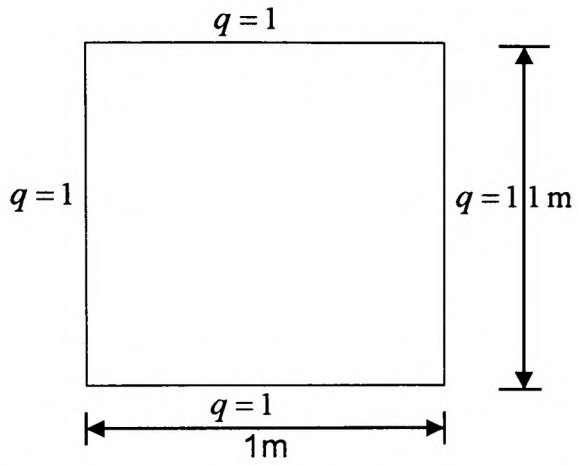

Figure 3.41 Definition of the second problem

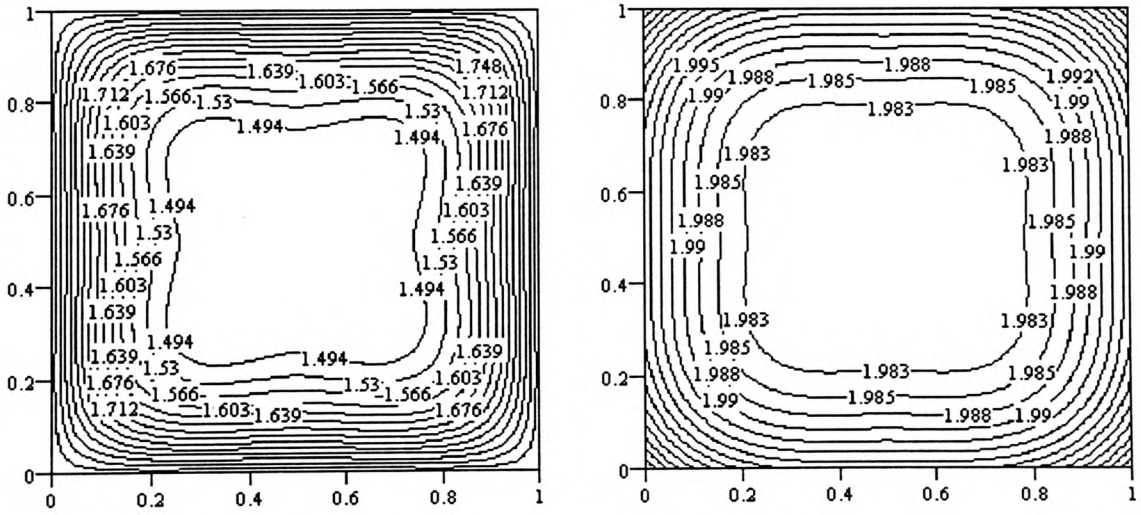

Figure 3.42a Potential distribution ϕ by the BEM and FDM, respectively

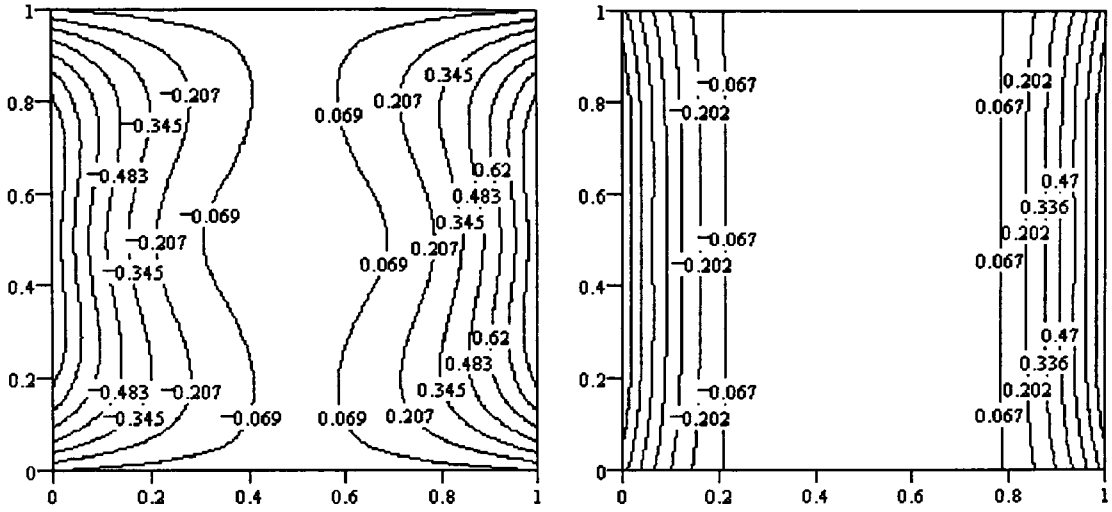

Figure 3.42b Flux distribution qx_1 by the BEM and FDM, respectively

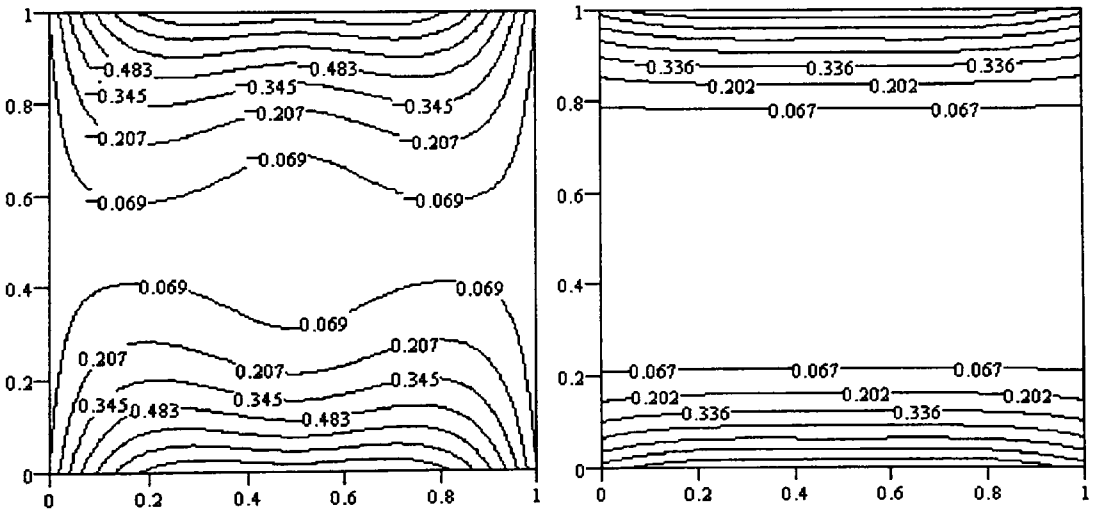

Figure 3.42c Flux distribution qx_2 by the BEM and FDM, respectively

In the domain considered, the unknown values of the potential and fluxes are calculated using the BEM and the FDM. There is good agreement between the BEM results and the FDM results given in Figure (3.42). The agreement is both quantitatively and qualitatively good. In both methods, on the two vertical and horizontal sides, the value of the potential is close to 2. In the two situations, the potential is symmetric with respect to the axes of x_1 and x_2, and the fluxes are skew symmetric with respect to related axes as expected. The corresponding derivatives are zero along the lines $x_1 = 0.5$ and $x_2 = 0.5$. The numbers on the graphs indicate the potential and potential derivatives in the related figures. The flux qx_2 has the same distribution as qx_1 when it is rotated by 90 degrees clockwise. As with the first example, the results are at time t=1.

3.11 Conclusions

In this chapter, the BEM method has been established for transient two-dimensional scalar wave problems. All result comparisons are good when comparison has been possible. Since, in nature, geomaterials are heterogeneous requiring much intricacy through dealing with the BEM, it is believed that the multimedia results presented here are worthy of mention.

The internal flux kernels are derived for the time functions used in this study. The results related to these kernels are presented.

Also, the above results give confidence for the work of the next chapter, where considerations are given to the problem of two-dimensional elastic wave propagation, which are similarly based but more involved.

CHAPTER 4

TWO DIMENSIONAL TIME DOMAIN BEM FOR ELASTIC WAVE PROPAGATION

4.1 Introduction

In the previous chapter, two-dimensional scalar wave problems have been dealt with generally, and the BEM solutions to the problems presented. Now, in this chapter, two-dimensional elastic wave problems are considered in the same fashion. Similar to the scalar case the fundamental solutions are considered. The two-dimensional time domain direct boundary element formulation for the elastic waves is set up in terms of the dynamic reciprocal relation applied to the fundamental solution and actual states. The BEM solutions of the Cauchy-Navier equations are presented and discussed for isotropic elastic homogeneous media as well as piecewise homogeneous media.

4.2 Integral Equation Formulation for Two Dimensional Elastic Wave

In Chapter 2 it was shown that the governing equation of the two-dimensional elastic wave equation through a homogeneous isotropic elastic body Ω enclosed by the boundary B is given by:

$$c_2^{\,2} u_{l,kk} + (c_1^{\,2} - c_2^{\,2}) u_{k,kl} + b_l = \ddot{u}_l \tag{4.1}$$

In this equation $\mathbf{u}$, $\mathbf{b}$ and $\ddot{\mathbf{u}}$ are functions of position and time, and represent the displacement, body force and acceleration vectors respectively, whilst c_1 and c_2 are the P and S-wave velocities. Stokes (1849) first obtained the solution to equation (4.1).

It follows that the fundamental solution satisfies equation (4.1) as follows:

$$c_2^{\,2} u^s_{l,kk} + (c_1^{\,2} - c_2^{\,2}) u^s_{k,kl} + b^s_l = \ddot{u}^s_l \tag{4.2}$$

4.2.1 Elastodynamic Fundamental Solutions

If a fundamental solution of the governing partial differential equation (4.1) is known, then the BEM can be applied. For the domain and its boundary, the fundamental solution is a solution that satisfies the governing equation (4.2) except at the load point where a removable singularity must exist. The solution results from a concentrated load applied at point $\mathbf{y}^i$ in the l direction where the body force is of the type (Eringen et al., 1975),

$$\rho b_k^s = \delta(t)\delta(\mathbf{x}-\mathbf{y}^i)\delta_{lk} \tag{4.3}$$

When the load is applied at point $\mathbf{y}^i$ at t=0, the displacements at point $\mathbf{x}$ in the infinite domain to the fundamental solution state can be written as:

$$u_k^s = u_{lk}^s e_l \tag{4.4}$$

and similarly the tractions

$$p_k^s = p_{lk}^s e_l \tag{4.5}$$

where e_l is the component of unit vector in the load direction. The effect of the load is propagated from the load point $\mathbf{y}^i$ to infinity. Here each component of the displacements u_k at point $\mathbf{x}$ due to a point load $\mathbf{y}^i$ along $\mathbf{e}$ can be written as equation (4.4) where u_{lk}^s shows the displacement along k due to the load point $\mathbf{y}^i$ in the l direction. Similarly p_{lk}^s represents the boundary traction along the k-direction due to the load point $\mathbf{y}^i$ in the l direction in equation (4.5).

Similar to the scalar case in Chapter 3, the two-dimensional fundamental solution for the elastic case is obtained (Achenbach, 1975, Eringen et al., 1975) from its three-dimensional counterpart by integrating along the third spatial direction. As can be seen

from Figure (3.1), the fundamental solution corresponds to an infinite line of forces along x_3 direction perpendicular to $x_1 - x_2$ plane. It follows that

$$u^s_{lk(2D)} = \int_{-\infty}^{\infty} u^s_{lk(3D)} dx_3 \tag{4.6}$$

where $u^s_{lk(3D)}$ denotes the three-dimensional fundamental solution displacements which will be derived in Chapter 6 and is given (e.g. Eringen et al., 1975, Achenbach,1975) by:

$$\begin{aligned} u^s_{lk(3D)} = \frac{1}{4\pi\rho R}\{&\frac{t}{R^2}(3R_{,l}R_{,k} - \delta_{lk})[H(t-\frac{R}{c_1}) - H(t-\frac{R}{c_1})] \\ &+ R_{,l}R_{,k}[\frac{1}{c_1^2}\delta(t-\frac{R}{c_1}) - \frac{1}{c_2^2}\delta(t-\frac{R}{c_2})] + \frac{\delta_{lk}}{c_2^2}\delta(t-\frac{R}{c_2})\} \end{aligned} \tag{4.7}$$

where R is the distance between the field point $\mathbf{x}$ and load point $\mathbf{y}^i$ in the three-dimensional fundamental solution. If R^2 is replaced by $r^2 + x_3^2$ in equation (4.7) using Figure (3.1), then in a similar way to the scalar case, equation (4.6) may be evaluated (Eringen et al., 1975) to give:

$$\begin{aligned} u^s_{lk} = \frac{1}{2\pi\rho}\{&\frac{1}{c_1}\frac{H(c_1t-r)}{r^2}[r_{,l}r_{,k}(2R_1 + \frac{r^2}{R_1}) - R_1\delta_{lk}] \\ &- \frac{1}{c_2}\frac{H(c_2t-r)}{r^2}[r_{,l}r_{,k}(2R_2 + \frac{r^2}{R_2}) - (2R_2 + \frac{r^2}{R_2})\delta_{lk}]\} \end{aligned} \tag{4.8}$$

where $R_\alpha = \sqrt{c_\alpha^2 t^2 - r^2}$ and r is the distance from the load point $\mathbf{y}^i$ to any point under consideration, for the two-dimensional fundamental solution, and H is the Heaviside function. It is important to recognise that the field point $\mathbf{x}$ and load point $\mathbf{y}^i$ are in two dimensions for equation (4.8) whilst they are in three dimensions for equation (4.7).

The Stokes' tensor u_{lk}^{s} represents the displacement component in the k-direction at time t and position $\mathbf{x} = (x_1, x_2)$ due to a concentrated load acting in the l-direction at point $\mathbf{y}^i$ at time τ. When the load is applied at τ the variable t in the fundamental solution is replaced by $t-\tau$ when applying the Riemann convolution. Thus, equation (4.8) can be written as:

$$u_{lk}^{s} = \frac{1}{2\pi\rho}\{\frac{1}{c_1}\frac{H[c_1(t-\tau)-r]}{r^2}[r_{,l}r_{,k}(2R_1+\frac{r^2}{R_1})-R_1\delta_{lk}]$$

$$-\frac{1}{c_2}\frac{H[c_2(t-\tau)-r]}{r^2}[r_{,l}r_{,k}(2R_2+\frac{r^2}{R_2})-(2R_2+\frac{r^2}{R_2})\delta_{lk}]\} \qquad (4.9)$$

$$= h_{lk}^{(1)}H[c_1(t-\tau)-r]+h_{lk}^{(2)}H[c_2(t-\tau)-r] = u_{lk}^{s(1)}+u_{lk}^{s(2)}$$

with $R_\alpha = \sqrt{c_\alpha^2(t-\tau)^2 - r^2}$.

As was done for the scalar case in Chapter 3, the Hadamard's method of descent is used to evaluate the two-dimensional fundamental solution from the three-dimensional fundamental solution.

The displacement at $\mathbf{x}$ produced by the load at $\mathbf{y}^i$ is equal to the displacement at $\mathbf{y}^i$ produced by the same load at $\mathbf{x}$, that is $u_{lk}^{s}(\mathbf{x},t;\mathbf{y}^i,\tau) = u_{lk}^{s}(\mathbf{y}^i,t;\mathbf{x},\tau)$.

As can be seen from the fundamental solution the disturbance emitted initially from the load point $\mathbf{y}^i$ is received at point $\mathbf{x}$ any time after $t = r/c_1$ (Eringen et al., 1975).

The stress tensor can be obtained from equation (4.8) using Hooke's law

$$\sigma_{km}^{s} = \rho(c_1^2 - 2c_2^2)u_{j,j}^{s}\delta_{km} + \rho c_2^2(u_{k,m}^{s} - u_{m,k}^{s}) \qquad (4.10)$$

When a load point is applied in the 'l' direction the 'km' component of the stress tensor can be obtained from

$$\sigma^s_{km} = \sigma^s_{lkm} e_l \tag{4.11}$$

In addition the stress tensor may be obtained using similar methods. Since the tensor is obtained as tractions on the boundary it is necessary to find the boundary tractions. Now the tractions on a boundary point, once a load is applied in the normal **n** direction, may be computed as:

$$p^s_{lk} = \sigma^s_{lkm} n_m \tag{4.12}$$

Thus the fundamental traction solutions may be given (e.g. Eringen et al., 1975) by:

$$p^s_{lk} = \frac{1}{2\pi\rho}\{-\frac{H(c_1 t - r)}{c_1}[b_{lk}(2R_1 + \frac{r^2}{R_1}) + d_{lk}\frac{r^3}{R_1^3}] + \frac{\delta(c_1 t - r)}{c_1} d_{lk}(2R_1 + \frac{r^2}{R_1})$$

$$+\frac{H(c_2 t - r)}{c_2}[a_{lk}\frac{r}{R_2^3} + b_{lk}(2R_2 + \frac{r^2}{R_2}) + d_{lk}\frac{r^3}{R_1^3}] - \frac{\delta(c_2 t - r)}{c_2}[\frac{a_{lk}}{R_2} + d_{lk}(2R_2 + \frac{r^2}{R_2})]\} \tag{4.13}$$

where

$$R_\alpha = \sqrt{c_\alpha^2 t^2 - r^2}$$

$$a_{lk} = \mu(\frac{\lambda}{\mu} n_k r_{,l} + \delta_{lk}\frac{\partial r}{\partial n} + n_l r_{,k})$$

$$b_{lk} = \frac{-2\mu}{r^3}(n_k r_{,l} + n_l r_{,k} + \delta_{lk}\frac{\partial r}{\partial n} - 4\frac{\partial r}{\partial n} r_{,l} r_{,k}) \tag{4.14}$$

$$d_{lk} = \frac{-2\mu}{r^2}(\frac{\lambda}{2\mu} n_k r_{,l} + \frac{\partial r}{\partial n} r_{,l} r_{,k})$$

In the above $\frac{\partial r}{\partial n} = r_{,i} n_i$ with $r_{,k} \equiv \frac{\partial r}{\partial x_k}$.

The two-dimensional fundamental solutions have the following properties (Aki et al., 1980, Eringen et al., 1975):

i) Causality:

$$u^s_{lk}(\mathbf{x}, t; \mathbf{y}^i, \tau) = 0 \quad \text{if} \quad c_1(t - \tau) < r$$

which means that the field point can feel the effects of the load only after the load has been applied.

ii) Reciprocity:

$$u_{lk}^{s}(\mathbf{x},t;\mathbf{y}^{i},\tau)=u_{lk}^{s}(\mathbf{y}^{i},-\tau;\mathbf{x},-t)$$

This property is the same as the scalar case.

iii) Time translation:

$$u_{lk}^{s}(\mathbf{x},t+t_1;\mathbf{y}^{i},\tau+t_1)=u_{lk}^{s}(\mathbf{x},t;\mathbf{y}^{i},\tau)$$

This property is also the same as the scalar case.

Note that the fundamental traction solution obeys the above properties. It is also noted that the fundamental displacement solution is symmetric in terms of tensors whilst the fundamental traction solution is not.

4.2.2 Integral Representation

The elastodynamic reciprocal relation was obtained between the two states in Chapter 2. If the body forces (4.3) is applied at the interior load point $\mathbf{y}^{i}$, then by using the sifting property of the Dirac delta function, equation (2.47) may be transformed into

$$u_l^{i}(\mathbf{y}^{i},t)=\int_B[(u_{lk}^{s}*p_k)-(u_k*p_{lk}^{s})](\mathbf{x},t)dB$$

$$+\int_\Omega\rho[(u_{lk}^{s}*b_k)(\mathbf{x},t)+u_{0k}(\mathbf{x})\dot{u}_{lk}^{s}(\mathbf{x},t)+v_{0k}(\mathbf{x})u_{lk}^{s}(\mathbf{x},t)]d\Omega \qquad (4.15)$$

Assume vanishing body forces and initial rest, namely $b_k=0$, $u_{0k}=0$, $v_{0k}=0$. Then equation (4.15) reduces to

$$u_l^{i}(\mathbf{y}^{i},t)=\int_B(u_{lk}^{s}*p_k)(\mathbf{x},t)dB-\int_B(u_k*p_{lk}^{s})(\mathbf{x},t)dB \qquad (4.16)$$

Using the time convolution, equation (4.16) can be written explicitly as:

$$u_l^i(\mathbf{y}^i,t) = \int_0^{t^+}\int_B u_{lk}^s(\mathbf{x},t-\tau,\mathbf{y}^i)p_k(\mathbf{x},\tau)dBd\tau - \int_0^{t^+}\int_B u_k(\mathbf{x},\tau)p_{lk}^s(\mathbf{x},t-\tau,\mathbf{y}^i)dBd\tau \qquad (4.17)$$

where the t^+ value is the same as in the scalar case. The representation (4.17) expresses the displacement value u_l at the interior point $\mathbf{y}^i$ at time t in terms of boundary displacements and tractions at time τ.

4.2.3 Boundary Integral Equation

Now the time-domain boundary integral equation can be obtained by combining the two states of the governing differential equation of motion (4.1). The singular behaviour of the fundamental solution at $\mathbf{y}^i = \mathbf{x}$ means that the integral representation cannot be taken directly on the boundary B. Therefore the boundary integral equations are established through the usual limiting process, following the same lines as in the scalar case. The equality of the singularities of the dynamic and static fundamental solutions at $\mathbf{y}^i = \mathbf{x}$ plays an essential role in the limiting process to be performed.

Thus, from Figure (4.1), the integrals in equation (4.17) can be written as the limiting process when $\varepsilon \to 0$ for boundaries B_ε and B,

$$I_1 = \int_B (u_{lk}^s * p_k)(\mathbf{x},t)dB = \lim_{\varepsilon\to 0}\int_{B-B_\varepsilon}(u_{lk}^s * p_k)(\mathbf{x},t)dB + \lim_{\varepsilon\to 0}\int_{B_\varepsilon}(u_{lk}^s * p_k)(\mathbf{x},t)dB \qquad (4.18)$$

and similarly for the second integral

$$I_2 = \int_B (p_{lk}^s * u_k)(\mathbf{x},t)dB = \lim_{\varepsilon\to 0}\int_{B-B_\varepsilon}(p_{lk}^s * u_k)(\mathbf{x},t)dB + \lim_{\varepsilon\to 0}\int_{B_\varepsilon}(p_{lk}^s * u_k)(\mathbf{x},t)dB \qquad (4.19)$$

In order to simplify the second integrals in the right hand side of equations (4.18) and

(4.19), consider the fundamental solutions of the static counterpart of equation (4.1) are (Bonnet, 1998, Brebbia et al., 1992, Paris, 1997) given by:

$$u_{lk}^{s1} = \frac{1}{8\pi\mu(1-\upsilon)}[(4\upsilon-3)\delta_{lk}\ln r + r_{,l}r_{,k}] \tag{4.20}$$

$$p_{lk}^{s1} = -\frac{1}{4\pi(1-\upsilon)r}\{[(1-2\upsilon)\delta_{lk} + 2r_{,l}r_{,k}]\frac{\partial r}{\partial n} + (1-2\upsilon)(n_l r_{,k} - n_k r_{,l})\} \tag{4.21}$$

where u_{lk}^{s1} and p_{lk}^{s1} are the displacement and traction fundamental solutions, for the elastostatic case.

The last integrals on the right hand side of equations (4.20) and (4.21) are of the same type as in the elastostatic case when $t \to 0$ and $r \to 0$ (Dominguez, 1993, Bonnet, 1998). Therefore, the final integrals in equations (4.17) and (4.18) are evaluated by replacing u_{lk}^{s} and p_{lk}^{s} with u_{lk}^{s1} and p_{lk}^{s1}, respectively.

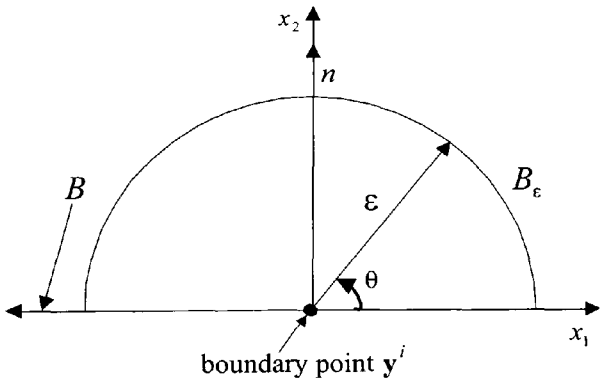

Figure 4.1 Illustration of the Cauchy principle integral

Thus, for the small semi-circle, when $\varepsilon \to 0$, the final integrals in equations (4.17) and (4.18) are:

$$\lim_{\varepsilon\to 0} p_k^i \int_{B_\varepsilon} u_{lk}^{s1} dB = \lim_{\varepsilon\to 0} \frac{1}{8\pi(1-\upsilon)\mu} \int_{B_\varepsilon} [(4\upsilon-3)\delta_{lk} \ln r + r_{,l} r_{,k}] dB \tag{4.22}$$

$$\lim_{\varepsilon\to 0} u_k^i \int_{B_\varepsilon} p_{lk}^{s1} dB = \lim_{\varepsilon\to 0} u_k^i \int_{B_\varepsilon} -\frac{1}{4\pi(1-\upsilon)r} \{[(1-2\upsilon)\delta_{lk} + 2r_{,l} r_{,k}] \frac{\partial r}{\partial n} + (1-2\upsilon)(n_l r_{,k} - n_k r_{,l})\} dB \tag{4.23}$$

With the help of Figure (4.1) it follows that

$$\varepsilon \equiv r, \qquad \frac{\partial r}{\partial n} = 1, \qquad dB = \varepsilon d\theta, \qquad r_{,i} = n_i$$

$$r_{,1} = \cos\theta, \qquad r_{,2} = \sin\theta, \qquad n_l r_{,k} - n_k r_{,l} = 0 \tag{4.24}$$

The integrals then, for the case of $l = k = 1$ are:

$$\lim_{\varepsilon\to 0} p_1^i \int_{B_\varepsilon} u_{11}^{s1} dB = \frac{1}{8\pi(1-\upsilon)\mu} \lim_{\varepsilon\to 0} p_1^i \int_0^\pi [(4\upsilon-3)\ln\varepsilon + \cos^2\theta]\varepsilon d\theta = 0 \tag{4.25}$$

and

$$\lim_{\varepsilon\to 0} u_1^i \int_{B_\varepsilon} p_{11}^{s1} dB = \lim_{\varepsilon\to 0} u_1^i \int_0^\pi -\frac{1}{4\pi(1-\upsilon)\varepsilon} [(1-2\upsilon) + 2\cos^2\theta]\varepsilon d\theta = -\frac{1}{2} u_1^i \tag{4.26}$$

Taking $l = k = 2$, the same results are obtained as above, and for the case of $l \neq k$, both integrals give zero. So, the above calculations can be rewritten by:

$$\lim_{\varepsilon\to 0} u_k^i \int_{B_\varepsilon} p_{lk}^{s1} dB = -\frac{1}{2} \delta_{lk} u_k^i \tag{4.27}$$

Using the calculations (4.25) and (4.27), the limiting form when $\varepsilon \to 0$ of the identities (4.18) and (4.19) are:

$$I_1 = \int_B (u_{lk}^s * p_k)(\mathbf{x}, t) dB \tag{4.28}$$

$$I_2 = \int_B (p_{lk}^s * u_k)(\mathbf{x},t)dB - \frac{1}{2}\delta_{lk}u_k^i(\mathbf{y}^i,t)$$
$$= \int_B (p_{lk}^s * u_k)(\mathbf{x},t)dB - \frac{1}{2}u_l^i(\mathbf{y}^i,t) \tag{4.29}$$

Note that the integral investigated (4.18) is not affected by the singularity at the point $\mathbf{y}^i$, because the corresponding integral is equal to zero. Also note that the time convolution has not been considered in equations (4.22) and (4.23) since the kernels are static. Thus the actual states of the displacement $u_k(\mathbf{x},t)$ and traction $p_k(\mathbf{x},t)$ are taken as constant during the integration.

From equations (4.18), (4.19), (4.28) and (4.29), the integral equation required for a boundary point is:

$$\frac{1}{2}\delta_{lk}u_k^i(\mathbf{y}^i,t) = \int_B (u_{lk}^s * p_k)(\mathbf{x},t)dB - \int_B (p_{lk}^s * u_k)(\mathbf{x},t)dB \tag{4.30}$$

where the integrals have the sense of a Cauchy principal value.

Thus, the integral representation for the two-dimensional elastodynamic problem for any point is:

$$\alpha_{lk}^i u_k^i = \int_B (u_{lk}^s * p_k)(\mathbf{x},t)dB - \int_B (p_{lk}^s * u_k)(\mathbf{x},t)dB \tag{4.31}$$

where

$$\alpha_{lk}^i = \begin{cases} \delta_{lk} & \text{if} \quad \mathbf{y}^i \in \Omega \\ \frac{1}{2}\delta_{lk} & \text{if} \quad \mathbf{y}^i \in B \\ 0. & \text{if} \quad \mathbf{y}^i \notin (\Omega \cup B) \end{cases} \tag{4.32}$$

By means of the convolution equation (4.31) may be written explicitly as

$$\alpha_{lk}^{i} u_k^i(\mathbf{y}^i,t) = \int_0^{t^+}\int_B u_{lk}^s(\mathbf{x},t-\tau;\mathbf{y}^i)p_k(\mathbf{x},\tau)dBd\tau - \int_0^{t^+}\int_B p_{lk}^s(\mathbf{x},t-\tau;\mathbf{y}^i)u_k(\mathbf{x},\tau)dBd\tau \qquad (4.33)$$

where t^+ value is the same as in the scalar case. In the fundamental traction solution (4.13), the term

$$\frac{1}{[c_\alpha^2(t-\tau)^2 - r^2]^{1/2}}\delta[c_\alpha(t-\tau)-r] \qquad (4.34)$$

becomes singular at $c_\alpha^2(t-\tau)^2 = r^2$ and then the fundamental solution require some further transformation (Mansur, 1983, Antes, 1985) for numerical treatment. The space derivative of the displacement fundamental solution (4.9), can be written as:

$$u_{lk,j}^s = \sum_{\alpha=1}^{2}\{H[c_\alpha(t-\tau)-r]h_{lk,j}^{(\alpha)} - r_{,j}h_{lk}^{(\alpha)}\delta[c_\alpha(t-\tau)-r]\} \qquad (4.35)$$

On the other hand the time derivative, with respect to τ, of the fundamental solution is:

$$\dot{u}_{lk}^s = \sum_{\alpha=1}^{2}\{H[c_\alpha(t-\tau)-r]\dot{h}_{lk}^{(\alpha)} - h_{lk}^{(\alpha)}\delta[c_\alpha(t-\tau)-r]\} \qquad (4.36)$$

Using equation (4.36), then equation (4.35) can be rewritten as to eliminate the delta function:

$$u_{lk,j}^s = \sum_{\alpha=1}^{2}\{H[c_\alpha(t-\tau)-r](h_{lk,j}^{(\alpha)} - \frac{r_{,j}}{c_\alpha}\dot{h}_{lk}^{(\alpha)}) + \frac{r_{,j}}{c_\alpha}\dot{u}_{lk}^{s(\alpha)}\} \qquad (4.37)$$

Thus, one can substitute equation (4.37), in the fundamental traction solution to obtain

$$p_{lk}^s = [\rho(c_1^2 - 2c_2^2)u_{lj,j}^s\delta_{km} + \rho c_2^2(u_{lk,m}^s - u_{lm,k}^s)]n_m \qquad (4.38)$$

Substituting the last equation into equation (4.31), and the result then is integrated by parts with respect to time to give

$$\alpha_{lk}^{i}u_{k}^{i}(\mathbf{y}^{i},t)=\int_{0}^{t^{+}}\int_{B}u_{lk}^{s}(\mathbf{x},t-\tau;\mathbf{y}^{i})p_{k}(\mathbf{x},\tau)dBd\tau$$

$$-\int_{0}^{t^{+}}\int_{B}[z_{lk}^{s}(\mathbf{x},t-\tau;\mathbf{y}^{i})u_{k}(\mathbf{x},\tau)-w_{lk}^{s}(\mathbf{x},t-\tau;\mathbf{y}^{i})\dot{u}_{k}(\mathbf{x},\tau)]dBd\tau \tag{4.39}$$

where

$$z_{lk}^{s}=\frac{c_2^2}{2\pi c_1^2}\{\frac{\partial r}{\partial n}[\delta_{lk}(\frac{2}{rR_1}+\frac{4R_1}{r^3})-2r_{,l}r_{,k}(\frac{c_1(t-\tau)-r}{R_1^3}+\frac{4}{rR_1}+\frac{8R_1}{r^3})]$$

$$+n_l r_{,k}(\frac{4}{rR_1}+\frac{4R_1}{r^3})+n_k r_{,l}(-\frac{\lambda}{\mu}\frac{c_1(t-\tau)-r}{R_1^3}+\frac{2}{rR_1}+\frac{4R_1}{r^3})\}$$

$$+\frac{c_2}{2\pi}\{\frac{\partial r}{\partial n}[-\delta_{lk}(\frac{2}{rR_2}+\frac{4R_2}{r^3}+\frac{c_2(t-\tau)-r}{R_2^3})+2r_{,l}r_{,k}(\frac{c_2(t-\tau)-r}{R_2^3}$$

$$+\frac{4}{rR_2}+\frac{8R_2}{r^3})]-r_{,k}n_l(\frac{2}{rR_2}+\frac{4R_2}{r^3}+\frac{c_2(t-\tau)-r}{R_2^3})-r_{,l}n_k(\frac{2}{rR_2}+\frac{4R_2}{r^3})\} \tag{4.40}$$

and

$$w_{lk}^{s}=\frac{1}{2\pi}\{\frac{c_2^2}{c_1^2R_1}[2r_{,l}r_{,k}\frac{\partial r}{\partial n}+\frac{\lambda}{\mu}r_{,l}n_k]+\frac{1}{R_2}[(\delta_{lk}-2r_{,l}r_{,k})\frac{\partial r}{\partial n}+r_{,k}n_l]\} \tag{4.41}$$

For non-smooth boundaries see, for instance, Brebbia (1984), Brebbia et al. (1992) and Banerjee (1994).

4.3 Boundary Elements for 2D Elastodynamic Problems

The integral representation has previously been established in terms of the two elastodynamic states from the principle of elastodynamic reciprocal relation. Since an analytical solution of the boundary integral equation is not always possible, it is necessary to consider numerical solutions. For numerical integration the boundary elements have been illustrated in Chapter 3 and shown in Figure (3.3).

4.3.1 Time Interpolations of Boundary Variables

Analytical boundary integrations of the kernels are first evaluated in equation (4.39) to obtain a formulation with particular assumptions concerning the distribution of the boundary displacements, and tractions over time. Analytical time integration of the kernels used is performed by Dominguez (1993). Similar to the scalar case in Chapter 3, constant variation in the traction, and linear variation in the displacement with time will be considered. Dividing time into n equal intervals, $t = n\Delta t$, and using the time approximation of the actual state values one can write:

$$u_k(\mathbf{x},\tau) = \sum_m \eta^m(\tau) u_k^m(\mathbf{x})$$

$$p_k(\mathbf{x},\tau) = \sum_m \mu^m(\tau) p_k^m(\mathbf{x}) \tag{4.42}$$

where $\eta^m(\tau)$ and $\mu^m(\tau)$ are the interpolation shape functions (see Chapter 3). In addition u_k^m and p_k^m indicate the displacement and traction in k-direction, respectively, at time $t_m = m\Delta t$ for the point $\mathbf{x}$.

The choice of the time interpolation functions is not arbitrary even if it is so in principle, as can be seen from the last chapter. However, the discussions previously for the choice of the time interpolation functions will not be repeated here. The purposes of the use of such time functions can be found in Chapter 3.

For any boundary node and given time step equation (4.39) can be written as:

$$\alpha_{lk}^i u_k^{ni} = \sum_{m=1}^{n}\sum_{j=1}^{N} \int_{B_j} U_{lk}^{nm} p_k^{mj}(\mathbf{x}) dB - \sum_{m=1}^{n}\sum_{j=1}^{N} \int_{B_j} Q_{lk}^{nm} u_k^{mj}(\mathbf{x}) dB \tag{4.43}$$

where

$$U_{lk}^{nm} = \int_0^{t^+} u_{lk}^s(\mathbf{x},t)\mu^m(\tau)d\tau \tag{4.44}$$

and:

$$Q_{lk}^{nm} = \int_0^{t^+} [z_{lk}^s(\mathbf{x},t-\tau;\mathbf{y}^i)\eta^m(\tau) - w_{lk}^s(\mathbf{x},t-\tau;\mathbf{y}^i)\dot{\eta}^m(\tau)]d\tau \tag{4.45}$$

Here u_{lk}^s, z_{lk}^s, w_{lk}^s, $\eta^m(\tau)$ and $\mu^m(\tau)$ are given by equations (4.9), (4.40), (4.41), (3.35) and (3.36) respectively. Using (3.36) and (4.44), it may be shown (Dominguez, 1993) that

$$U_{lk}^{nm} = \delta_{lk}(E_1 - E_2) + 2r_{,l}r_{,k}E_2 \tag{4.46}$$

where

$$E_1 = \frac{1}{4\pi\rho c_1^2}(u^1 + \frac{c_1^2}{c_2^2}u^2)$$

$$E_2 = \frac{1}{4\pi\rho c_1^2}(v^1 - \frac{c_1^2}{c_2^2}v^2) \tag{4.47}$$

with the mass density ρ.

Now considering $\eta_\alpha = \max[1, \frac{c_\alpha(t_n - \tau_{m-1})}{r}]$ and $\theta_\alpha = \max[1, \frac{c_\alpha(t_n - \tau_m)}{r}]$, expressions u^α and v^α in (4.47) are categorised to clearly obtain U_{lk}^{nm} in equation (4.46),

Case 1: $0 < \tau_1^* < \tau_{m-1}$ and $0 < \tau_2^* < \tau_1^* < \tau_{m-1}$

$$u^\alpha = 0, \qquad v^\alpha = 0 \tag{4.48a}$$

with $\tau_\alpha^* = t_n - r/c_\alpha$.

Case 2: $\tau_{m-1} < \tau_1^* < \tau_m$ and $0 < \tau_2^* < \tau_{m-1}$

$$u^1 = \cosh^{-1}(\eta_1), \qquad u^2 = 0,$$

$$v^1 = \eta_1(\eta_1^2 - 1)^{1/2}, \quad v^2 = 0. \tag{4.48b}$$

Case 3: $\tau_{m-1} < \tau_1^* < \tau_m$ and $\tau_{m-1} < \tau_2^* < \tau_m$

$$u^1 = \cosh^{-1}(\eta_1), \quad u^2 = \cosh^{-1}(\eta_2),$$

$$v^1 = \eta_1(\eta_1^2 - 1)^{1/2}, \quad v^2 = \eta_2(\eta_2^2 - 1)^{1/2} \tag{4.48c}$$

Case 4: $\tau_m < \tau_1^*$ and $0 < \tau_2^* < \tau_{m-1}$

$$u^1 = \cosh^{-1}(\eta_1) - \cosh^{-1}(\theta_1), \quad u^2 = 0,$$

$$v^1 = \eta_1(\eta_1^2 - 1)^{1/2} - \theta_1(\theta_1^2 - 1)^{1/2}, \quad v^2 = 0. \tag{4.48d}$$

Case 5: $\tau_m < \tau_1^*$ and $\tau_{m-1} < \tau_2^* < \tau_m$

$$u^1 = \cosh^{-1}(\eta_1) - \cosh^{-1}(\theta_1), \quad u^2 = \cosh^{-1}(\theta_1)$$

$$v^1 = \eta_1(\eta_1^2 - 1)^{1/2} - \theta_1(\theta_1^2 - 1)^{1/2}, \quad v^2 = \eta_2(\eta_2^2 - 1)^{1/2} \tag{4.48e}$$

Case 6: $\tau_m < \tau_1^*$ and $\tau_m < \tau_2^*$

$$u^\alpha = \cosh^{-1}(\eta_\alpha) - \cosh^{-1}(\theta_\alpha)$$

$$v^\alpha = \eta_\alpha(\eta_\alpha^2 - 1)^{1/2} - \theta_\alpha(\theta_\alpha^2 - 1)^{1/2} \tag{4.48f}$$

Similarly, from equation (3.35) for the time integral of traction, equation (4.45) may be evaluated analytically (Dominguez, 1993) to give:

$$Q_{lk}^{nm} = \frac{1}{r}[(\delta_{lk}\frac{\partial r}{\partial n} + n_l r_{,k})a^1 + 2\frac{\partial r}{\partial n} r_{,l} r_{,k} a^2 + n_k r_{,l} a^3] \tag{4.49}$$

where

$$a^1 = -\frac{\mu}{\pi\rho c_1^2}(p^1 - \frac{c_1^2}{c_2^2}p^2 + \frac{c_1^2}{c_2^2}q^2)$$

$$a^2 = \frac{\mu}{\pi\rho c_1^2}(2p^1 - 2\frac{c_1^2}{c_2^2}p^2 - \frac{1}{2}q^1 + \frac{c_1^2}{2c_2^2}q^2)$$

$$a^3 = -\frac{\mu}{\pi\rho c_1^2}(p^1 - \frac{c_1^2}{c_2^2}p^2 + \frac{\lambda}{2\mu}q^1) \tag{4.50}$$

Knowing $\beta_\alpha = \max[1, \frac{c_\alpha(t_n - \tau_{m+1})}{r}]$, expressions p^α and q^α in equations (4.50) are given for different cases as follows:

Case 1: $0 < \tau_1^* < \tau_{m-1}$ and $0 < \tau_2^* < \tau_1^* < \tau_{m-1}$

$$p^\alpha = 0 \tag{4.51a}$$

$$q^\alpha = 0 \tag{4.52a}$$

Case 2: $\tau_{m-1} < \tau_1^* < \tau_m$ and $0 < \tau_2^* < \tau_{m-1}$

$$p^1 = \frac{t - \tau_{m-1}}{3\Delta t}\frac{(\eta_1^2 - 1)^{3/2}}{\eta_1}, \quad p^2 = 0 \tag{4.51b}$$

$$q^1 = \frac{t - \tau_{m-1}}{\Delta t}\frac{(\eta_1^2 - 1)^{1/2}}{\eta_1}, \quad q^2 = 0 \tag{4.52b}$$

Case 3: $\tau_{m-1} < \tau_1^* < \tau_m$ and $\tau_{m-1} < \tau_2^* < \tau_1^* < \tau_m$

$$p^1 = \frac{t - \tau_{m-1}}{3\Delta t}\frac{(\eta_1^2 - 1)^{3/2}}{\eta_1}, \quad p^2 = \frac{t - \tau_{m-1}}{3\Delta t}\frac{(\eta_2^2 - 1)^{3/2}}{\eta_2} \tag{4.51c}$$

$$q^1 = \frac{t - \tau_{m-1}}{\Delta t}\frac{(\eta_1^2 - 1)^{1/2}}{\eta_1}, \quad q^2 = \frac{t - \tau_{m-1}}{\Delta t}\frac{(\eta_2^2 - 1)^{1/2}}{\eta_2} \tag{4.52c}$$

Case 4: $\tau_m < \tau_1^* < \tau_{m+1}$ and $0 < \tau_2^* < \tau_{m-1}$

$$p^1 = \frac{t - \tau_{m-1}}{3\Delta t}\frac{(\eta_1^2 - 1)^{3/2}}{\eta_1} - 2\frac{t - \tau_m}{3\Delta t}\frac{(\theta_1^2 - 1)^{3/2}}{\theta_1}, \quad p^2 = 0 \tag{4.51d}$$

$$q^1 = \frac{t - \tau_{m-1}}{\Delta t}\frac{(\eta_1^2 - 1)^{1/2}}{\eta_1} - 2\frac{t - \tau_m}{\Delta t}\frac{(\theta_1^2 - 1)^{1/2}}{\theta_1}, \quad q^2 = 0 \tag{4.52d}$$

Case 5: $\tau_m < \tau_1^* < \tau_{m+1}$ and $\tau_{m-1} < \tau_2^* < \tau_m$

$$p^1 = \frac{t-\tau_{m-1}}{3\Delta t}\frac{(\eta_1^2-1)^{3/2}}{\eta_1} - 2\frac{t-\tau_m}{3\Delta t}\frac{(\theta_1^2-1)^{3/2}}{\theta_1}, \quad p^2 = \frac{t-\tau_{m-1}}{3\Delta t}\frac{(\eta_2^2-1)^{3/2}}{\eta_2} \tag{4.51e}$$

$$q^1 = \frac{t-\tau_{m-1}}{\Delta t}\frac{(\eta_1^2-1)^{1/2}}{\eta_1} - 2\frac{t-\tau_m}{\Delta t}\frac{(\theta_1^2-1)^{1/2}}{\theta_1}, \quad q^2 = \frac{t-\tau_{m-1}}{\Delta t}\frac{(\eta_2^2-1)^{1/2}}{\eta_2} \tag{4.52e}$$

Case 6: $\tau_m < \tau_1^* < \tau_{m+1}$ and $\tau_m < \tau_2^* < \tau_1^* < \tau_{m+1}$

$$p^1 = \frac{t-\tau_{m-1}}{3\Delta t}\frac{(\eta_1^2-1)^{3/2}}{\eta_1} - 2\frac{t-\tau_m}{3\Delta t}\frac{(\theta_1^2-1)^{3/2}}{\theta_1},$$

$$p^2 = \frac{t-\tau_{m-1}}{3\Delta t}\frac{(\eta_2^2-1)^{3/2}}{\eta_2} - 2\frac{t-\tau_m}{3\Delta t}\frac{(\theta_2^2-1)^{3/2}}{\theta_2} \tag{4.51f}$$

$$q^1 = \frac{t-\tau_{m-1}}{\Delta t}\frac{(\eta_1^2-1)^{1/2}}{\eta_1} - 2\frac{t-\tau_m}{\Delta t}\frac{(\theta_1^2-1)^{1/2}}{\theta_1},$$

$$q^2 = \frac{t-\tau_{m-1}}{\Delta t}\frac{(\eta_2^2-1)^{1/2}}{\eta_2} - 2\frac{t-\tau_m}{\Delta t}\frac{(\theta_2^2-1)^{1/2}}{\theta_2} \tag{4.52f}$$

Case 7: $\tau_{m+1} < \tau_1^*$ and $0 < \tau_2^* < \tau_{m-1}$

$$p^1 = \frac{t-\tau_{m-1}}{3\Delta t}\frac{(\eta_1^2-1)^{3/2}}{\eta_1} - 2\frac{t-\tau_m}{3\Delta t}\frac{(\theta_1^2-1)^{3/2}}{\theta_1} + \frac{t-\tau_{m+1}}{3\Delta t}\frac{(\beta_1^2-1)^{3/2}}{\beta_1}, \quad p^2 = 0 \tag{4.51g}$$

$$q^1 = \frac{t-\tau_{m-1}}{\Delta t}\frac{(\eta_1^2-1)^{1/2}}{\eta_1} - 2\frac{t-\tau_m}{\Delta t}\frac{(\theta_1^2-1)^{1/2}}{\theta_1} + \frac{t-\tau_{m+1}}{\Delta t}\frac{(\beta_1^2-1)^{3/2}}{\beta_1}, \quad q^2 = 0 \tag{4.52g}$$

Case 8: $\tau_{m+1} < \tau_1^*$ and $\tau_{m-1} < \tau_2^* < \tau_m$

$$p^1 = \frac{t-\tau_{m-1}}{3\Delta t}\frac{(\eta_1^2-1)^{3/2}}{\eta_1} - 2\frac{t-\tau_m}{3\Delta t}\frac{(\theta_1^2-1)^{3/2}}{\theta_1} + \frac{t-\tau_{m+1}}{3\Delta t}\frac{(\beta_1^2-1)^{3/2}}{\beta_1},$$

$$p^2 = \frac{t-\tau_{m-1}}{3\Delta t}\frac{(\eta_2^2-1)^{3/2}}{\eta_2} \tag{4.51h}$$

$$q^1 = \frac{t-\tau_{m-1}}{\Delta t}\frac{(\eta_1^2-1)^{1/2}}{\eta_1} - 2\frac{t-\tau_m}{\Delta t}\frac{(\theta_1^2-1)^{1/2}}{\theta_1} + \frac{t-\tau_{m+1}}{\Delta t}\frac{(\beta_1^2-1)^{3/2}}{\beta_1},$$

$$q^2 = \frac{t-\tau_{m-1}}{\Delta t}\frac{(\eta_2^2-1)^{1/2}}{\eta_2} \tag{4.52h}$$

Case 9: $\tau_{m+1} < \tau_1^*$ and $\tau_m < \tau_2^* < \tau_{m+1}$

$$p^1 = \frac{t-\tau_{m-1}}{3\Delta t}\frac{(\eta_1^2-1)^{3/2}}{\eta_1} - 2\frac{t-\tau_m}{3\Delta t}\frac{(\theta_1^2-1)^{3/2}}{\theta_1} + \frac{t-\tau_{m+1}}{3\Delta t}\frac{(\beta_1^2-1)^{3/2}}{\beta_1},$$

$$p^2 = \frac{t-\tau_{m-1}}{3\Delta t}\frac{(\eta_2^2-1)^{3/2}}{\eta_2} - 2\frac{t-\tau_m}{3\Delta t}\frac{(\theta_2^2-1)^{3/2}}{\theta_2} \tag{4.51i}$$

$$q^1 = \frac{t-\tau_{m-1}}{\Delta t}\frac{(\eta_1^2-1)^{1/2}}{\eta_1} - 2\frac{t-\tau_m}{\Delta t}\frac{(\theta_1^2-1)^{1/2}}{\theta_1} + \frac{t-\tau_{m+1}}{\Delta t}\frac{(\beta_1^2-1)^{3/2}}{\beta_1},$$

$$q^2 = \frac{t-\tau_{m-1}}{\Delta t}\frac{(\eta_2^2-1)^{1/2}}{\eta_2} - 2\frac{t-\tau_m}{\Delta t}\frac{(\theta_2^2-1)^{1/2}}{\theta_2} \tag{4.52i}$$

Case 10: $\tau_{m+1} < \tau_1^*$ and $\tau_{m+1} < \tau_2^* < \tau_1^*$

$$p^\alpha = \frac{t-\tau_{m-1}}{3\Delta t}\frac{(\eta_\alpha^2-1)^{3/2}}{\eta_\alpha} - 2\frac{t-\tau_m}{3\Delta t}\frac{(\theta_\alpha^2-1)^{3/2}}{\theta_\alpha} + \frac{t-\tau_{m+1}}{3\Delta t}\frac{(\beta_\alpha^2-1)^{3/2}}{\beta_\alpha} \tag{4.51j}$$

$$q^\alpha = \frac{t-\tau_{m-1}}{\Delta t}\frac{(\eta_\alpha^2-1)^{1/2}}{\eta_\alpha} - 2\frac{t-\tau_m}{\Delta t}\frac{(\theta_\alpha^2-1)^{1/2}}{\theta_\alpha} + \frac{t-\tau_{m+1}}{\Delta t}\frac{(\beta_\alpha^2-1)^{3/2}}{\beta_\alpha} \tag{4.52j}$$

4.3.2 Boundary Discretization

The discretization of the boundary of the domain has been given in the previous chapter. The spatial variations of the field variables, and the geometry can be approximated by the interpolation functions as used for the scalar waves. The boundary displacements and tractions are assumed to be constant over each element.

Using the spatial interpolation functions ψ_j, the boundary displacements, and tractions (4.42) across an arbitrary element j can be rewritten as:

$$u_k(\mathbf{x},\tau) = \sum_j \sum_m \eta^m(\tau)\psi_j(\mathbf{x})u_k^{mj}$$

$$p_k(\mathbf{x},\tau) = \sum_j \sum_m \mu^m(\tau)\psi_j(\mathbf{x})p_k^{mj} \tag{4.53}$$

where m and j denote time and space respectively, and $k = 1, 2$ relates to k-direction. Using the spatial approximations with a set of elements B_j, j=1,2,...,N, on the boundary B, equation (4.43) can be written as:

$$\alpha_{lk}^i u_k^{ni} = \sum_{m=1}^{n}\sum_{j=1}^{N}[\int_{B_j} U_{lk}^{nm}\psi_j(\mathbf{x})dB]p_k^{mj} - \sum_{m=1}^{n}\sum_{j=1}^{N}[\int_{B_j} Q_{lk}^{nm}\psi_j(\mathbf{x})dB]u_k^{mj} \tag{4.54}$$

where u_k^{ni} denotes the displacement, at point i, in the k-direction at time step n.

4.3.2.1 Evaluation of Spatial Integrals

To solve equation (4.39) numerically, the boundary quantities are approximated spatially and temporally. When only the boundary B is discretized, the kernels U_{lk}^{nm} and Q_{lk}^{nm} have to be integrated spatially over all boundary elements. During the integration there is a singularity when $t_n = \tau_m$ and $r \to 0$. This singularity has the same behaviour with the elastostatic case.

If the load point $\mathbf{y}^i$ is not on the integration element then the above integrals are evaluated using the usual Gaussian numerical quadrature of maximum fourteenth order. The order of the integration is taken this high because of the discontinuous variation of the fundamental solution with respect to r.

The integration to be evaluated is expressed by means of the homogeneous co-ordinate $-1 \le \zeta \le 1$ along the elements. With the spatial discretization, and using equation (3.51), equation (4.54) takes the following form for the two-dimensional elastic wave problems,

$$\alpha_{lk}^{i} u_k^{ni} = \sum_{m=1}^{n} \sum_{j=1}^{N} [\int_{-1}^{1} U_{lk}^{nm} \psi_j |J| d\zeta] p_k^{mj} - \sum_{m=1}^{n} \sum_{j=1}^{N} [\int_{-1}^{1} Q_{lk}^{nm} \psi_j |J| d\zeta] u_k^{mj} \tag{4.55}$$

where $|J|$ is the Jacobian of the transformation, and was given previously in Chapter 3 (see equation 3.51).

The boundary is divided into N elements, and because of the constant elements considered here the displacement u_k and traction p_k in the k-direction are assumed to be constant over each element and equal to the value at the mid-element node. After the prescribed nodal values, the number of unknown field variables is $2N$.

4.3.2.2 Evaluation of Singular Integrals

When the field and load points are in the same element at the first time step, the integrals become singular. In case of $r \to 0$, the integrals are performed analytically (Dominguez, 1993). In that case, the value Q_{lk}^{nm} is an antisymmetric function, and its spatial integral gives zero. Then, the traction fundamental solution is zero. Taking equation (4.46), the integral of displacement fundamental solution can be evaluated in a local co-ordinate system. The transformation matrix T, in terms of global components of the normal vector, can be defined as:

$$T = \begin{bmatrix} -n_2 & n_1 \\ n_1 & n_2 \end{bmatrix} \tag{4.56}$$

The matrix G in local co-ordinate system can be written with the help of the transformation matrix as:

$$G^{nm} = T\begin{bmatrix} G'^{nm}_{11} & 0 \\ 0 & G'^{nm}_{22} \end{bmatrix} T^T \tag{4.57}$$

or in expanded form,

$$G^{nm} = \begin{bmatrix} n_1^2 G'^{nm}_{11} + n_2^2 G'^{nm}_{22} & n_1 n_2 (G'^{nm}_{22} - G'^{nm}_{11}) \\ n_1 n_2 (G'^{nm}_{22} - G'^{nm}_{11}) & n_2^2 G'^{nm}_{11} + n_1^2 G'^{nm}_{22} \end{bmatrix} \tag{4.58}$$

The off-diagonal terms of U^{nm}_{lk} are zero and the diagonal terms are:

$$U^{nm}_{11} = \frac{1}{4\pi\rho}[\frac{1}{c_1^2}(u^1 + v^1) + \frac{1}{c_2^2}(u^2 - v^2)] \tag{4.59}$$

and

$$U^{nm}_{22} = \frac{1}{4\pi\rho}[\frac{1}{c_1^2}(u^1 - v^1) + \frac{1}{c_2^2}(u^2 + v^2)] \tag{4.60}$$

where u^α and v^α are given by equations in (4.48). Then,

$$\begin{aligned} IG_1(c,t) &= \int_0^s \cosh^{-1}(\frac{ct}{r})dr = \int_0^s \ln[\frac{ct}{r} + ((\frac{ct}{r})^2 - 1)^{1/2}]dr \\ &= ct[\frac{1}{L}\cosh^{-1} L + \sin^{-1}\frac{1}{L}] \end{aligned} \tag{4.61}$$

$$IG_2(c,t) = \int_0^s \frac{ct}{r}[(\frac{ct}{r})^2 - 1]^{1/2}]dr = -ct[(L^2 - 1)^{1/2} + \sin^{-1}\frac{1}{L}] \tag{4.62}$$

where

$$s = \max[ct, \frac{\Delta x}{2}], \quad L = \max[1, \frac{ct}{(\Delta x/2)}].$$

Thus,

$$G_{11}^{'nm} = \frac{1}{2\pi\rho}\sum_{\alpha=1}^{2}\frac{1}{c_\alpha^2}\{IG_1(c_\alpha, t_n - \tau_{m-1}) - IG_1(c_\alpha, t_n - \tau_m) - (-1)^\alpha[IG_2(c_\alpha, t_n - \tau_{m-1}) - IG_2(c_\alpha, t_n - \tau_m)]\} \tag{4.63}$$

$$G_{22}^{'nm} = \frac{1}{2\pi\rho}\sum_{\alpha=1}^{2}\frac{1}{c_\alpha^2}\{IG_1(c_\alpha, t_n - \tau_{m-1}) - IG_1(c_\alpha, t_n - \tau_m) + (-1)^\alpha[IG_2(c_\alpha, t_n - \tau_{m-1}) - IG_2(c_\alpha, t_n - \tau_m)]\} \tag{4.64}$$

with the element length Δx.

4.3.3 The Boundary Element Equation

For each boundary element j one can write

$$G_{lk}^{nmij} = \int_{B_j} U_{lk}^{nm}\psi_j dB \tag{4.65}$$

$$\hat{H}_{lk}^{nmij} = \int_{B_j} Q_{lk}^{nm}\psi_j dB\,. \tag{4.66}$$

equation (4.66) may also be redefined as:

$$H_{lk}^{nmij} = \begin{cases} \hat{H}_{lk}^{nmij} + \alpha_{lk}^{i} & \text{if } i = j \text{ and } n = m \\ \hat{H}_{lk}^{nmij} & \text{if } i \neq j \text{ or } n \neq m \end{cases} \tag{4.67}$$

Here, the boundary of the domain is discretized with constant elements. Now, using the spatial integrals, equation (4.54) can be written as:

$$\sum_{m=1}^{n}\sum_{j=1}^{N} H_{lk}^{nmij} u_k^{mj} - \sum_{m=1}^{n}\sum_{j=1}^{N} G_{lk}^{nmij} p_k^{mj} = 0 \tag{4.68}$$

where N represents the total number of boundary elements. More compactly, this becomes:

$$\sum_{m=1}^{n}[\mathbf{H}^{nm}\mathbf{u}^{m} - \mathbf{G}^{nm}\mathbf{p}^{m}] = \mathbf{0} \tag{4.69}$$

Here, $\mathbf{G}^{nm}$ and $\mathbf{H}^{nm}$ are two $N \times N$ matrices which are calculated by spatial integration for each element, and $\mathbf{u}^{m}$ and $\mathbf{p}^{m}$ are the column vectors of boundary nodal quantities. The evaluation of the boundary integrals in space and time, and prescription of the boundary conditions, results in an algebraic equation with $2N$ unknowns.

4.3.4 Solution Procedure

The procedure will now be considered in the same way as for the scalar case. The only exception is the number of unspecified field variables. After the prescribed values at a boundary node, there are now two unknowns, while only one unknown in the scalar case. For the sake of completeness, the solution procedure is repeated here.

At time t, the number knowns and unknowns are equal in the matrix equation (4.69). If the boundary quantities $\mathbf{u}^{m}$ and $\mathbf{p}^{m}$ are known for the time m=1,2,...,n-1, then for each time step n, the solution can be found. Thus, taking the unknowns on the left, equation (4.71) can be rewritten as:

$$\mathbf{H}^{nn}\mathbf{u}^{n} = \mathbf{G}^{nn}\mathbf{p}^{n} + \sum_{m=1}^{n-1}[\mathbf{G}^{nm}\mathbf{p}^{m} - \mathbf{H}^{nm}\mathbf{u}^{m}] \tag{4.70}$$

Here the last part of the right hand side of equation (4.70) is known. The unknowns in the above equation consist of boundary displacements and tractions. For example, if the boundary displacement quantities are prescribed, then the tractions are unknowns at these boundary nodes. Rearranging the columns of $\mathbf{G}^{nm}$ and $\mathbf{H}^{nm}$ according to the boundary conditions the last equation may be expressed as:

$$\mathbf{A}^n\mathbf{X}^n = \mathbf{R}^n \tag{4.71}$$

where the right hand side $\mathbf{R}^n$ is the sum of terms over the previous steps, and the known boundary conditions for time step n multiplied by their coefficient matrix. The last equation is a linear equation system, and, in that equation, $\mathbf{X}^n$ and $\mathbf{A}^n$ are respectively the unknown vector, and the system matrix for time step n.

It may be noted that a new $\mathbf{R}^n$ in equation (4.71) has to be computed for each time step. If the time step size is constant, the $\mathbf{G}^{nn}$, $\mathbf{H}^{nn}$ and $\mathbf{A}^n$ matrices do not change from time step to time step. So, the system matrix is organised only once, thus it can be written as $\mathbf{A}^n \equiv \mathbf{A}$. For the solution of equation (4.71) see the Appendix.

4.4 Infinite Domains

It should be noted that behaviour of the field variables at infinity is almost identical to the two-dimensional scalar wave cases. The main difference is to take displacements and tractions rather than potential and flux. Thus repeating the argument for the displacements and tractions, and using Figure (3.7), equation (4.31) can be written in the form:

$$\alpha_{lk}^i u_k^i = \int_B [(u_{lk}^s * p_k) - (p_{lk}^s * u_k)](\mathbf{x},t)dB + \lim_{r\to\infty} \int_{B_r} [(u_{lk}^s * p_k) - (p_{lk}^s * u_k)](\mathbf{x},t)dB \tag{4.72}$$

If all the loads causing the motion are inside the region Ω, then, there is no wave to propagate to the interior from infinity. Therefore, the displacement and tractions must behave in such a way that the second integral in equation (4.72) must equivalent to zero be (Eringen et al., 1975).

Since the displacement vector **u** can be decomposed into its irrotational and solenoidal parts (Eringen et al., 1975, Dominguez, 1993), then:

$$\mathbf{u} = \mathbf{u}^{(1)} + \mathbf{u}^{(2)} \tag{4.73}$$

From the analytical structure of the fundamental solutions, it follows that each vector satisfies the radiation and regularity conditions:

$$\lim_{r\to\infty} r^{1/2}[\frac{\partial \mathbf{u}^{(1)}}{\partial r} + \frac{1}{c_1}\dot{\mathbf{u}}^{(1)}] = \mathbf{0}, \qquad \lim_{r\to\infty}(r^{-1/2}\mathbf{u}^{(1)}) = \mathbf{0}$$

$$\lim_{r\to\infty} r^{1/2}[\frac{\partial \mathbf{u}^{(2)}}{\partial r} + \frac{1}{c_2}\dot{\mathbf{u}}^{(2)}] = \mathbf{0}, \qquad \lim_{r\to\infty}(r^{-1/2}\mathbf{u}^{(2)}) = \mathbf{0} \tag{4.74}$$

These conditions express the fact that the energy at infinity is outgoing, in other words, there is no source at infinity. Thus, it may be seen that the boundary integral equation (4.31) is valid for infinite domains as well as the finite domains. There is no need to discretize the external boundary B_r as $r \to \infty$ (see Figure 3.7).

4.5 Multimedia

So far, in this chapter, the boundary elements for homogeneous linear elastic isotropic materials have been considered.

In many cases, media that are not homogeneous but consist of several subdomains each one being homogeneous, are modelled. This idea is represented in Figure (3.8), with a domain consisting of two subdomains which are Ω_1 and Ω_2. For the elastic case, the equations formulated for each homogeneous domain separately are:

$$\sum_{m=1}^{n}\left\{\begin{bmatrix}\mathbf{H}_{11}^{nm} & \mathbf{H}_{1I}^{nm}\end{bmatrix}\begin{bmatrix}\mathbf{u}_1^m \\ \mathbf{u}_{1I}^m\end{bmatrix} - \begin{bmatrix}\mathbf{G}_{11}^{nm} & \mathbf{G}_{1I}^{nm}\end{bmatrix}\begin{bmatrix}\mathbf{p}_1^m \\ \mathbf{p}_{1I}^m\end{bmatrix}\right\} = \mathbf{0} \tag{4.75}$$

for subdomain Ω_1. Here, for time $t_m = m\Delta t$, $\mathbf{u}_1^m$ and $\mathbf{p}_1^m$ indicate the nodal displacements and tractions at the boundary B_1 whilst $\mathbf{u}_{1I}^m$ and $\mathbf{p}_{1I}^m$ stand for the nodal displacements and tractions at the interface when it belongs to B_1. It may be seen that the

corresponding coefficient matrices $\mathbf{H}_{1I}^{nm}$ and $\mathbf{G}_{1I}^{nm}$ are for the interface when it belongs to B_1, whilst $\mathbf{H}_{11}^{nm}$ and $\mathbf{G}_{11}^{nm}$ show the corresponding matrices for B_1, excluding the interface, in the subdomain Ω_1. Similarly

$$\sum_{m=1}^{n}\left\{\begin{bmatrix}\mathbf{H}_{22}^{nm} & \mathbf{H}_{2I}^{nm}\end{bmatrix}\begin{bmatrix}\mathbf{u}_{2}^{m} \\ \mathbf{u}_{2I}^{m}\end{bmatrix}-\begin{bmatrix}\mathbf{G}_{22}^{nm} & \mathbf{G}_{2I}^{nm}\end{bmatrix}\begin{bmatrix}\mathbf{p}_{2}^{m} \\ \mathbf{p}_{2I}^{m}\end{bmatrix}\right\}=\mathbf{0} \tag{4.76}$$

for subdomain Ω_2.

Equations (4.75, 4.76) are not sufficient to find the displacements and tractions, because at each interface both field variables are unknown. When the two homogeneous subdomains Ω_1 and Ω_2 are considered, the interface displacements are continuous across the interface, and the tractions associated with each subdomain are in dynamical equilibrium, unless there is any separation at the interface. These conditions can be written as:

$$\mathbf{u}_{1I}^{m}=\mathbf{u}_{2I}^{m} \tag{4.77}$$

$$\mathbf{p}_{1I}^{m}=-\mathbf{p}_{2I}^{m} \tag{4.78}$$

Equations (4.77) and (4.78) are called compatibility conditions and dynamical equilibrium conditions, respectively.

So, for the elastic wave problems, the integral equation is constructed in terms of the interface variables of the subdomain as well as the boundary variables. At the interface, both the displacements and the tractions are unknown, so that the number of unknowns and knowns are not equal. Then, considering equations (4.77) and (4.78) corresponding to the interface, the discrete equation system is constructed for the piecewise homogeneous medium, and the number of unknowns, and knowns now becomes equal.

This algebraic equation system can be solved simultaneously for all subdomains. It follows that the algebraic linear equation system can be written in compact form as,

$$\mathbf{D}\mathbf{X}^n = \mathbf{R}^n \tag{4.79}$$

in which $\mathbf{D}$ denotes the system matrix which consists of the matrix coefficients of both subdomains at time step n. The vector $\mathbf{X}^n$ is the unknown vector which contains the unknown boundary, the interface displacements, and tractions at time step n. In an equivalent way to the scalar case, the matrix $\mathbf{D}$ can be constructed in two different ways (see Chapter 3). The first way, where equations (4.77) and (4.78) are added directly to the system matrix, is used to consider multimedia problems. So, for each time step, the boundary and interface unknowns can be calculated from equation (4.79). The solution of equation (4.79) is stated in the Appendix.

The argument above can be repeated for more than two subdomains.

4.6 Internal Calculations

Once the unknown values of the displacement and traction have been calculated along the boundary, for time $t = \Delta t, 2\Delta t, ..., n\Delta t$, the displacement values can be evaluated at any internal point. Clearly, from equation (4.32), $\alpha_{lk}^i = \delta_{lk} \quad l,k = 1, 2$, for internal points. Hence:

$$u_l^{ni} = \sum_{m=1}^{n}\sum_{j=1}^{N} G_{lk}^{nmij} p_k^{mj} - \sum_{m=1}^{n}\sum_{j=1}^{N} \hat{H}_{lk}^{nmij} u_k^{mj} \tag{4.80}$$

where u_l^{ni} represents the value of the displacement in the l-direction at an internal point i at time step n. The coefficient functions G_{lk}^{nmij} and $\hat{H}_{lk}^{nmij}$ represent the integrations on the element j from the internal point i. Similar to the boundary computations, the functions depend only on the time difference n-m.

To calculate the displacement values inside a subdomain, only the subdomain boundary (interface) values are needed.

4.7 Results

The method given above is now used to solve the plane elastic wave equation. Bounded and unbounded cases for single medium and layered media are considered to observe their dynamical behaviour.

4.7.1 Single Medium Results

Consider the physical problem of solving equation (4.1) for one-layered medium. The geometry of the problem is shown in Figure (4.2) and is considered for comparison with the work of Reynolds (1978) who used the FDM to obtain similar results. The material velocities are c_1=2130 m/s and c_2=1230 m/s for shale. In Figure (4.2), the source is taken at the centre of the medium, while the receivers are positioned in a horizontal line at 10 m below the top boundary. The number of receivers, time increment, element length used, and source size are 169, 0.004 s, 5 m and 4 m, respectively. The receiver points are positioned equally. The medium is initially at rest.

In this physical problem the Dirichlet boundary conditions are used for the sides and bottom boundaries, whilst the top side is a free surface (see Figure 4.3). Figure (4.4) shows the stable results both horizontally and vertically, which contain large reflections from the side boundaries as well as the bottom. Both the horizontal and vertical results obtained by using the BEM (Figure 4.4) give excellent qualitative agreement with the Reynolds' results (Figure 4.5a, 4.5b). The first wave reaches the closest receiver at time 0.14 s. There is a weak shear wave received at 0.236 s, as can be seen from horizontal result in Figure (4.4). The first reflection wave comes from the bottom side, arriving at

0.42 s, whilst the second reflection wave first hits the top and follows the same path as the first.

The seismograms obtained from the physical geometry have time (in seconds), on the horizontal axis, and all displacement values received at the selected receiver points are on the vertical axis. The vertical axis (in meters) shows the length of the top side of the physical model (see Figure 4.2).

For the infinite medium, the BEM results (Figure 4.7) presented are compared with those found using the FDM by Reynolds (1978). He used his transparent boundary conditions to simulate a medium of infinite extent on the sides, as shown in Figure (4.6). The desired agreement between the BEM results (see Figure 4.7) and Reynolds' results (see Figures 4.8a, 4.8b) may be observed. However, Reynolds could not completely eliminate the side reflections as can be seen in his results, whilst the BEM completely eliminate such effects (see Figure 4.7). This shows the advantage of the BEM over the FDM for the medium of infinite extent. A MATHCAD program has been employed to present the graphical results.

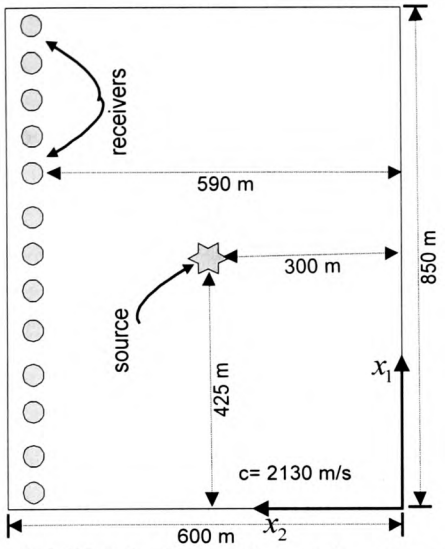

Figure 4.2 Physical model showing geometry of the medium used to generate seismograms in the elastic BEM program for one medium.

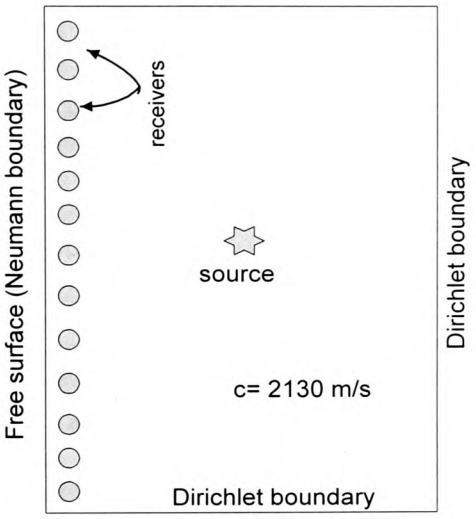

Figure 4.3 Definition of the boundary condition of the problem

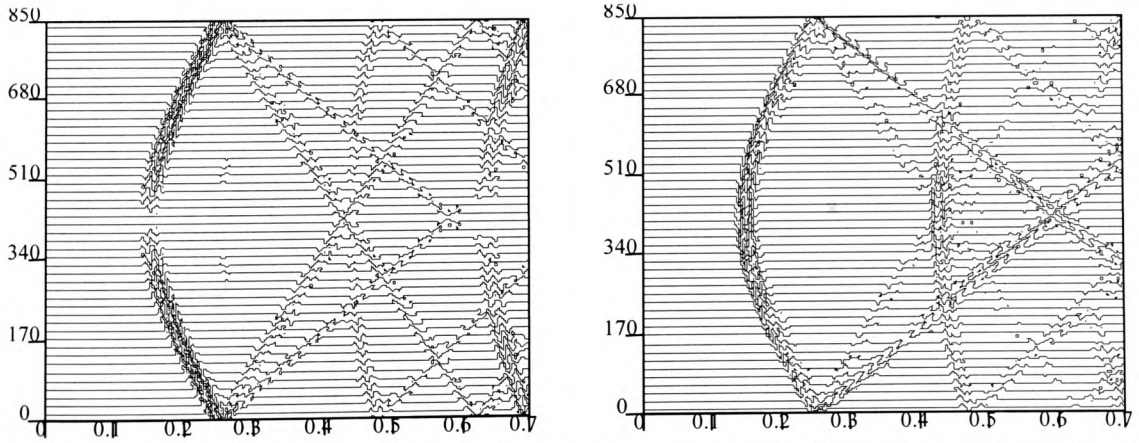

Figure 4.4 Synthetic horizontal and vertical seismograms generated from the BEM solution of the 2D elastic wave equation with the sides and top (Dirichlet) and bottom (Neumann) boundary conditions

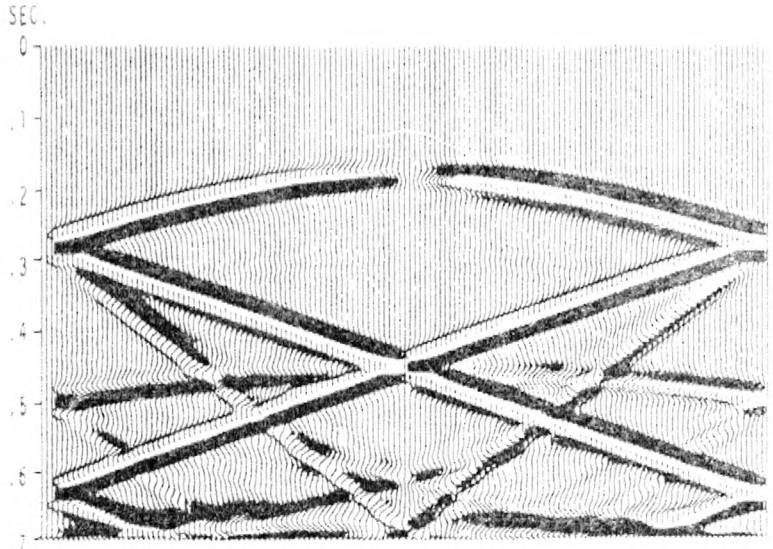

Figure 4.5a Synthetic horizontal seismogram with the Dirichlet boundary condition for Reynolds' result

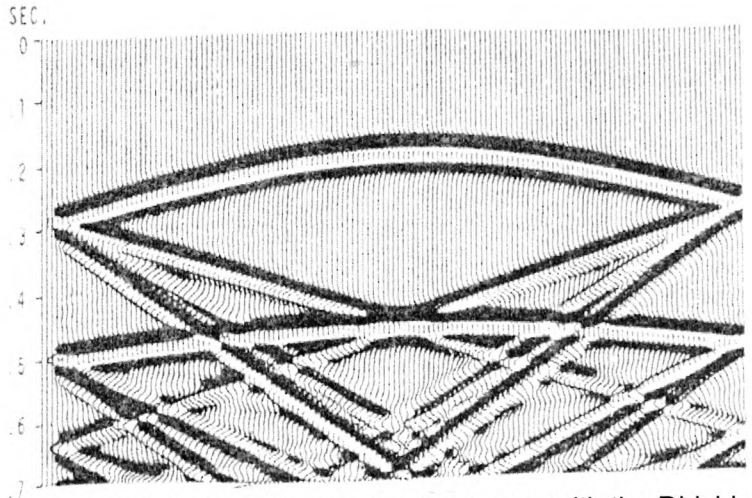

Figure 4.5b Synthetic vertical seismogram with the Dirichlet boundary condition for Reynolds' result

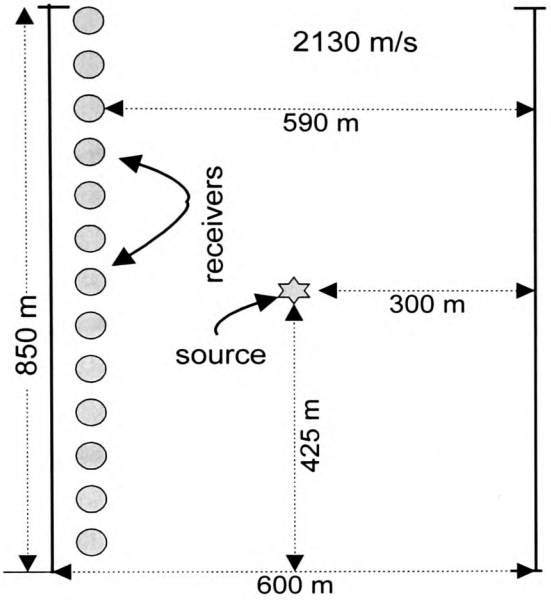

Figure 4.6 Physical model showing geometry of the medium used to generate seismograms in the elastic BEM program

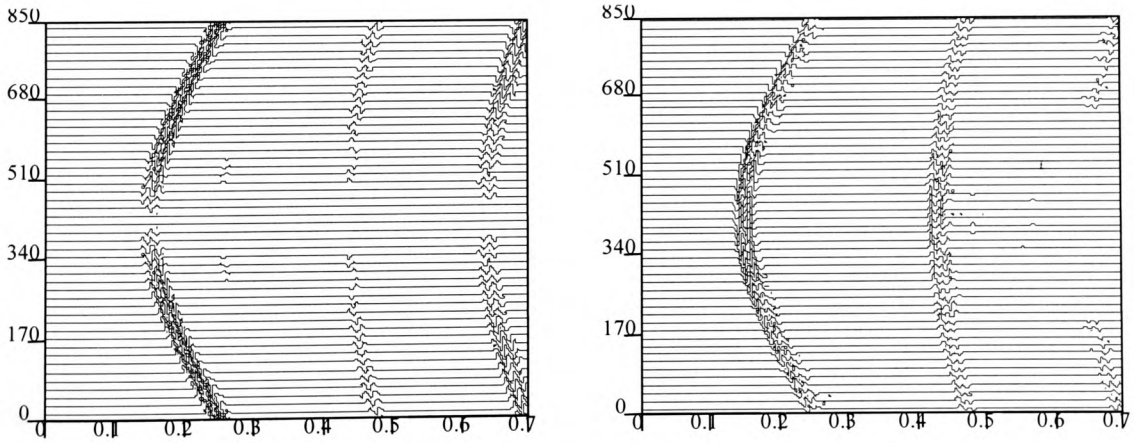

Figure 4.7 Synthetic horizontal and vertical seismogram generated from the BEM solution of the 2D elastic wave equation with the top (Neumann)-bottom (Dirichlet) boundary conditions for an infinite case of the medium.

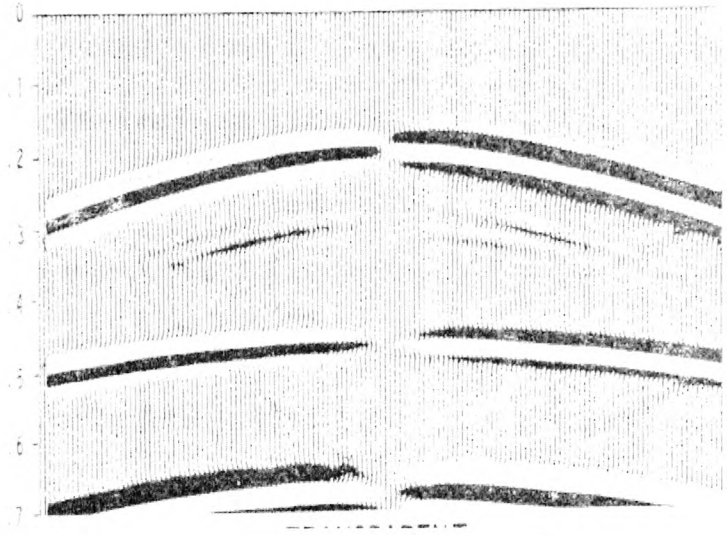

Figure 4.8a Synthetic horizontal seismogram with Transparent boundary condition for Reynolds' result

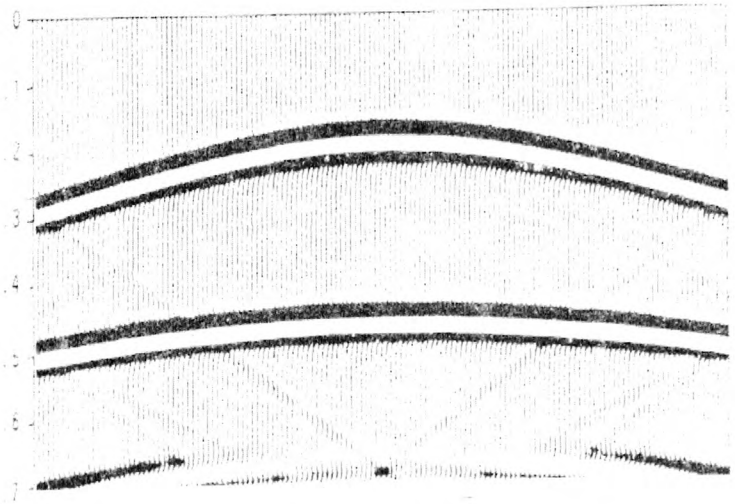

Figure 4.8b Synthetic vertical seismogram with Transparent boundary condition for Reynolds' result

4.7.2 Two Media Results

Now a two-layered medium, when the sides and bottom extending to infinity, are considered. The compressional wave velocities are taken to be 2440 m/s and 5500 m/s for the top and bottom layers respectively, with shear wave velocities of 1400 m/s and 3100 m/s. The results do not exhibit any reflections from the sides or bottom. The first compressional wave arrives at the closest receiver point at time 0.045 s. Clearly the wave arriving immediately after the first wave is a shear wave, as expected, for both horizontal and vertical results. It is noticeable that the first interface wave is received at time 0.144 s. This wave first impinges on the interface and then reflects.

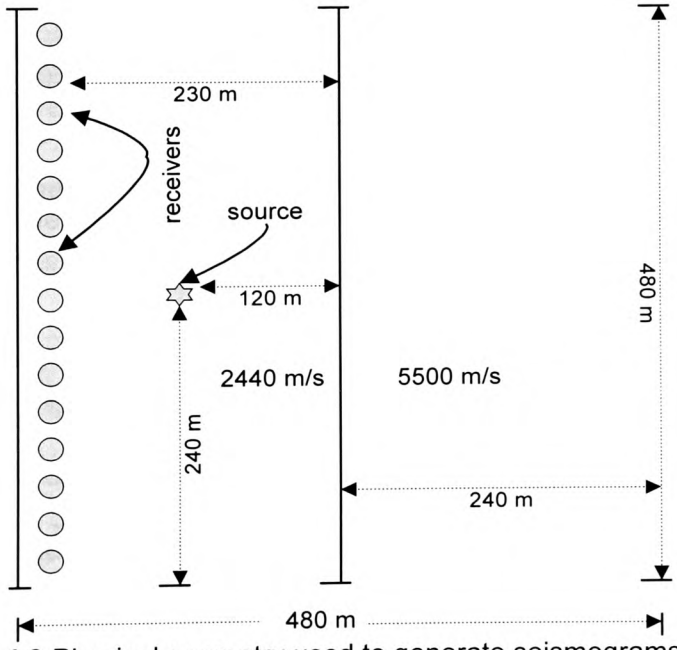

Figure 4.9 Physical geometry used to generate seismograms in the elastic BEM program for a two-layered medium

The second interface wave first strikes the top, and then continues in the same way as the first. It may be seen that the second wave is stronger than the first one. Because, the

interface wave, and the wave caused by the source boundary, coincide. The second interface wave is registered after approximately 0.24 s.

It is also not difficult to see that the waves arriving at 0.34 s and 0.43 s are the repetitions of the first and second interface waves. The interface waves repeated in the vertical axis are weaker than those in the horizontal axis, as can be seen in Figure (4.10).

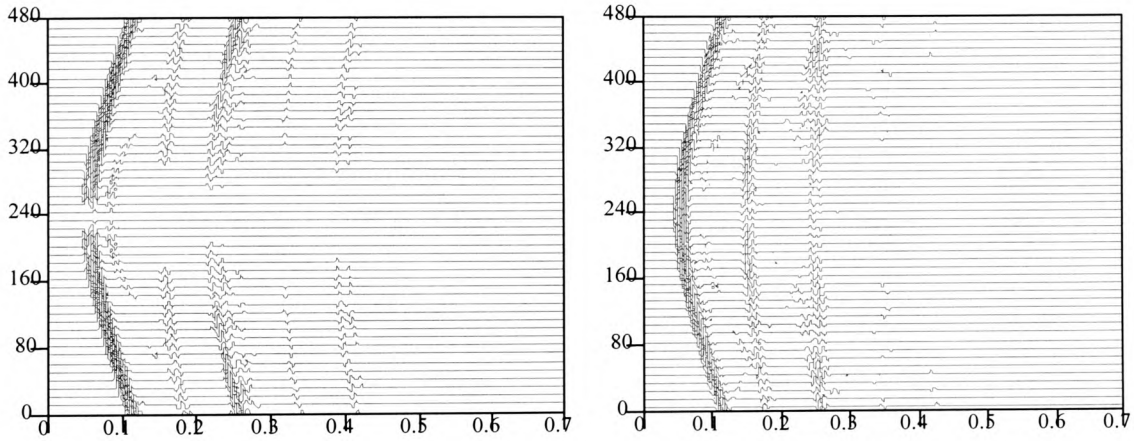

Figure 4.10 Synthetic horizontal and vertical seismogram generated from the BEM solution of the 2D elastic wave equation with the top Neumann boundary condition for the two-layered medium.

4.7.3 Multimedia Results

When the sides and bottom are of infinite extent, a three-layered medium is considered to examine the behaviour of the elastic waves, as shown in Figure (4.11). The distance between the flat interfaces is equal. The compressional wave velocities are given from the top layer to the bottom layer, as: 2130 m/s in shale, 4000 m/s in sandstone and 5800 m/s in basalt, with their shear wave velocities being 1230 m/s, 2400 m/s and 3500 m/s respectively. The co-ordinates of the source is (75,125), and its size is 1 m. The element

size used for the external boundary is 1.2 m, and the results obtained for the time increment of 0.00095 is stable.

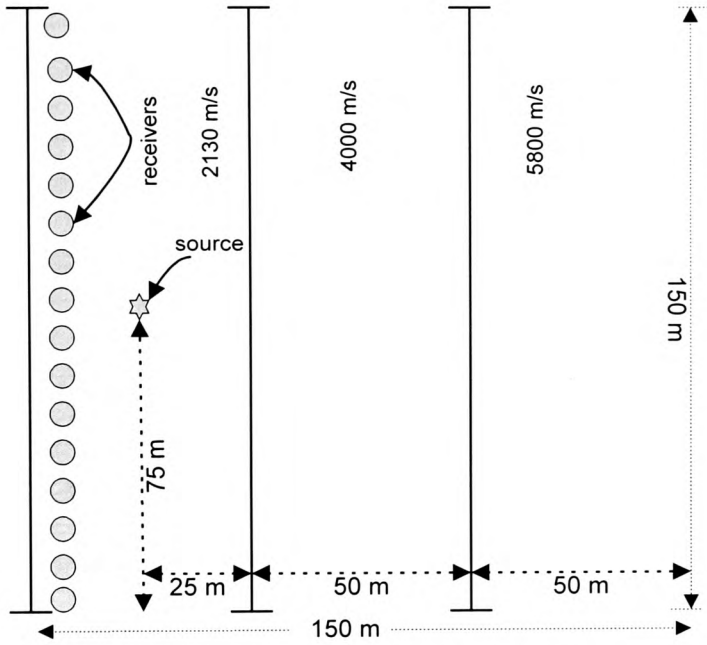

Figure 4.11 Physical geometry used to generate seismograms in the elastic BEM program for the multimedia

There are no reflections coming from the sides or bottom as expected. This is as expected. At time 0.0103 s, the first compressional wave reaches the closest receiver point. the wave following the first wave is a shear wave in the both horizontal and the vertical axes.

Consider the first interface. It is noticeable that the first interface wave is received at time 0.034 s. This wave first impinges on the interface and then reflects. The second interface wave first strikes the top and then continues in the same way as the first. The second wave is stronger than the first one because there is a visible wave coming from the second interface, coinciding with that interface wave. The synthetic seismograms also generate S-waves.

These results show the versatility of the method, although there are no available results to compare with the layered media results (Figures 4.10 and 4.12),.

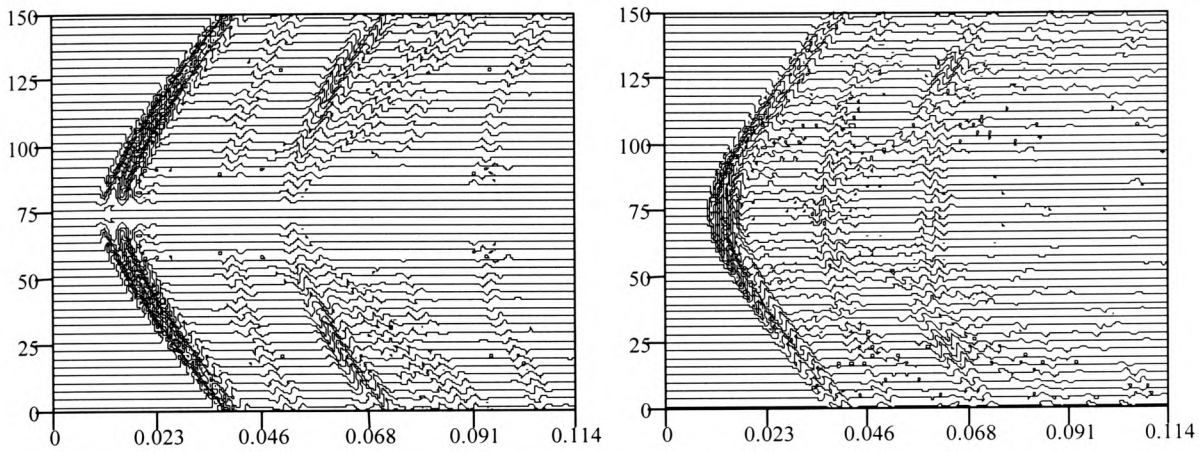

Figure 4.12 Synthetic horizontal and vertical seismogram generated from the BEM solution of the 2D elastic wave equation with the top Neumann boundary condition for an infinity case of three-layered medium.

4.8 Conclusions

In this chapter, the two-dimensional time domain elastic wave formulation in terms of dynamical reciprocity has been established. Using this formulation, the BEM solutions of the Cauchy-Navier equations have been presented for isotropic elastic homogeneous media. The numerical implementation of the method for simply connected regions was modified to multiply connected regions. In addition, the corresponding partial differential equations have been solved in terms of the modified formulations for piecewise homogeneous media.

CHAPTER 5

THREE-DIMENSIONAL TIME DOMAIN BEM FOR SCALAR WAVE PROPAGATION

5. 1 Introduction

Having gained confidence with the two-dimensional results in the previous chapters, this chapter is devoted to considering the more realistic three-dimensional geometries. First, the three-dimensional scalar wave equation is considered, this is then followed by three-dimensional elastic cases. After derivation of the fundamental solution, the three-dimensional time domain direct BEM formulation for the scalar waves is established by means of the dynamic reciprocal relation in which the fundamental solution and actual states are used. The time integration of the kernels is evaluated analytically. Also, evaluation of the singular integrals is dealt with using two different techniques, and relevant results are compared for isotropic elastic homogeneous and piecewise homogeneous media. Moreover the flux kernels for interior points are derived, and the corresponding flux results are discussed.

5.2 Integral Equation Formulation for the Three Dimensional Scalar Wave

In Chapter 2, the three-dimensional scalar wave equation (2.27) corresponding to a homogeneous isotropic elastic body Ω bounded by the boundary B, was derived. The actual and fundamental solution solutions are shown by ϕ and ϕ^s, respectively. The fundamental solution satisfies equation (2.27), namely,

$$c^2\phi^s_{,ii} + f^s = \ddot{\phi}^s \tag{5.1}$$

5.2.1 Fundamental Solutions

To apply the BEM, a fundamental solution of the differential equation must be known. For the domain Ω, and its boundary surface B, the fundamental solution is a solution that satisfies equation (2.27), for an infinite region with a unit impulse body source. Using the source (3.3) for this case, it follows that equation (5.1) becomes

$$\phi^s_{,ii} + \delta(t)\delta(\mathbf{x}-\mathbf{y}^i) = \frac{1}{c^2}\ddot{\phi}^s \tag{5.2}$$

To derive the three-dimensional fundamental solution, the Fourier integral representation may be used (Greenberg, 1971, Barton, 1991, Haberman, 1998):

$$\phi^s(\mathbf{x},t;\mathbf{y}^i,\tau) = \frac{c^2}{(2\pi)^3}\int_\Omega \frac{e^{-j\mathbf{w}.\mathbf{r}}\sin cw(t-\tau)}{cw}d\Omega \tag{5.3}$$

with $\mathbf{w}.\mathbf{r} = wr\cos\alpha$ and $j^2 = -1$.

Consider a sphere of radius w as shown in Figure (5.1). The differential surface area dB and differential volume $d\Omega$ (see Figure 5.1) needed in spherical co-ordinates may be written as:

$$dB = w^2\sin\alpha d\alpha d\theta, \qquad d\Omega = w^2\sin\alpha d\alpha d\theta dw \tag{5.4}$$

Substituting (5.4) into equation (5.3), it follows that

$$\phi^s(\mathbf{x},t;\mathbf{y}^i,\tau) = \frac{c^2}{(2\pi)^3}\iiint \frac{e^{-jwr\cos\alpha}\sin cw(t-\tau)}{cw}w^2\sin\alpha d\alpha dw d\theta \tag{5.5}$$

In the above $w = |\mathbf{w}|$ and $r = |\mathbf{x}-\mathbf{y}^i|$ where i is fixed.

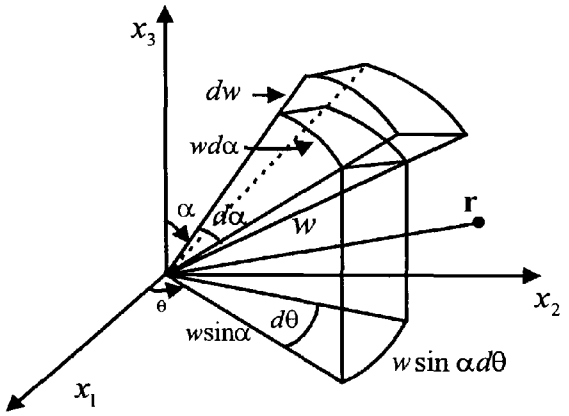

Figure 5.1 Infinitesimal volume determined in spherical co-ordinates

In equation (5.5), the integration is taken over the entire space, so that $0 < \alpha < \pi$, $0 < \theta < 2\pi$ and $0 < w < \infty$ as shown in Figure (5.1).

$$\int_0^{2\pi} d\theta = 2\pi, \qquad \int_0^{\pi} e^{-jwr\cos\alpha} w\sin\alpha d\alpha = \frac{2}{r}\sin wr \tag{5.6}$$

Using (5.6), it follows that,

$$\begin{aligned} \phi^s(\mathbf{x},t;\mathbf{y}^i,\tau) &= \frac{2c}{(2\pi)^2 r}\int_0^{\infty} \sin wr \sin cw(t-\tau)dw \\ &= \frac{c}{4\pi^2 r}\int_0^{\infty}\{\cos w[r-c(t-\tau)] + \cos w[r+c(t-\tau)]\}dw \end{aligned} \tag{5.7}$$

However, Haberman (1998) has shown that

$$\frac{1}{\pi}\int_0^{\infty}\cos wx dw = \delta(x) \tag{5.8}$$

and so

$$\phi^s(\mathbf{x},t;\mathbf{y}^i,\tau)=\frac{c}{4\pi r}\{\delta[r-c(t-\tau)]+\delta[r+c(t-\tau)]\} \tag{5.9}$$

Since $r\geq 0$ and $t>\tau$, the second Dirac delta function is zero. Then, using $\delta[r-c(t-\tau)]=\delta[c(t-\tau)-r]$ (Stephenson, 1996) it may be shown that:

$$\phi^s(\mathbf{x},t;\mathbf{y}^i,\tau)=\frac{c}{4\pi r}\delta[c(t-\tau)-r]=\frac{1}{4\pi r}\delta[(t-\tau)-r/c] \tag{5.10}$$

where r is the distance between the field point $\mathbf{x}$ and load point $\mathbf{y}^i$ in the three-dimensional fundamental solution. It may be noted that ϕ^s is the field at time t and position $\mathbf{x}$, due to an impulsive unit point source. As can be seen from the fundamental solution (5.10), the disturbance sent initially from the load point $\mathbf{y}^i$ is received at point $\mathbf{x}$ only at time $r=c(t-\tau)$, and then is zero (Eringen et al., 1975). Also for all $t>\tau$, it is also zero at $r=0$.

The causality, reciprocity and time translation properties given in Chapter 3 are also available for the three-dimensional fundamental solutions.

The normal derivative of the fundamental solution may be found to be:

$$q^s(\mathbf{x},t;\mathbf{y}^i,\tau)=\frac{\partial\phi^s(\mathbf{x},t;\mathbf{y}^i,\tau)}{\partial n}=\frac{\partial r}{\partial n}\frac{\partial\phi^s}{\partial r}=[\frac{-1}{4\pi r^2}\delta(t-\tau-r/c)-\frac{1}{4\pi r}\delta'(t-\tau-r/c)]\frac{\partial r}{\partial n}$$

$$=[\frac{-1}{4\pi r^2}\delta(t-\tau-r/c)-\frac{1}{4\pi rc}\dot{\delta}(t-\tau-r/c)]\frac{\partial r}{\partial n} \tag{5.11}$$

where the time derivative is with respect to τ, whilst the space derivative is with respect to $\mathbf{x}$, and where

$$\delta'(t-\tau-r/c)=\frac{1}{c}\dot{\delta}(t-\tau-r/c) \tag{5.12}$$

5.2.1.1 Comparison of the Fundamental Solutions (2D and 3D Solutions)

The fundamental solution of the three-dimensional scalar wave equation (5.10), for $\tau = 0$, represents a disturbance. The disturbance emitted initially from the load point $\mathbf{y}^i$ is received at time $t = r/c$ at the field point $\mathbf{x}$. In this case, the strength of the impulse decreases with r, and the solution becomes zero just after $t = r/c$ (see Figure 5.2b). It can be seen from the definition of the Dirac delta function, and Figure (5.2b) that, for $t < r/c$ or $t > r/c$, no perturbation is felt at any time except at $t = r/c$.

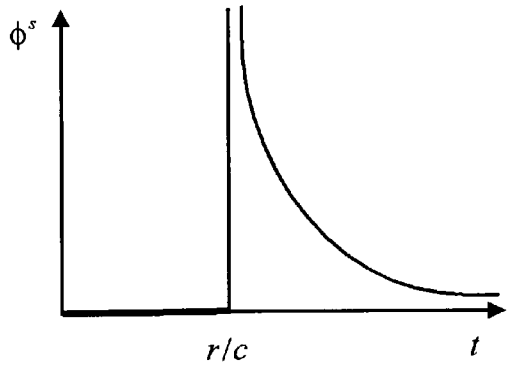

(a) The two-dimensional fundamental solution

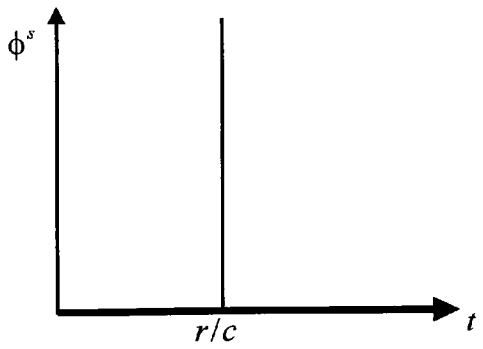

(b) The three-dimensional fundamental solution

Figure 5.2 Comparison of the 2D and 3D fundamental solutions

On the other hand the two-dimensional fundamental solution (3.13) does not depend on an impulse applied at a single point, but rather on an infinite number of points on the line source (see Figure 3.1). The disturbance emitted from the source points $\mathbf{y}^i$ on the line source is received at the field point $\mathbf{x}$ not only at time $t = r/c$, but also any time in the interval $r/c < t < \infty$ (see Figure 5.2a). Thus, there is a 'tail' (Eringen et al., 1975) in the two-dimensional solutions as can be seen in Figure (5.2a). The tail may be one of the reasons that the boundary element solution may become unstable.

Schematic representations of the two and three-dimensional fundamental solutions as a function of time can be seen in Figures (5.2a) and (5.2b) for a fixed position. Note that here, $\mathbf{x} = (x_1, x_2)$, $\mathbf{y}^i = (y_1, y_2)$ and $\mathbf{x} = (x_1, x_2, x_3)$, $\mathbf{y}^i = (y_1, y_2, y_3)$ for the two and three-dimensional cases respectively. More comprehensive discussion to this difference may be found in, for example, Morse et al. (1953) Greenberg (1971) and Eringen et al. (1975), Barton (1991).

5.2.2 Boundary Integral Equation

With the zero body source and zero initial conditions, equation (3.17) can be rewritten, for the three-dimensional case, as:

$$\phi(\mathbf{y}^i, t) = \int_B (\phi^s * q)(\mathbf{x}, t) dB - \int_B (q^s * \phi)(\mathbf{x}, t) dB \tag{5.13}$$

Equation (5.13) is now considered for the case of the body source on the smooth boundary. In this case, due to the singular behaviour of the fundamental solutions at $\mathbf{y}^i = \mathbf{x}$ when $\mathbf{y}^i \in B$, integral equation must be established through a limiting process to remove singularities. The domain Ω can then be enlarged (Mansur et al., 1985, Brebbia et al. 1992, Bonnet, 1998) by a small hemi-sphere of radius ε, as shown in Figure (5.3). The

point $\mathbf{y}^i$ is considered at the centre of the small sphere of infinitesimally small radius ε, with $\varepsilon \to 0$.

In equation (5.13), the integrals can be evaluated when $r \to 0$ with the help of Figure (5.3). Hence, the integrals in equation (5.13) can be written as the limiting process when $\varepsilon \to 0$ for boundary surfaces B_ε and B. Thus,

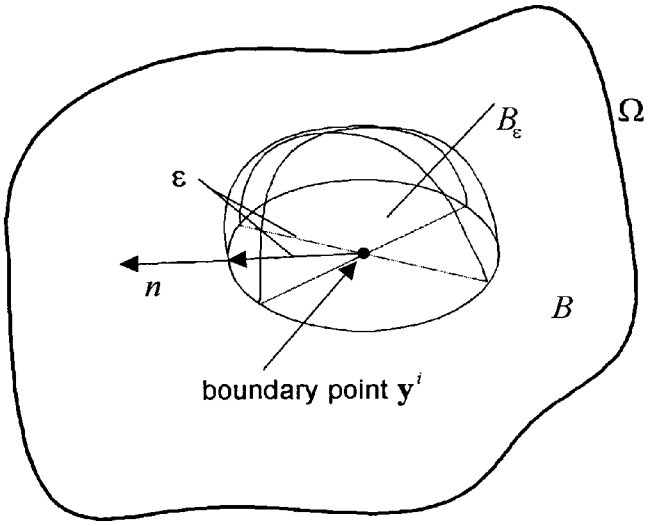

Figure 5.3 Illustration of the Cauchy Principal Value

$$I_1 = \int_B (\phi^s * q)(\mathbf{x},t)dB = \lim_{\varepsilon\to 0} \int_{B-B_\varepsilon} (\phi^s * q)(\mathbf{x},t)dB + \lim_{\varepsilon\to 0} \int_{B_\varepsilon} (\phi^s * q)(\mathbf{x},t)dB \qquad (5.14)$$

and:

$$I_2 = \int_B (q^s * \phi)(\mathbf{x},t)dB = \lim_{\varepsilon\to 0} \int_{B-B_\varepsilon} (q^s * \phi)(\mathbf{x},t)dB + \lim_{\varepsilon\to 0} \int_{B_\varepsilon} (q^s * \phi)(\mathbf{x},t)dB \qquad (5.15)$$

The singular behaviour of the dynamical and static fundamental solutions is the same. Therefore, during the evaluation of the second integrals in equations (5.14) and (5.15), the dynamical fundamental solutions are replaced by their static counterparts and given (Bonnet, 1998, Brebbia et al., 1992):

$$\phi^{s1} = \frac{1}{4\pi r}, \qquad q^{s1} = -\frac{\partial r}{\partial n}\frac{1}{4\pi r^2} \tag{5.16}$$

where ϕ^{s1} and q^{s1} are the three-dimensional potential and flux fundamental solutions for the static case.

Hence, these integrals are calculated by replacing ϕ^s and q^s with ϕ^{s1} and q^{s1}, respectively, for the small hemi-sphere, when $\varepsilon \to 0$. The last integrals in equations (5.14) and (5.15) are then:

$$\lim_{\varepsilon\to 0}\int_{B_\varepsilon} q\phi^{s1}dB = \lim_{\varepsilon\to 0}[-q\frac{2\pi\varepsilon^2}{4\pi\varepsilon}] = 0 \tag{5.17}$$

$$\lim_{\varepsilon\to 0}\int_{B_\varepsilon} \phi q^{s1}dB = \lim_{\varepsilon\to 0}[-\phi\frac{2\pi\varepsilon^2}{4\pi\varepsilon^2}] = -\frac{1}{2}\phi \tag{5.18}$$

where $2\pi\varepsilon^2$ is the surface of the hemi-sphere. Note that time convolution has not been used in equations (5.17) and (5.18) since the kernels are static, whilst the actual potential ϕ and flux q values are time-dependent. Using (5.17) and (5.18), the identities (5.14) and (5.15) are:

$$I_1 = \int_B (\phi^s * q)(\mathbf{x},t)dB \tag{5.19}$$

$$I_2 = \int_B (q^s * \phi)(\mathbf{x},t)dB - \frac{1}{2}\phi(\mathbf{y}^i,t) \tag{5.20}$$

Employing equations (5.13), (5.19) and (5.20), the integral equation for a boundary point is:

$$\frac{1}{2}\phi(\mathbf{y}^i,t) = \int_B (\phi^s * q)(\mathbf{x},t)dB - \int_B (q^s * \phi)(\mathbf{x},t)dB \tag{5.21}$$

where the integrals have the sense of a Cauchy principal value.

For points $\mathbf{y}^i$, located outside $\Omega \cup B$, the potential is equal to zero. Then, the left-hand side of equation (3.17) is equal to zero for the three-dimensional case, that is, $\phi(\mathbf{y}^i, t) = 0$. Thus, the integral representation for the three-dimensional scalar wave problems for any point can be condensed to:

$$\alpha^i \phi(\mathbf{y}^i, t) = \int_B (q * \phi^s)(\mathbf{x}, t) dB - \int_B (\phi * q^s)(\mathbf{x}, t) dB \tag{5.22}$$

where

$$\alpha^i(\mathbf{y}^i) = \begin{cases} 1. & \text{if} \quad \mathbf{y}^i \in \Omega \\ 1/2 & \text{if} \quad \mathbf{y}^i \in B \\ 0. & \text{if} \quad \mathbf{y}^i \notin (\Omega \cup B) \end{cases} \tag{5.23}$$

Using the convolution, equation (5.22) may be written explicitly as:

$$\alpha^i \phi(\mathbf{y}^i, t) = \int_0^t \int_B \phi^s(\mathbf{x}, t-\tau; \mathbf{y}^i) q(\mathbf{x}, \tau) dB d\tau - \int_0^t \int_B q^s(\mathbf{x}, t-\tau; \mathbf{y}^i) \phi(\mathbf{x}, \tau) dB d\tau \tag{5.24}$$

In equation (5.24), the components of the solution states, ϕ^s and q^s, are given by equations (5.10) and (5.11) respectively. Similar approaches for non-smooth boundaries can be found, for example, in Banerjee (1994), Brebbia et al. (1992), Guiggiani (1992) and Paris et al. (1997).

5.3 Boundary Elements for 3D Problems

So far, the integral representation has been instituted in terms of the two dynamical states from the principle of dynamic reciprocity, and boundary integral equation has been established. As it is impossible to obtain an analytical solution of the boundary integral equation except for trivial geometries, it is necessary to employ numerical methods. In the present work, for the numerical integration, the boundary surface is approximated by

flat surfaces (or planes), that are called boundary elements in a three-dimensional geometry as shown in Figure (5.4).

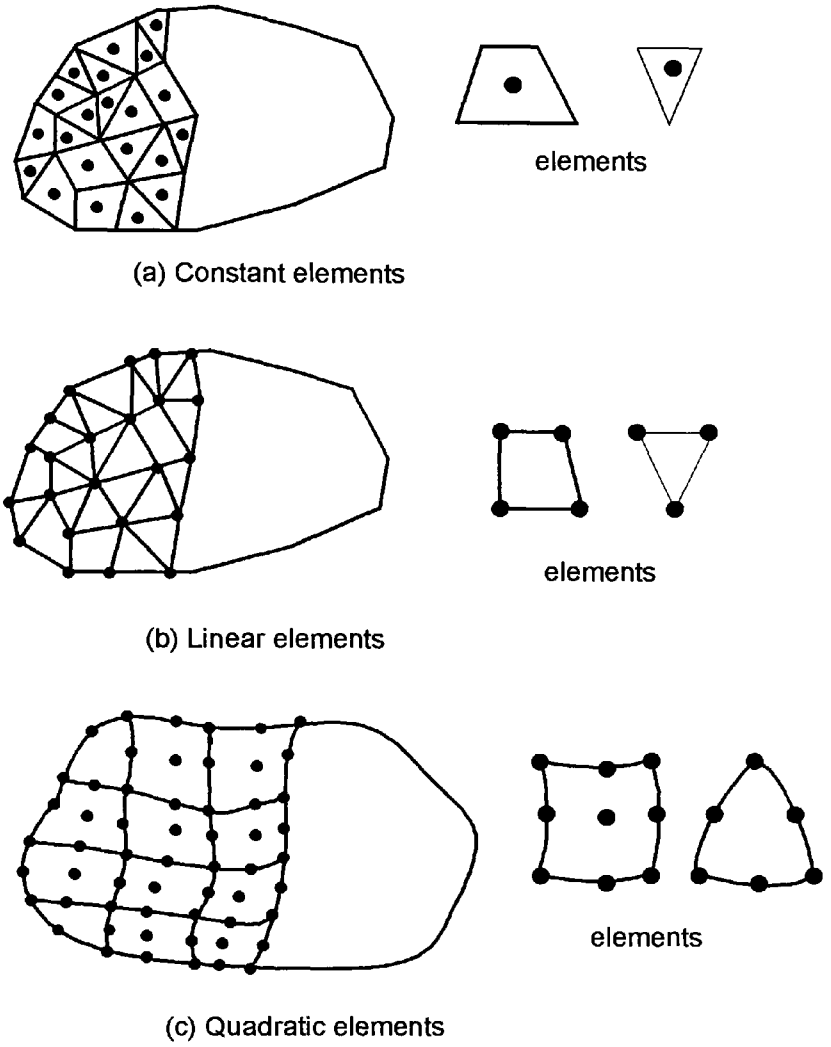

Figure 5.4 Quadrilateral and Triangular elements for 3D problems

In an element, nodal points are positions where dependent variable values are to be approximately determined. If the nodal points are taken to be in the centre of the element surface, then the boundary elements are called constant (see Figure 5.4.a), and if they are taken to be at the corner points of the element, then they are called linear, as shown in

Figure (5.4.b). An element is called a quadratic element if the element is also required to have a node between the two corners, as well as at the centre (for quadrilateral) of the element (see Figure 5.4.c).

5.3.1 Time Interpolations of Boundary Variables

Implementation of the method requires assumptions about the temporal distribution of the boundary variables. Formulation of the interpolation functions for the boundary parameters follows the procedure given in Chapter 3. Namely, temporal variations of the boundary flux q and boundary potential ϕ are constant and linear respectively. Having divided time into n equal intervals, $t = n\Delta t$, similar to the two-dimensional problems, to obtain the approximate solution of the boundary integral equation let:

$$\phi(\mathbf{x},\tau) = \sum_m \eta^m(\tau)\phi^m(\mathbf{x})$$

$$q(\mathbf{x},\tau) = \sum_m \mu^m(\tau)q^m(\mathbf{x}) \tag{5.25}$$

where $\eta^m(\tau)$ and $\mu^m(\tau)$ are the temporal interpolation shape functions, as given in the earlier chapters. In addition, ϕ^m and q^m indicate the potential and flux, respectively, at time $t_m = m\Delta t$ at point $\mathbf{x}$, similar to the two-dimensional case. The choice of the interpolation time functions has been discussed in detail in Chapter 3. For any given boundary node at time step n, after the time approximations have been used, equation (5.24) can be written as:

$$\alpha^i\phi^{ni} = \sum_{m=1}^{n}[\int_B U^{nm}q^m(\mathbf{x})dB] - \sum_{m=1}^{n}[\int_B Q^{nm}\phi^m(\mathbf{x})dB] \tag{5.26}$$

where

$$U^{nm} = \int_{\Delta t_m} \phi^s(\mathbf{x}, t-\tau; \mathbf{y}^i)\mu^m(\tau)d\tau = \frac{1}{4\pi r}\int_{\tau_{m-1}}^{\tau_m} \delta[(t-r/c)-\tau]d\tau$$

$$= \frac{1}{4\pi r}[H(t_n - \tau_{m-1} - r/c) - H(t_n - \tau_m - r/c)] \tag{5.27}$$

and:

$$Q^{nm} = \int_{\Delta t_m} q^s(\mathbf{x}, t-\tau; \mathbf{y}^i)\eta^m(\tau)d\tau$$

$$= \int_{\tau_{m-1}}^{\tau_m} (\frac{\tau - \tau_{m-1}}{\Delta t})q^s(\mathbf{x}, t-\tau; \mathbf{y}^i)d\tau + \int_{\tau_m}^{\tau_{m+1}} (\frac{\tau_{m+1} - \tau}{\Delta t})q^s(\mathbf{x}, t-\tau; \mathbf{y}^i)d\tau \tag{5.28}$$

The solutions ϕ^s and q^s are given by equations (5.10) and (5.11) respectively. In equation (5.26), n indicates the final time (i.e. $t = n\Delta t$), whilst the actual potential value is shown by ϕ^{ni} at point $\mathbf{y}^i$ on the boundary at time step n.

Taking (5.27), the effect of the load at the field point $\mathbf{x}$ at time $t = t_n$ can be given depending on whether or not the disturbance reached the field point. To obtain the time integral for the potential, three possible situations have been considered and are described by the cases below:

Case 1: $\tau_m < \tau^* = t_n - \frac{r}{c}$

Disturbances within the interval $[\tau_{m-1}, \tau_m]$ are:

$$U^{nm} = 0 \tag{5.29}$$

Case 2: $\tau_{m-1} < \tau^* \leq \tau_m$

The field point has received the effect within only this interval. So that:

$$U^{nm} = \frac{1}{4\pi r} \tag{5.30}$$

Case 3: $\tau^* \leq \tau_{m-1}$

There is no effect yet which has been received by the field point, so that:

$$U^{nm} = 0 \tag{5.31}$$

Similarly, for the time integral of the flux equation (5.28), four possible cases must be considered. Hence from equation (5.28), the time integration for the flux kernel, for the three-dimensional case, may be given as:

Case 1: $\tau_{m+1} < \tau^*$

$$Q^{nm} = 0 \tag{5.32}$$

Case 2: $\tau_m < \tau^* \leq \tau_{m+1}$

$$Q^{nm} = \frac{\partial r}{\partial n}\frac{a_2}{4\pi r c \Delta t} \tag{5.33}$$

where a_2 is formally the same as in Chapter 3.

Case 3: $\tau_{m-1} < \tau^* \leq \tau_m$

$$Q^{nm} = -\frac{\partial r}{\partial n}\frac{a_0}{4\pi r c \Delta t} \tag{5.34}$$

where a_0 is formally the same as in Chapter 3.

Case 4: $\tau^* \leq \tau_{m-1}$

$$Q^{nm} = 0 \tag{5.35}$$

It is important to emphasise that the kernels obtained in the above, agree with the kernels obtained *implicitly* during time integration by Dominguez (1993).

It is also noticeable that, by taking $n = m$ from the above equations the three-dimensional static potential and flux fundamental solutions can be easily found, and seen to be the same as with the solutions (5.16).

5.3.2 Boundary Discretization

The boundary surface of the domain is discretized into a number of connected elements, see for example Figure (5.5). Over each element, the spatial variation of the potentials and fluxes and the geometry are described. The variations can be chosen with arbitrary order. In the present study for the three-dimensional problems, the co-ordinates at any point over any element are expressed using linear quadrilateral elements, whilst the field variables are represented by constant quadrilateral elements. The co-ordinates using linear interpolation functions can represent the geometry of an element,

$$\mathbf{x}(\zeta) = \varphi_\alpha(\zeta)\mathbf{x}^\alpha, \quad 1 \le \alpha \le 4 \tag{5.36}$$

where

$$\varphi_1(\zeta) = \frac{1}{4}(1-\zeta_1)(1-\zeta_2)$$

$$\varphi_2(\zeta) = \frac{1}{4}(1+\zeta_1)(1-\zeta_2)$$

$$\varphi_3(\zeta) = \frac{1}{4}(1+\zeta_1)(1+\zeta_2)$$

$$\varphi_4(\zeta) = \frac{1}{4}(1-\zeta_1)(1+\zeta_2) \tag{5.37}$$

with the homogeneous co-ordinates $\zeta = \zeta(\zeta_1, \zeta_2)$.

The nodal values of the potential and flux on the boundary are approximated by using the spatial interpolation function ψ_j for the node j to write equation (5.25),

$$\phi(\mathbf{x},\tau) = \sum_j \sum_m \eta^m(\tau)\psi_j(\mathbf{x})\phi^{mj}$$

$$q(\mathbf{x},\tau) = \sum_j \sum_m \mu^m(\tau)\psi_j(\mathbf{x})q^{mj} \tag{5.38}$$

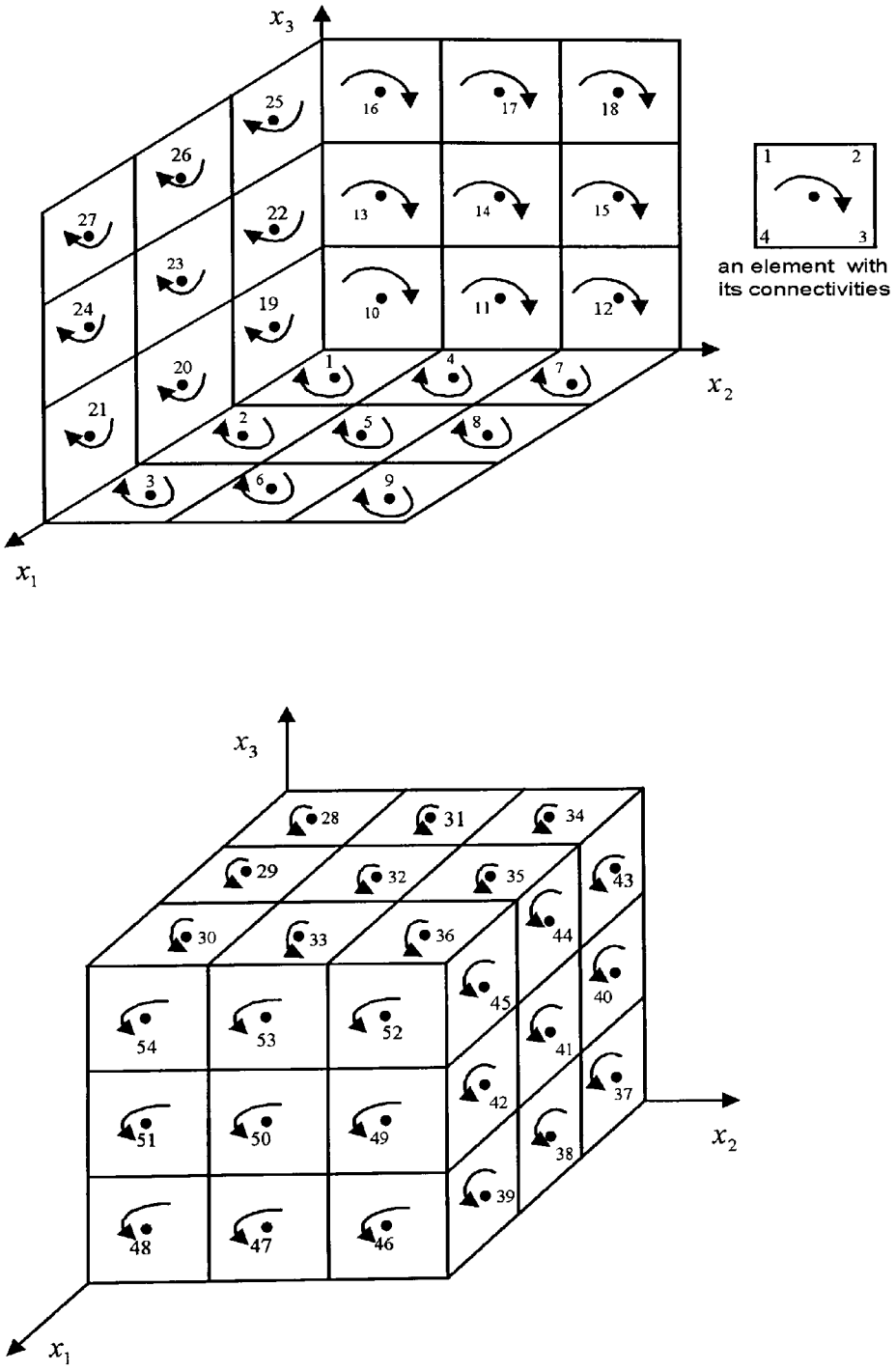

Figure 5.5 Discretization of a boundary surface

where ϕ^{mj} and q^{mj} denote the potential and its normal derivative, respectively, at node j for time $t_m = m\Delta t$. Furthermore, when the field variables are constant over the element in approximation (5.38) $\psi_j(\mathbf{x}) = 1$.

When the elements are isoparametric, the interpolation functions are identical so that $\psi_j(\zeta) = \varphi_\alpha(\zeta)$.

After discretization of the boundary B into B_j, j=1,2,...,N, equation (5.26) can be written as:

$$\alpha^i \phi^{ni} = \sum_{m=1}^{n}\sum_{j=1}^{N}[\int_{B_j} U^{nm}\psi_j(\mathbf{x})dB]q^{mj} - \sum_{m=1}^{n}\sum_{j=1}^{N}[\int_{B_j} Q^{nm}\psi_j(\mathbf{x})dB]\phi^{mj} \qquad (5.39)$$

5.3.2.1 Evaluation of Spatial Integrals

As mentioned in the two-dimensional problems, in the BEM only the boundary surface B is discretized, as opposed to the FDM and FEM in which the domain is also discretized. After the discretization, the kernels U^{nm} and Q^{nm} have to be integrated spatially over the all boundary elements. In Figure (5.5), a discretization by using constant elements of a cube is given as an example. As the flat boundaries are used, constant elements are preferred.

The co-ordinates of the corner points of the boundary elements are used. The numbers of the corner points of one element are given in an order by the right hand screw rule, following the outward normal vector to the element. Four corner points are given for quadrilateral elements. Since a triangular element is accepted as a degenerated quadrilateral element (in the case of singularity), four corner points are used for a triangular element as well. Also the numbering direction, depending on the outward normal, is shown in Figure (5.5).

If the load point $\mathbf{y}^i$ is not on the integration element, the integrals $\int_{B_j} U^{nm}\psi_j dB$ and $\int_{B_j} Q^{nm}\psi_j dB$ are evaluated using a standard Gaussian quadrature of maximum order of fourteenth, due to the same reason as before. The integrals are expressed using the homogeneous co-ordinates ζ_1, ζ_2 of the elements. From Figure (5.6) the differential area is

$$dB = \left|\frac{\partial \mathbf{x}}{\partial \zeta_1} \times \frac{\partial \mathbf{x}}{\partial \zeta_2}\right| d\zeta_1 d\zeta_2 = |\mathbf{J}| d\zeta_1 d\zeta_2 \tag{5.40}$$

where $|\mathbf{J}|$ is the Jacobian of the transformation.

By using equation (5.36) for element j:

$$\frac{\partial \mathbf{x}^j}{\partial \zeta_k} = \left(\frac{\partial x_1}{\partial \zeta_k}, \frac{\partial x_2}{\partial \zeta_k}, \frac{\partial x_3}{\partial \zeta_k}\right)^j = \frac{\partial \varphi_\alpha}{\partial \zeta_k}\mathbf{x}^j \tag{5.41}$$

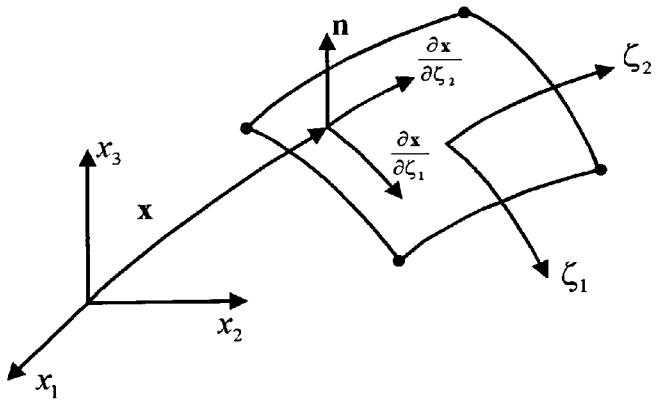

Figure 5.6 Transformation of the co-ordinates for the Gaussian integration

Then, using the base vectors and omitting node j,

$$\frac{\partial \mathbf{x}}{\partial \zeta_1} \times \frac{\partial \mathbf{x}}{\partial \zeta_2} = \left(\frac{\partial x_2}{\partial \zeta_1}\frac{\partial x_3}{\partial \zeta_2} - \frac{\partial x_3}{\partial \zeta_1}\frac{\partial x_2}{\partial \zeta_2}, \frac{\partial x_3}{\partial \zeta_1}\frac{\partial x_1}{\partial \zeta_2} - \frac{\partial x_1}{\partial \zeta_1}\frac{\partial x_3}{\partial \zeta_2}, \frac{\partial x_1}{\partial \zeta_1}\frac{\partial x_2}{\partial \zeta_2} - \frac{\partial x_2}{\partial \zeta_1}\frac{\partial x_1}{\partial \zeta_2}\right)$$
$$= (s_1, s_2, s_3) \tag{5.42}$$

The magnitude of the Jacobian is

$$|\mathbf{J}| = (s_1^2 + s_2^2 + s_3^2)^{1/2} \tag{5.43}$$

So with equations (5.40) and (5.43), equation (5.39) can be written as:

$$\alpha^i \phi^{ni} = \sum_{m=1}^{n}\sum_{j=1}^{N}\left[\int_{-1}^{1}\int_{-1}^{1} U^{nm}\psi_j |\mathbf{J}| d\zeta_1 d\zeta_2\right] q^{mj} - \sum_{m=1}^{n}\sum_{j=1}^{N}\left[\int_{-1}^{1}\int_{-1}^{1} Q^{nm}\psi_j |\mathbf{J}| d\zeta_1 d\zeta_2\right] \phi^{mj} \tag{5.44}$$

In equation (5.44), lower and upper limits for the Gaussian integrations are 0 and 1, respectively, for the triangular elements.

The same transformation of the co-ordinates can be used during the internal integration.

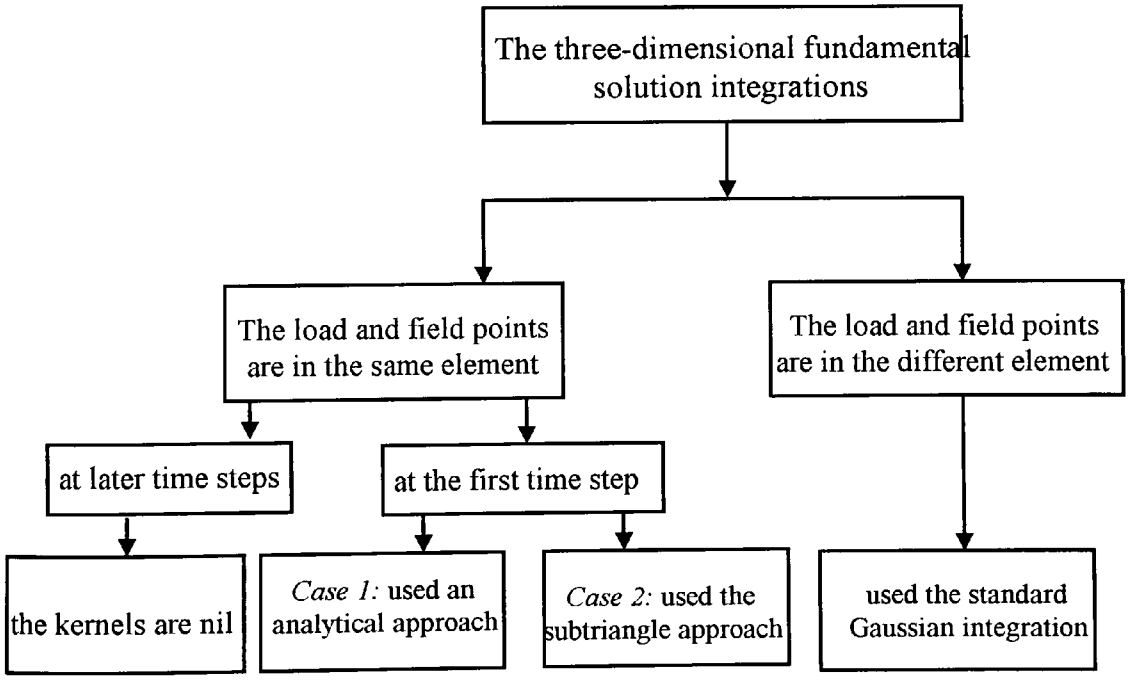

Figure 5.7 Integration Scheme

5.3.2.2 Evaluation of Singular Integrals

There are two types of integrals, singular and non-singular as can be seen in Figure (5.7). The integrals become singular when $r \rightarrow 0$ for the first time step. In the previous section, the integrals have been considered when $r \neq 0$. Now the integrals are discussed when $r = 0$ at the first time step. At later time steps, the integration of the potential kernel is zero, when $r = 0$.

As previously stated, the singularity is of the same order as its static counterpart. In the singularity case, the fundamental flux solution is zero, since $\partial r / \partial n = 0$. Therefore, only the fundamental potential solution is integrated using two approaches:

***Case 1 (Analytical Approach)*:** In this approach the singular integral is evaluated analytically. When the load and field points are coincident at first time step, the spatial term in equation (5.30) is integrated over the element area to which the load and field points belong. In this case, the integration is evaluated in a circle defined by the wave front in the plane of the element.

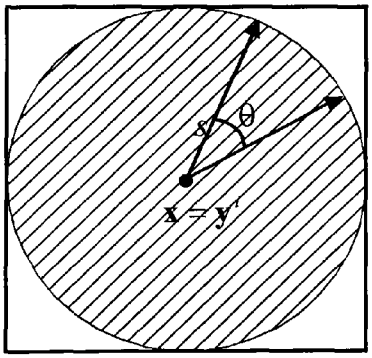

Figure 5.8 Integration element during the singularity

Then with the help of Figure (5.8) one can write using equation (5.30) in polar co-ordinates:

$$\frac{1}{4\pi}\int_{B_i}\frac{1}{r}dB_i = \frac{1}{4\pi}\int_0^{2\pi s}\int_0\frac{1}{r}rdrd\theta = \frac{1}{4\pi}2\pi s = s/2 \qquad (5.45)$$

where s is the wave front radius of the rectangular element.

Case 2 (Subtriangle Approach): The integration of the potential fundamental solution is evaluated when the load and field points are in the same element. To achieve this, the element is first divided into four sub-triangles as in Figure (5.9). Then, each sub-element is considered as an independent quadrilateral element by taking two corners at the same node. The integration is performed for each sub-element using the standard Gaussian integration. So, the singularity is removed by taking each sub-element as a quadrilateral element. In a similar manner, this approach can also be used for the triangular elements.

It is important to see that *case 2* takes about 25% more computing time in comparison to *case 1*. For both cases, the results are to be presented, and it will be seen that there is excellent agreement between the solutions.

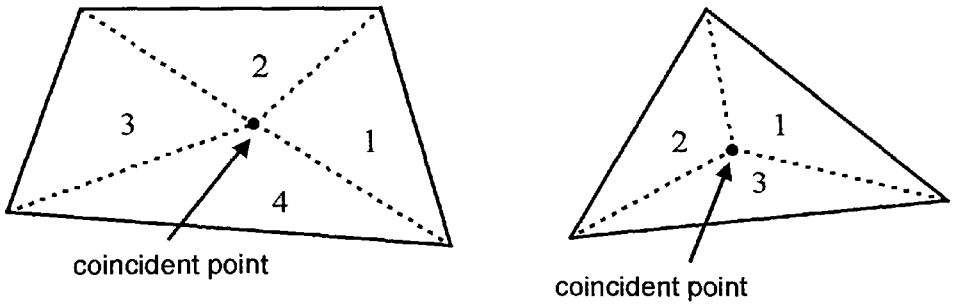

Figure 5.9 Subdivision of constant surface elements for the singular integration

5.3.3 The Boundary Element Equation

After the geometry and boundary variables have been discretized, in terms of the spatial and time integrals for all boundary elements, the algebraic linear equation system is

formed. To write the BEM equation for each element, equations (3.55-3.59) of Chapter 3 are used. However notice that, these equations are used here for the surface of the three dimensional geometries. Then, by solving the linear equation system obtained from all boundary elements, the unknown field variables are computed for each time step n using the solution procedure given in Chapter 3.

5.4 Infinite Domains

For convenience, the medium is taken to be of infinite extent. For example, consider Figure (5.10). For such domains one can take the sides of the domain at infinity, such that $r \to \infty$, whilst the top and bottom sides are bounded. Thus, one can write $B = B_1 + B_2^t + B_2^b$; where B_1, B_2^t and B_2^b denote the top boundary, bottom boundary and internal boundary surfaces, respectively. The external boundary surface is shown by B_r when extending to infinity. In Figure (5.10), $\mathbf{x}$ and $\mathbf{y}^i$ stand for the load and field points, respectively. Using the boundary definitions in the above, equation (5.24) can then be written in the following form:

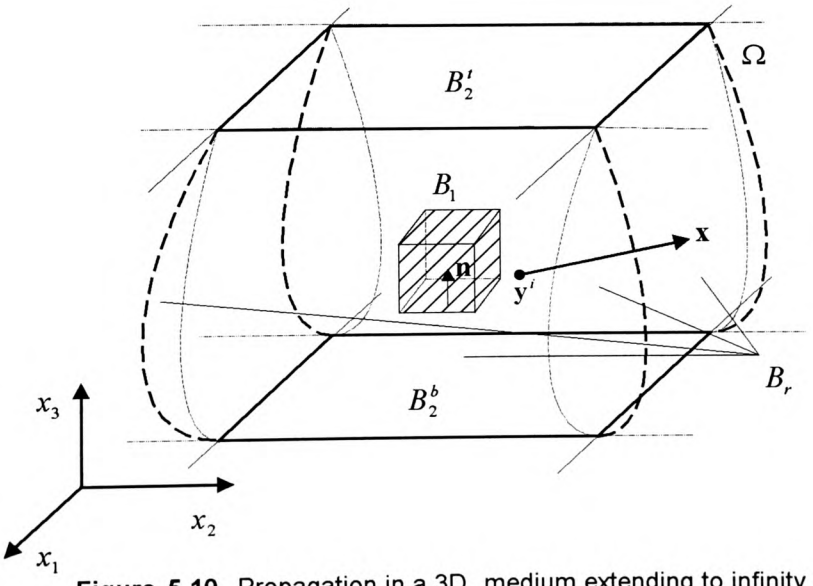

Figure 5.10 Propagation in a 3D medium extending to infinity

$$\alpha^i\phi(\mathbf{y}^i,t)=\int_B[(\phi^s*q)-(q^s*\phi)](\mathbf{x},t)dB+\lim_{r\to\infty}\int_{B_r}[(\phi^s*q)-(q^s*\phi)](\mathbf{x},t)dB \qquad (5.46)$$

When all the loads producing the motion are inside a finite domain, then there is no wave to propagate to the interior from the far field. Therefore, the potential and its normal derivative must behave in such a way that the last integral in equation (5.46) must be zero (Eringen et al., 1975, Bonnet, 1998). Consideration of the analytical structure of the three-dimensional fundamental solutions (5.10, 5.11) gives:

$$\lim_{r\to\infty}\phi=0, \qquad \lim_{r\to\infty}r(\frac{\partial\phi}{\partial r}+\frac{1}{c}\dot{\phi})=0 \qquad (5.47)$$

Similar to the two-dimensional case, the regularity and radiation conditions (5.47), ensure the uniqueness of the solution (Eringen et al., 1975). Thus, the boundary integral equation (5.24) remains valid for infinite domains, as well as for bounded domains. Hence, the discretization of the external boundary surface B_r is not required, as $r\to\infty$. This argument may be repeated for semi-infinite domains as well as the infinite domains.

5.5 Multimedia

Various homogeneous media will now be studied. The geometry is illustrated in Figure (5.11) for the simplest case where the domain is subdivided into two subdomains Ω_1 and Ω_2 with a flat interface. With reference to Figure (5.11) two BEM equations (3.64) and (3.65) can be used for subdomains Ω_1 and Ω_2, respectively. Both field variables are unknown on the interface. Therefore, it is required that the common nodal points on the boundary surfaces B_1 and B_2 are at the same potential, and the fluxes associated with each subdomain are in dynamical equilibrium. These conditions are expressed using the interface equations (3.66, 3.67). It must be remembered that, the equations are used here for the three-dimensional geometries.

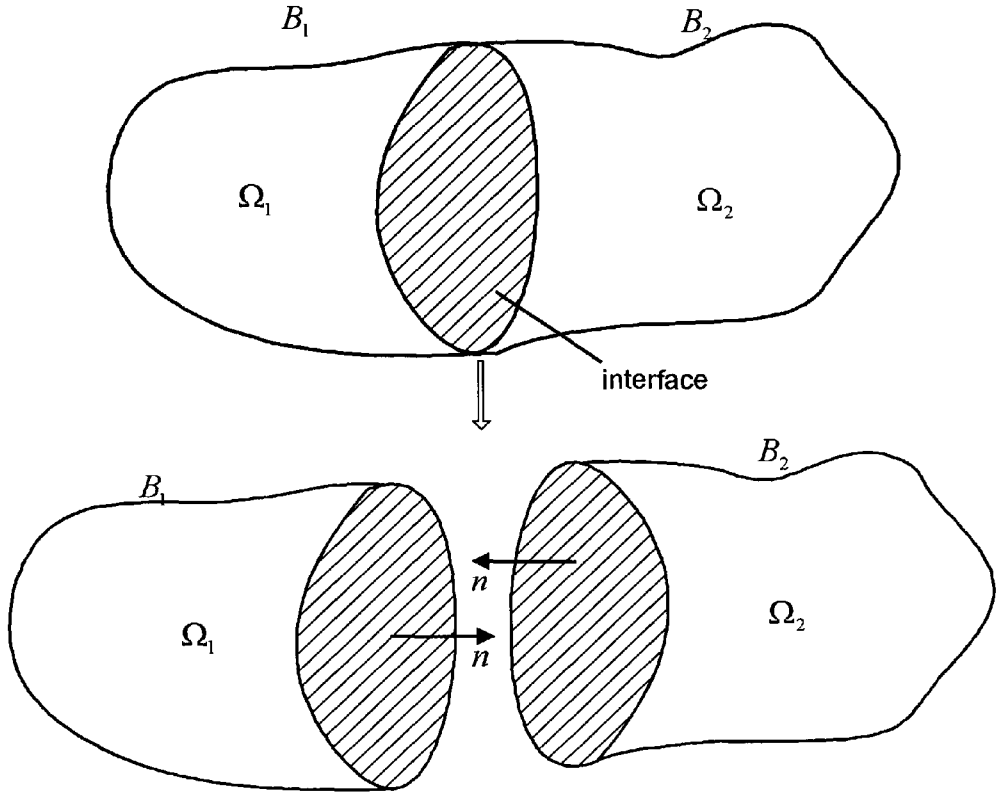

Figure 5.11 Two subdomains of the medium

In the same way as the two dimensional problems, the integral equation is constructed in terms of the interface variables of the subdomain, as well as the boundary variables. The use of equations (3.66) and (3.67), for the current geometries corresponding to the interface, makes the number of unknowns and knowns equal. The discrete equation system is then built for the piecewise homogeneous media, and simultaneously solved for all subdomains. It follows that the algebraic equation system including the interface equations can be written in the form of equation (3.68). Following the same procedure as described in Chapter 3, equation (3.68) is solved for the present case. Needless to say that the same argument can be repeated for more than two subdomains.

5.6 Internal Calculations

In the BEM analysis, the internal points to be considered are optional. To compute the internal field variable values, the equations related to them are obtained. The internal flux kernels are derived for different cases, depending on whether or not the effect has been received by the field point.

5.6.1 Internal Potentials

So far, the numerical formulation determined has focused on finding the unspecified boundary values. When the field variables on the boundary are known, for time $t = \Delta t, 2\Delta t, \ldots, n\Delta t$, then the internal potential value at chosen points can be readily calculated. For the boundary node j and internal point i, considering the time difference n-m, the interior integral representation can be written with the same discretization for time and boundary integrals as follows:

$$\phi^{ni} = \sum_{m=1}^{n} \sum_{j=1}^{N} (G^{nmij} q^{mj} - \hat{H}^{nmij} \phi^{mj}) \tag{5.48}$$

5.6.2 Internal Fluxes

If the field quantities on the boundary are known for $t = \Delta t, 2\Delta t, \ldots, n\Delta t$, then the internal fluxes can be calculated using the internal kernels. The internal flux kernels are derived in the same way as their 2D counterparts. The coefficients depend on the boundary node j, internal point i, and time difference n-m. The internal fluxes can then be calculated. Differentiation of equation (5.48) gives the following equation:

$$q_k^{ni} = \frac{\partial \phi^{ni}}{\partial y_k} = \sum_{m=1}^{n} \sum_{j=1}^{N} \left(\frac{\partial G^{nmij}}{\partial y_k} q^{mj} - \frac{\partial \hat{H}^{nmij}}{\partial y_k} \phi^{mj} \right) \tag{5.49}$$

To avoid clustering of notation, the index 'i' of the load point $\mathbf{y}^i$ is omitted. In equation (5.49), q_k^{ni} denotes the flux in the k-direction at an internal point i at time step n. From the last equation,

$$\frac{\partial G^{nmij}}{\partial y_k} = \int_B \frac{\partial U^{nm}}{\partial y_k} \psi_j dB \tag{5.50}$$

where ψ_j is the same as given before. Then

$$\frac{\partial U^{nm}}{\partial y_k} = \int_{\Delta t_m} \frac{\partial}{\partial y_k} \phi^s(\mathbf{x}, t-\tau; \mathbf{y}) \mu^m(\tau) d\tau \tag{5.51}$$

Three different situations are considered:

Case 1: $\tau_m < \tau^*$

Disturbances which take place within the interval $[\tau_{m-1}, \tau_m]$ are:

$$\frac{\partial U^{nm}}{\partial y_k} = 0 \tag{5.52}$$

Case 2: $\tau_{m-1} < \tau^* \leq \tau_m$

The effect received by the field point is:

$$\frac{\partial U^{nm}}{\partial y_k} = \frac{1}{4\pi} \frac{r_{,k}}{r^2} \tag{5.53}$$

where τ^* and $\mu^m(\tau)$ are the same as given before, and $r_{,k} \equiv \frac{\partial r}{\partial x_k} \equiv \frac{r_k}{r}$ with $r_k \equiv x_k - y_k$.

Case 3: $\tau^* \leq \tau_{m-1}$

There is no effect at the field point, so that:

$$\frac{\partial U^{nm}}{\partial y_k} = 0 \tag{5.54}$$

In a similar manner to equation (5.51), the interior flux kernel is:

$$\frac{\partial \hat{H}^{nmij}}{\partial y_k} = \int_B \frac{\partial Q^{nm}}{\partial y_k} \psi_j dB \tag{5.55}$$

with

$$\frac{\partial Q^{nm}}{\partial y_k} = \int_{\Delta t_m} \frac{\partial}{\partial y_k} [q^s(\mathbf{x}, t-\tau; \mathbf{y})] \eta^m(\tau) d\tau \tag{5.56}$$

where $\eta^m(\tau)$ is the same as given before.

Now consideration of four possible situations is given as follows:

Case 1: $\tau_m < \tau^*$

$$\frac{\partial Q^{nm}}{\partial y_k} = 0 \tag{5.57}$$

Case 2: $\tau_m < \tau^* \leq \tau_{m+1}$

$$\frac{\partial Q^{nm}}{\partial y_k} = \frac{a_2}{4\pi r c \Delta t} \left[\frac{2r_{,k}}{r} \frac{\partial r}{\partial n} + \frac{\partial}{\partial y_k} \left(\frac{\partial r}{\partial n} \right) \right] \tag{5.58}$$

where the expression $\frac{\partial}{\partial y_k}\left(\frac{\partial r}{\partial n}\right)$ is the same as in equation (3.79) but here the three-dimensional situation is used.

Case 3: $\tau_{m-1} < \tau^* \leq \tau_m$

$$\frac{\partial Q^{nm}}{\partial y_k} = \frac{-a_0}{4\pi r c \Delta t} \left[\frac{2r_{,k}}{r} \frac{\partial r}{\partial n} + \frac{\partial}{\partial y_k} \left(\frac{\partial r}{\partial n} \right) \right] \tag{5.59}$$

Case 4: $\tau^* \leq \tau_{m-1}$

$$\frac{\partial Q^{nm}}{\partial y_k} = 0 \tag{5.60}$$

It is worth emphasising that by taking $n = m$ in equations (5.53), (5.58) and (5.59), the static flux kernels are obtained for the interior points as follows:

$$\frac{\partial U^{nn}}{\partial y_k} = \frac{1}{4\pi}\frac{r_{,k}}{r^2} \tag{5.61}$$

$$\frac{\partial Q^{nn}}{\partial y_k} = -\frac{1}{4\pi r^2}[\frac{2r_{,k}}{r}\frac{\partial r}{\partial n} + \frac{\partial}{\partial y_k}(\frac{\partial r}{\partial n})] \tag{5.62}$$

At the same time, one can also check the equations (5.61) and (5.62) using the solutions (5.16).

Similar to the two-dimensional case, to calculate the internal unknowns inside a subdomain, only the subdomain boundary (interface) coefficients are used.

5.7 Numerical Aspects

As was pointed out for the two-dimensional problems, choice of appropriate time step size is very important for the transient dynamic problems. To analyse the sensitivity of the time step size and element size, the BEM solution for a single internal point (50,50,45) is presented in a medium extending to infinity on the sides and bottom (see Figure 5.12). In the solution, the natural boundary condition is specified for the discretized boundary. As always for the field variables on the source, homogeneous Dirichlet boundary conditions are prescribed. The elements are uniform for the external boundary with their size being 4m×4m, while 3m×3m for the source.

The time step size used for the element meshes is computed and selected using the relationship:

$$\Delta t = \frac{1}{c}\sqrt{\frac{\Delta x_1 \Delta x_2}{\pi}} \tag{5.63}$$

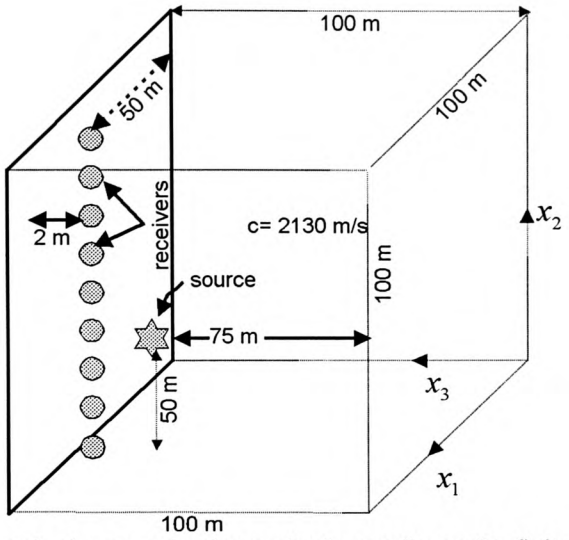

Figure 5.12 Physical geometry for a single medium of infinite extent used to generate seismograms in the 3D scalar BEM program

where Δx_1 and Δx_2 are the lengths of the sides of the rectangular element used. Equation (5.63) expresses the time required for the wave, which emanated from the geometrical centre of an element to cover a circular area equivalent to the rectangular area of the element (similar to Figure 5.8). Note that a formula similar to (5.63) for the elastodynamic problems was used by Karabalis et al. (1984).

When the relation (5.63) is not considered for the optimum time step, then there appear two alternatives: a small time step size, and a large time step size. It may be seen that the wave travels less than 100% of the element surface for a small time interval. On the other hand, for the selection of a large time step, the wave travels more than 100% of the element surface. A series of studies were conducted to show the appropriate time step size as follows.

When the time step is such that the wave travels around 100% of the area of an element, then a stable solution can be obtained (see Figure 5.13a). The solution is obtained for a single point in an unbounded medium. For the bounded medium, complete seismograms obtained from the recorded traces will be given in the next section. If a bounded medium were considered here, even the small forms of the wave would be recognisable.

If the wave travels less than 80% of the element surface within a time interval, the solution diverges and so looses stability (see Figures 5.13b,c).

It has been observed that when the wave travels around 1400% of an element surface, the solution remains valid (Figure 5.13d). In other words, for very large time steps, the solution is valid. However, for the larger time step sizes, small reflection events can not be seen when the medium is of finite extent. Results exemplifying this observation are not given in this section.

Similar to two-dimensional observation, the choice of element meshes affects the solution. In order to represent the distribution of the wave travelling accurately and efficiently, the boundary surface has been discretized into reasonably small element meshes. Since very small meshes cause accumulation of numerical errors and restriction of storage space, researchers need to be careful in their choice of element size. Moreover non-uniformity gives rise to observable effect, only when the difference between the element meshes is large.

It is apparent from Figure (5.13a) that agreement between the cases is excellent when the time step size is computed from the formula (5.63). In *case 1*, evaluation of the singular integrals needs to be performed only over the area of element (see Figure 5.8). When this restriction is not considered, agreement between *case 1* and *case 2* is not as good as in

Figure (5.13a). At the same time, the solution looks to be more sensitive for selection of time step in *case 2* than in *case 1*(see Figures 5.13b,c).

The observations stated here agree with the examinations carried out in two dimensions. In a later section, full results for all interior points will be given in the related seismograms.

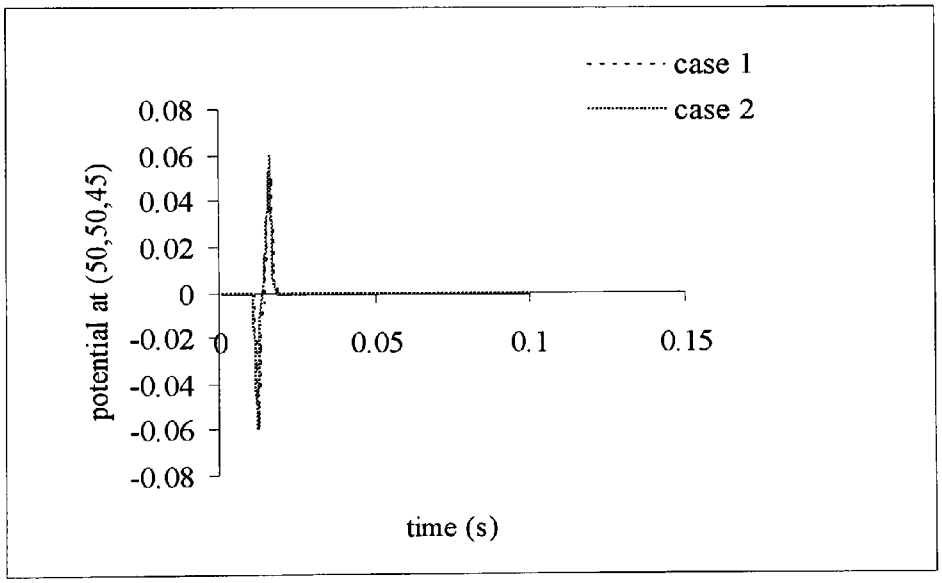

Figure 5.13a Plot of potential ϕ versus time for point (50,50,45) with *case 1* and *case 2*, for $\Delta t = 0.001$

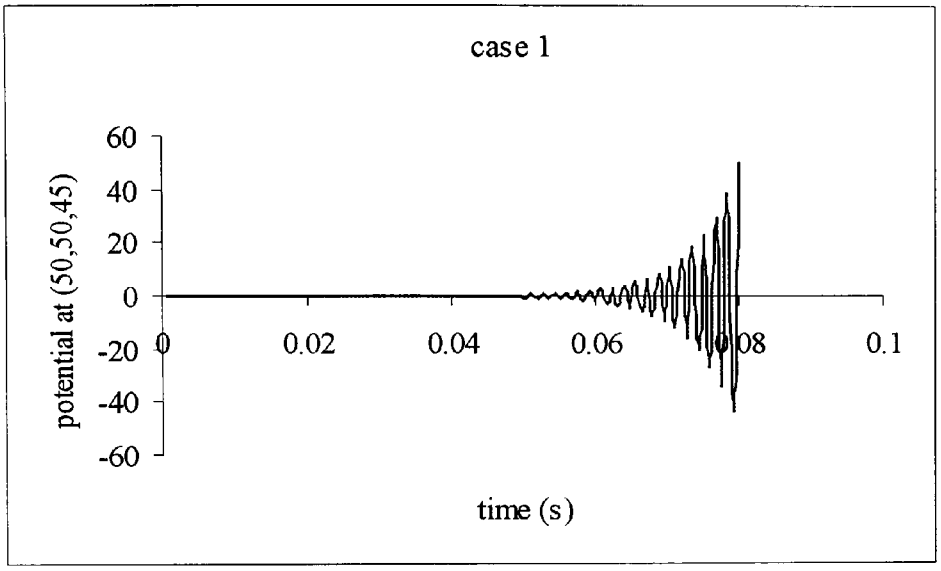

Figure 5.13b Plot of potential ϕ versus time for point (50,50,45) with *case 1* and for $\Delta t = 0.0008$

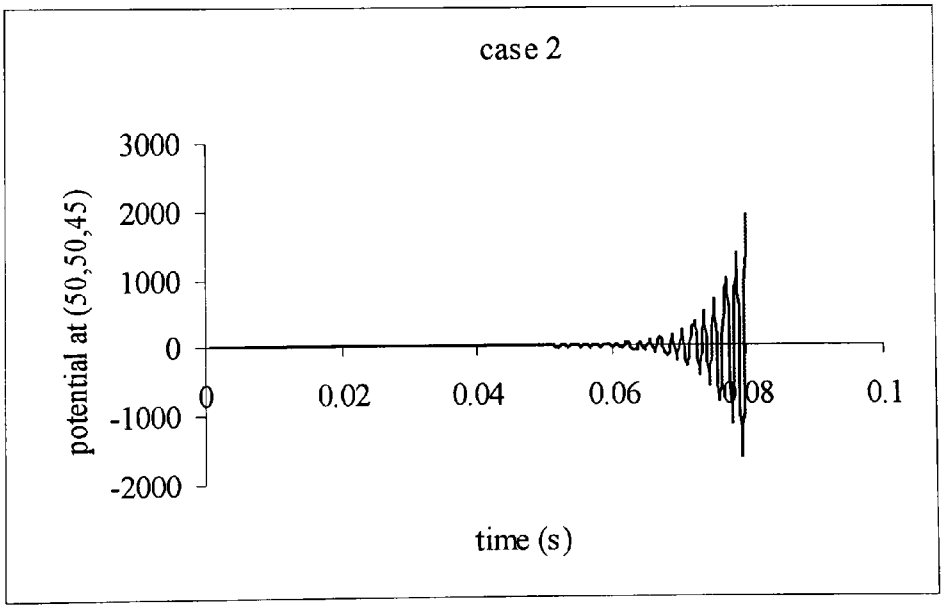

Figure 5.13c Plot of potential ϕ versus time for point (50,50,45) with *case 2* and for $\Delta t = 0.0008$

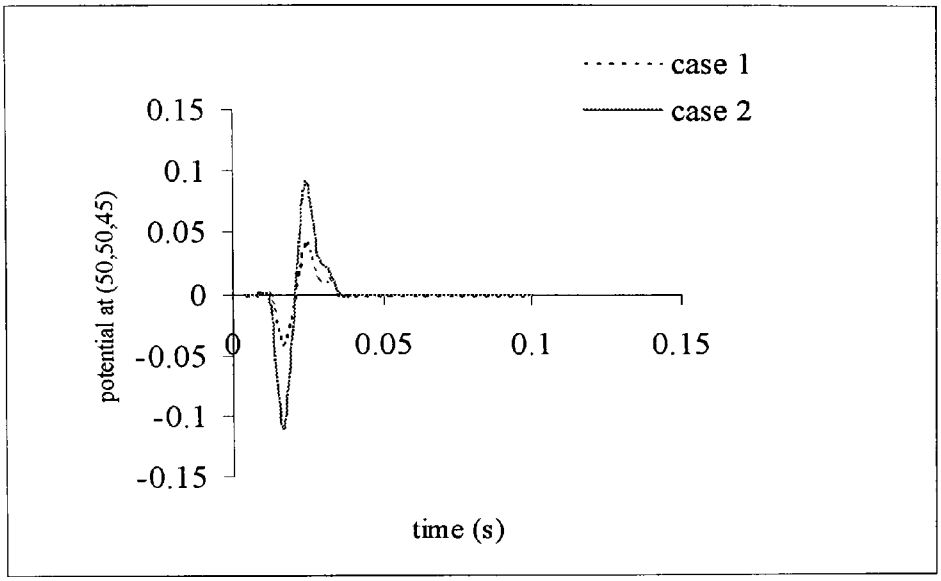

Figure 5.13d Plot of potential ϕ versus time for point (50,50,45) with *case 1* and *case 2*, for $\Delta t = 0.004$

5.8 Results

The methodology described in the previous sections is applied here to determine the responses from three-dimensional, homogeneous, or piecewise homogeneous rock structures of both finite, and infinite extent. With the help of the two-dimensional programs used in the previous chapters, additional computer programs have been produced to solve the scalar wave problems in three dimensions for a single medium and multimedia. In addition, the algorithms resolve internal flux problems. Results are displayed using a MATHCAD program.

5.8.1 Single Medium Results

Evaluation of the singular integrals is essential in the BEM, and these integrals are calculated in *case 1*, which is an analytical approach, and *case 2*, which is an approach

first used by Lachat (1975) for static problems. In the present work, this approach is extended to the case of time domain. The two approaches are compared in the following.

5.8.1.1 Single Medium of Infinite Extent

Consider the problem of solving the acoustic equation (2.27) for a single-layered medium extending to infinity on the sides and bottom surfaces. A cubic domain geometry is taken to infer the disturbances, when the sides and bottom extending to infinity (see Figure 5.12). The material velocity is $c = 2130$ m/s for shale. The source is located at a depth of 25 m, whilst the receivers are spaced equally and positioned in a horizontal line at 2 m below the top surface (see Figure 5.12). The number of receivers used is 99. To obtain this synthetic seismogram, the boundary elements are uniform. The time increment and source position are 0.001 s and (50,50,75). In the three-dimensional study, the source is taken as an internal boundary, which is a small cube. On the side of finite extent in the domain, the natural boundary conditions are specified. The Dirichlet boundary condition is prescribed for the sides of the small cube with side length 3-m. Results are given here an 4m×4m element discretization.

The results have been acquired for the two cases as shown in Figures (5.14) and (5.15). The registered signals are presented to simulate the medium of infinite extent on the sides and bottom, as is seen in Figure (5.12).

In the seismograms for the physical geometry, time runs along the horizontal axis and all displacement values received at the selected receiver points are on the vertical axis. In case of the medium of infinite extent, the first wave is received at time 0.011 s. There is no reflected wave coming from the sides or bottom, as expected. The synthetic seismograms presented give the required agreement between the two cases.

5.8.1.2 The Bounded Medium

Consider an acoustic problem of solving equation (2.27) in a three-dimensional portion of an unbounded medium. The medium is a 100mx100mx100m cubic domain and is excited by a source located in the domain (see Figure 5.16). The positions of the source and receivers are the same as in the previous section. In the physical geometry the top edge is taken as a free surface, whilst the Dirichlet boundary conditions are used for the rest of the boundary surface. The results are presented here for 6.25m×6.25m element meshes and 0.0016 s time increment.

Figures (5.17) and (5.18) show the results, which contain reflections from the side boundaries. The results produced for the different cases in the figures give the desired agreement.

In Figures (5.17) and (5.18), the first wave reaches the nearest receiver at time 0.011 s. After 0.0019 s of the arrival of the first wave, a reflected wave originates from the top boundary and coincides with the first wave. The wave reflected from the bottom is received at about 0.081 s. In these figures, the waves reflecting from the side boundaries can be seen even though they are weaker than the waves reflected from the sides in the 2D case in Chapter 3.

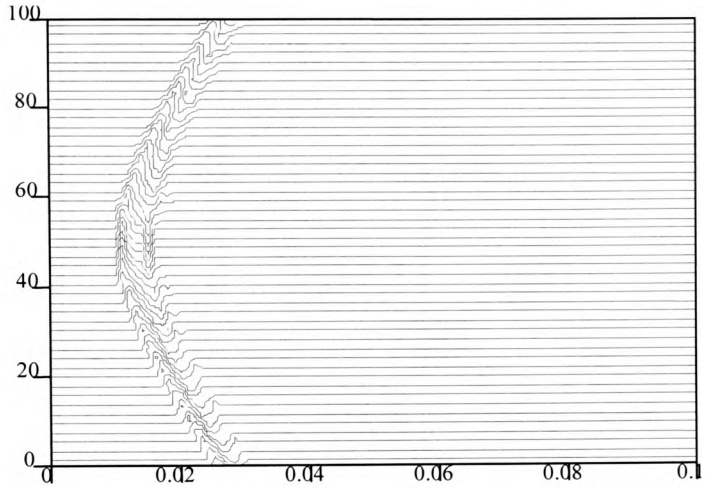

Figure 5.14 Synthetic seismograms introduced for the medium of infinite extent from the BEM with ***case 1***

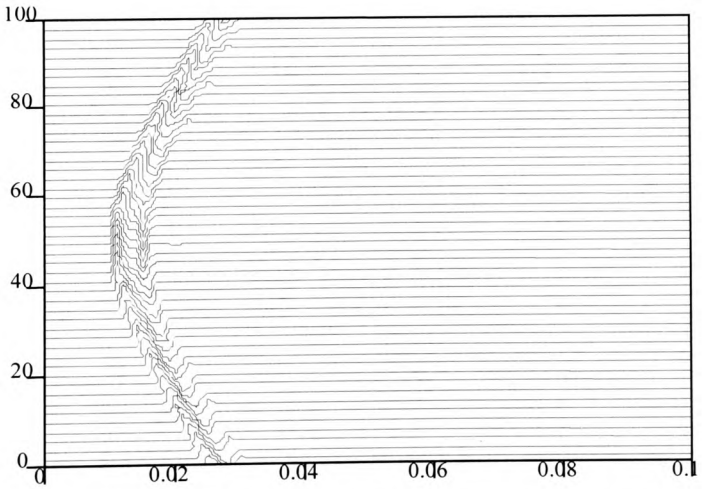

Figure 5.15 Synthetic seismograms introduced for the medium of infinite extent from the BEM with ***case 2***

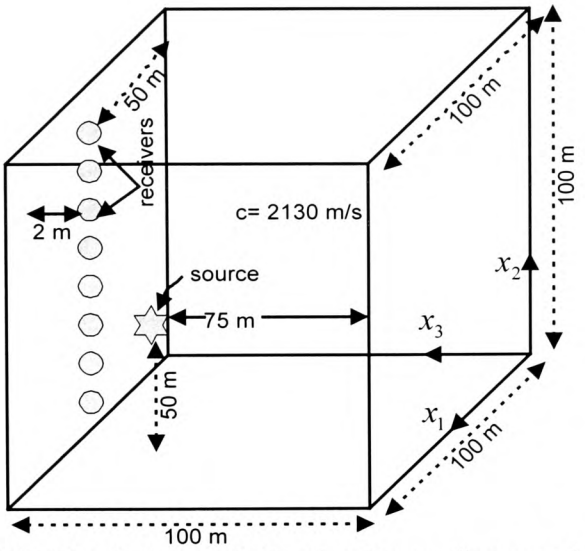

Figure 5.16 Physical model showing the medium used to generate seismograms in the 3D scalar BEM program

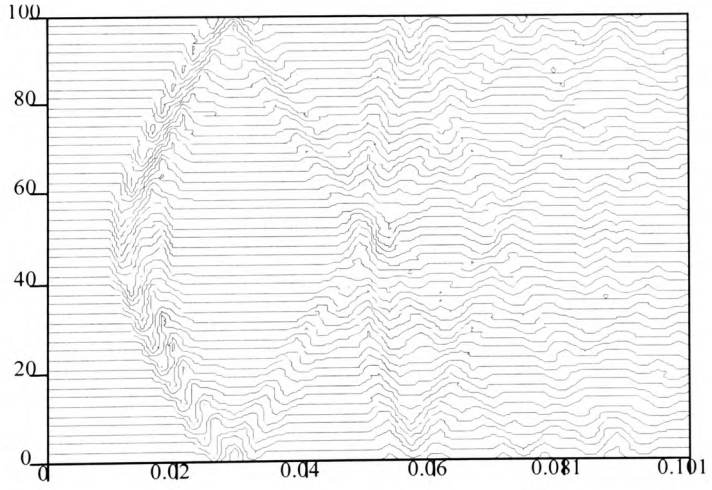

Figure 5.17 Synthetic seismograms from the BEM for the single medium with ***case 1***

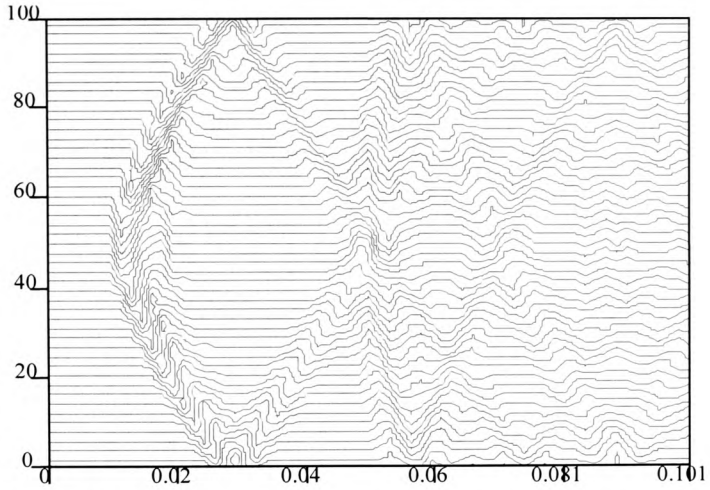

Figure 5.18 Synthetic seismograms from the BEM for the single medium with ***case 2***

5.8.2 Two Media Results

Consider now the case of two media with differing acoustic properties. The physical medium of infinite extent is defined in Figure (5.19). The material velocities of the layers in the medium are 1500 m/s for the upper seawater and 2440 m/s for the lower marls. The medium is employed to acquire the behaviour of the wave at registration points, and only the interface and top boundary surfaces are disctretized. The Neumann boundary conditions are exploited for the top surface, while the same boundary conditions as for the single medium case are prescribed for the source.

Figures (5.20) and (5.21) indicate the results for the two-layered medium of infinite extent for the two approaches considered. The aimed agreement is obtained from comparison of Figures (5.20) and (5.21). The reflected wave from the source is seen immediately after the first wave. The first interface wave is visible, whilst the second interface wave is very weak.

As expected, the results for the medium being discussed show no reflections from the sides and bottom. The first interface wave, arising at 0.0487 s strikes the interface and then reflects. As for the second interface wave appearing at 0.082 s, this first impinges on the top side and then pursues in the same way as the first.

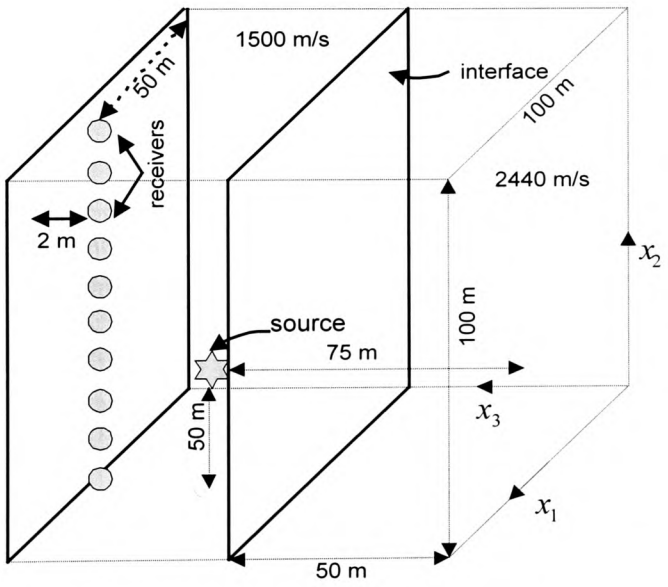

Figure 5.19 Physical model showing a two-layered medium used to generate seismograms in the 3D scalar BEM program.

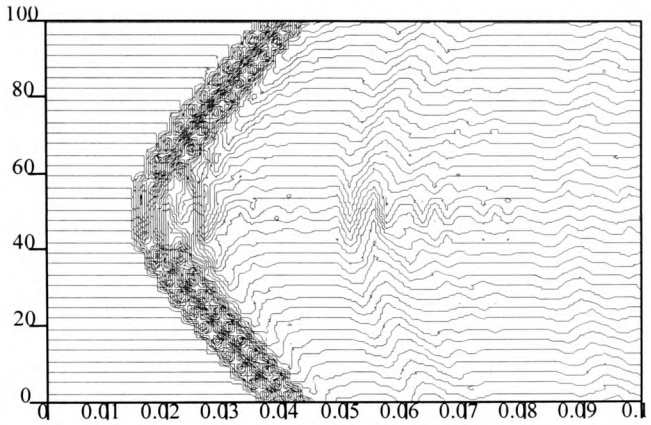

Figure 5.20 Synthetic seismograms introduced for the two-layered medium from the BEM with ***case 1***

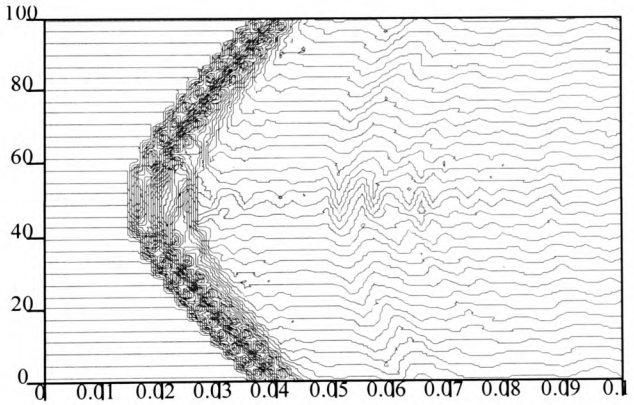

Figure 5.21 Synthetic seismograms introduced for the two-layered medium from the BEM with ***case 2***

5.9 Results of the Potential and Flux Distributions

In the previous section the wave behaviour through single and two media structures has been analysed at selected receiver points with relevant results presented. In this section, potential and flux distributions through a plane in the region under consideration are presented.

Some numerical results to the planes in the 3D domains have been produced using the BEM for two different circumstances. The relevant three-dimensional kernels derived previously, see equations 5.62-5.64 and 5.67-5.70, are used together with specified boundary conditions. The geometry of the model for the examples examined, is shown in the corresponding figures, with the use of 4 boundary elements for each side for the isotropic homogeneous region of interest. The results calculated for the two situations are qualitatively and quantitatively in a good agreement.

The internal potential ϕ and fluxes qx_1, qx_2 and qx_3 in the shaded regions are computed by employing the Dirichlet conditions for the boundary. The graphical results given for these cases are indicated in the following figures. The values on the contours show either the potential or its derivatives at internal points in the related figures. In the applications examined, the results are calculated by considering *cases 1*and *2* in the BEM. The results presented are for an elapsed time of 0.15 s, and the speed of wave propagation of 1500 m/s. The distance between any two internal points is 10 m. The boundary elements are uniform, with 24 elements being used. The potential and its derivatives are obtained at the internal nodes where they were unknown-the shaded planes shown in Figures (5.21, 5.24 and 5.27).

Example 1.1: *Dirichlet Problem*

In the domain of interest, the potential and flux values have been calculated using both approaches. Details of the problem with plane $x_1 = 50$ are given in Figure (5.21). Reasonable agreement between the two results is shown in Figures (5.22), and (5.23).

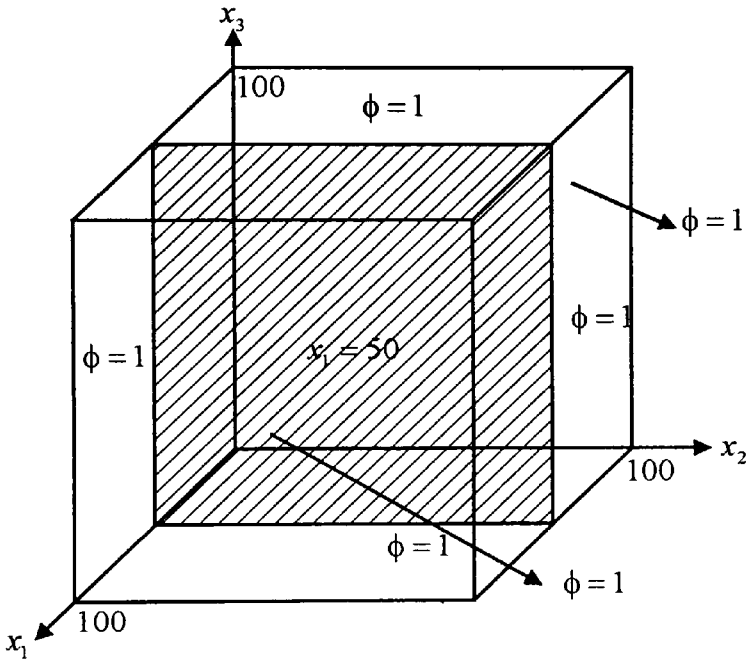

Figure 5.21 The definiton of the problem with the shaded plane

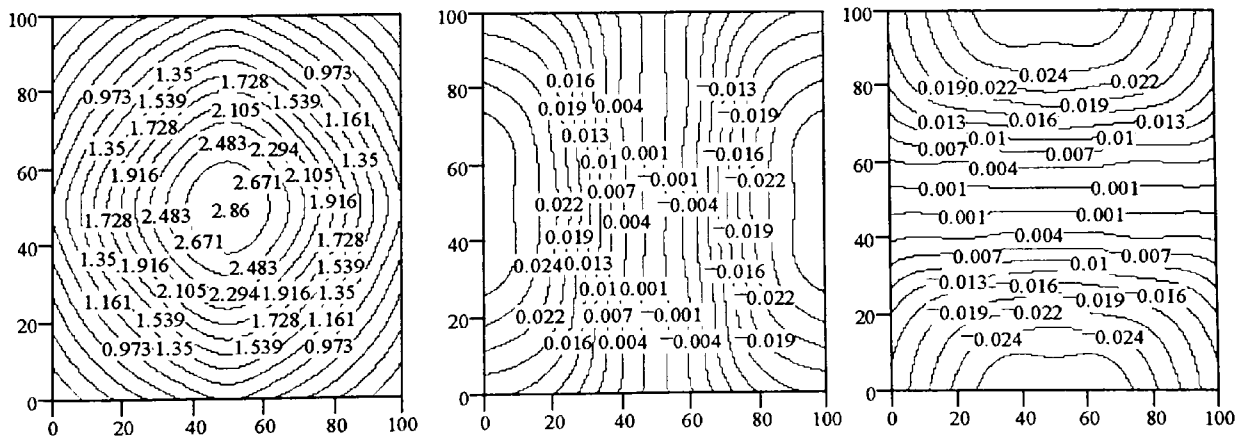

Figure 5.22 Internal potential ϕ and internal fluxes qx_2, qx_3 distributions in the plane $x_1 = 50$ by ***Case 1***, respectively

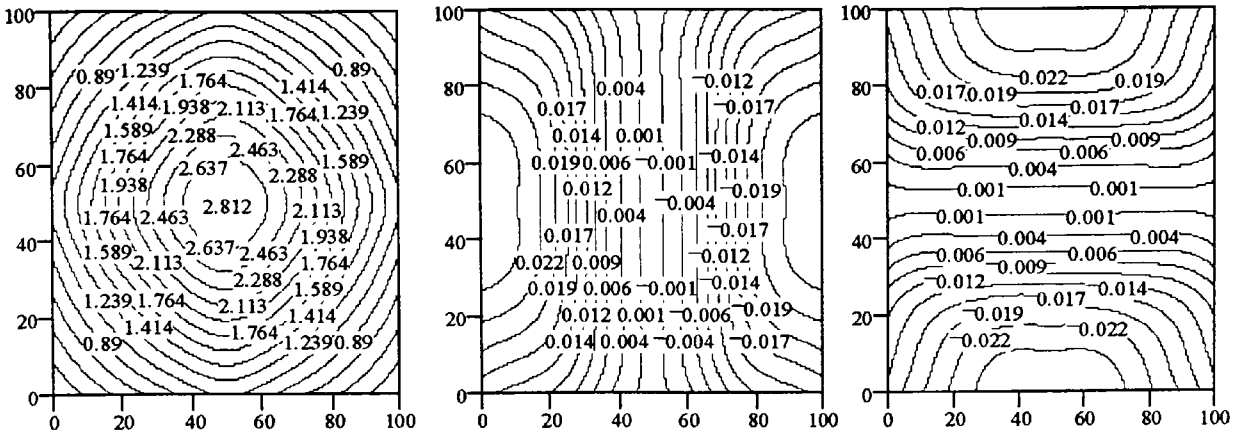

Figure 5.23 Internal potential ϕ and internal fluxes qx_2, qx_3 distributions in the plane $x_1 = 50$ by ***Case 2***, respectively

Example 1.2: *Dirichlet Problem*

In this example in order to obtain the distributions, the previous geometry is considered with the same physical conditions, but this time for plane $x_2 = 50$. Expected agreement between the distributions (Figure 5.25 and 5.26) are clearly seen.

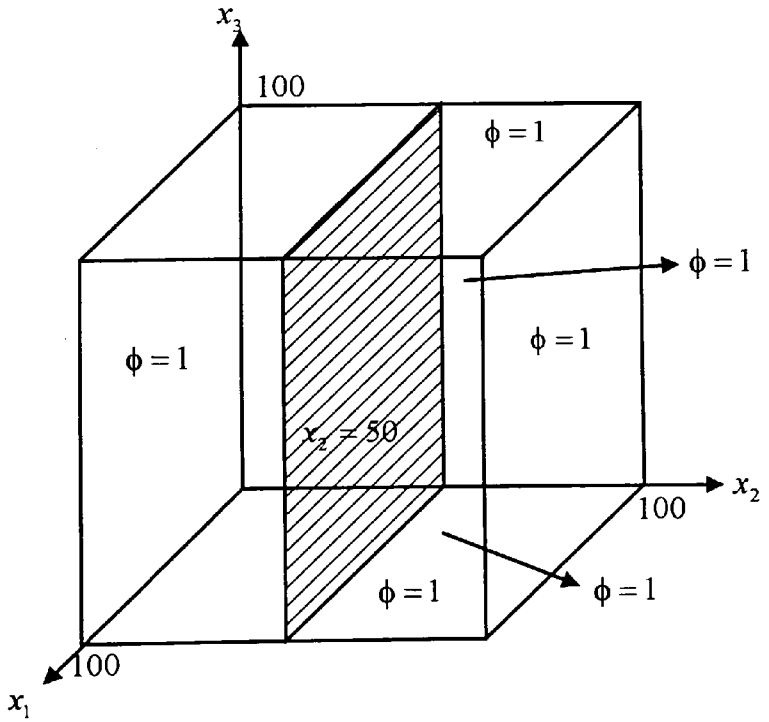

Figure 5.24 The definiton of the problem with the shaded plane

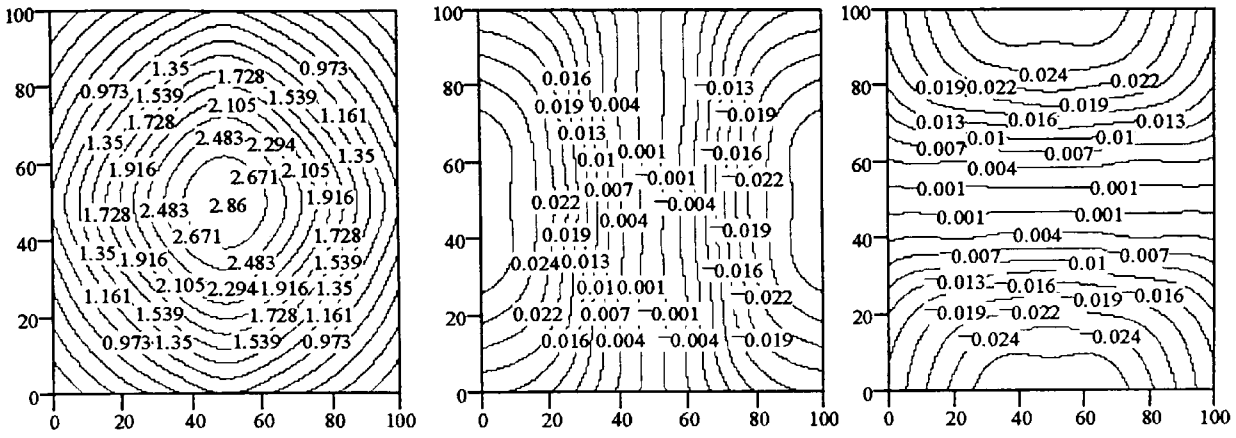

Figure 5.25 Internal potential ϕ and internal fluxes qx_1, qx_3 distributions in the plane $x_2 = 50$ by ***Case 1***, respectively

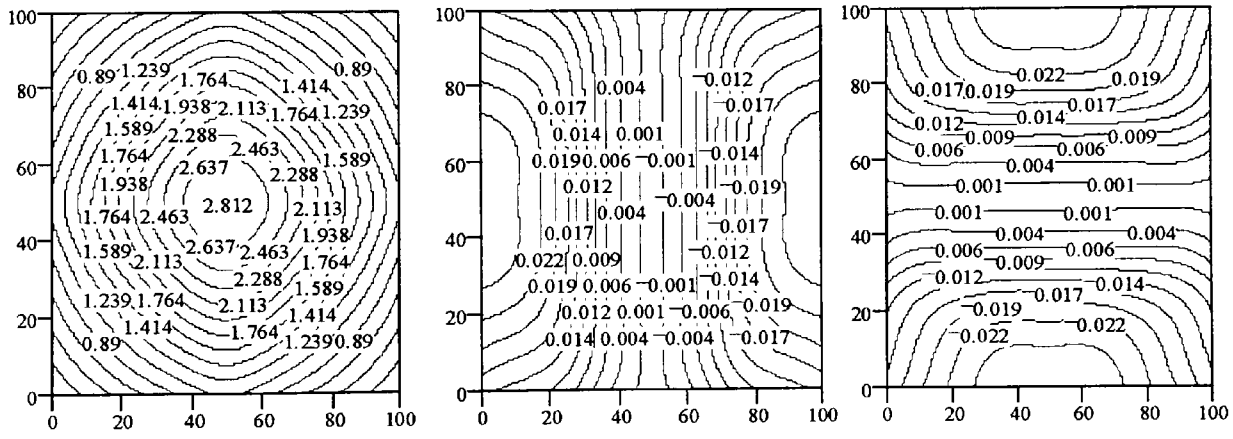

Figure 5.26 Internal potential ϕ and internal fluxes qx_1, qx_3 distributions in the plane $x_2 = 50$ by ***Case 2***, respectively

Example 1.3: *Dirichlet Problem*

In the present case of the above examples, the same geometry is used with the same conditions to find the distributions in plane $x_3 = 50$. The agreement between the distributions (see Figure 5.28 and 5.29) are obtained again.

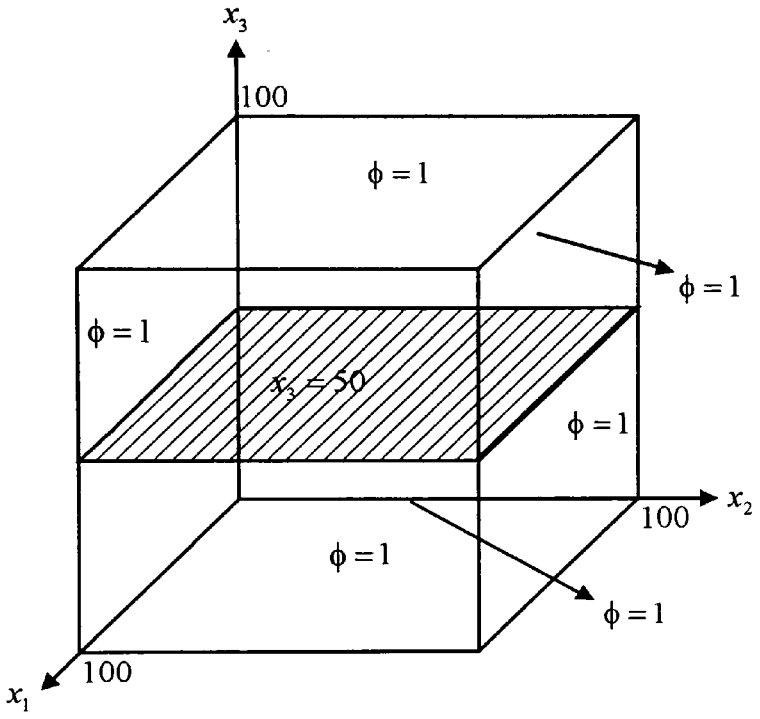

Figure 5.27 The definiton of the problem with the shaded plane

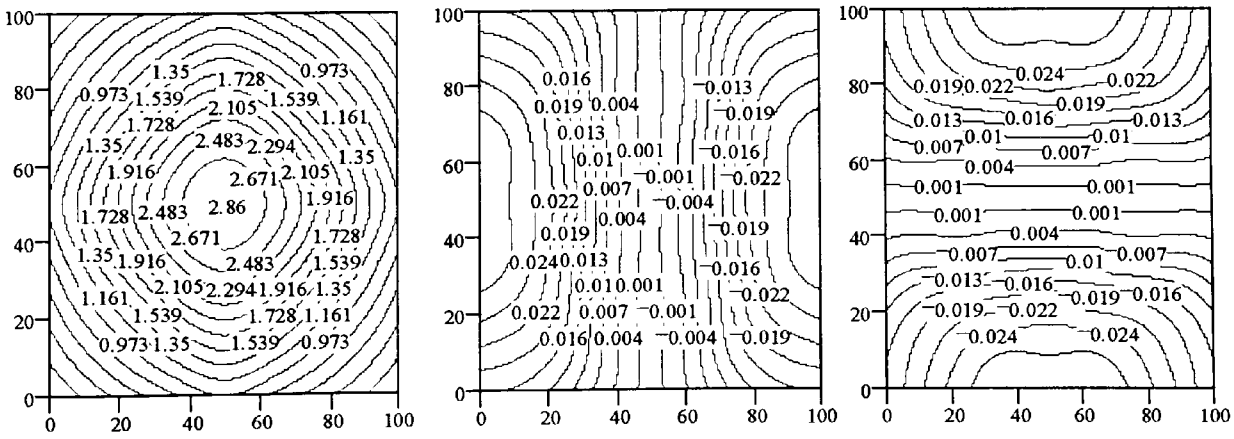

Figure 5.28 Internal potential ϕ and internal fluxes qx_1, qx_2 distributions in the plane $x_3 = 50$ by ***Case 1***, respectively

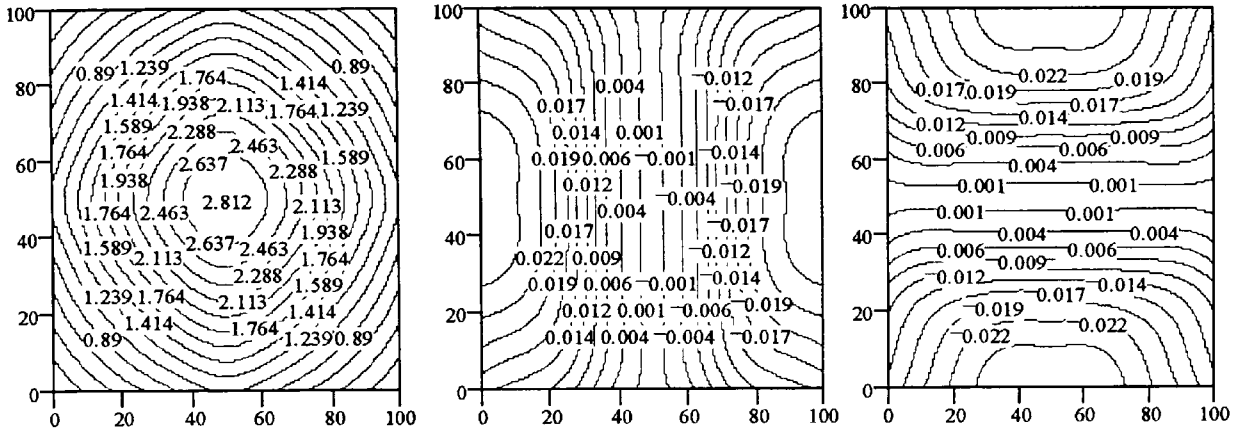

Figure 5.29 Internal potential ϕ and internal fluxes qx_1, qx_2 distributions in the plane $x_3 = 50$ by ***Case 2***, respectively

The unknown values of the potential and fluxes are calculated using the two approaches. There is both quantitatively and qualitatively excellent agreement in the results obtained using both *case 1* and *case 2* as seen in the above related figures. In both cases, the value of the potential is at its minimum on the two vertical and horizontal sides. In the two situations, the potential is symmetric with respect to the axes of the plane taken, and the fluxes are skew symmetric with respect to related axes of the shaded planes. The corresponding derivatives are zero along the middle lines, which are perpendicular to the related axes in the shaded plane. It can clearly be seen that planes $x_1 = 50$, $x_2 = 50$ and $x_3 = 50$ in the region have the same distributions, as required.

5.10 Conclusions

This chapter has developed the direct time domain BEM for the three-dimensional scalar wave problems. This formulation has also been extended to multimedia. All results presented agree with others where comparisons are possible. Using the formulations, results have been presented for homogeneous and piecewise homogeneous materials.

Moreover the singular integrals, which are at the heart of the BEM, have been evaluated successfully using two different approaches.

The internal flux kernels have clearly been derived and the results related to these kernels have been presented.

Also the above results give confidence for the work of the following chapter where attention is paid to the problems of the three-dimensional elastic wave propagation which are based on similar principles but are of a greater complexity.

CHAPTER 6

THREE DIMENSIONAL TIME DOMAIN BEM FOR ELASTIC WAVE PROPAGATION

6.1 Introduction

Complex elastodynamic problems are now solved through three-dimensional rock structures. As in the previous chapters, the fundamental solutions are first derived. To obtain the numerical solution of the partial differential equation, the three-dimensional time domain direct boundary element formulation is determined in terms of the dynamic reciprocal relation. As in earlier chapters singular integrals are evaluated using two different approaches. In both cases, the solutions of the Cauchy-Navier equations are presented for isotropic elastic homogeneous media. For both cases, the stable solutions are in close agreement.

6.2 Integral Equation Formulation

In Chapter 2, the governing equation of the three-dimensional elastic wave equation was shown (see equation 2.43). Stokes (1849) was the first to obtain the three-dimensional solution to that equation.

When the fundamental solution $\mathbf{u}^s$ of the field is substituted into equation (2.43), then:

$$c_2^{\,2} u^s_{l,kk} + (c_1^{\,2} - c_2^{\,2}) u^s_{k,kl} + b^s_l = \ddot{u}^s_l \qquad (6.1)$$

6.2.1 Elastodynamic Fundamental Solutions

To establish the three-dimensional BEM in terms of the equations of the elastodynamics, it is necessary to derive the fundamental solution. For the domain and its boundary, the

fundamental solution is a solution which satisfies the governing equation (6.1) except at the load point where a removable singularity is required. The body force (4.3), for the three-dimensional case, is given by:

$$\rho b_k^s = \delta(t)\delta(\mathbf{x}-\mathbf{y}^i)\delta_{lk} \tag{6.2}$$

The displacements (4.4) and tractions (4.5) are now applied with the three-dimensional case.

Given that $\delta(\mathbf{x}-\mathbf{y}^i) = -\frac{1}{4\pi}\nabla^2(\frac{1}{r})$ (e.g. Brebbia et al., 1992), then the body forces can be written as:

$$\rho\mathbf{b} = g(t)\delta(\mathbf{x}-\mathbf{y}^i)\mathbf{e} = -\frac{g(t)}{4\pi}\nabla^2(\frac{1}{r})\mathbf{e} = \frac{g(t)}{4\pi}(\nabla\times\nabla\times\frac{\mathbf{e}}{r} - \nabla\nabla\cdot\frac{\mathbf{e}}{r}) \tag{6.3}$$

where $g(t)$ is the magnitude. In determining equation (6.3) the following identity has been used:

$$\nabla^2\mathbf{u} = \nabla\nabla\cdot\mathbf{u} - \nabla\times\nabla\times\mathbf{u} \tag{6.4}$$

In addition, using equation (4.73), Navier's equation (2.43) can be written in the two uncoupled forms:

$$c_1^2\nabla^2\mathbf{u}^{(1)} - g(t)\nabla\nabla\cdot(\frac{\mathbf{e}}{4\pi\rho r}) = \ddot{\mathbf{u}}^{(1)}$$

$$c_2^2\nabla^2\mathbf{u}^{(2)} + g(t)\nabla\times\nabla\times(\frac{\mathbf{e}}{4\pi\rho r}) = \ddot{\mathbf{u}}^{(2)} \tag{6.5}$$

Any two vector potentials $\mathbf{V}^1$ and $\mathbf{V}^2$ can be used to decompose $\mathbf{u}$ into its irrotational and solenoidal parts (Eringen et al., 1975) by writing

$$\mathbf{u} = \nabla(\nabla\cdot\mathbf{V}^1) - \nabla\times\nabla\times\mathbf{V}^2 \tag{6.6}$$

It then follows that

$$c_\alpha^2 \nabla^2 \mathbf{V}^{(\alpha)} - g(t)\frac{\mathbf{e}}{4\pi\rho r} = \ddot{\mathbf{V}}^{(\alpha)} \tag{6.7}$$

and

$$c_\alpha^2 \nabla^2 V^{(\alpha)} - \frac{g(t)}{4\pi\rho r} = \ddot{V}^{(\alpha)} \tag{6.8}$$

where $\mathbf{V}^{(\alpha)} = V^{(\alpha)}\mathbf{e}$, $\alpha = 1, 2$.

Thus, the solution for the elastic wave problems is reduced to the solution of a pair of scalar wave equations in an infinite domain. The solution of equation (6.8) has been determined by Eringen et al. (1975) and has the following form:

$$V^{(\alpha)}(\mathbf{x},t) = -\frac{1}{16\pi^2 c_\alpha^2 \rho}\int_{\Omega_\infty} \frac{g(t-|\mathbf{y}-\mathbf{x}|/c_\alpha)}{|\mathbf{y}-\mathbf{y}^i||\mathbf{y}-\mathbf{x}|} d\Omega(\mathbf{y}) \tag{6.9}$$

To evaluate the last integral in infinite space, a spherical co-ordinate system is considered with origin at the point $\mathbf{y}^i$, and with polar axis in the direction of $\mathbf{x}-\mathbf{y}^i$ as shown in Figure (6.1).

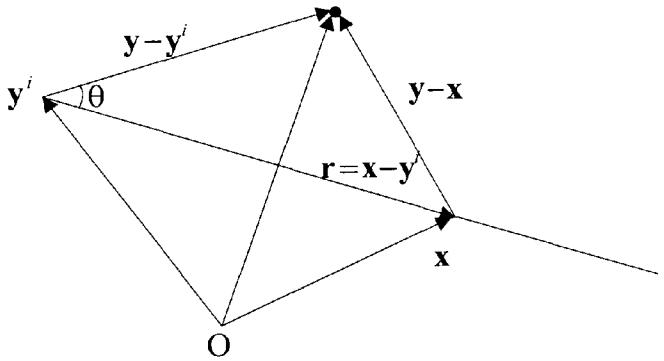

Figure 6.1 Relations between the variable points used for the derivation (from Eringen et al., 1975)

Clearly:

$$|\mathbf{r}| = r, \qquad |\mathbf{y} - \mathbf{y}^i| = \xi, \qquad |\mathbf{y} - \mathbf{x}| = (\xi^2 + r^2 - 2r\xi\cos\theta)^{1/2} \tag{6.10}$$

and so the integral (6.9) can be transformed into:

$$V^{(\alpha)}(\mathbf{x},t) = -\frac{1}{8\pi c_\alpha^2 \rho}\int_0^\infty\int_0^\pi \frac{g(t-(\xi^2+r^2-2r\xi\cos\theta)^{1/2}/c_\alpha)}{\xi(\xi^2+r^2-2r\xi\cos\theta)^{1/2}}\xi^2\sin\theta d\theta d\xi \tag{6.11}$$

Moreover using the transformation $a = (\xi^2 + r^2 - 2r\xi\cos\theta)^{1/2}/c_\alpha$, the integral (6.11) becomes:

$$V^{(\alpha)}(\mathbf{x},t) = -\frac{1}{8\pi c_\alpha \rho r}\int_0^\infty\int_{|\xi-r|/c_\alpha}^{(\xi+r)/c_\alpha} g(t-a)da d\xi \tag{6.12}$$

From Figure (6.2) and as was stated by Eringen et al. (1975), the integral (6.12) may be expressed as follows,

$$V^{(\alpha)}(\mathbf{x},t) = -\frac{1}{8\pi c_\alpha \rho r}\{\int_0^{r/c_\alpha}\int_{r-ac_\alpha}^{r+ac_\alpha} g(t-a)d\xi da + \int_{r/c_\alpha}^{\infty}\int_{ac_\alpha-r}^{ac_\alpha+r} g(t-a)d\xi da\}$$

$$= -\frac{1}{4\pi\rho r}\{\int_0^{r/c_\alpha} a g(t-a)da + \frac{r}{c_\alpha}\int_{r/c_\alpha}^{\infty} g(t-a)da\} \tag{6.13}$$

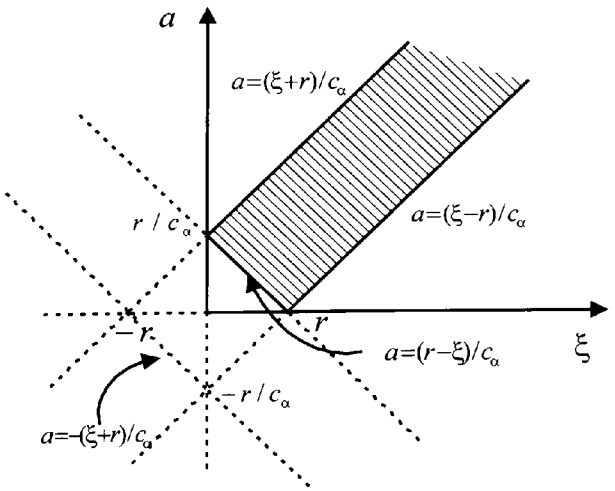

Figure 6.2 Domain (shaded) of integration in equation (6.13)

Using $a = \lambda r$, equation (6.13) may be written in the following convenient form:

$$V^{(\alpha)}(\mathbf{x},t) = -\frac{r}{4\pi\rho}\{\int_0^{1/c_\alpha}\lambda g(t-\lambda r)d\lambda + \frac{1}{c_\alpha}\int_{1/c_\alpha}^{\infty} g(t-\lambda r)d\lambda\} \tag{6.14}$$

From (6.14) it follows that

$$V^{(\alpha)}_{,lk}(\mathbf{x},t) = -\frac{1}{4\pi\rho r}\{(3r_{,l}r_{,k}-\delta_{lk})\int_0^{1/c_\alpha}\lambda g(t-\lambda r)d\lambda - \frac{r_{,l}r_{,k}}{c_\alpha^2}g(t-\frac{r}{c_\alpha})\} \tag{6.15}$$

If

$$u^{(1)}_{lk} = V^{(1)}_{,lk}, \quad u^{(2)}_{lk} = -V^{(2)}_{,lk} + V^{(2)}_{,jj}\delta_{lk} \tag{6.16}$$

then

$$u^{(1)}_{lk} = -\frac{1}{4\pi\rho r}\{(3r_{,l}r_{,k}-\delta_{lk})\int_0^{1/c_1}\lambda g(t-\lambda r)d\lambda - \frac{r_{,l}r_{,k}}{c_1^2}g(t-\frac{r}{c_1})\} \tag{6.17}$$

and

$$u^{(2)}_{lk} = \frac{1}{4\pi\rho r}\{(3r_{,l}r_{,k}-\delta_{lk})\int_0^{1/c_2}\lambda g(t-\lambda r)d\lambda - \frac{r_{,l}r_{,k}}{c_2^2}g(t-\frac{r}{c_2}) + \frac{\delta_{lk}}{c_2^2}g(t-\frac{r}{c_2})\} \tag{6.18}$$

Using expression (4.73), in three dimensions, the total displacement is given by:

$$\begin{aligned} u^s_{lk} = u^{(1)}_{lk} + u^{(2)}_{lk} = \frac{1}{4\pi\rho r}\{(3r_{,l}r_{,k}-\delta_{lk})\int_{1/c_1}^{1/c_2}\lambda g(t-\lambda r)d\lambda \\ + r_{,l}r_{,k}[\frac{1}{c_1^2}g(t-\frac{r}{c_1}) - \frac{1}{c_2^2}g(t-\frac{r}{c_2})] + \frac{\delta_{lk}}{c_2^2}g(t-\frac{r}{c_2})\} \end{aligned} \tag{6.19}$$

When $g(t) = \delta(t)$

$$\int_{1/c_1}^{1/c_2}\lambda\delta(t-\lambda r)d\lambda = \frac{t}{r^2}[H(t-r/c_1) - H(t-r/c_2)] \tag{6.20}$$

then equation (6.19) becomes:

$$u_{lk}^{s} = \frac{1}{4\pi\rho r}\{\frac{t}{r^2}(3r_{,l}r_{,k} - \delta_{lk})[H(t-\frac{r}{c_1}) - H(t-\frac{r}{c_2})] + r_{,l}r_{,k}[\frac{1}{c_1^2}\delta(t-\frac{r}{c_1}) - \frac{1}{c_2^2}\delta(t-\frac{r}{c_2})] + \frac{\delta_{lk}}{c_2^2}\delta(t-\frac{r}{c_2})\} \tag{6.21}$$

Similar derivations can also be found in Achenbach (1975) and Bonnet (1998). This three-dimensional fundamental solution is known as the Stokes' displacement tensor (1849).

The Stokes' tensor u_{lk}^{s} represents the displacement component in the l-direction at time t and position $\mathbf{x} = (x_1, x_2, x_3)$ due to a concentrated load acting in the k-direction at a point $\mathbf{y}^i$. When the load is applied at time τ, the variable t in the fundamental solution is replaced by $t-\tau$ when applying the Riemann convolution. Thus, equation (6.21) has the form:

$$u_{lk}^{s} = \frac{1}{4\pi\rho r}\{\frac{t-\tau}{r^2}(3r_{,l}r_{,k} - \delta_{lk})[H(t-\tau-\frac{r}{c_1}) - H(t-\tau-\frac{r}{c_2})] + r_{,l}r_{,k}[\frac{1}{c_1^2}\delta(t-\tau-\frac{r}{c_1}) - \frac{1}{c_2^2}\delta(t-\tau-\frac{r}{c_2})] + \frac{\delta_{lk}}{c_2^2}\delta(t-\tau-\frac{r}{c_2})\} \tag{6.22}$$

The displacement at $\mathbf{x}$ produced by the load at $\mathbf{y}^i$ is equal to the displacement at $\mathbf{y}^i$ produced by the same load at $\mathbf{x}$, that is, $u_{lk}^{s}(\mathbf{x}, t; \mathbf{y}^i, \tau) = u_{lk}^{s}(\mathbf{y}^i, t; \mathbf{x}, \tau)$.

Thus the stress tensor can be obtained from equation (6.22) using Hooke's law as follows,

$$\sigma_{km}^{s} = \rho(c_1^2 - 2c_2^2)u_{j,j}^{s}\delta_{km} + \rho c_2^2(u_{k,m}^{s} + u_{m,k}^{s}) \tag{6.23}$$

When a load point is applied in the 'l' direction, the 'km' component of the stress tensor can be obtained using

$$\sigma^s_{km} = \sigma^s_{lkm} e_l \tag{6.24}$$

where

$$\sigma^s_{lkm} = \frac{1}{4\pi r^2}\{\frac{b^1}{r^2}[\delta_{km}r_{,l} + \delta_{kl}r_{,m} + \delta_{lm}r_{,k} - 5r_{,l}r_{,k}r_{,m}]$$

$$+ 2b^2[6r_{,l}r_{,k}r_{,m} - \delta_{km}r_{,l} - \delta_{kl}r_{,m} - \delta_{lm}r_{,k}]$$

$$+ \frac{2rb^3}{c_2} r_{,l}r_{,k}r_{,m} - \delta_{km}r_{,l}b^4(1 - 2\frac{c_2^2}{c_1^2}) - b^5(\delta_{kl}r_{,m} + \delta_{lm}r_{,k})\}$$

$$= \sigma^{s(1)}_{lkm} + \sigma^{s(2)}_{lkm} \tag{6.25}$$

with

$$b^1 = 6c_2^2(t-\tau)[H(t-\tau-r/c_1) - H(t-\tau-r/c_2)]$$

$$b^2 = \delta(t-\tau-r/c_2) - \frac{c_2^2}{c_1^2}\delta(t-\tau-r/c_1)$$

$$b^3 = \dot{\delta}(t-\tau-r/c_2) - \frac{c_2^3}{c_1^3}\dot{\delta}(t-\tau-r/c_1)$$

$$b^4 = \delta(t-\tau-r/c_1) + \frac{r}{c_1}\dot{\delta}(t-\tau-r/c_1)$$

$$b^5 = \delta(t-\tau-r/c_2) + \frac{r}{c_2}\dot{\delta}(t-\tau-r/c_2) \tag{6.26}$$

The stress tensor may also be obtained using similar methods. The tractions on a boundary point may be computed using:

$$p^s_{lk} = \sigma^s_{lkm} n_m = \rho[(c_1^2 - 2c_2^2)u^s_{j,j}\delta_{km} + \rho c_2^2(u^s_{k,m} + u^s_{m,k})]n_m \tag{6.27}$$

where **n** is the vector normal to be boundary. Thus the fundamental traction solution may be explicitly written as:

$$p_{lk}^{s} = \frac{1}{4\pi r^2}\{\frac{b^1}{r^2}[(\delta_{lk} - 5r_{,l}r_{,k})\frac{\partial r}{\partial n} + r_{,l}n_k + r_{,k}n_l]$$

$$+ 2b^2[(6r_{,l}r_{,k} - \delta_{lk})\frac{\partial r}{\partial n} - r_{,l}n_k - r_{,k}n_l] + \frac{2b^3 r}{c_2}r_{,l}r_{,k}\frac{\partial r}{\partial n} \qquad (6.28)$$

$$- b^4(1 - 2\frac{c_2^2}{c_1^2})r_{,l}n_k - b^5(\delta_{lk}\frac{\partial r}{\partial n} + r_{,k}n_l)\}$$

where $\frac{\partial r}{\partial n} = r_{,i}n_i$ with $r_{,k} \equiv \frac{\partial r}{\partial x_k}$.

The three-dimensional displacement solution has the causality, reciprocity and time translation properties, as was also the case for the two-dimensional solution.

6.2.1.1 Comparison of the Elastodynamic Fundamental Solutions (2D and 3D)

It is worth noting the difference between the two-dimensional (4.8), and three-dimensional (6.21) elastodynamic fundamental solutions. In the three-dimensional case, the disturbance emitted from the load point $\mathbf{y}^i$ is received at point $\mathbf{x}$ from time $t = r/c_1$ (arrival of the compressional wave) up to time $t = r/c_2$ (arrival of the shear wave). Impulses are received at $t = r/c_1$ and $t = r/c_2$. As was stated in Chapter 4, in the two-dimensional case the disturbance emitted initially from the load point $\mathbf{y}^i$ is received at point $\mathbf{x}$ any time after $t = r/c_1$. In other words, the three-dimensional fundamental solution returns to zero after the passage of the shear wave whilst the two-dimensional fundamental solution does not have sudden end, but rather a 'tail'. As was pointed out in the scalar case, the tail may be one of the reasons for the possible instability. This problem has been discussed in Tian (1990).

6.2.2 Integral Representation

In Chapter 2, the elastodynamic reciprocal relation was given in terms of the two states. With zero body forces namely, $b_k = 0$, and initial conditions $u_{0k} = 0$ and $v_{0k} = 0$ equation (4.16), for the three-dimensional elastodynamic problems, can be written as:

$$u_l^i(\mathbf{y}^i,t) = \int_B [(u_{lk}^s * p_k) - (u_k * p_{lk}^s)](\mathbf{x},t)dB \tag{6.29}$$

Using time convolution, equation (6.29) can be rewritten explicitly, giving:

$$u_l^i(\mathbf{y}^i,t) = \int_0^{t^+}\int_B u_{lk}^s(\mathbf{x},t-\tau,\mathbf{y}^i)p_k(\mathbf{x},\tau)dBd\tau - \int_0^{t^+}\int_B u_k(\mathbf{x},\tau)p_{lk}^s(\mathbf{x},t-\tau,\mathbf{y}^i)dBd\tau \tag{6.30}$$

where the t^+ value is the same as in the two-dimensional case. The representation (6.30) expresses the displacement value u_l at an interior point $\mathbf{y}^i$ at time t in terms of boundary displacements and tractions at time τ.

6.2.3 Boundary Integral Equation

The integral representation (6.29) was derived when the load point $\mathbf{y}^i$ is inside the domain. Consideration of the body force on the boundary requires special care to remove the singularities, which occur when the load point also becomes the field point, namely $\mathbf{x} = \mathbf{y}^i$. When the point $\mathbf{y}^i$ is on a smooth surface, the domain Ω can be enlarged (Brebbia et al., 1992, Paris et al., 1997) by a small hemi-sphere of radius ε as shown in Figure (6.3). As was shown in Chapter 4, the point $\mathbf{y}^i$ is then a point on the boundary of the domain.

In equation (6.30), the integrals can be evaluated when the singularity takes place. From Figure (6.3), the integrals in equation (6.29) can be written as the limiting process when $\varepsilon \to 0$ for boundary surfaces B_ε and B. Hence

$$I_1 = \int_B (u_{lk}^s * p_k)(\mathbf{x},t)dB = \lim_{\varepsilon\to 0} \int_{B-B_\varepsilon} (u_{lk}^s * p_k)(\mathbf{x},t)dB + \lim_{\varepsilon\to 0} \int_{B_\varepsilon} (u_{lk}^s * p_k)(\mathbf{x},t)dB \quad (6.31)$$

and for the second integral:

$$I_2 = \int_B (p_{lk}^s * u_k)(\mathbf{x},t)dB = \lim_{\varepsilon\to 0} \int_{B-B_\varepsilon} (p_{lk}^s * u_k)(\mathbf{x},t)dB + \lim_{\varepsilon\to 0} \int_{B_\varepsilon} (p_{lk}^s * u_k)(\mathbf{x},t)dB \quad (6.32)$$

For simplification of the second integrals on the right hand side of equations (6.31) and (6.32), the fundamental solutions of the static counterpart of equation (2.43) are considered and given by (Brebbia et al., 1992, Paris et al., 1997):

$$u_{lk}^{s1} = \frac{1}{16\pi\mu(1-\upsilon)} \frac{1}{r}[(3-4\upsilon)\delta_{lk} + r_{,l}r_{,k}] \quad (6.33)$$

$$p_{lk}^{s1} = -\frac{1}{8\pi(1-\upsilon)r^2}\{[(1-2\upsilon)\delta_{lk} + 3r_{,l}r_{,k}]\frac{\partial r}{\partial n} + (1-2\upsilon)(n_l r_{,k} - n_k r_{,l})\} \quad (6.34)$$

where u_{lk}^{s1} and p_{lk}^{s1} are the three-dimensional elastostatic displacement and traction fundamental solutions.

The three-dimensional static solutions are now used with the geometry of Figure (6.3) to evaluate the last integrals in equations (6.31) and (6.32). This is achieved by replacing u_{lk}^s and p_{lk}^s, with u_{lk}^{s1} and p_{lk}^{s1}, respectively, for the small hemisphere when $\varepsilon \to 0$. Thus:

$$\lim_{\varepsilon\to 0} p_k^i \int_{B_\varepsilon} u_{lk}^{s1} dB = \frac{1}{8\pi(1-\upsilon)\mu} \lim_{\varepsilon\to 0} p_k^i \int_{B_\varepsilon} [(4\upsilon-3)\delta_{lk} \ln r + r_{,l}r_{,k}]dB \quad (6.35)$$

$$\lim_{\varepsilon\to 0} u_k^i \int_{B_\varepsilon} p_{lk}^{s1} dB = \lim_{\varepsilon\to 0} u_k^i \int_{B_\varepsilon} -\frac{1}{8\pi(1-\upsilon)r}\{[(1-2\upsilon)\delta_{lk} + 3r_{,l}r_{,k}]\frac{\partial r}{\partial n} + (1-2\upsilon)(n_l r_{,k} - n_k r_{,l})\}dB \tag{6.36}$$

With the help of Figure (6.3) it follows that

$$\varepsilon \equiv r, \quad \frac{\partial r}{\partial n} = 1, \quad dB = \varepsilon^2 \cos\gamma d\gamma d\theta, \quad r_{,i} = n_i$$

$$r_{,1} = \cos\gamma\cos\theta, \quad r_{,2} = \cos\gamma\sin\theta, \quad r_{,3} = \sin\gamma, \quad n_l r_{,k} - n_k r_{,l} = 0 \tag{6.37}$$

The integrals for the case of $l = k = 1$ are:

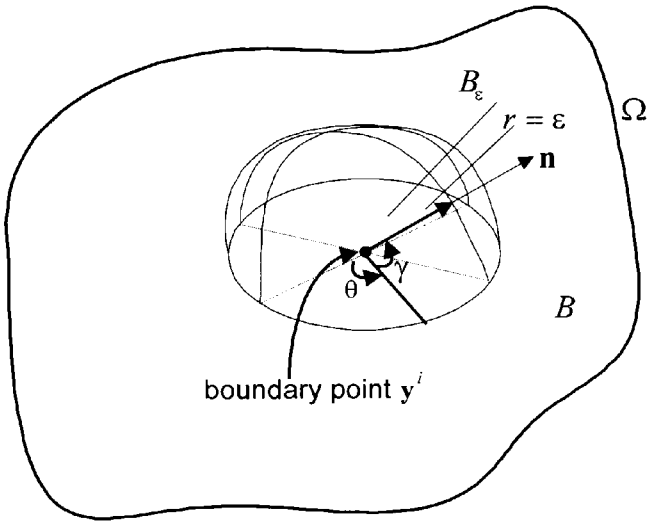

Figure 6.3 Illustration of the Cauchy Principal Value

$$\lim_{\varepsilon\to 0} p_1^i \int_{B_\varepsilon} u_{11}^{s1} dB = \frac{1}{8\pi(1-\upsilon)\mu} \lim_{\varepsilon\to 0} p_1^i \int_0^{2\pi} \int_0^{\pi/2} \frac{1}{\varepsilon}[(3-4\upsilon) + \cos^2\gamma\cos^2\theta]\varepsilon^2 \cos\gamma d\gamma d\theta = 0 \tag{6.38}$$

and:

$$\lim_{\varepsilon\to 0} u_1^i \int_{B_\varepsilon} p_{11}^{s1} dB = \lim_{\varepsilon\to 0} u_1^i \int_0^{2\pi} \int_0^{\pi/2} -\frac{1}{8\pi(1-\upsilon)\varepsilon^2}[(1-2\upsilon)+\cos^2\gamma\cos^2\theta]\varepsilon^2\cos\gamma d\gamma d\theta$$

$$= u_1^i \int_0^{2\pi} \int_0^{\pi/2} -\frac{1}{8\pi(1-\upsilon)}[(1-2\upsilon)+\cos^2\gamma\cos^2\theta]\cos\gamma d\gamma d\theta \qquad (6.39)$$

$$= -\frac{1}{2}u_1^i$$

A similar approach applies when $l = k = 2$ and $l = k = 3$. For the case of $l \neq k$, both integrals are zero. Thus,

$$\lim_{\varepsilon\to 0} p_k^i \int_{B_\varepsilon} u_{lk}^{s1} dB = 0 \qquad (6.40)$$

$$\lim_{\varepsilon\to 0} u_k^i \int_{B_\varepsilon} p_{lk}^{s1} dB = -\frac{1}{2}\delta_{lk}u_k^i \qquad (6.41)$$

When $\varepsilon \to 0$ and it follows that the identities (6.31) and (6.32) are:

$$I_1 = \int_B (u_{lk}^s * p_k)(\mathbf{x},t)dB \qquad (6.42)$$

$$I_2 = \int_B (p_{lk}^s * u_k)(\mathbf{x},t)dB - \frac{1}{2}\delta_{lk}u_k^i(\mathbf{y}^i,t)$$
$$= \int_B (p_{lk}^s * u_k)(\mathbf{x},t)dB - \frac{1}{2}u_l^i(\mathbf{y}^i,t) \qquad (6.43)$$

Notice that the singularity at the point $\mathbf{y}^i$ does not affect the integral (6.31), since the last integral in that equation is equal to zero. Since the static kernels are used, the time convolution was not considered in equations (6.35) and (6.36). Thus, the displacement $u_k(\mathbf{x},t)$ and traction $p_k(\mathbf{x},t)$ are taken as constant during the integration.

So equations (6.31), (6.32), (6.42) and (6.43) give the required integral equation for a boundary point as follows:

$$\frac{1}{2}\delta_{lk}u_k^i(\mathbf{y}^i,t) = \int_B [(u_{lk}^s * p_k) - (p_{lk}^s * u_k)](\mathbf{x},t)dB \tag{6.44}$$

where the integrals have the same sense as the Cauchy principal value.

It may also be noted that at points $\mathbf{y}^i$ located outside $\Omega \cup B$ the displacement is equal to zero. Hence the left-hand side of equation (6.29) is also equal to zero, that is, $u_l^i(\mathbf{y}^i,t) = 0$. Thus, the integral representation for the three-dimensional elastodynamic problem for any point in or outside the domain is:

$$\alpha_{lk}^i u_k^i = \int_B [(u_{lk}^s * p_k) - (p_{lk}^s * u_k)](\mathbf{x},t)dB \tag{6.45}$$

where

$$\alpha_{lk}^i = \begin{cases} \delta_{lk} & \text{if} \quad \mathbf{y}^i \in \Omega \\ \frac{1}{2}\delta_{lk} & \text{if} \quad \mathbf{y}^i \in B \\ 0. & \text{if} \quad \mathbf{y}^i \notin (\Omega \cup B) \end{cases} \tag{6.46}$$

By means of the convolution, equation (6.45) may be rewritten explicitly:

$$\alpha_{lk}^i u_k^i(\mathbf{y}^i,t) = \int_0^{t^+}\int_B u_{lk}^s(\mathbf{x},t-\tau;\mathbf{y}^i)p_k(\mathbf{x},\tau)dBd\tau - \int_0^{t^+}\int_B p_{lk}^s(\mathbf{x},t-\tau;\mathbf{y}^i)u_k(\mathbf{x},\tau)dBd\tau \tag{6.47}$$

where t^+ value has the same value as for the scalar case.

Non-smooth boundaries are discussed in, for example, Guiggiani et al. (1990), Paris et al. (1997), and Brebbia et al. (1992).

6.3 Boundary Elements for 3D Elastodynamic Problems

The integral representation has been established in terms of the two elastodynamic states from the principle of elastodynamic reciprocal relation. Since an analytical solution of the boundary integral equation is not always possible it is necessary to consider

numerical solutions. For the numerical integration the boundary elements have been illustrated in Chapter 5, as shown in Figure (5.4).

6.3.1 Time Interpolations of Boundary Variables

To obtain a numerical solution of the partial differential equation by applying the BEM, the time integration is first evaluated analytically. Constant variation in tractions and linear variation in displacements with time is used.

Consider $t = n\Delta t$. To obtain the approximate solution of the boundary integral equation, the field variables are used in the following form:

$$u_k(\mathbf{x},\tau) = \sum_m \eta^m(\tau) u_k^m(\mathbf{x})$$

$$p_k(\mathbf{x},\tau) = \sum_m \mu^m(\tau) p_k^m(\mathbf{x}) \tag{6.48}$$

where $\eta^m(\tau)$ and $\mu^m(\tau)$ are the interpolation shape functions given in Chapter 3. In addition u_k^m and p_k^m indicate the displacement and traction in the k-direction, respectively. Once again the displacements are approximated by the linear time functions, and the tractions are represented by the piecewise constant functions.

For any given boundary node at time step n, equation (6.47) can be written as:

$$\alpha_{lk}^i u_k^{ni} = \sum_{m=1}^{n} \int_B U_{lk}^{nm} p_k^m(\mathbf{x}) dB - \sum_{m=1}^{n} \int_B Q_{lk}^{nm} u_k^m(\mathbf{x}) dB \tag{6.49}$$

where

$$U_{lk}^{nm} = \int_0^{t^+} u_{lk}^s(\mathbf{x}, t-\tau; \mathbf{y}^i) \mu^m(\tau) d\tau \tag{6.50}$$

and:

$$Q_{lk}^{nm} = \int_0^{t^+} p_{lk}^s(\mathbf{x}, t-\tau; \mathbf{y}^i)\eta^m(\tau)d\tau \tag{6.51}$$

The solutions u_{lk}^s and p_{lk}^s were previously given by equations (6.22) and (6.28) respectively. Using expression (3.36) in equation (6.50), it is possible to determine the effect of the field point $\mathbf{x}$, at time $t = t_n$ when the load is applied at $\mathbf{y}^i$ between τ_{m-1} and τ_m. Equation (6.50) thus becomes:

$$U_{lk}^{nm} = \frac{1}{4\pi\mu r}\left\{\left(\frac{3c_2^2}{r^2}T_3 + \frac{c_2^2}{c_1^2}T_1 - T_2\right)r_{,l}r_{,k} + \left(T_2 - \frac{c_2^2}{r^2}T_3\right)\delta_{lk}\right\} \tag{6.52}$$

where

$$T_\alpha = \int_{\tau_{m-1}}^{\tau_m} \delta(\tau_\alpha^* - \tau)d\tau = H(\tau_\alpha^* - \tau_{m-1}) - H(\tau_\alpha^* - \tau_m) \tag{6.53}$$

$\alpha = 1,2$ and

$$T_3 = \int_{\tau_{m-1}}^{\tau_m} (t-\tau)[H(\tau_1^* - \tau) - H(\tau_2^* - \tau)]d\tau \tag{6.54}$$

where $\tau_\alpha^* = t_n - r/c_\alpha$.

In equation (6.54) the related integrals can be obtained for three different cases as follows,

1. $\tau_\alpha^* < \tau_{m-1}$:

$$\int_{\tau_{m-1}}^{\tau_m} (t-\tau)H(\tau_\alpha^* - \tau)d\tau = 0 \tag{6.55}$$

2. $\tau_\alpha^* > \tau_m$:

$$\int_{\tau_{m-1}}^{\tau_m} (t-\tau)H(\tau_\alpha^* - \tau)d\tau = (\Delta t)^2(n - m + \frac{1}{2}) \tag{6.56}$$

3. $\tau_{m-1} \le \tau_\alpha^* < \tau_m$:

$$\int_{\tau_{m-1}}^{\tau_m} (t-\tau) H(\tau_\alpha^* - \tau) d\tau = \frac{(\Delta t)^2}{2}(n-m+1)^2 - \frac{r^2}{2c_\alpha^2} \tag{6.57}$$

Now from equations (6.53-6.57) distinct cases are grouped to obtain U_{lk}^{nm} in equation (6.52) as follows:

Case 1: $0 < \tau_1^* < \tau_{m-1}$ and $0 < \tau_2^* < \tau_1^* < \tau_{m-1}$

$$T_1 = T_2 = T_3 = 0 \tag{6.58}$$

Case 2: $\tau_{m-1} < \tau_1^* < \tau_m$ and $0 < \tau_2^* < \tau_{m-1}$

$$T_1 = 1, \quad T_2 = 0, \quad T_3 = \frac{(\Delta t)^2}{2}(n-m+1)^2 - \frac{r^2}{2c_1^2} \tag{6.59}$$

Case 3: $\tau_{m-1} < \tau_1^* < \tau_m$ and $\tau_{m-1} < \tau_2^* < \tau_m$

$$T_1 = 1, \quad T_2 = 1, \quad T_3 = \frac{r^2}{2}\left(\frac{1}{c_2^2} - \frac{1}{c_1^2}\right) \tag{6.60}$$

Case 4: $\tau_m < \tau_1^*$ and $0 < \tau_2^* < \tau_{m-1}$

$$T_1 = 0, \quad T_2 = 0, \quad T_3 = (\Delta t)^2 (n-m+\frac{1}{2}) \tag{6.61}$$

Case 5: $\tau_m < \tau_1^*$ and $\tau_{m-1} < \tau_2^* < \tau_m$

$$T_1 = 0, \quad T_2 = 1, \quad T_3 = (\Delta t)^2 [(n-m+\frac{1}{2}) - \frac{1}{2}(n-m+1)^2] + \frac{r^2}{2c_2^2} \tag{6.62}$$

Case 6: $\tau_m < \tau_1^*$ and $\tau_m < \tau_2^*$

$$T_1 = T_2 = T_3 = 0 \tag{6.63}$$

Using equation (3.35) in equation (6.51), the effect may be obtained on the field point **x** at time $t = t_n$ when the load is applied at point $\mathbf{y}^i$ from τ_{m-1} to τ_m and from τ_m to τ_{m+1}. Equation (6.51) thus becomes:

$$Q_{lk}^{nm} = \frac{1}{4\pi r^2}[r_{,l}r_{,k}\frac{\partial r}{\partial n}K_1 + (\delta_{lk}\frac{\partial r}{\partial n} + r_{,k}n_l)K_2 + r_{,l}n_k K_3] \tag{6.64}$$

where

$$K_1 = -\frac{5A_1}{r^2} + 12A_2 + \frac{2rA_3}{c_2}$$

$$K_2 = \frac{A_1}{r^2} - 2A_2 - A_5$$

$$K_3 = \frac{A_1}{r^2} - 2A_2 - A_4(1 - 2\frac{c_2^2}{c_1^2})$$

Using equations (6.28) and (3.35) in equation (6.64),

$$A_\alpha = \int_{\Delta t_m} b^\alpha \eta^m(\tau)d\tau \tag{6.65}$$

where $1 \le \alpha \le 5$.

Now from equation (6.65) cases are categorised depending on whether or not the related wave reached the field point,

Case 1: $0 < \tau_1^* < \tau_{m-1}$ and $0 < \tau_2^* < \tau_1^* < \tau_{m-1}$

$$A_1 = A_2 = A_3 = A_4 = A_5 = 0 \tag{6.66}$$

Case 2: $\tau_{m-1} < \tau_1^* < \tau_m$ and $0 < \tau_2^* < \tau_{m-1}$

$$A_1 = c_2^2(\Delta t)^2[(n-m+1)^3 - \frac{3r^2(n-m+1)}{c_1^2(\Delta t)^2} + \frac{2r^3}{c_1^3(\Delta t)^3}]$$

$$A_2 = -\frac{c_2^2}{c_1^2 \Delta t}(\tau_1^* - \tau_{m-1})$$

$$A_3 = -\frac{c_2^3}{c_1^3 \Delta t}$$

$$A_4 = (\tau_1^* - \tau_{m-1} + \frac{r}{c_1}) / \Delta t = n - m + 1$$

$$A_5 = 0 \tag{6.67}$$

Case 3: $\tau_{m-1} < \tau_1^* < \tau_m$ and $\tau_{m-1} < \tau_2^* < \tau_1^* < \tau_m$

$$A_1 = 3(n-m+1)r^2(1-\frac{c_2^2}{c_1^2}) + \frac{2r^3}{\Delta t}c_2^2(\frac{1}{c_1^3} - \frac{1}{c_2^3})$$

$$A_2 = [\tau_2^* - \tau_{m-1} - \frac{c_2^2}{c_1^2}(\tau_1^* - \tau_{m-1})] / \Delta t$$

$$A_3 = (1 - \frac{c_2^3}{c_1^3}) / \Delta t$$

$$A_4 = (\tau_1^* - \tau_{m-1} + \frac{r}{c_1}) / \Delta t = n - m + 1$$

$$A_5 = (\tau_2^* - \tau_{m-1} + \frac{r}{c_2}) / \Delta t = n - m + 1 \tag{6.68}$$

Case 4: $\tau_m < \tau_1^* < \tau_{m+1}$ and $0 < \tau_2^* < \tau_{m-1}$

$$A_1 = c_2^2(\Delta t)^2\{6(n-m) - (n-m-1)^3 + \frac{3r^2(n-m-1)}{c_1^2(\Delta t)^2} - \frac{2r^3}{c_1^3(\Delta t)^3}\}$$

$$A_2 = \frac{c_2^2}{c_1^2}(\tau_1^* - \tau_{m+1}) / \Delta t$$

$$A_3 = \frac{c_2^3}{c_1^3 \Delta t}$$

$$A_4 = -(\tau_1^* - \tau_{m+1} + \frac{r}{c_1})/\Delta t = -(n-m-1)$$

$$A_5 = 0 \tag{6.69}$$

Case 5: $\tau_m < \tau_1^* < \tau_{m+1}$ and $\tau_{m-1} < \tau_2^* < \tau_m$

$$A_1 = c_2^2(\Delta t)^2[-2(n-m)^3 + \frac{3r^2}{(\Delta t)^2}(\frac{n-m-1}{c_1^2} + \frac{n-m+1}{c_2^2}) - \frac{2r^3}{(\Delta t)^3}(\frac{1}{c_1^3} + \frac{1}{c_2^3})]$$

$$A_2 = [\tau_2^* - \tau_{m-1} + \frac{c_2^2}{c_1^2}(\tau_1^* - \tau_{m+1})]/\Delta t$$

$$A_3 = (1 + \frac{c_2^3}{c_1^3})/\Delta t$$

$$A_4 = -(\tau_1^* - \tau_{m+1} + \frac{r}{c_1})/\Delta t = -(n-m-1)$$

$$A_5 = (\tau_2^* - \tau_{m-1} + \frac{r}{c_2})/\Delta t = n-m+1 \tag{6.70}$$

Case 6: $\tau_m < \tau_1^* < \tau_{m+1}$ and $\tau_m < \tau_2^* < \tau_1^* < \tau_{m+1}$

$$A_1 = c_2^2(\Delta t)^2[\frac{3r^2}{(\Delta t)^2}(n-m-1)(\frac{1}{c_1^2} - \frac{1}{c_2^2}) - \frac{2r^3}{(\Delta t)^3}(\frac{1}{c_1^3} - \frac{1}{c_2^3})]$$

$$A_2 = -\frac{1}{\Delta t}[\tau_2^* - \tau_{m+1} - \frac{c_2^2}{c_1^2}(\tau_1^* - \tau_{m+1})]$$

$$A_3 = \frac{1}{\Delta t}(\frac{c_2^3}{c_1^3} - 1)$$

$$A_4 = -\frac{1}{\Delta t}(\tau_1^* - \tau_{m+1} + \frac{r}{c_1}) = -(n-m-1)$$

$$A_5 = -\frac{1}{\Delta t}(\tau_2^* - \tau_{m+1} + \frac{r}{c_2}) = -(n-m-1) \tag{6.71}$$

Case 7: $\tau_{m+1} < \tau_1^*$ and $0 < \tau_2^* < \tau_{m-1}$

$$A_1 = 6c_2^2(\Delta t)^2(n-m)$$

$$A_2 = A_3 = A_4 = A_5 = 0 \tag{6.72}$$

Case 8: $\tau_{m+1} < \tau_1^*$ and $\tau_{m-1} < \tau_2^* < \tau_m$

$$A_1 = c_2^2(\Delta t)^2[6(n-m) - (n-m+1)^3 + \frac{3(n-m+1)r^2}{c_2^2(\Delta t)^2} - \frac{2r^3}{c_2^3(\Delta t)^3}]$$

$$A_2 = (\tau_2^* - \tau_{m-1})/\Delta t$$

$$A_3 = \frac{1}{\Delta t},\ A_4 = 0$$

$$A_5 = (\tau_2^* - \tau_{m-1} + \frac{r}{c_2})/\Delta t = n-m+1 \tag{6.73}$$

Case 9: $\tau_{m+1} < \tau_1^*$ and $\tau_m < \tau_2^* < \tau_{m+1}$

$$A_1 = c_2^2(\Delta t)^2[(n-m-1)^3 - \frac{3r^2(n-m-1)}{c_2^2(\Delta t)^2} + \frac{2r^3}{c_2^3(\Delta t)^3}]$$

$$A_2 = -\frac{1}{\Delta t}(\tau_2^* - \tau_{m+1})$$

$$A_3 = -\frac{1}{\Delta t},\quad A_4 = 0$$

$$A_5 = -\frac{1}{\Delta t}(\tau_2^* - \tau_{m+1} + \frac{r}{c_2}) = -(n-m-1) \tag{6.74}$$

Case 10: $\tau_{m+1} < \tau_1^*$ and $\tau_{m+1} < \tau_2^* < \tau_1^*$

$$A_1 = A_2 = A_3 = A_4 = A_5 = 0 \tag{6.75}$$

It may be noted that for the case of $n = m$ in equations (6.52) and (6.60), the displacement kernel becomes:

$$U_{lk}^{nn} = \frac{1}{16\pi\mu(1-\upsilon)}\frac{1}{r}[(3-4\upsilon)\delta_{lk} + r_{,l}r_{,k}] \tag{6.76}$$

Moreover from (6.64) and (6.68) the traction kernel are:

$$Q_{lk}^{nn} = -\frac{1}{8\pi(1-\upsilon)r^2}\{[(1-2\upsilon)\delta_{lk} + 3r_{,l}r_{,k}]\frac{\partial r}{\partial n} + (1-2\upsilon)(n_l r_{,k} - n_k r_{,l})\} \tag{6.77}$$

As previously stated these equations are the three-dimensional Kelvin's elastostatic fundamental solutions (see equations 6.33 and 6.34).

6.3.2 Boundary Discretization

The boundary surface of the domain is discretized into a number of connected elements. The spatial variation of the field variables and the geometry must be described for each element. The field variables can be approximated arbitrarily in space. The co-ordinates at any point over any element surface are expressed by means of their nodal values using linear quadrilateral elements, whilst the field variables are represented by constant quadrilateral elements. The geometry of an element using linear interpolation functions (5.37) is represented by (5.36).

The displacement and traction fields on the boundary are approximated using the spatial interpolation function ψ_j for the node j. Thus from (6.48),

$$u_k(\mathbf{x},\tau) = \sum_j \sum_m \eta^m(\tau)\psi_j(\mathbf{x})u_k^{mj}$$

$$p_k(\mathbf{x},\tau) = \sum_j \sum_m \mu^m(\tau)\psi_j(\mathbf{x})p_k^{mj} \tag{6.78}$$

where m and j refer to time and space respectively, and $k = 1, 2, 3$ relates to the k-direction. When the field variables are constant over the element in approximation (6.78) $\psi_j(\mathbf{x}) = 1$. In case of an isoparametric element, the interpolation functions are identical.

Using these approximations equation (6.49) becomes:

$$\alpha_{lk}^{i} u_k^{ni} = \sum_{m=1}^{n}\sum_{j=1}^{N}[\int_{B_j} U_{lk}^{nm}\psi_j(\mathbf{x})dB]p_k^{mj} - \sum_{m=1}^{n}\sum_{j=1}^{N}[\int_{B_j} Q_{lk}^{nm}\psi_j(\mathbf{x})dB]u_k^{mj} \tag{6.79}$$

6.3.2.1 Evaluation of Spatial Integrals

When the boundary B is discretized, the computation of the kernels U_{lk}^{nm} and Q_{lk}^{nm} involves the integrals of the type

$$\int_{B_j} U_{lk}^{nm}\psi_j dB \quad \text{and} \quad \int_{B_j} Q_{lk}^{nm}\psi_j dB \tag{6.80}$$

When the load and field points coincide, the above integrals are evaluated using a standard Gaussian quadrature. The integrals are expressed in terms of the homogeneous co-ordinates ζ_1, ζ_2 for the elements.

Thus using equations (5.40-5.43), equation (6.79) can be written as:

$$\alpha_{lk}^{i} u_k^{ni} = \sum_{m=1}^{n}\sum_{j=1}^{N}[\int_{-1}^{1}\int_{-1}^{1} U_{lk}^{nm}\psi_j|\mathbf{J}|d\zeta_1 d\zeta_2]p_k^{mj} - \sum_{m=1}^{n}\sum_{j=1}^{N}[\int_{-1}^{1}\int_{-1}^{1} Q_{lk}^{nm}\psi_j|\mathbf{J}|d\zeta_1 d\zeta_2]u_k^{mj} \tag{6.81}$$

Similar transformation of co-ordinates is used during the internal integrations.

The boundary surface is divided into N elements, and because of the constant elements considered here the displacement u_k and traction p_k in the k-direction are assumed to be constant over each element, and equal to the value at the centre of the element. After the prescribed values, the number of unknown quantities is $3N$ with three directions.

6.3.2.2 Evaluation of Singular Integrals

In the last section the evaluation of the non-singular integrals, when $r \neq 0$, has been discussed. Consider now the case of singular integrals. During the integration there exists a singularity if and only if the load point is also a field point at the first time interval. The

need for singular and non-singular integrals is schematised in Figure (6.4). The singularity of the fundamental solutions can be treated in two different ways as follows:

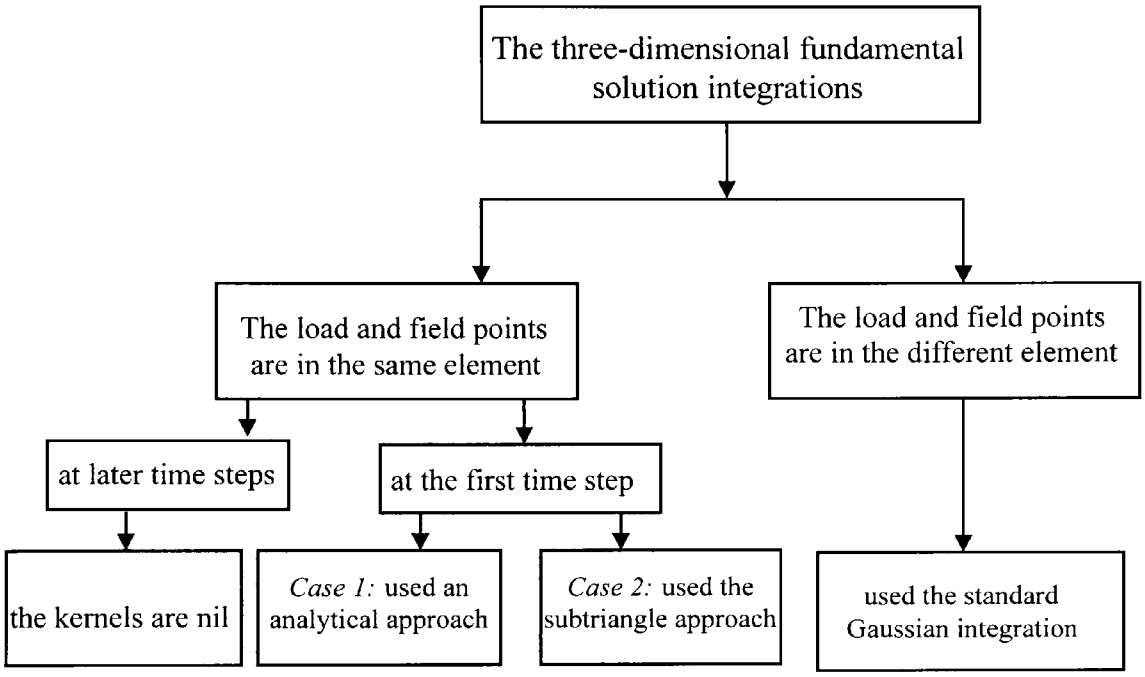

Figure 6.4 Integration Scheme

***Case 1 (Analytical)*:** When the singularity occurs, recalling equations (6.76) and (6.77), the spatial integrals are evaluated analytically using Cruse's method (1969).

Here, the integrals are to be evaluated in the sense of the Cauchy principal value in which the region very close to the load point is to be excluded from the integral. The integral is obtained as the region recoils toward zero area (see Figure 6.5). So, for example for the displacement integral, has the form,

$$G_{lk} = \frac{1}{16\pi\mu(1-\upsilon)} \lim_{\rho_1 \to 0} \int_{-\theta_2}^{\theta_1} (r(\theta) - \rho_1)[(3-4\upsilon)\delta_{lk} + r_{,l} r_{,k}]d\theta \qquad (6.82)$$

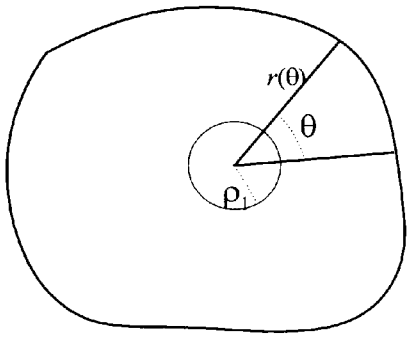

Figure 6.5 Transformation to polar co-ordinates

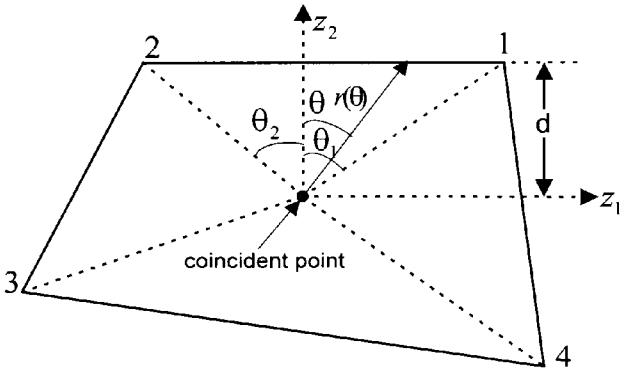

Figure 6.6 Scheme for analytical integration of the singularity case

Thus using a quadrilateral in the local co-ordinate system, see Figure (6.6), the kernels can be integrated as line integrals.

Therefore, one can evaluate (6.76) in polar co-ordinates such that the displacement integral becomes,

$$G_{lk}\Big|_2^1 = \frac{1}{16\pi\mu(1-\upsilon)} \int_{-\theta_2}^{\theta_1} r(\theta)[(3-4\upsilon)\delta_{lk} + r_{,l}r_{,k}]d\theta \tag{6.83}$$

In the local variables:

$$r_{,k} = e_{1k}\sin\theta + e_{2k}\cos\theta \tag{6.84}$$

where $e_{1k} = \frac{\partial z_1}{\partial x_k}$ and $e_{2k} = \frac{\partial z_2}{\partial x_k}$ are the direction cosines of the z_1 and z_2 axes.

From Figure (6.6) for side 2-1, taking $r(\theta) = d/\cos\theta$ and, using (6.84), equation (6.83) can be integrated so that:

$$G_{lk}\Big|_2^1 = \frac{1}{16\pi\mu(1-\upsilon)}\{(3-4\upsilon)\delta_{lk}\ln(\sec\theta+\tan\theta) + e_{1l}e_{1k}[-\sin\theta + \ln(\sec\theta+\tan\theta)] + e_{2l}e_{2k}\sin\theta - (e_{1l}e_{2k}+e_{2l}e_{1k})\cos\theta\}\Big|_{-\theta_2}^{\theta_1} \tag{6.85}$$

In evaluation of integral of the traction kernel, it is only necessary to consider the term of $\frac{1}{r^2}(n_l r_{,k} - n_k r_{,l})$ since $\partial r/\partial n = 0$. Clearly, for the case of $l = k$, then $Q_{ll} = 0$. Thus, for the case of $l \neq k$, using

$$e_{lkm}e_{rsm}n_r(\frac{1}{r})_{,s} = \frac{\mathrm{I}}{r^2}(n_k r_{,l} - n_l r_{,k}) \tag{6.86}$$

the integral of the traction kernel (6.77) can then be written as:

$$H_{lk}\Big|_2^1 = \bar{k}e_{lkm}\int_{\Delta B} e_{rsm}n_r(\frac{1}{r})_{,s}\,dB \tag{6.87}$$

with $\bar{k} = (1-2\upsilon)/8\pi(1-\upsilon)$.

Using Stokes' theorem the surface integral (6.87) is reduced to the line integral:

$$H_{lk}\Big|_2^1 = \bar{k}e_{lkm}\oint\frac{1}{r}dx_k \tag{6.88}$$

where $dx_k = e_{1k}dz_1 + e_{2k}dz_2$.

From Figure (6.6) it can be seen that $dz_2 = 0$. Then equation (6.88) becomes

$$H_{lk}\Big|_2^1 = \bar{k}e_{lkm}\oint\frac{1}{r}dx_k = \bar{k}e_{lkm}e_{1k}\oint\frac{1}{r}dz_1 = \bar{k}e_{lkm}e_{1k}\sinh^{-1}(z_1/z_2)$$

$$= \bar{k} e_{lkm} e_{1k} \ln(r + z_1)\Big|_{z_1^2}^{z_1^1} \tag{6.89}$$

Repeating the above operations along sides 3-2, 4-3 and 1-4, the combined integrals of the displacement and traction kernels are:

$$G_{lk}^{nnii} = G_{lk}\Big|_2^1 + G_{lk}\Big|_3^2 + G_{lk}\Big|_4^3 + G_{lk}\Big|_1^4 \tag{6.90}$$

and

$$H_{lk}^{nnii} = H_{lk}\Big|_2^1 + H_{lk}\Big|_3^2 + H_{lk}\Big|_4^3 + H_{lk}\Big|_1^4 \tag{6.91}$$

***Case 2 (Subtriangle Approach)*:** In the case of the singularity, $\partial r / \partial n = 0$, and as stated previously, for any plane boundary it can be shown that $Q_{ll}^{nn} = 0$. For the case of $l \neq k$ the terms $Q_{lk}^{nn} \neq 0$. These non-zero terms express a *weak* coupling between the horizontal and vertical motions (Karabalis et al., 1986). Assuming vertical loads produce *only* vertical motions, whilst horizontal loads cause *only* horizontal motions (Karabalis et al., 1984, 1986), those non-zero terms can be neglected. As a result of this simplification the influence terms Q_{lk}^{nn} are zero for the plane boundary elements.

When the load point is also a field point, the element is divided into four sub-triangles (see Figure 5.9). Taking each sub-triangle as an independent quadrilateral element, the singularity is removed and integrated using the standard Gaussian quadrature. Details of the approach can be found in Chapter 5.

It is emphasised that *case 2* requires about 25% more computing time in comparison to *case 1*.

6.3.3 The Boundary Element Equation

After evaluating temporal and space (singular and regular) integrals using all the boundary elements, the algebraic equation system is established similar to the two-dimensional elastodynamic problems in Chapter 4. Namely, equations (4.65-4.69) are used here again. It must be remembered that these equations are used here for three-dimensional geometries. Thus unspecified field variables can be found for each time step n, using the same procedure as of Chapter 4.

6.4 Infinite Domains

To extend the validity of the boundary integral equation (6.47) to media of infinite extent of the form ($\mathbb{R}^2$-B), one must introduce certain conditions on the behaviour at infinity of the actual state (u_k, p_k). Following considerations similar to those invoked for scalar wave problems (see Figure 5.10) equation (6.47) can be written in the form:

$$\alpha_{lk}^{i} u_k^i = \int_B [(u_{lk}^s * p_k) - (p_{lk}^s * u_k)](\mathbf{x}, t) dB + \lim_{r \to \infty} \int_{B_r} [(u_{lk}^s * p_k) - (p_{lk}^s * u_k)](\mathbf{x}, t) dB \qquad (6.92)$$

When all loads causing the motion are inside a finite domain then there is no wave to propagate to the interior from infinity. Therefore, the displacement and tractions must behave in such a way that, the second integral in equation (6.92), vanishes in the limit as $r \to \infty$.

Using (4.73) for the three-dimensional problems, and from the analytical structure of the fundamental displacement and traction solutions (6.22, 6.28), each vector satisfies the radiation and regularity conditions like the two-dimensional solutions.

6.5 Calculation of the Internal Displacements

The BEM formulation has concentrated on obtaining the unknown boundary displacements and tractions. In terms of the boundary values known for $t = \Delta t, 2\Delta t, ..., n\Delta t$, the internal displacements can be found for the given points. From equation (6.46), the value $\alpha_{lk}^{i} = \delta_{lk}$, $l,k = 1, 2, 3$ for any point inside the domain. Considering the time difference *n-m*, the internal displacements can easily be calculated at time step *n*. The equation required can then be written as:

$$u_l^{ni} = \sum_{m=1}^{n}\sum_{j=1}^{N} G_{lk}^{nmij} p_k^{mj} - \sum_{m=1}^{n}\sum_{j=1}^{N} \hat{H}_{lk}^{nmij} u_k^{mj} \qquad (6.93)$$

where *i* and *j* denote the internal and boundary points, respectively.

It is noted that equation (6.93) is evaluated numerically using the usual Gaussian quadrature in a similar way to that of the boundary integrations.

6.6 Results

In this section, the behaviour of the elastic wave, through three-dimensional rock structures is considered in the medium of finite and infinite extent. With the help of the two-dimensional programs used in the previous chapters, subprograms together with a main program have been produced to solve the three-dimensional elastic wave propagation problems.

Evaluation of the singular integrals is essential in the BEM and these integrals are obtained for c*ase 1*, which is analytical, and c*ase 2*, which is an extension of the Lachat (1975) approach to dynamic problems. Note that Lachat used it for static problems. The two approaches are compared in the following results.

6.6.1 The Bounded Medium

Consider the problem of solving equation (2.43) in a three-dimensional medium of infinite extent. The material properties, $c_1 = 2130$ m/s and $c_2 = 1230$ m/s, are for shale. As can be seen in Figure (6.7), the source is located at the centre of the medium whilst equally spaced receivers are positioned in a horizontal line at 2 m below the top surface. The geometrical definition of the model can be seen in Figure (6.7), and the top boundary is taken as a free surface boundary condition. The Dirichlet boundary conditions are used for the remaining boundary surfaces. In order to take into account the distribution of the travelling waves, the surface of the domain has been discretized into uniform 9m×9m element meshes.

The synthetic seismograms (Figures 6.8 and 6.9) are produced for the physical geometry shown by Figure (6.7). In these seismograms, time runs along the horizontal axis, and all registered displacement values at the selected receiver points are on the vertical axis. The number of receivers taken is 89. To obtain the seismograms the boundary elements put to use are uniform for the external boundary. The time increment and source position are 0.001 s and (45,45,45). The source is taken as an internal boundary being a small cube. The Dirichlet boundary condition is prescribed for the sides of the small cube with side length 3-m.

In both Figures (6.8) and (6.9), the first wave reaches the receiver at time 0.02 s. The S-wave appears at time 0.035 s. The wave reflected from the bottom is received at about time 0.0625 s. In these figures, the waves coming from the side boundaries are weaker than the waves reflected from the sides in 2D case in Chapter 4. This observation also holds for scalar waves. It has been observed that, non-uniformity of the elements and the

number of elements affect the stability of the solution. The effect of non-uniformity on the results is addressed in the results for a medium of infinite extent as will be seen in the following section. Increasing the number of elements can redress this problem subject to the limitation of storage space.

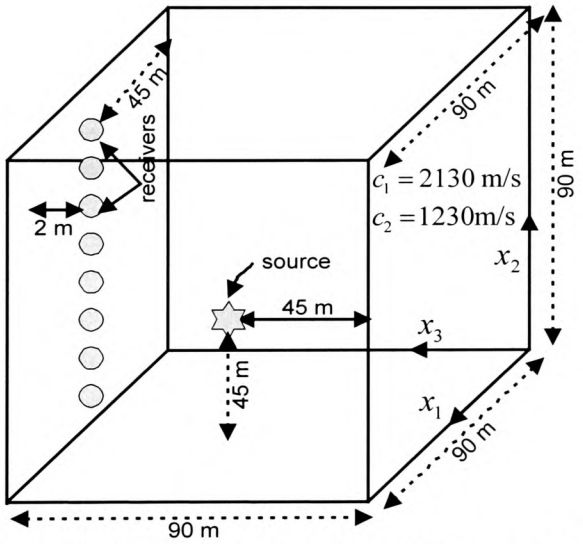

Figure 6.7 Physical model showing the medium used to generate seismograms in the 3D elastic BEM program

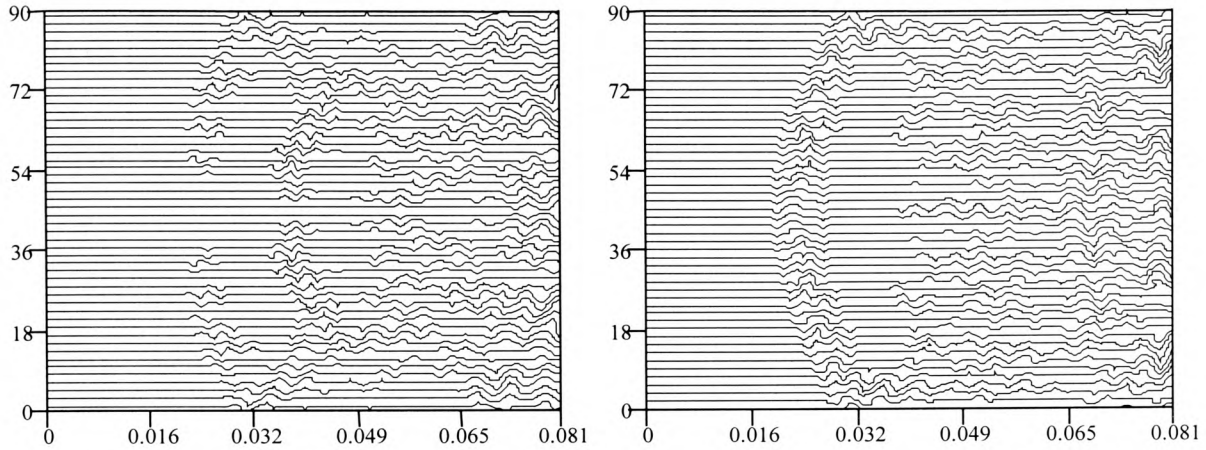

Figure 6.8 Synthetic horizontal and vertical seismograms generated from the BEM solution of the 3D elastic wave equation with the top (Neumann) and sides and bottom (Dirichlet) boundary conditions for the bounded medium- ***Case 1***.

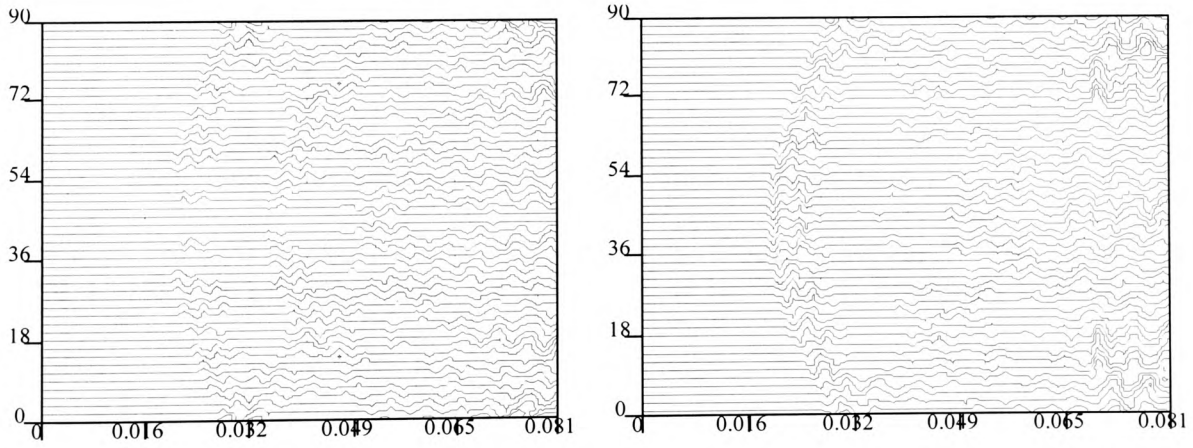

Figure 6.9 Synthetic horizontal and vertical seismograms generated from the BEM solution of the 3D elastic wave equation with the top (Neumann) and sides and bottom (Dirichlet) boundary conditions for the bounded medium - ***Case 2***.

6.6.2 The Medium of Infinite Extent

The physical geometry given in Figure (6.10) extends to infinity from the sides and bottom. The elastic results are given in Figures (6.11) and (6.12). As can be seen from Figures (6.11) and (6.12), excellent agreement is obtained. The boundary elements used are uniform for the external boundary. The time increment, source size and element size taken are 0.00079 s, 2mx2mx2m and 5mx5m respectively.

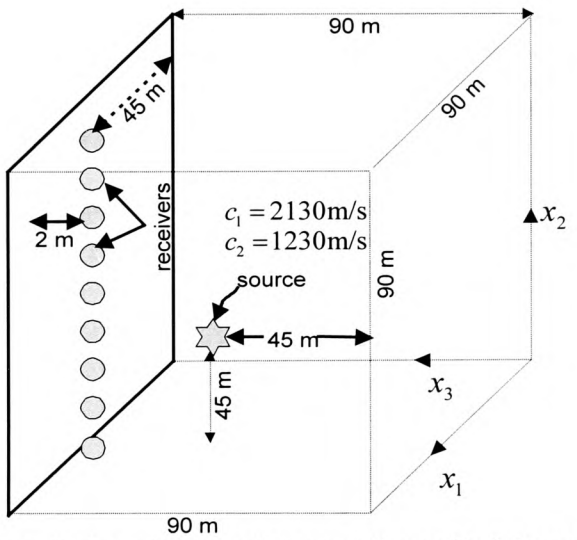

Figure 6.10 Physical model showing a medium of infinite extent used to generate seismograms in the 3D elastic BEM program

In the medium of infinite extent, the first wave is received at time 0.02 s. There is no reflected wave from the sides or bottom as expected. The S-wave starts to arrive at the nearest receiver at time 0.035 s. One can notice that the S-wave is weaker in the horizontal seismogram than in the vertical one, as observed in two dimensions. The strength of the waves is affected from the source size and time increment. Very clear results have been obtained for the boundless medium. The results presented demonstrate

the BEM to be most satisfactory and more easily applicable for unbounded media than bounded media.

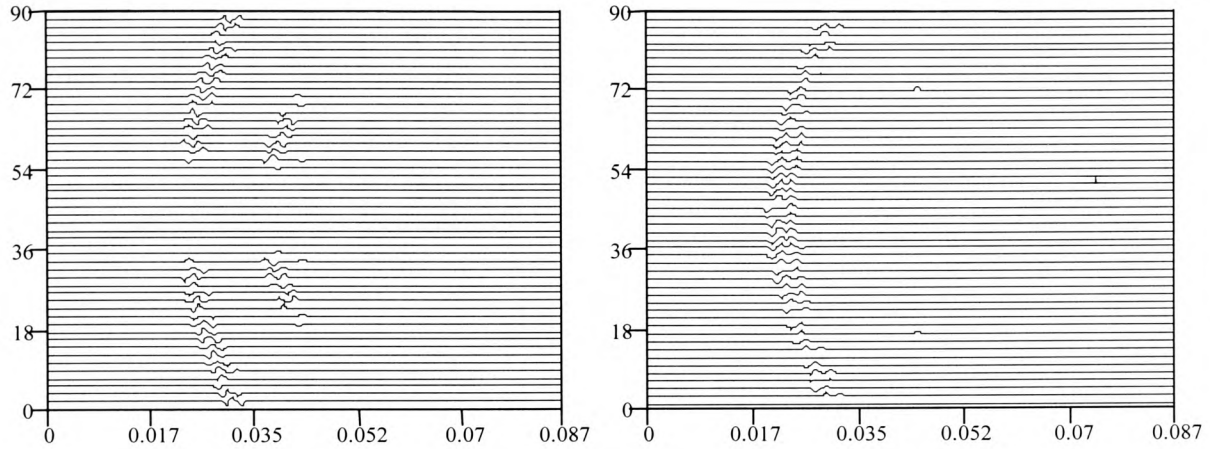

Figure 6.11 Synthetic horizontal and vertical seismograms generated from the BEM solution of the 3D elastic wave equation (with the top-Neumann boundary conditions) for the medium of infinite extent-***Case 1***.

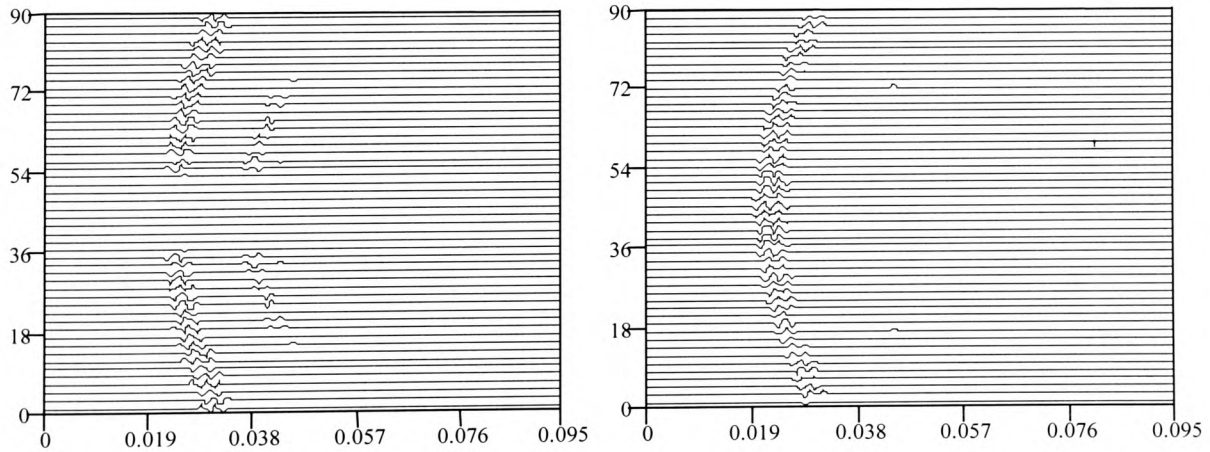

Figure 6.12 Synthetic horizontal and vertical seismograms generated from the BEM solution of the 3D elastic wave equation (with the top-Neumann boundary conditions) for the medium of infinite extent-***Case 2***.

6.7 Conclusions

A new numerical formulation for the three-dimensional BEM has been presented with the help of the two-dimensional case. After the fundamental solutions were considered, the displacement and traction kernels were derived. The fundamental importance of the singular integrals in BEM has led us to evaluate them using two alternative approaches. For each method, BEM solutions have been presented. The results have agreed perfectly, and are seen to be stable. The clarity of the unbounded media results is better than that for the bounded media results.

CHAPTER 7

MAIN CONCLUSIONS AND RECOMMENDATIONS FOR THE FUTURE RESEARCH

The main aims of the thesis were to use the BEM as a satisfactory numerical approach to model seismic wave propagation, and also to clearly determine whether the method could be applied to more sophisticated seismological problems.

In this regard the two-dimensional scalar wave problems have been analyzed to identify dynamic behavior through different types of materials. Having obtained stable and accurate solutions for many two-dimensional scalar wave problems, the more complex elastic waves were investigated. The results were discussed for the scalar and elastic wave problems in two dimensions, for one-medium and also for layered media. These results were used as a basis to examine the more realistic three-dimensional scalar and elastic wave problems.

A time domain direct BEM was employed for solutions for all types of wave propagation problems. Certain programs of Dominguez (1993) were extended by writing additional subroutines to compute internal variables for a single medium in two-dimensions. In addition, to ascertain scalar and elastic wave behavior in layered media, these extended programs were further expanded using subroutines for each layer in turn. To solve the more complex three-dimensional scalar and elastic wave problems in homogeneous and piecewise homogeneous media, programs were developed which were based upon their two-dimensional counterparts.

The displacements and its normal derivatives are represented by linear and constant time variation, respectively. By means of these temporal variations all time integrations were determined analytically for both wave types, and both dimensions. New two-dimensional kernels have been evaluated. All kernels for boundary and internal points have also been derived for three-dimensional scalar waves. In addition, it is noted that the three-dimensional elastodynamic boundary kernels have been presented in this work.

Note that in Chapters 5 and 6 the singular integrals have been evaluated using two alternative approaches for both three-dimensional scalar and elastic wave problems. In the case of a singularity, use of analytical integration results in a time saving of approximately 25%.

Several wave propagation problems have been examined. In particular, scalar, and elastic waves were discussed in both two and three dimensions, and for one-medium, and layered media. It was observed that, the sensitivity of the solutions for the selection of time step and element size in elastic waves is more than that for scalar waves. Perhaps one of the most important reasons for this is the structural intricacy of the fundamental solutions. As a result of this complexity, too many parameters are used during the numerical solution. The number of the linear equations affects the stability. The number of equations in elastodynamic problems is clearly more than for scalar cases. Clearly, more equations give rise to more operations, which in turn cause a greater accumulation of round-off errors.

On the other hand, the desire for stable results requires more elements which in turn increase the dimension of the algebraic equation system. It must be emphasized that very few elements may not represent small changes as required. It is therefore recommended

that a reasonable number of elements must be employed. This number can be determined by researchers depending on the nature of the problem to be solved.

The solutions are more stable for media of infinite extent than for media of finite extent. Despite the fact that the existence of the interfaces make the solution of the problem more prone to instability, the present analysis shows that, the BEM is capable of treating layered media problems. Even though the examples presented show that the time domain direct BEM is stable for practical applications, future work should concentrate on the analysis of numerical solutions, which give unconditional stability.

To determine the dynamical response of two- and three-dimensional geophysical structures, the boundary has been composed of a number of 'linear line' and flat rectangular elements, respectively. Two or more layers can be connected together at an interface to shape a body with an arbitrary number of connected layers. The size of the source considered should not be too small to simulate meaningful changes in the media of interest.

Generally, reflected waves in three dimensions are weaker than that in two dimensions. The interface reflections are clearly visible from the seismograms even though they are weaker in three dimensions.

In an elastic isotropic and homogeneous plane body the potential, and flux changes across the body have been examined in two, and three dimensions.

To solve the wave equations in multimedia additional interface equations have been added directly to the algebraic equation system. An alternative approach is available to deal with the interface variables. In this alternative, the interface variables can be eliminated without using additional interface equations. It should be noted that use of the suggested approach would give some flexibility for the storage of dynamical history. In

addition, the number of the algebraic equations will be less than that used in the present work. However this method renders its flexibility due to its structural complexity.

The work for the 2D and 3D scalar and elastic wave propagation may be extended to include non-zero initial and body force contributions. To achieve this, Dual Reciprocity BEM (Partridge et al., 1992) can be considered.

The method has been demonstrated to be useful, and applicable in the solution of displacement wave propagation problems. Similarly, the dynamical behavior of the stress components can be studied in 2D and 3D geometries. The wave equations can also be solved for borehole geometries in two and three dimensions.

When a fundamental solution is known, the BEM can be applied. A possible improvement to this approach includes the coupling of the BEM with the FEM. This would retain the advantages of the BEM, but not require the fundamental solutions and evaluation of singular integrals. In such an approach, the modelling of non-linear behavior is also possible, see for example, Wolf et al. (1999).

In addition, the results presented here for the 2D and 3D elastic wave propagation may be extended to include thermoelasticity problems.

The FEM and different domain methods are readily available to solve wave propagation problems, but require full discretization of the domain of interest, and extra effort to deal with infinite and semi-infinite domains.

It is anticipated that code employing implicit full pivoting, would be more effective in solving the linear algebraic equation system for the case of large multimedia problems, because of the presence of zero matrix elements. Such a solver would allow the exclusion of some zero values from the system matrix. This exclusion would reduce the storage space by approximately 20%. Considering LU decomposition of a band

diagonal matrix, partial-pivoting solvers are already available, see for example, Press et al. (1992). However, it is believed that the solver recommended gives more accurate and stable solution to the algebraic equation.

APPENDIX

Solution of the Linear Equation Systems

Throughout the present the Crout algorithm was used for the solution of the real system of linear equations of types (3.61, 4.71). The coefficient matrix **A** is factorized into its upper and lower triangular matrices. A discussion of the approach can be found in Bowdler et al. (1966). The computer program was developed by Dominguez (1993).

In multi-layered problems the Gaussian elimination method with implicit full pivoting is used for the solution of the equation systems (3.68, 4.79). The program of Monro (1985) was used to solve the corresponding linear equation systems. In this research a program was written in which the system matrix is factorized into LU form with implicit full pivoting. This was tested to obtain the same results given in Figure (3.19). Using the new program, the results obtained are as follows.

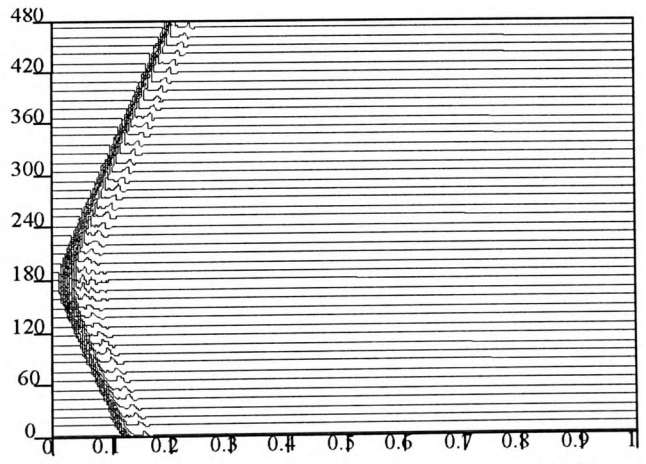

Figure A.1 The same result obtained with Figure 3.19 using the new solver

REFERENCES

Achenbach, J. D., 1975, *Wave propagation in elastic solids*, North-Holland

Ahmad, S., 1986, Linear and nonlinear dynamic analysis boundary element method, *Ph.D. Thesis*, State University of New York, Buffalo.

Ahmad, S. and Banerjee, P. K., 1988, Time domain transient elastodynamic analysis of 3D solids by BEM, *International Journal of Numerical Methods in Engineering*, Vol. 26, pp. 1709-1728.

Ahmad, S. and Banerjee, P. K., 1988, Multi-domain BEM for two-dimensional problems of elastodynamics, *International Journal of Numerical Methods in Engineering*, Vol. 26, pp. 891-911.

Aki, K. and Richards, P. G., 1980, *Quantitative seismology - theory and methods*, San Francisco: W.H. Freeman and Co.

Antes, H., 1985, A boundary element procedure for transient wave propagation in two-dimensional isotropic elastic media, *Finite Element Analysis and Design*, Vol. 1, pp. 313-322.

Antes, H., Steinfeld, B. and Trondle, G., 1991, Recent developments in dynamic stress analyses by time domain BEM, *Engineering Analysis with Boundary Elements*, Vol. 8, No 4, pp. 176-184.

Arai, M., Adachi, T. and Matsumoto, H., 1999, Boundary element analysis for unsteady elastodynamic problems based on the Laplace transform, JSME International Journal Series A, Vol. 42, No. 4, pp. 507-514

Banaugh, R. P. and Goldsmith, W., 1963, Diffraction of steady elastic waves by surfaces of arbitrary shape, *J. Appl. Mech.*, Vol. 30, pp. 589-597.

Banerjee, P. K., 1994, *The boundary element methods in engineering*, McGraw-Hill, London.

Banerjee, P. K., Ahmad, S. and Manolis, G. D., 1986, Transient elastodynamic analysis of 3D problems by BEM, *International Journal of Earthquake Engineering and Structural Dynamics*, Vol. 14, pp. 933-949.

Banerjee, P. K. and Butterfield, R., 1981, *Boundary Element Methods in Engineering Science*, McGraw-Hill, London.

Barton, G., 1991, *Elements of Green's functions and propagation: Potentials, diffusion and waves*, Oxford Science Publications

Becker, A. A., 1992, *The Boundary Element Method in Engineering*, McGraw-Hill, London.

Bedford, A. and Drumheller, D. S., 1994, *Introduction to elastic wave propagation*, John Wiley and Sons

Beer, G. and Watson, J. O., 1992, *Introduction to Finite and Boundary Elements for Engineers*, John Wiley-Sons, West Sussex, England.

Ben-Menahem, A. and Singh, S. J., 1981, *Seismic Waves and Sources*, Springer-Verlag, Berlin.

Beskos, D. E., 1988, Boundary element methods in geomechanics, *Boundary Elements X. Proc. of the 10th Int. Conf. on Boundary Elements (Brebbia Ed.)*, Springer-Verlag, pp. 3-28.

Beskos, D. E., 1987a, Boundary element methods in mechanics, Amsterdam, North Holland.

Beskos, D. E., 1987b, Boundary element method in dynamic analysis, *Applied Mechanics Review*, Vol. 40, No 1, pp. 1-23.

Beskos, D. E., 1997, Boundary element methods in dynamic analysis: Part II (1986-1996), *Applied Mechanics Review*, Vol. 50, No. 3, pp. 149-197.

Birgisson, B., 1996, A two-dimensional dynamic direct boundary element method for piecewise homogeneous elastic media, *Ph.D. Thesis*, University of Minnesota, USA.

Birgisson, B. and Crouch, S. L., 1998, Elastodynamic boundary element method for piecewise homogeneous media, *International Journal for Numerical Methods in Engineering*, Vol. 42, pp. 1045-1069.

Birgisson, B., Siebrits, E. and Peirce, A. P., 1999, Elastodynamic direct boundary element methods with enhanced numerical stability properties, *International Journal for Numerical Methods in Engineering*, Vol. 46, pp. 871-888.

Bluck, M. J. and Walker, M. J., 1996, Analysis of three-dimensional transient acoustic wave propagation using the boundary integral equation method, *International Journal for Numerical Methods in Engineering*, Vol. 39, pp. 1419-1431.

Bonnet, M., 1998, *Boundary integral equation methods for solids and fluids*, John Wiley and Sons, New York

Bowdler, H. J., Martin, R. S., Peters, G. and Wilkonson, J. H., 1966, Solution of real and complex systems of linear equations, *Numerische Mathematik*, Vol. 8, pp. 217-234.

Brabham, P. J., McDonald, R. J. and McCarroll, D., 1999, The use of shallow seismic techniques to characterize sub-surface Quaternary deposits: the example of Porth Neigwl (Hells Mouth Bay), Gwynedd, N. Wales, *Quarterly Journal of Engineering Geology*, Vol. 32, pp. 119-137.

Brebbia, C.A., 1978, *The boundary element method for engineers*, Pentech Press, London.

Brebbia, C. A., Telles, J. C. F. and Wrobel, L. C., 1984, *Boundary element techniques*, Berlin, Springer-Verlag.

Brebbia, C. A., 1991, Two different approaches for transforming domain integrals to the boundary, *Mathematical and Computer Modelling*, Vol. 15, No. 3-5, pp. 43-58

Brebbia, C.A. and Dominguez, J., 1992, *Boundary elements-an Introductory course*, Second Edition, CMP, Southampton, Boston.

Bullen, K.A., 1976, *An introduction to theory of seismology*, Cambridge University Press.

Carrer, J. A. M. and Mansur, W. J., 1994, Space derivatives in the time domain BEM analysis for the scalar wave equation, *Engineering Analysis with Boundary Elements*, Vol. 13, pp. 67-74.

Carrer, J. A. M. and Mansur, W. J., 1996, Time-domain BEM analysis for the 2D scalar wave equation: Initial conditions contributions to space and time derivatives, *International Journal for Numerical Methods in Engineering*, Vol. 39, pp. 2169-2188.

Carrer, J. A. M. and Mansur, W. J., 1999, Stress and velocity in 2D elastodynamic analysis by the boundary element method, *Engineering Analysis with Boundary Elements*, Vol. 23, No. 3, pp. 233-245.

Coda, H. B. and Venturini, W. S., 1995, Three-dimensional transient BEM analysis, *Computers and Structures*, Vol. 56, No. 5, pp. 751-768.

Coda, H. B. and Venturini, W. S., 1996, A simple comparison between two 3D time domain elastodynamic boundary element formulations, *Engineering Analysis with Boundary Elements*, Vol. 17, pp. 33-44.

Cole, D. M., Kosloff, D. D. and Minster, J. B., 1978, A numerical boundary integral equation method for elastodynamics. I, *Bulletin of the Seismological Society of America*, Vol. 68, No. 5, pp. 1331-1357

Crouch, S. L. and Starfield, A. M., 1983, *Boundary element methods in solid mechanics*, George Allen and Unwin Publishers.

Cruse, T. A., 1968, A direct formulation and numerical solution of the general transient elastodynamic problem II, *Journal of Mathematical Analysis and Applications*, Vol. 22, pp. 341-355.

Cruse, T. A., and Rizzo, F. J., 1968, A direct formulation and numerical solution of the general transient elastodynamic problem I, *Journal of Mathematical Analysis and Applications*, Vol. 22, pp. 244-259.

Cruse, T. A., 1969, Numerical solutions in three-dimensional elastostatics, *Int. J. Solids Structures*, Vol. 5, pp. 1259-1274.

Cruse, T. A., 1974, An improved boundary integral equation method for three dimensional elastic stress analysis, *Computers and Structures*, Vol. 4, pp. 741-754.

Das, S. and Aki, K., 1977, A numerical study of two-dimensional spontaneous rupture propagation, *Geophys. J. R. Astr. Soc.*, Vol. 50, pp. 643-668

Demir, I., 1998, Seismic wave modelling using finite difference methods, *Ph.D. Thesis*, University of Glamorgan, UK

Dominguez, J. and Gallego, R., 1989, Time domain boundary elements: a comparative study, *Advances in boundary elements, Vol. 3, C.A. Brebbia (Ed.)*, pp. 319-329.

Dominguez, J., 1993, *Boundary element in dynamics*, CMP, Southampton.

Dominguez, J. and Gallego, R., 1991a, The time domain boundary element method for elastodynamic problems, *Mathematical and Computer Modelling*, Vol. 15, No, 3-5, pp. 119-129.

Dominguez, J., and Meise, T., 1991, On the use of the BEM for wave propagation in infinite domains, *Engineering Analysis with Boundary Elements*, Vol. 8, pp. 132-138.

Doyle, H. A., 1995, *Seismology*, Wiley, England.

El-Zafrany, A., 1993, Techniques of the Boundary Element Method, Ellis Horwood Ltd.

Eringen, A. C. and Suhubi, E. S., 1975, *Elastodynamics, Vol. II, Linear Theory*, Academic Press, New York.

Friedman, M. B. and Shaw, R. P., 1962, Diffraction of pulses by cylindrical obstacles of arbitrary cross section, *ASME Journal of Applied Mechanics*, Vol. 29, pp. 40-46

Gallego, R. and Dominguez, J., 1996, Hypersingular BEM for transient elastodynamics, *International Journal for Numerical Methods in Engineering*, Vol. 39, pp. 1681-1705.

Gilbert, J. E. and Knobs, R. J., 1967, Stability of general systems, *Archive for Rational Mechanics and Analysis*, Vol. 25, pp. 271-284

Graff, K. F, 1975, *Wave motion in elastic solids*, Oxford: Clarendon Press.

Greenberg, M. D., 1971, *Application of Green's Functions in Science and Engineering*, Prentice-Hall, New Jersey

Guiggiani, M., 1992, Computing principle value integrals in 3-D BEM for time harmonic elastodynamics – a direct approach, *Communications in Applied Numerical Methods*, Vol. 8, pp. 141-149.

Guiggiani, M. and Gigante, A., 1990, A general algorithm for multidimensional Cauchy principle value integrals in the boundary element method, *ASME Journal of Applied Mechanics*, Vol. 57, pp. 906-915.

Haberman, R., 1998, *Elementary applied partial differential equations-With Fourier series and boundary value problems*, Prentice-Hall.

Hall, W. S., 1994, *The boundary element method*, The Netherlands: Kluwer Academic Publishers

Hudson, J. A., 1980, *Excitation and wave propagation*, Cambridge University Press.

Israil, A. S. M. and Banerjee, P. K., 1990a, Advanced development of time-domain BEM for 2D scalar wave propagation, *International Journal for Numerical Methods in Engineering*, Vol. 29, pp. 1003-1020.

Israil, A. S. M. and Banerjee, P. K., 1990b, Advanced time-domain formulation of BEM for 2D transient elastodynamics, *International Journal for Numerical Methods in Engineering*, Vol. 29, pp. 1421-1440.

Israil, A. S. M. and Banerjee, P. K., 1991a, 2-D transient interior flux by time-domain boundary element method, *Communications in Applied Numerical Methods*, Vol. 7, pp. 411-420.

Israil, A. S. M. and Banerjee, P. K., 1991b, Interior stress calculations in 2-D time domain transient BEM analysis, *International Journal of Solids and Structures*, Vol. 27, No. 7, pp. 915-927.

Jaswon, M. A., 1963, Integral equation methods in potential theory-I, *Proc. Roy. Soc.*, London, A275, pp. 23-32.

Karabalis, D. L. and Beskos, D. E., 1984, Dynamic response of 3D rigid surface foundations by time domain boundary element method, *Earthquake Engineering and Structural Dynamics*, Vol. 12, pp. 73-93

Karabalis, D. L. and Beskos, D. E., 1986, Dynamic response of 3D embedded foundations by time domain boundary element method, *Computer Methods in Applied Mechanics and Engineering*, Vol. 56, pp. 91-119

Karabalis, D. L., 1991, A simplified 3-D time domain BEM for dynamic soil-structure interaction problems, *Engineering Analysis with Boundary Elements*, Vol. 8, No. 3, pp. 139-145.

Lachat, J. C., 1975, A further development of the boundary integral technique for elastostatics, *Ph.D. Thesis*, University of Southampton

Lachat, J. C. and Watson, J. O., 1976, Effective numerical treatment of boundary integral equations: A formulation for three-dimensional elastostatics, *International Journal for Numerical Methods in Engineering*, Vol. 10, pp. 991-1005.

Loken, M. C., 1992, A three-dimensional boundary element method for linear elastodynamics, *Ph.D. Thesis*, University of Minnesota, USA.

Love, A. E. H., 1944, A treatise on the mathematical theory of elasticity, Dover, New York.

Mack, M. G., 1991, A three-dimensional boundary element method for elastodynamics, *Ph.D. Thesis*, University of Minnesota, USA.

Mackerle, J. and Brebbia, C. A., 1988, *The boundary element reference book*, CMP, Springer-Verlag, Southampton, Boston.

Manolis, G. D., 1983, A comparative study on three boundary element method approaches to problems in elastodynamics, *International Journal for Numerical Methods in Engineering*, Vol. 19, pp. 73-91.

Manolis, G. D. and Beskos, D. E., 1981, Dynamic stress concentration studies by boundary integrals and Laplace transform, *International Journal for Numerical Methods in Engineering*, Vol. 17, pp. 573-599.

Manolis, G. D. and Beskos, D. E., 1988, *Boundary element methods in elastodynamics*, Unwin and Hyman, London.

Mansur, W. J., 1983, A time-stepping technique to solve wave propagation problems using the Boundary Element Method, *Ph.D. Thesis*, University of Southampton, UK

Mansur, W. J. and Brebbia, C. A., 1982, Numerical implementation of the boundary element method for two-dimensional transient scalar wave propagation problems, *Applied Mathematical Modelling*, Vol. 6, pp. 299-306.

Mansur, W. J. and Brebbia, C. A., 1985, Transient elastodynamics, in *Topics in boundary element research, Vol. 2: Time dependent and vibration problems, C.A. Brebbia (Ed.)*, pp. 124-155

Mansur, W. J. and Carrer, J. A. M., 1993, Two-dimensional transient BEM analysis for the scalar wave equation: Kernels, *Engineering Analysis with Boundary Elements*, Vol. 12, pp. 283-288.

Mansur, W. J., Carrer, J. A. M. and Siqueira, E. F. N., 1998, Time discontinuous linear traction approximation in time-domain BEM scalar wave propagation analysis, *International Journal for Numerical Methods in Engineering*, Vol. 42, pp. 667-683.

Mikhlin, S. G., 1957, *Integral equations*, Oxford: Pergamon Press.

Monro, D. M., 1985, *Fortran 77*, London: Edward Arnold Publishers

Morse, P. M. and Feshbach, H., 1953, *Methods of theoretical physics*, McGraw-Hill.

Muskhelishivili, N. I., 1963, *Some basic problems of the mathematical theory of elasticity*, Groningen: Noordhoff Publishing.

Nardini, D. and Brebbia, C. A., 1983, A new approach to free vibration analysis using boundary elements, *App. Math. Modelling*, Vol. 7, pp. 157-162.

Nardini, D. and Brebbia, C. A., 1985, Boundary integral formulation of mass matrices for dynamic analysis, *Topics in Boundary Element Research, Vol. 2, C. A. Brebbia (Ed.)*, pp. 191-208, Springer-Verlag, Berlin.

Nowak, A. J. and Neves, A. C., 1994, *The multiple reciprocity boundary element method*, CMP, Elsevier, Southampton, Boston.

Paris, F. and Canas, J., 1997, *Boundary element method: Fundamentals and applications*, Oxford Science Publications.

Partridge, P. W., Brebbia, C. A. and Wrobel, L. C., 1992, *The dual reciprocity boundary element method*, CMP, Southampton, Boston.

Peirce, A. and Siebrits, E., 1996, Stability analysis of model problems for elastodynamic boundary element discretizations, *Numerical Methods for Partial Differential Equations*, Vol. 12, pp. 585-613.

Peirce, A. and Siebrits, E., 1997, Stability analysis and design of time-stepping schemes for general elastodynamic boundary element models, *International Journal for Numerical Methods in Engineering*, Vol. 40, pp. 319-342.

Press, W. H., Teukolsky, S. A., Vetterling, W. T. and Flannery, B. P., 1992, *Numerical recipes in Fortran*, Second edition, Cambridge University Press.

Reynolds, A. C., 1978, Boundary conditions for the numerical solution of wave propagation problems, *Geophysics*, Vol. 43, No 6, pp. 1099-1110.

Richter, C., 1997, *Topics in Engineering: A Green's Function Time-Domain BEM of Elastodynamics, Brebbia, C. A. and Connor, J. J. (Eds.)*, Vol. 31, CMP, Southampton, UK

Rizos, D. C. and Karabalis, D. L., 1994, An advanced direct time domain BEM formulation for general elastodynamic problems, *Computational Mechanics*, Vol. 15, pp. 249-269.

Rizzo, F. J., 1967, An integral equation approach to boundary value problems of classical elastostatics, *Q. Appl. Math.*, Vol. 25, No 1, pp. 83-95.

Siebrits, E., Birgisson, B., Peirce, A. P. and Crouch, S. L., 1997, On the numerical stability of the time domain boundary element methods, *International Journal of Blasting and Fragmentation*, Vol. 1, pp. 305-316.

Siebrits, E. and Peirce, A. P., 1995, The stability properties of time domain elastodynamic boundary element methods, in *Boundary Element Methods XVII*, Southampton, pp. 45-53.

Sokolnikoff, I. S., 1956, *Mathematical theory of elasticity*, London, New York: McGraw-Hill.

Spyrakos, C. C. and Antes, H., 1986, Time-domain boundary element method approaches in elastodynamics: A comparative study, *Computers and Structures*, Vol. 24, No. 4, pp. 529-535.

Stephenson, G., 1996, *Partial Differential Equations for Scientist and Engineers*, Imperial College Press.

Stokes, G. D., 1849, On the dynamical theory of diffraction, *Trans. Cambridge Philos. Soc.*, Vol. 9, pp. 1-62

Symm, G. T., 1963, Integral equation methods in potential theory II, *Proc. Roy. Soc.*, A275, pp. 401-415.

Tian, Y., 1990, Boundary element methods in elastodynamics, *Ph.D. Thesis*, University of Minnesota, USA.

Trevelyan, J., 1994, *Boundary elements for engineers: Theory and applications*, CMP, Southampton, Boston.

Wang, Canyun and Takemiya, H., 1992, Analytical elements of time domain BEM for two-dimensional scalar wave problems, *International Journal for Numerical Methods in Engineering*, Vol. 33, pp. 1737-1754.

Wang, Chung-Cheng, Wang, H. and Liou, G., 1997, Quadratic time domain BEM formulation for 2D elastodynamic transient analysis, *Int. J. Solids and Struct.*, Vol. 34, No 1, pp. 129-151.

Wen, P. H., Aliabadi, M. H. and Young, A., 1999, A time dependent formulation of dual boundary element for 3D dynamic crack problems, *International Journal for Numerical Methods in Engineering*, Vol. 45, pp. 1887-1905.

Wheeler, L. T. and Sternberg, E., 1968, Some theorems in classical elastodynamics, *Arch. Rational Mech. Anal.*, Vol. 31, pp. 51-90

White, J. E. and Sengbush, R. L., 1987, *Production Seismology Volume 10*, Geophysical Press, London, Amsterdam

Wolf, J. P. and Song, C., 1999, *Finite element modelling of unbounded media*, John Wiley and Sons.

Yu, G., Mansur, W. J. and Carrer, J. A. M., 1999, The linear θ method for 2D elastodynamic BE analysis, *Computational Mechanics*, Vol. 24, p. 2, pp. 82-89.

Yu, G., Mansur, W. J., Carrer, J. A. M. and Gong, L., 2000, Stability of Galerkin and collocation time domain boundary element methods as applied to the scalar wave equation, *Computers and Structures*, Vol. 74, pp. 495-506.

Zienkiewicz, O. C., 1977, *The finite element method*, Third edition, London: McGraw-Hill